NUMERICAL AND EXACT DENSITY FUNCTIONAL STUDIES OF LIGHT ATOMS IN STRONG MAGNETIC FIELDS

By

WUMING ZHU

A DISSERTATION PRESENTED TO THE GRADUATE SCHOOL
OF THE UNIVERSITY OF FLORIDA IN PARTIAL FULFILLMENT
OF THE REQUIREMENTS FOR THE DEGREE OF
DOCTOR OF PHILOSOPHY

UNIVERSITY OF FLORIDA

2005

Dedicated to Mom, to Dad,
and to my wife.

ACKNOWLEDGMENTS

First of all, I would like to thank Professor Samuel B. Trickey, my research advisor and committee chair, for the guidance he provided throughout the course of my graduate study at the University of Florida. His patience and constant encouragement are truly appreciated. Besides physics, I have also learned a lot from him about life and language skills which also are indispensable for becoming a successful physicist.

I would also like to thank Professor Hai-Ping Cheng, Professor Jeffrey L. Krause, Professor Susan B. Sinnott, and Professor David B. Tanner for serving in my supervisory committee, and for the guidance and advice they have given me. Professor David A. Micha is acknowledged for his help when I was in his class and for being a substitute committee member in my qualifying exam.

My gratitude goes to Dr. John Ashley Alford II for many helpful discussions, and to Dr. Chun Zhang, Dr. Lin-Lin Wang, and Dr. Mao-Hua Du for their academic and personal help. Besides them, many other friends have also enriched my life in Gainesville. They are Dr. Rongliang Liu, Dr. Linlin Qiu, Dr. Xu Du, Dr. Zhihong Chen, and Dr. Lingyin Zhu, who have moved to other places to advance their academic careers, and Guangyu Sun, Haifeng Pi, Minghan Chen, Yongke Sun, and Hui Xiong, who are continuing to make progress in their Ph.D. research.

Many thanks go to the incredible staff at the Department of Physics and at QTP. I especially would like to thank Darlene Latimer, Coralu Clements, and Judy Parker for the

assistance they provided during my graduate study. Financial support from NSF grants DMR-0218957 and DMR-9980015 is acknowledged.

Lastly, I thank my parents, who will never read this dissertation but can feel as much as I do about it, for their boundless love. I thank my wife for her special patience and understanding during the days I wrote my dissertation, and for all the wonderful things she brings to me.

TABLE OF CONTENTS

LIST OF TABLES

LIST OF FIGURES

Abstract of Dissertation Presented to the Graduate School
of the University of Florida in Partial Fulfillment of the
Requirements for the Degree of Doctor of Philosophy

NUMERICAL AND EXACT DENSITY FUNCTIONAL STUDIES OF LIGHT ATOMS IN STRONG MAGNETIC FIELDS

By

Wuming Zhu

August 2005

Chair: Samuel B. Trickey
Major Department: Physics

Although current density functional theory (CDFT) was proposed almost two decades ago, rather little progress has been made in development and application of this theory, in contrast to many successful applications that ordinary density functional theory (DFT) has enjoyed. In parallel with early DFT exploration, we have made extensive studies on atom-like systems in an external magnetic field. The objectives are to advance our comparative understanding of the DFT and CDFT descriptions of such systems. A subsidiary objective is to provide extensive data on light atoms in high fields, notably those of astrophysical interest.

To address the cylindrical symmetry induced by the external field, an efficient, systematic way to construct high quality basis sets within anisotropic Gaussians is provided. Using such basis sets, we did extensive Hartree-Fock and DFT calculations on helium through carbon atoms in a wide range of B fields. The applicability and

limitations of modern DFT and CDFT functionals for atomic systems in such fields is analyzed.

An exactly soluble two-electron model system, Hooke's atom (HA), is studied in detail. Analogously with known results for zero field, we developed exact analytical solutions for some specific confinement and field strengths. Exact DFT and CDFT quantities for the HA in *B* fields, specifically exchange and correlation functionals, were obtained and compared with results from approximate functionals. Major qualitative differences were identified. A major overall conclusion of the work is that the vorticity variable, introduced in CDFT to ensure gauge invariance, is rather difficult to handle computationally. The difficulty is severe enough to suggest that it might be profitable to seek an alternative gauge-invariant formulation of the current-dependence in DFT.

CHAPTER 1
BASICS OF DENSITY FUNCTIONAL THEORY AND CURRENT DENSITY FUNCTIONAL THEORY

Introduction

Ambient and low-temperature properties of normal bulk materials are largely determined by knowledge of the motion of the nuclei in the field of the electrons. In essence, this is a statement that the Born-Oppenheimer approximation [1] is widely relevant. For materials drawn from the lighter elements of the periodic table, the electrons even can be treated non-relativistically [2]. While doing some electronic structure calculations on α-quartz [3], and some classical inter-nuclear potential molecular dynamics (MD) simulations on silica-like nano-rods [4], a feature of modern computational materials physics became obvious. Very little is done with external magnetic fields. This scarcity seems like a missed opportunity.

Even with no external field, within the Born-Oppenheimer approximation, a non-relativistic approach to solution of the N-electron Schrödinger equation is not a trivial task. For simple systems, e.g. the He atom, highly accurate approximate variational wavefunctions exist [5], but these are too complicated to extend. Much of the work of modern quantum chemistry involves extremely sophisticated sequences of approximations to the exact system wavefunction [6]. The Hartree-Fock (HF) approximation, which uses a single Slater determinant as the approximation to the many-electron wavefunction, usually constitutes the first step toward a more accurate, sophisticated method. Several approaches, such as configuration interaction (CI), many-

body perturbation theory (MBPT), and coupled cluster (CC), are widely used in practice to improve HF results. It is worthwhile mentioning that such methods are extremely demanding computationally. Their computational cost scales as some high power of the number of electrons, typically 5-7th power. Thus these methods are only affordable for systems having up to tens of electrons. An external magnetic field which could not be treated perturbatively would make things much worse. The largest system that has been investigated with the full CI method as of today is a four-electron system, beryllium atom [7, 8]. On the other hand, people always have interests in larger systems and more accurate results than those achievable, no matter how fast and how powerful the computers are; thus theorists continue to conceive all kinds of clever approximations and theories to cope with this problem.

Density functional theory (DFT) [9, 10] is an alternative approach to the many-electron problem that avoids explicit contact with the *N*-electron wavefunction. DFT developed mostly in the materials physics community until the early 1990s when it reappeared in the quantum chemistry community as a result of the success of new approximate functionals. These aspects will be discussed below. Two other aspects are worth emphasizing. DFT has been remarkably successful in predicting and interpreting materials properties. Almost none of those predictions involve an external magnetic field. Particularly in Florida, with the National High Magnetic Field Laboratory, that is striking.

Even for very simple atoms, inclusion of an external *B* field is not easy. Only recently have the calculations on the helium atom in a high field been pushed beyond the HF approximation [11, 12, 13]. Although a version of DFT called current density

functional theory (CDFT) [14, 15, 16] exists for external magnetic fields, it has seen very little application or development. As discussed below, there is a lack of good approximate CDFT functionals and a lack of studies on which to try to build such improved functionals. One of the foundations of the success of ordinary DFT has been the availability of exact analytical and highly precise numerical data for atoms for comparison of various functionals and understanding their behavior. The main purpose of this dissertation is to find how the effect of an external magnetic field on electron motion should be incorporated in the DFT functional. In particular, I obtain numerical results on various atom-like systems in an external field, with and without CDFT approximate functionals. In addition, I give exact solutions for a model two-electron atom in a nonzero external B field, the so-called Hooke's atom (HA), that has provided valuable insight for DFT at $B = 0$.

Density Functional Theory

Attempts to avoid calculation of the many-electron wavefunction began almost simultaneously with the emergence of modern quantum mechanics. In 1927, Thomas and Fermi proposed a model in which the electron kinetic energy is expressed as a functional of the electron density, totally neglecting exchange and correlation effects [17]. The kinetic energy density is assumed to be solely determined by the electron density at that point, and approximated by the kinetic energy density of a non-interacting uniform electron gas having the same density. Later this approach was called the "local density approximation" (LDA) in DFT. The Thomas-Fermi (TF) model was refined subsequently by Dirac to include exchange effects (anti-symmetry of identical-particle wavefunction) and by von Weizsäcker to include spatial gradient corrections for the kinetic energy. The result is called the TFDW model. Though useful, it fails as a candidate for a model of

materials behavior. Teller proved that the model will not provide binding even for a simple diatomic molecule [17].

The modern form of DFT is rooted in the 1964 paper of Hohenberg and Kohn [9] which put forth two basic theorems, and the subsequent paper by Kohn and Sham [10], which gave an ingenious scheme for the use of those theorems. A difficulty with the KS scheme is that it lumps all of the subtlety of the many-electron problem, exchange and correlation, in one approximation. The popularity of DFT depends on the availability of reasonably accurate, tractable approximate functionals. To make the point clear and establish notation, next I give the bare essentials of ordinary DFT.

Foundations for DFT

The Hamiltonian of an interacting *N*-electron system is

$$\hat{H} = -\frac{1}{2}\sum_{i=1}^{N}\nabla_i^2 + \sum_{i=1}^{N}\upsilon(\vec{r}_i) + \frac{1}{2}\sum_{\substack{i,j=1 \\ i\neq j}}^{N}\frac{1}{|\vec{r}_i - \vec{r}_j|} \tag{1.1}$$

where $\vec{r}_i$ labels the space coordinate of the *i*th electron. Hartree atomic units are used throughout. The Schrödinger equation specifies the map from the external potential $\upsilon(\vec{r}_i)$ to the ground state many-body wavefunction, and the electron number density can be obtained by integrating out *N*-1 space variables. Schematically,

$$\upsilon(\vec{r}) \rightarrow \Psi(\vec{r}_1, \vec{r}_2, \ldots, \vec{r}_N) \rightarrow n(\vec{r}) \tag{1.2}$$

Hohenberg and Kohn noticed that the inversion of the above maps is also true [9], even though it is not as obvious as above. Because of the key importance of this observation, their proof is included here. For simplicity, they considered the spin independent, non-degenerate ground states. Let the Hamiltonian $\hat{H}$, ground state

wavefunction Ψ, density $n(\vec{r})$, and energy E associated with the specific external potential $\upsilon(\vec{r})$,

$$\upsilon(\vec{r}) :\mapsto \hat{H}, \Psi, n(\vec{r}), E. \tag{1.3}$$

Similarly define a primed system,

$$\upsilon'(\vec{r}) :\mapsto \hat{H}', \Psi', n'(\vec{r}), E'. \tag{1.4}$$

where $\upsilon(\vec{r}) \neq \upsilon'(\vec{r}) + C$, and hence $\Psi \neq \Psi'$. By the variational principle,

$$E = \left\langle \Psi \middle| \hat{H} \middle| \Psi \right\rangle < \left\langle \Psi' \middle| \hat{H} \middle| \Psi' \right\rangle = \left\langle \Psi' \middle| \hat{H}' \middle| \Psi' \right\rangle + \int n'(\vec{r}) \left(\upsilon(\vec{r}) - \upsilon'(\vec{r}) \right) \tag{1.5}$$

Interchanging the primed and unprimed systems gives us another inequality. Summation of those two inequalities leads to a contradiction $E + E' < E + E'$ if we assume $n'(\vec{r}) = n(\vec{r})$. Thus, different potentials must generate different ground state electron densities. Equivalently speaking, the knowledge of the ground state density $n(\vec{r})$ uniquely determines the external potential $\upsilon(\vec{r})$ up to a physically irrelevant addictive constant. This assertion is referred as Hohenberg-Kohn (HK) theorem I. Now the maps in eqn. (1.2) are both bijective,

$$\upsilon(\vec{r}) \leftrightarrow \Psi(\vec{r}_1, \vec{r}_2, \ldots, \vec{r}_N) \leftrightarrow n(\vec{r}) \tag{1.6}$$

An immediate consequence of HK theorem I is that the ground state electron density $n(\vec{r})$ can be chosen as the basic variable to describe the interacting *N*-electron system, since it is as good as the many-body wavefunction. Here "as good as" means that the ground state density $n(\vec{r})$ contains no more or less information about the system than the wavefunction does. It does not mean the density is a variable as easy as, or as hard as, the many-body wavefunction to handle. Actually, since the density is a 3-dimensional

physically observable variable, whereas the spatial part of wavefunction is a 3*N*-dimensional variable, the density is a much simpler variable to manipulate and to think about. On the other hand, by switching from the wavefunction to the density, we also lose some tools from quantum mechanics (QM) which we are quite adept at using. For example, in QM, an observable can be calculated by evaluating the expectation value of its corresponding operator. This approach often does not work in DFT. The best we can say is that the observable is a functional of the ground state density. In contrast to the explicit dependence on the wavefunction in the QM formulas for the expectation value, the implicit dependence on the ground state density in DFT is rarely expressible in a form useful for calculation. Most such functionals are not known as of today. Among them, the most exploited and the most successful one is the exchange-correlation energy functional, which is amenable to approximations for large varieties of systems. Another one being extensively studied but not so successfully is the kinetic energy functional, already mentioned in the paragraph about TF-type models.

While DFT is a whole new theory that does not need to resort to the many-body wavefunction, to make use of the Rayleigh-Ritz variational principle to find the ground state energy E_0, we retain that concept for a while. By the so-called constrained search scheme independently given by Lieb [18] and Levy [19] in 1982, all the trial wavefunctions are sorted into classes according to the densities $n'(\vec{r})$ to which they give rise. The minimization is split into two steps,

$$E_0 = \min_{\Psi'} \left\langle \Psi' \middle| \hat{H} \middle| \Psi' \right\rangle = \min_{n'(\vec{r})} \left\{ \int \upsilon(\vec{r}) n'(\vec{r}) d\vec{r} + F_{LL}\left[n'(\vec{r}) \right] \right\} \tag{1.7}$$

where $F_{LL}\left[n' \right] \equiv \min_{\Psi' \to n'} \left\langle \Psi' \middle| \hat{T} + U \middle| \Psi' \right\rangle$ (1.8)

The Lieb-Levy functional F_{LL} is defined on all the possible densities realizable from some anti-symmetric, normalized N-particle functions, or N- representable densities. Both the densities of degenerate states and even excited states are included. One good thing about F_{LL} is that we have a simple criterion for N- representable densities: all non-negative, integrable densities are N- representable.

The Kohn-Sham Scheme

The HK theorem showed that the ground state energy of a many-electron system can be obtained by minimizing the energy functional $E\left[n'\left(\vec{r}\right)\right]$. TF-type models constitute a direct approach to attack this problem, in which energy functionals are constructed as explicit approximate forms dependent upon the electron density. However, the accuracy of TF-type models is far from acceptable in most applications, and there are seemingly insurmountable difficulties to improve those models significantly. The reason is that the kinetic energy functionals in TF-type models bring in a large error. To circumvent this difficulty, an ingenious indirect approach to the kinetic energy was invented by Kohn and Sham [10]. A fictitious non-interacting system having the same ground state electron density as the one under study is introduced. Because the kinetic energy of this KS system, $T_{s,}$ can be calculated exactly, and because T_s includes almost all the true kinetic energy T, the dominant part of the error in TF-type models is eliminated. Since then, DFT has become a practical tool for realistic calculations.

It is advantageous to decompose the total energy in the following way,

$$E[n] = F_{LL}\left[n\left(\vec{r}\right)\right] + \int \upsilon(\vec{r})n(\vec{r})d\vec{r}$$

$$= T[n] + E_{ee}[n] + \int \upsilon(\vec{r})n(\vec{r})d\vec{r}$$

$$= T_s[n] + J + \int \upsilon(\vec{r}) n(\vec{r}) d\vec{r} + E_x^{HF} + V_c[n] + \left(T[n] - T_s[n]\right) \tag{1.9}$$

where E_{ee} is the total QM electron-electron interaction energy, $J = \frac{1}{2}\iint \frac{n(\vec{r})n(\vec{r}')}{|\vec{r} - \vec{r}'|} d\vec{r} d\vec{r}'$ is the classical electron-electron repulsion energy, E_x^{HF} is the conventional exchange energy, and V_c is the conventional correlation energy. T_s is defined in terms of the non-interacting system as usual,

$$T_s = -\frac{1}{2}\sum_{i=1}^{N} \left\langle \phi_i \middle| \nabla^2 \middle| \phi_i \right\rangle \tag{1.10}$$

Then E_x^{HF} is replaced by $E_x[n]$, the exchange energy calculated using the single-determinant HF formula but with the same orbitals in T_s, and E_c is defined as all the remaining energy

$$E_c[n] = V_c[n] + \left(T[n] - T_s[n]\right) + \left(E_x^{HF} - E_x[n]\right) \tag{1.11}$$

The total energy is finally expressed as

$$E[n] = T_s[n] + J + \int \upsilon(\vec{r}) n(\vec{r}) d\vec{r} + E_{xc}[n] \tag{1.12}$$

where $E_{xc}[n] = E_x[n] + E_c[n]$. (1.13)

Each of the first three terms in eqn. (1.12) usually makes a large contribution to the total energy, but they all can be calculated exactly. The remainder, E_{xc}, is normally a small fraction of the total energy and is more amenable to approximation than the kinetic energy. Even though the equations in this section are all exact, approximations to the E_{xc} functional ultimately must be introduced.

The variational principle leads to the so-called Kohn-Sham self-consistent equations,

$$\left[-\frac{\nabla^2}{2}+\upsilon_s(\vec{r})\right]\phi_i(\vec{r})=\varepsilon_i\phi_i(\vec{r}) \tag{1.14}$$

where $$\upsilon_s(\vec{r})=\upsilon(\vec{r})+\upsilon_H(\vec{r})+\upsilon_{xc}^{dft}(\vec{r}) \tag{1.15}$$

$$\upsilon_H(\vec{r})=\int\frac{n(\vec{r}\,')}{\left|\vec{r}-\vec{r}\,'\right|}d\vec{r}\,' \tag{1.16}$$

$$\upsilon_{xc}^{dft}(\vec{r})=\frac{\delta E_{xc}[n(\vec{r})]}{\delta n(\vec{r})} \tag{1.17}$$

and $$n(\vec{r})=\sum_{i=1}^{N}\left|\phi_i(\vec{r})\right|^2. \tag{1.18}$$

Again, Hartree atomic units are used throughout. Equations (1.14) - (1.18) constitute the basic formulas for KS calculations. The detailed derivation and elaborations can be found in the abundant literature on DFT, for example, references 20-22.

Since the foundations of DFT were established, there have been many generalizations to this theory. The most important include spin density functional theory (SDFT) [23], DFT for multi-component systems [24, 25], thermal DFT for finite temperature ensembles [26], DFT of excited states, superconductors [27], relativistic electrons [28], time-dependent density functional theory (TDDFT) [29], and current density functional theory (CDFT) for systems with external magnetic fields [14-16]. Among them, SDFT is the most well-developed and successful one. TDDFT has attracted much attention in recent years and shows great promise. Compared to the thousands of papers published on DFT and SDFT, we have fewer than 80 papers on CDFT in any form. Thus CDFT seems to be the least developed DFT generalization, perhaps surprisingly since there is a great deal of experimental work on systems in external *B* fields. That disparity is the underlying motivation for this thesis.

Current Density Functional Theory (CDFT)

Basic Formulations

One of the striking features of the very limited CDFT literature is the extremely restricted choice of functionals. A second striking feature is that most of the work using CDFT has been at $B = 0$, in essence using CDFT either to gain access to magnetic susceptibility [30, 31] or to provide a richer parameterization of the $B = 0$ ground state than that provided by SDFT [32]. In order to comprehend the challenge it is first necessary to outline the essentials of CDFT.

For an interacting N-electron system under both a scalar potential $\upsilon(\vec{r})$ and a vector potential $\vec{A}(\vec{r})$, its Hamiltonian reads,

$$\hat{H}_{tot} = \sum_i \left[\frac{1}{2} \left(\frac{\nabla_i}{i} + \vec{A}(\vec{r}_i) \right)^2 + \upsilon(\vec{r}_i) \right] + \frac{1}{2} \sum_{i \neq j} \frac{1}{|\vec{r}_i - \vec{r}_j|} \tag{1.19}$$

The paramagnetic current density $\vec{j}_p(\vec{r})$ is the expectation value of the corresponding operator $\vec{J}_p^{op}(\vec{r})$,

$$\vec{j}_p(\vec{r}) = \left\langle \Psi(\vec{r}_1, \vec{r}_2, \cdots, \vec{r}_N) \,|\, \vec{J}_p^{op}(\vec{r}) \,|\, \Psi(\vec{r}_1, \vec{r}_2, \cdots, \vec{r}_N) \right\rangle \tag{1.20}$$

where $$\vec{J}_p^{op}(\vec{r}) = \frac{1}{2i} \left[\hat{\Psi}^+(\vec{r}) \nabla \hat{\Psi}(\vec{r}) - \hat{\Psi}(\vec{r}) \nabla \hat{\Psi}^+(\vec{r}) \right] \tag{1.21}$$

in terms of the usual fermion field operators.

CDFT is an extension of DFT to include the vector potential $\vec{A}(\vec{r})$. The original papers [14-16] followed the HK argument by contradiction and purported thereby to prove not only that the ground state is uniquely parameterized by the density $n(\vec{r})$ and paramagnetic current density $\vec{j}_p(\vec{r})$, but also that the $\upsilon(\vec{r})$ and $\vec{A}(\vec{r})$ are uniquely

determined. Later it was found that a subtlety was overlooked. It is obvious that two Hamiltonians with different scalar external potentials cannot even have a common eigenstate, e.g., the first map in eqn. (1.6) is bijective, but this is not true when a vector potential is introduced. It is possible that two sets of potentials $\upsilon(\vec{r})$, $\vec{A}(\vec{r})$ and $\upsilon'(\vec{r})$, $\vec{A}'(\vec{r})$ could have the same ground state wavefunction. This non-uniqueness was later realized [33]. Fortunately, the HK-like variational principle only needs the one-to-one map between ground state wavefunction and densities, without recourse to the system's external potentials being functionals of densities [34]. To avoid the difficulties of representability problems, we follow the Lieb-Levy constrained search approach.

Sort all the trial wavefunctions according to the densities $n(\vec{r})$ and $\vec{j}_p(\vec{r})$ they would generate. The ground state wavefunction, which generates correct densities, will give the minimum of the total energy.

$$\begin{aligned} E_0 &= \min_{\Psi'} \left\langle \Psi' \middle| \hat{H}_{tot} \middle| \Psi' \right\rangle \\ &= \min_{n'(\vec{r}),\vec{j}'_p(\vec{r})} \left\{ \int \left(\upsilon(\vec{r}) + \frac{\vec{A}^2(\vec{r})}{2} \right) n'(\vec{r}) d\vec{r} + \int \vec{A}(\vec{r}) \cdot \vec{j}'_p(\vec{r}) + F\left[n'(\vec{r}), \vec{j}'_p(\vec{r}) \right] \right\} \end{aligned} \tag{1.22}$$

where $F\left[n', \vec{j}'_p \right] \equiv \min_{\Psi' \to n', \vec{j}'_p} \left\langle \Psi' \middle| \hat{T} + U \middle| \Psi' \right\rangle$ (1.23)

A non-physical non-interacting KS system is now introduced, which generates correct densities $n(\vec{r})$ and $\vec{j}_p(\vec{r})$. The functional F is customarily decomposed as

$$F\left[n, \vec{j}_p \right] = T_s\left[n, \vec{j}_p \right] + J + E_{xc}^{cdft}\left[n, \vec{j}_p \right] \tag{1.24}$$

The variational principle gives us the self-consistent equations

$$\left[\frac{1}{2} \left(\frac{\nabla}{i} + \vec{A}_{eff}(\vec{r}) \right)^2 + \upsilon_{eff}^{cdft}(\vec{r}) \right] \phi_i(\vec{r}) = \varepsilon_i \phi_i(\vec{r}) \tag{1.25}$$

where $\vec{A}_{eff}(\vec{r}) = \vec{A}(\vec{r}) + \vec{A}_{xc}(\vec{r})$ (1.26)

$$\upsilon_{eff}^{cdft}(\vec{r}) = \left[\upsilon(\vec{r}) + \upsilon_H(\vec{r}) + \upsilon_{xc}^{cdft}(\vec{r})\right] + \frac{1}{2}\left[\vec{A}^2(\vec{r}) - \vec{A}_{eff}^2(\vec{r})\right] \tag{1.27}$$

It is easy to see that $\upsilon_{eff}^{cdft}(\vec{r})$ reduces to $\upsilon_s(\vec{r})$ when we set $\vec{A}_{xc}(\vec{r}) = 0$. Exchange-correlation potentials are defined as functional derivatives,

$$\vec{A}_{xc}(\vec{r}) = \left.\frac{\delta E_{xc}^{cdft}\left[n(\vec{r}), \vec{j}_p(\vec{r})\right]}{\delta \vec{j}_p(\vec{r})}\right|_{n(\vec{r})} \tag{1.28}$$

$$\upsilon_{xc}^{cdft}(\vec{r}) = \left.\frac{\delta E_{xc}^{cdft}\left[n(\vec{r}), \vec{j}_p(\vec{r})\right]}{\delta n(\vec{r})}\right|_{\vec{j}_p(\vec{r})} \tag{1.29}$$

The electron density $n(\vec{r})$ can be calculated just as in eqn. (1.18). The paramagnetic current density is constructed from the KS orbitals according to

$$\vec{j}_p(\vec{r}) = \frac{1}{2i}\sum_i \left[\phi_i^*(\vec{r})\nabla\phi_i(\vec{r}) - \phi_i(\vec{r})\nabla\phi_i^*(\vec{r})\right] \tag{1.30}$$

The total energy expression of the system is

$$\begin{aligned} E_{tot}^{cdft} &= T_s + J + E_{xc}^{cdft}\left[n(\vec{r}), \vec{j}_p(\vec{r})\right] + \int n(\vec{r})\left\{\upsilon(\vec{r}) + \frac{\vec{A}^2(\vec{r})}{2}\right\}d\vec{r} + \int \vec{j}_p(\vec{r})\cdot\vec{A}(\vec{r})d\vec{r} \\ &= \sum \varepsilon_i - J + E_{xc}^{cdft}\left[n(\vec{r}), \vec{j}_p(\vec{r})\right] - \int \upsilon_{xc}^{cdft}(\vec{r})n(\vec{r})d\vec{r} - \int \vec{j}_p(\vec{r})\cdot\vec{A}_{xc}(\vec{r})d\vec{r} \end{aligned} \tag{1.31}$$

Equation (1.25) can be rewritten as

$$\left[\frac{1}{2}\left(\frac{\nabla}{i} + \vec{A}(\vec{r})\right)^2 + \left(\upsilon(\vec{r}) + \upsilon_H(\vec{r}) + \upsilon_{xc}^{cdft}(\vec{r})\right) + \frac{1}{2i}\left(\vec{A}_{xc}(\vec{r})\cdot\nabla + \nabla\cdot\vec{A}_{xc}(\vec{r})\right)\right]\phi_i(\vec{r}) = \varepsilon_i\phi_i(\vec{r}) \tag{1.32}$$

which is more suitable for application.

Vignale-Rasolt-Geldart (VRG) Functional

On grounds of gauge-invariance, Vignale and Rasolt argued that the exchange-correlation functional E_{xc}^{cdft} should be expressed as a functional of $n(\vec{r})$ and the so-called voticity [14-16]

$$\vec{v}(\vec{r}) \equiv \nabla \times \frac{\vec{j}_p(\vec{r})}{n(\vec{r})} \tag{1.33}$$

Following their proposal, if we choose $\vec{v}(\vec{r})$ as the second basic variable in CDFT,

$$E_{xc}^{cdft}[n(\vec{r}), \vec{j}_p(\vec{r})] = \tilde{E}_{xc}^{cdft}[n(\vec{r}), \vec{v}(\vec{r})] \tag{1.34}$$

exchange-correlation potentials can be found from functional derivatives

$$\vec{A}_{xc}(\vec{r}) = \frac{1}{n(\vec{r})}\left(\nabla \times \frac{\delta \tilde{E}_{xc}^{cdft}[n, \vec{v}]}{\delta \vec{v}(\vec{r})}|_{n(\vec{r})} \right) \tag{1.35}$$

$$\upsilon_{xc}^{cdft}(\vec{r}) = \frac{\delta \tilde{E}_{xc}^{cdft}[n, \vec{v}]}{\delta n(\vec{r})}|_{\vec{v}(\vec{r})} - \vec{A}_{xc}(\vec{r}) \cdot \frac{\vec{j}_p(\vec{r})}{n(\vec{r})} \tag{1.36}$$

To make use of the already proven successful DFT functionals, it is useful to separate the exchange-correlation functional into a current-independent term and an explicitly current-dependent term,

$$\tilde{E}_{xc}^{cdft}[n(\vec{r}), \vec{v}(\vec{r})] = E_{xc}^{dft}[n(\vec{r})] + \Delta E_{xc}[n(\vec{r}), \vec{v}(\vec{r})] \tag{1.37}$$

The current-independent term can be any widely used XC functional, such as LDA, or the generalized gradient approximation (GGA) functional. The current-dependent term is presumably small, and should vanish for zero current system, for example, the ground state of the helium atom.

Next we proceed in a slightly different, more general way. By homogeneous scaling of both the $n(\vec{r})$ and $\vec{j}_p(\vec{r})$, Erhard and Gross deduced that the current-dependent exchange functional scales homogeneously as [35]

$$E_x^{cdft}[n^\lambda, \vec{j}_p^\lambda] = \lambda E_x^{cdft}[n, \vec{j}_p] \tag{1.38}$$

where λ is the scaling factor. $n^\lambda = \lambda^3 n$ and $\vec{j}_p^\lambda = \lambda^4 \vec{j}_p$ are scaled charge density and paramagnetic current density, respectively. Assuming that the exchange part dominates the exchange-correlation energy, a local approximation for the E_{xc}^{cdft} takes the form

$$\tilde{E}_{xc}^{cdft}[n(\vec{r}), \vec{v}(\vec{r})] = E_{xc}^{dft}[n(\vec{r})] + \int g([n(\vec{r}), \vec{v}(\vec{r})], \vec{r}) \,|\, \vec{v}(\vec{r}) \,|^2 \, d\vec{r} \tag{1.39}$$

The foregoing expression is derived based on the assumption that $\vec{v}(\vec{r})$ is a basic variable in CDFT. A further (drastic) approximation is to assume

$$g([n(\vec{r}), \vec{v}(\vec{r})], \vec{r}) = g(n(\vec{r})) \tag{1.40}$$

which is done in the VRG approximation. By considering the perturbative energy of a homogeneous electron gas (HEG) in a uniform *B* field (the question whether the HEG remains uniform after the *B* field is turned on was not discussed), Vignale and Rasolt[14-16] gave the form for *g*,

$$g(\vec{r}) = g(n(\vec{r})) = \frac{k_F}{24\pi^2}\left[\frac{\chi(n(\vec{r}))}{\chi_0(n(\vec{r}))} - 1\right] \tag{1.41}$$

Here k_F is the Fermi momentum, χ and χ_0 are the orbital magnetic susceptibilities for the interacting and non-interacting HEG, respectively. From the tabulated data for $1 \le r_s \le 10$ in reference 36, Lee, Colwell, and Handy (LCH) obtained a fitted form [31],

$$s_{LCH} = \chi / \chi_0 = (1.0 + 0.028 r_s) e^{-0.042 r_s} \tag{1.42}$$

where $r_s = \left(\frac{3}{4\pi n}\right)^{1/3}$. (1.43)

accordingly, $g_{LCH} = \frac{k_F}{24\pi^2}(s_{LCH} - 1)$ (1.44)

Orestes, Marcasso, and Capelle proposed two other fits, both polynomial [37]

$$s_{OMC3} = 0.9956 - 0.01254 r_s - 0.0002955 r_s^2 \quad (1.45)$$

$$s_{OMC5} = 1.1038 - 0.499 r_s^{1/3} + 0.4423\sqrt{r_s} - 0.06696 r_s + 0.0008432 r_s^2 \quad (1.46)$$

Those fits all give rise to divergence problems in the low density region. A cutoff function needs to be introduced, which will be discussed in the next chapter.

Survey on the Applications of CDFT

The VRG functional has been applied in the calculation of magnetizabilities [30, 31], nuclear shielding constants [38], and frequency-dependent polarizabilities [39, 40] for small molecules, and ionization energies for atoms [37, 41]. In those calculations, the vector potential was treated perturbatively. Fully self-consistent calculations are still lacking. None of those studies has a conclusive result. The first calculation in Handy's group was plagued with problems arising from an insufficiently large basis set [31]. In their second calculation, they found that the VRG functional would cause divergences and set $g(n(\vec{r})) = 0$ for r_s >10. The small VRG contribution was overwhelmed by the limitations of the local density functional [38]. The VRG contribution to the frequency-dependent polarizability was also found to be negligible, and several other issues emerge as more important than explicitly including the current density functional [40]. Contrary to the properties of small molecules studied by Handy's group, Orestes *et al.* found that the current contribution to the atomic ionization energy is non-negligible, even though use of VRG did not improve the energy systematically [37].

All those investigations are based on the assumption that the VRG functional at least can give the correct order of magnitude of current contributions to the properties under study. Actually this is not guaranteed. The errors from ordinary DFT functionals and from the current part are always intertwined. To see how much the current term contributes, an exact solution is desired.

Vignale's group has never done any actual numerical calculation based on the VRG functional. Either for an electronic system [42, 43] or for an electron-hole liquid [44, 45], they used Danz and Glasser's approximation [46] for the exchange, and the random phase approximation for the correlation energy, which is known to be problematic in the low density regime. The kinetic energy was approximated from a non-interacting particle model or a TF-type model. Even though correlation effects were included in their formulas, the numerical errors introduced in each part were uncontrollable, and their calculations could only be thought as being very crude at best. This is somewhat inconsistent with invoking CDFT to do a better calculation than the ordinary DFT calculation does.

While the fully CDFT calculations on three-dimensional (3D) systems are scarce, there are more applications of CDFT to 2D systems. Examples include the 2D Wigner crystal transition [47], quantum dots [48], and quantum rings [49] in a magnetic field. In these cases, the E_{xc}^{cdft} was interpolated between the zero-field value from the Monte Carlo calculation by Tanatar and Ceperley [50], and the strong field limit [51].

Other Developments in CDFT

Some formal properties and virial theorems for CDFT have been derived from density scaling arguments [35, 52-54] or density matrix theory [55]. A connection

between CDFT and SDFT functionals is also established [56]. Those formal relations could be used as guidance in the construction of CDFT functionals, but as of today, there is no functional derived from them as far as I know.

CDFT is also extended to TDDFT in the linear response regime [57], which is called time-dependent CDFT (TD-CDFT). There is not much connection between TD-CDFT [57] and the originally proposed CDFT formulation [14-16]. Notice an important change in reference 57, the basic variables are electron density $n(\vec{r})$ and *physical* current density $\vec{j}(\vec{r})$, as opposed to the *paramagnetic* current density $\vec{j}_p(\vec{r})$, which is argued in references 14-16 to be the basic variable. In TD-CDFT, the frequency dependent XC kernel functions are approximated from the HEG [58, 59], and the formalism is used in the calculations of polarizabilities of polymers and optical spectra of group IV semiconductors [60, 61, 62]. TD-CDFT has also been extended to weakly disordered systems [63] and solids [64].

CHAPTER 2
ATOMS IN UNIFORM MAGNETIC FIELDS – THEORY

Single Particle Equations

When a uniform external magnetic field B, which we choose along the z direction, is imposed on the central field atom, its symmetry goes over to cylindrical. The Hamiltonian of the system commutes with a rotation operation about the direction of the B field, so the magnetic quantum number m is still a good quantum number. The natural gauge origin for an atom-like system is its center, e.g. the position of its nucleus. In the coulomb gauge, the external vector potential is expressed as

$$\vec{A}(\vec{r}) = \frac{1}{2}\vec{B} \times \vec{r} \tag{2.1}$$

The total many-electron Hamiltonian (in Hartree atomic units) then becomes

$$\hat{H} = \sum_{i=1}^{N}\left[-\frac{1}{2}\nabla_i^2 - \frac{Z}{r_i} + \frac{B^2}{8}\left(x_i^2 + y_i^2\right) + \frac{B}{2}\left(m_i + 2m_{s,i}\right)\right] + \frac{1}{2}\sum_{\substack{i,j=1 \\ i \neq j}}^{N}\frac{1}{\left|\vec{r}_i - \vec{r}_j\right|} \tag{2.2}$$

where Z is the nuclear charge, $\vec{r}_i$, m_i, $m_{s,i}$ are the space coordinate, magnetic quantum number, and spin z component for the ith electron.

Hartree-Fock Approximation

In the Hartree-Fock (HF) approximation, correlation effects among electrons are totally neglected. The simplest case is restricted Hartree-Fock (RHF), which corresponds to a single-determinant variational wavefunction of doubly occupied orbitals. We use $\phi_i(\vec{r})$ to denote single-particle orbitals. For spin-unrestricted Hartree-Fock (UHF)

theory, different spatial orbitals are assigned to the spin-up (α) and spin-down (β) electrons. The resulting single-particle equation is

$$\left[-\frac{\nabla^2}{2}+\upsilon_H\left(\vec{r}\right)-\frac{Z}{r}+\frac{B^2}{8}\left(x^2+y^2\right)+\frac{B}{2}\left(m_i+2m_{s,i}\right)\right]\phi_i^{HF}\left(\vec{r}\sigma\right) \\ -\sum_j\int d\vec{r}'\frac{\phi_j^{*HF}\left(\vec{r}'\sigma\right)\phi_i^{HF}\left(\vec{r}'\sigma\right)}{\left|\vec{r}-\vec{r}'\right|}\phi_j^{HF}\left(\vec{r}\sigma\right)=\varepsilon_{i,\sigma}^{HF}\phi_i^{HF}\left(\vec{r}\sigma\right) \tag{2.3}$$

Notice that exchange contributes only for like-spin orbitals.

Simple DFT Approximation

It seems plausible to assume that the $\vec{A}_{xc}$ contribution to the total energy is small compared to the ordinary DFT E_{xc}. Then the zeroth-order approximation to the CDFT exchange-correlation functional $E_{xc}^{cdft}\left[n,\vec{j}_p\right]$ can be taken to be the same form as the XC functional in ordinary DFT, $E_{xc}\left[n\right]$, with the current dependence in the XC functional totally neglected. Notice that in this scheme, the interaction between the B field and the orbitals is still partially included. From eqn. (1.28), we see that this approximation amounts to setting the XC vector potential identically zero everywhere, $\vec{A}_{xc}\left(\vec{r}\right)=0$. The corresponding single-particle Kohn-Sham equation is

$$\hat{h}^{dft}\phi_i^{dft}\left(\vec{r}\sigma\right)=\varepsilon_{i,\sigma}^{dft}\phi_i^{dft}\left(\vec{r}\sigma\right) \tag{2.4}$$

where $\hat{h}^{dft}=-\frac{\nabla^2}{2}+\upsilon_H\left(\vec{r}\right)-\frac{Z}{r}+\frac{B^2}{8}\left(x^2+y^2\right)+\frac{B}{2}\left(m_i+2m_{s,i}\right)+\upsilon_{xc}^{dft}\left(\vec{r}\right)$ (2.5)

The scalar XC potential is defined as in eqn. (1.17).

CDFT Approximation

In this case, both the density dependence and the current dependence of the XC energy functional $E_{xc}^{cdft}\left[n,\vec{j}_p\right]$ are included. If we knew the exact form of this functional,

this scheme in principal would be an exact theory including all many-body effects. In practice, just as in ordinary DFT, the XC functional must be approximated. Unfortunately very little is known about it. A major theme of this work is to develop systematic knowledge about the exact CDFT functional and the one available general-purpose approximation, VRG. The CDFT KS equation reads

$$\hat{h}^{cdft}\phi_i^{cdft}\left(\vec{r}\sigma\right)=\varepsilon_{i,\sigma}^{cdft}\phi_i^{cdft}\left(\vec{r}\sigma\right) \tag{2.6}$$

where $\hat{h}^{cdft}=\left(\hat{h}^{dft}-\upsilon_{xc}^{dft}\left(\vec{r}\right)\right)+\upsilon_{xc}^{cdft}\left(\vec{r}\right)+\frac{1}{2i}\left(\vec{A}_{xc}\cdot\nabla+\nabla\cdot\vec{A}_{xc}\right)$ (2.7)

and $\upsilon_{xc}^{cdft}\left(\vec{r}\right)$ is defined by eqn. (1.29). Notice the last term means $\nabla\cdot\left(\vec{A}_{xc}\phi_{i,\sigma}\right)$ when the operator is applied to a KS orbital.

Exchange-correlation Potentials

For ordinary DFT, both LDA and GGA approximations were implemented. Specifically, the XC functionals include HL [65], VWN [66, 67], PZ [68], PW92 [69], PBE [70], PW91 [71], and BLYP [72-75]. jPBE is an extension of the PBE functional that includes a current term [32], but does not treat $\vec{j}_p$ as an independent variable, which means $\vec{A}_{xc}\left(\vec{r}\right)=0$. For GGAs, the XC scalar potential is calculated according to

$$\upsilon_{xc}^{dft}\left(\vec{r}\right)=\frac{\delta E_{xc}^{GGA}\left[n\left(\vec{r}\right),\nabla n\left(\vec{r}\right)\right]}{\delta n\left(\vec{r}\right)}=\frac{\partial E_{xc}^{GGA}}{\partial n\left(\vec{r}\right)}-\nabla\cdot\frac{\partial E_{xc}^{GGA}}{\partial\nabla n\left(\vec{r}\right)} \tag{2.8}$$

Before considering any specific approximate XC functional in CDFT, we point out several cases for which CDFT should reduce to ordinary DFT. The errors in those DFT calculations are solely introduced by the approximate DFT functionals, *not* by neglecting the effects of the current. Such systems can provide estimates of the accuracy of DFT

functionals. Comparing their residual errors with the errors in corresponding current-carrying states can give us some clues about the magnitude of current effects.

The ground states of several small atoms have zero angular momentum for sufficiently small external fields. These are the hydrogen atom in an arbitrary field, the helium atom in $B < 0.711$ au. [76] (1 au. of B field $= 2.3505 \times 10^5$ Tesla), the lithium atom in $B < 0.1929$ au. [77], and the beryllium atom in $B < 0.0612$ au. [8]. Since their paramagnetic current density $\vec{j}_p$ vanishes everywhere, the proper CDFT and DFT descriptions must coincide. Notice (for future reference) that their density distributions are not necessarily spherically symmetric. This argument also holds for positive ions with four or fewer electrons and any closed shell atom.

If we admit the vorticity $\vec{\nu}(\vec{r})$ to be one basic variable in CDFT, as proposed by Vignale and Rasolt [14-16], there is another kind of system for which the DFT and CDFT descriptions must be identical. As Lee, Handy, and Colwell pointed out [38], for any system that can be described by a single complex wavefunction $\psi(\vec{r})$, $\vec{\nu}(\vec{r})$ vanishes everywhere. The proof is trivial,

$$\vec{\nu}(\vec{r}) = \nabla \times \frac{\vec{j}_p(\vec{r})}{n(\vec{r})} = \frac{1}{2i} \nabla \times \frac{\psi^* \nabla \psi - \psi \nabla \psi^*}{\psi \psi^*} = \frac{1}{2i} \nabla \times \nabla \left[\ln\left(\frac{\psi}{\psi^*} \right) \right] = 0$$

Cases include any single electron system, and the singlet states for two-electron systems in which the two electrons have the same spatial parts, such as H_2 and HeH^+ molecules. Notice that the system can have non-vanishing paramagnetic current density, $\vec{j}_p(\vec{r}) \neq 0$. A puzzling implication would seem to be that the choice of parameterization by $\vec{\nu}(\vec{r})$ is not adequate to capture all the physics of imposed B fields.

For CDFT calculations, we have mainly investigated the VRG functional already introduced. It is the only explicitly parameterized CDFT functional designed for $B > 0$ and applicable to 3D systems that we have encountered in the literature:

$$\Delta E_{xc}^{VRG}\left[n(\vec{r}),\vec{v}(\vec{r})\right]=\int g\left(n(\vec{r})\right)\left|\vec{v}(\vec{r})\right|^2 d\vec{r} \tag{2.9}$$

where $g\left(n(\vec{r})\right)$ and $\vec{v}(\vec{r})$ are defined in (1.41) and (1.33).

Substitution of (2.9) into (1.35) gives the expression for the vector XC potential,

$$\vec{A}_{xc}(\vec{r})=\frac{2}{n(\vec{r})}\nabla\times\left[g\left(n(\vec{r})\right)\vec{v}(\vec{r})\right] \tag{2.10}$$

In actual calculations it generally was necessary to compute the curl in this equation numerically. In CDFT, the scalar potential has two more terms beyond those found in ordinary DFT, namely

$$\upsilon_{xc}^{cdft}(\vec{r})=\upsilon_{xc}^{dft}(\vec{r})+\frac{dg(n)}{dn}\left|\vec{v}(\vec{r})\right|^2-\vec{A}_{xc}\left(\vec{r}\right)\cdot\frac{\vec{j}_p\left(\vec{r}\right)}{n(\vec{r})} \tag{2.11}$$

There are three fits for $g\left(n\right)$ to the same set of data tabulated in the range of $1\le r_s\le 10$ from random phase approximation (RPA) on the diamagnetic susceptibility of a uniform electron gas [36], namely eqns. (1.42), (1.45) and (1.46). Their derivatives are

$$\frac{dg_{LCH}}{dn}=\frac{dr_s}{dn}\cdot\frac{dg_{LCH}}{dr_s}$$

$$=-\frac{r_s}{3n}\cdot\frac{1}{24\pi^2}\left(\frac{9\pi}{4}\right)^{1/3}\left\{\frac{1}{r_s^2}-e^{-0.042r_s}\left[0.042\left(0.028+\frac{1}{r_s}\right)+\frac{1}{r_s^2}\right]\right\} \tag{2.12}$$

$$\frac{dg_{OMC3}}{dn}=-\frac{r_s}{3n}\cdot\frac{1}{24\pi^2}\left(\frac{9\pi}{4}\right)^{1/3}\left(\frac{0.0044}{r_s^2}-0.0002955\right) \tag{2.13}$$

$$\frac{dg_{OMC5}}{dn} = -\frac{r_s}{3n}\cdot\frac{1}{24\pi^2}\left(\frac{9\pi}{4}\right)^{1/3}\left(-0.1038r_s^{-2} + 0.3327r_s^{-5/3} - 0.2212r_s^{-3/2} + 0.0008432\right) \tag{2.14}$$

The three fits are very close in the range of $1 \le r_s \le 10$, but differ wildly in other regions due to different chosen functional forms for $g(n)$. They all cause divergence problems in any low density region. Without improving the reliability, precision, and the valid range of the original data set, it seems impossible to improve the quality of the fitted functions. It is desirable to know its behavior in the low density region, especially for finite system calculations, but unfortunately, reference 36 did not give any data for r_s >10, nor do we know its asymptotic form. Because *dg/dn* is required for all *r*, hence for all *n*, yet $g(n)$ is undefined for low densities, we must introduce a cutoff function. After some numerical experiment we chose

$$g_{cutoff} = \frac{k_F}{24\pi^2}\left(c_1 + c_2 r_s\right)e^{-a_{cutoff} r_s} \tag{2.15}$$

where α_{cutoff} is the cutoff exponent, which determines how fast the function dies out. The two constants c_1 and c_2 are determined by the smooth connection between $g(n)$ and g_{cutoff} at the designated cutoff density n_{cutoff}.

$$g_{cutoff}\left(n_{cutoff}\right) = g_{LCH/OMC}\left(n_{cutoff}\right),\ \left.\frac{dg_{cutoff}}{dn}\right|_{n_{cutoff}} = \left.\frac{dg_{LCH/OMC}}{dn}\right|_{n_{cutoff}} \tag{2.16}$$

In this work, we use $n_{cutoff} = 0.001a_0^{-3}$, $\alpha_{cutoff} = 2.0a_0^{-1}$, unless other values are explicitly specified.

There is an identity about the vector XC potential $\vec{A}_{xc}$ derived from the VRG functional,

$$\begin{aligned}\int \vec{A}_{xc}(\vec{r})\cdot\vec{j}_p(\vec{r}) &= \int \frac{1}{n(\vec{r})}\nabla\times\left[2g(n(\vec{r}))\vec{v}(\vec{r})\right]\cdot\vec{j}_p(\vec{r})d\vec{r} \\ &= -\int 2g(n(\vec{r}))\vec{v}(\vec{r})\cdot\nabla\times\frac{\vec{j}_p(\vec{r})}{n(\vec{r})}d\vec{r} \\ &= -2\Delta E_{xc}^{VRG}\left[n(\vec{r}),\vec{v}(\vec{r})\right]\end{aligned} \tag{2.17}$$

Since $\int \vec{A}_{xc}(\vec{r})\cdot\vec{j}_p(\vec{r})$ and ΔE_{xc}^{VRG} can be computed independently, this equation can provide a useful check in the code for whether the mesh is adequate and whether numerical accuracy is acceptable.

CHAPTER 3
BASIS SET AND BASIS SET OPTIMIZATION

Survey of Basis Sets Used in Other Work

For numerical calculations, the single particle orbitals in eqn. (2.3), or (2.4), or (2.6), can be represented in several ways. One is straightforward discretization on a mesh. For compatibility with extended system and molecular techniques, however, we here consider basis set expansions. For zero *B* field, the usual choices are Gaussian-type orbitals (GTO), or, less commonly, Slater-type orbitals (STO). Plane wave basis sets are more commonly seen in calculations on extended systems. Large *B* fields impose additional demands on the basis set, as discussed below. Here we summarize various basis sets that have been used for direct solution of the few-electron Schrödinger equation and in variational approaches such as the HF approximation, DFT, etc.

For the one-electron problem, the hydrogen atom in an arbitrary *B* field, the typical treatment is a mixture of numerical mesh and basis functions. The wavefunction is expanded in spherical harmonics $Y_{lm}(\theta,\varphi)$ in the low field regime, and in Landau orbitals $\phi_{nm}^{Lan}(\rho,\varphi)$ for large *B* fields. Here *r*, θ, φ are spherical coordinates, and *z*, ρ, φ are cylindrical coordinates. The radial part (for low *B*) or the *z* part (for high *B*) of the wavefunction is typically represented by numerical values on a one-dimensional mesh [78]. In Chapter 5 we will also use this technique for the relative motion part of the Hooke's atom in a *B* field. Of course, the hydrogen atom has also been solved algebraically, an approach in which the wavefunction takes the form of a polynomial

multiplying an exponential. This is by no means a trivial task. To get an accurate description for the wavefunction, the polynomial may have to include thousands of terms, and the recursion relation for the polynomial coefficients is complicated [79-82].

The multi-channel Landau orbital expansion was also used in DFT calculations on many-electron atoms [83]. Another approach is the two-dimensional finite element method [84]. Dirac exchange-only or similar functionals were used in those two calculations. In the series of Hartree-Fock calculations on the atoms hydrogen through neon by Ivanov, and by Ivanov and Schmelcher, the wavefunctions were expressed on two-dimensional meshes [85-90, 76]. Slater-type orbitals were chosen by Jones, Ortiz, and Ceperley for their HF orbitals to provide the input to quantum Monte Carlo calculations, with the aim to develop XC functionals in the context of CDFT [91-93]. Later they found that the STO basis was not sufficient and turned to anisotropic Gaussian type orbitals (AGTO) [94]. Apparently their interests changed since no subsequent publications along this thread were found in the literature. Schmelcher's group also employed AGTOs in their full CI calculations on the helium [11-13], lithium [77], and beryllium [8] atoms. At present, AGTOs seem to be the basis set of choice for atomic calculations which span a wide range of field strengths. This basis has the flexibility of adjusting to different field strengths, and the usual advantage of converting the one-body differential eigenvalue problem into a matrix eigenvalue problem. Moreover, the one-center coulomb integral can be expressed in a closed form in this basis, though the expression is lengthy [11, 12]. The disadvantage of AGTOs is that one has to optimize their exponents nonlinearly for each value of the B field, which is not an easy task, and a

simple, systematic optimization is lacking. We will come back to this issue and prescribe an efficient, systematic procedure.

Spherical-GTO and Anisotropic-GTO Representations

As with any finite GTO basis, there is also the improper representation of the nuclear cusp. Given the predominance of GTO basis sets in molecular calculations and the local emphasis on their use in periodic system calculations, this limitation does not seem to be a barrier. Spherical GTOs are most widely used in electronic structure calculations on finite systems without external magnetic field. The periodic system code we use and develop, GTOFF [95], also uses a GTO basis. Several small molecules in high *B* fields were investigated by Runge and Sabin with relatively small GTO basis sets [96]. To understand the performance of GTOs in nonzero field and make a connection to the code GTOFF, our implementation includes both GTO and AGTO basis sets. The former is, of course, a special case of the latter, in which the exponents in the longitudinal and transverse directions are the same.

Spherical GTO Basis Set Expansion

The form of spherical Gaussian basis we used is

$$G_{lm}^{\alpha}\left(\vec{r}\right)=N_{lm}^{\alpha}r^{l}e^{-\alpha r^{2}}Y_{lm}\left(\theta,\varphi\right) \tag{3.1}$$

where N_{lm}^{α} is the normalization factor. The KS or Slater orbitals (DFT or HF) are expanded in the $G_{lm}^{\alpha}\left(\vec{r}\right)$,

$$\phi_{i}\left(\vec{r}\sigma\right)=\sum_{l}\left(\sum_{\alpha}a_{i,l}^{\alpha,\sigma}G_{lm}^{\alpha}\right)\left|\sigma\right\rangle=\sum_{l}R_{il}^{\sigma}\left(r\right)Y_{lm}\left(\theta,\varphi\right)\left|\sigma\right\rangle \tag{3.2}$$

where $R_{il}^{\sigma}\left(r\right)=r^{l}\sum_{\alpha}a_{i,l}^{\alpha,\sigma}N_{lm}^{\alpha}e^{-\alpha r^{2}}$ (3.3)

Notice m is understood as m_i, the magnetic quantum number of the ith orbital. For simplicity, the subscript i is omitted when that does not cause confusion. The electron density and its gradient can be evaluated conveniently as

$$\begin{aligned} n(\vec{r}) &= \sum_i \left|\phi_i(\vec{r})\right|^2 = \sum_i \left|\sum_l R_{il}(r) Y_{lm}(\theta,\varphi)\right|^2 \\ &= \sum_i \sum_{ll'} R_{il}(r) R_{il'}(r) Y^*_{lm}(\theta,\varphi) Y_{l'm}(\theta,\varphi) \end{aligned} \tag{3.4}$$

$$\begin{aligned} \nabla n(\vec{r}) = \hat{r} \sum_i \sum_{ll'} &\left[R_{il}(r) R'_{il'}(r) + R'_{il}(r) R_{il'}(r)\right] Y^*_{lm}(\theta,\varphi) Y_{l'm}(\theta,\varphi) \\ &+ \hat{\theta} \sum_i \sum_{ll'} \frac{R_{il}(r) R_{il'}(r)}{r} \frac{\partial}{\partial\theta}\left[Y^*_{lm}(\theta,\varphi) Y_{l'm}(\theta,\varphi)\right] \end{aligned} \tag{3.5}$$

The paramagnetic current density is

$$\vec{j}_p(\vec{r}) = \hat{\varphi} \frac{1}{r\sin\theta} \sum_i \sum_{ll'} m_i R_{il}(r) R_{il'}(r) Y^*_{lm}(\theta,\varphi) Y_{l'm}(\theta,\varphi) = \hat{\varphi}\, j_p(r,\theta) \tag{3.6}$$

and the curl of $\vec{j}_p(\vec{r})$ is

$$\begin{aligned} \nabla \times \vec{j}_p(\vec{r}) = \hat{r} \sum_i \sum_{ll'} m_i &\left[\frac{R_{il} R_{il'}}{r^2}\left(\frac{\partial Y^*_{lm}}{\partial\theta}\frac{Y_{l'm}}{\sin\theta} + \frac{\partial Y^*_{l'm}}{\partial\theta}\frac{Y_{lm}}{\sin\theta}\right)\right] \\ -\hat{\theta} \frac{1}{r\sin\theta} \sum_i \sum_{ll'} m_i &\left[\left(R_{il} R'_{il'} + R'_{il} R_{il'}\right) Y^*_{lm} Y_{l'm}\right] \end{aligned} \tag{3.7}$$

The vorticity is evaluated analytically according to

$$\begin{aligned} \vec{\nu}(\vec{r}) &= \nabla \times \frac{\vec{j}_p(\vec{r})}{n(\vec{r})} = -\frac{\nabla n(\vec{r})}{n^2(\vec{r})} \times \vec{j}_p(\vec{r}) + \frac{\nabla \times \vec{j}_p(\vec{r})}{n(\vec{r})} \\ &= \nu_r(r,\theta)\hat{r} + \nu_\theta(r,\theta)\hat{\theta} \end{aligned} \tag{3.8}$$

For the VRG functional, the vector XC potential is expressed in spherical coordinates as

$$\begin{aligned} \vec{A}_{xc}(\vec{r}) &= \hat{\varphi} \frac{2}{n(r,\theta)} \frac{1}{r} \left\{\frac{\partial}{\partial r}\left[r \cdot g\left(n(r,\theta)\right)\nu_\theta(r,\theta)\right] - \frac{\partial}{\partial\theta}\left[g\left(n(r,\theta)\right)\nu_r(r,\theta)\right]\right\} \\ &= \hat{\varphi}\, A_{xc}(r,\theta) \end{aligned} \tag{3.9}$$

The last term in eqn. (2.7) becomes

$$\nabla\cdot\left(\vec{A}_{xc}(\vec{r})\phi_{i,\sigma}(\vec{r})\right)=\vec{A}_{xc}(\vec{r})\cdot\nabla\phi_{i,\sigma}(\vec{r})+\phi_{i,\sigma}(\vec{r})\cdot\frac{1}{r\sin\theta}\frac{\partial A_{xc}(r,\theta)}{\partial\varphi}$$
$$=\vec{A}_{xc}(\vec{r})\cdot\nabla\phi_{i,\sigma}(\vec{r}) \qquad (3.10)$$

Appendix A includes the matrix elements in this basis for each term in the Hamiltonian.

Anisotropic GTO (AGTO) Basis Set Expansion

An external *B* field effectively increases the confinement of the electron motions in the *xy* plane, and causes an elongation of the electron density distribution along the *z* axis. It is advantageous to reflect this effect in the basis set by having different decay rates along directions parallel and perpendicular to the *B* field. AGTOs are devised precisely in this way:

$$\chi_j(\rho,z,\varphi)=N_j\rho^{n_{\rho_j}}z^{n_{z_j}}e^{-\alpha_j\rho^2-\beta_j z^2}e^{im_j\varphi},\qquad j=1,2,3,\cdots \qquad (3.11)$$

where $n_{\rho_j}=|m_j|+2k_j,$ $n_{z_j}=\pi_{z_j}+2l_j,$ with $k_j=0,1,\cdots$ $m_j=\cdots,-2,-1,0,1,2,\cdots$ $l_j=0,1,\cdots$ $\pi_{z_j}=0,1.$

and N_j is the normalization factor. If we let $\alpha_j=\beta_j$, this basis of course recovers the isotropic Gaussian basis, appropriate for $B = 0$. The basis sets used in reference 94 were limited only to $k_j=l_j=0$, which are more restrictive than those used by Becken and Schmelcher [11-13] and ours.

Single-particle wavefunctions expanded in AGTOs have the general form

$$\phi_i(\vec{r}\sigma)=\sum_j b_{ij}^{\sigma}\chi_j(\rho,z,\varphi)\left|\sigma\right\rangle \qquad (3.12)$$

Various quantities can be calculated in this basis according to their expressions in cylindrical coordinates,

$$\nabla\phi_i(\vec{r}) = \hat{\rho}\frac{\partial\phi_i}{\partial\rho} + \hat{z}\frac{\partial\phi_i}{\partial z} + \hat{\varphi}\frac{im_i}{\rho}\phi_i$$
$$= \sum_j b_{ij}\left[\hat{\rho}\left(\frac{n_{\rho_j}}{\rho} - 2\alpha_j\rho\right) + \hat{z}\left(\frac{n_{z_j}}{z} - 2\beta_j z\right) + \hat{\varphi}\frac{im_i}{\rho}\right]\chi_j(\rho,z,\varphi) \tag{3.13}$$

$$n(\vec{r}) = \sum_i |\phi_i(\vec{r})|^2 = \sum_i\left[\sum_j b_{ij}N_j\rho^{n_{\rho_j}}z^{n_{z_j}}e^{-\alpha_j\rho^2-\beta_j z^2}\right]^2 = n(\rho,z) \tag{3.14}$$

$$\nabla n(\vec{r}) = \hat{\rho}\frac{\partial n(\vec{r})}{\partial\rho} + \hat{z}\frac{\partial n(\vec{r})}{\partial z} = 2\sum_i\left\{\hat{\rho}\,\phi_i^*\frac{\partial\phi_i}{\partial\rho} + \hat{z}\,\phi_i^*\frac{\partial\phi_i}{\partial z}\right\} \tag{3.15}$$

$$\vec{j}_p(\vec{r}) = \hat{\varphi}\frac{1}{\rho}\sum_i m_i|\phi_i(\vec{r})|^2 = \hat{\varphi}\frac{1}{\rho}\sum_i m_i\left[\sum_j b_{ij}N_j\rho^{n_{\rho_j}}z^{n_{z_j}}e^{-\alpha_j\rho^2-\beta_j z^2}\right]^2 \tag{3.16}$$
$$= \hat{\varphi}\;\; j_p(\rho,z)$$

$$\nabla\times\vec{j}_p(\vec{r}) = \frac{1}{\rho}\sum_i 2m_i\left\{-\hat{\rho}\,\phi_i^*\frac{\partial\phi_i}{\partial z} + \hat{z}\,\phi_i^*\frac{\partial\phi_i}{\partial\rho}\right\} \tag{3.17}$$
$$= \hat{\rho}\left(\hat{\rho}\cdot\nabla\times\vec{j}_p(\vec{r})\right) + \hat{z}\left(\hat{z}\cdot\nabla\times\vec{j}_p(\vec{r})\right)$$

$$\vec{v}(\vec{r}) = \hat{\rho}\left[\frac{j_p\dfrac{\partial n}{\partial z}}{n^2(\vec{r})} + \frac{\hat{\rho}\cdot\nabla\times\vec{j}_p}{n(\vec{r})}\right] + \hat{z}\left[\frac{\hat{z}\cdot\nabla\times\vec{j}_p}{n(\vec{r})} - \frac{j_p\dfrac{\partial n}{\partial\rho}}{n^2(\vec{r})}\right] \tag{3.18}$$

$$= v_\rho(\rho,z)\hat{\rho} + v_z(\rho,z)\hat{z}$$

Again, for the VRG functional we have

$$\vec{A}_{xc}(\vec{r}) = \hat{\varphi}\frac{2}{n(\rho,z)}\left\{\frac{\partial}{\partial z}\left[g(n(\rho,z))v_\rho(\rho,z)\right] - \frac{\partial}{\partial\rho}\left[g(n(\rho,z))v_z(\rho,z)\right]\right\} \tag{3.19}$$

We follow the scheme in references 11-12 for evaluation of matrix elements, in which all the integrals, including Coulomb integrals, are expressed in closed form.

Connection between GTOs and AGTOs

As pointed out before, a GTO basis is a special case of an AGTO basis. Conversely, a particular AGTO can be expanded in GTOs.

$$\chi_j(\rho,z,\varphi) = N_j \rho^{n_{\rho_j}} z^{n_{z_j}} e^{-\alpha_j r^2} e^{im_j\varphi} \sum_{k=0}^{\infty} \frac{\left[(\alpha_j - \beta_j) z^2\right]^k}{k!}$$

$$= N_j \sum_{k=0}^{\infty} \frac{(\alpha_j - \beta_j)^k}{k!} r^{n_{\rho_j}+n_{z_j}+2k} e^{-\alpha_j r^2} e^{im_j\varphi} (\sin\theta)^{n_{\rho_j}} (\cos\theta)^{n_{z_j}+2k} \qquad (3.20)$$

It is easy to see this is a linear combination of $G_{lm_j}^{\alpha_j}$ with $l = n_{\rho_j} + n_{z_j} + 2k$, $k = 0, 1, 2, \cdots$

An ordinary contracted Gaussian basis is a fixed linear combination of several primitive Gaussians having same the *l* and *m* but different exponents α_j. Similarly, an AGTO can also be thought as a contracted GTO that contains infinitely many GTOs (in principle) having the same exponent and *m* but different *l* values with increment of 2. This establishes the equivalence of the two kinds of orbitals. The relative efficiency of the AGTO basis in cylindrically confined systems is apparent for $B \neq 0$.

Primary and Secondary Sequences in AGTO

While the AGTO basis provides extra flexibility, its optimization is more complicated than for a GTO set of comparable size. Kravchenko and Liberman investigated the performance of AGTO basis sets in one-electron systems, the hydrogen atom and the hydrogen molecular ion, and showed that they could provide accuracy of 10^{-6} Hartree or better [97]. Jones, Ortiz, and Ceperley estimated their basis set truncation error for the helium atom in $B < 8$au. to be less than one milihartree in the total atomic energy of about 2 Hartrees [94].

Even-tempered Gaussian (ETG) sequences often are used in zero-field calculations. For a sequence of primitive spherical Gaussians having the same quantum numbers, their exponents are given by

$$\alpha_j = \beta_j = pq^j, \qquad j = 1, 2, \cdots N_b. \qquad (3.21)$$

where p and q are determined by

$$\begin{aligned} \ln p &= a \ln(q-1) + a' \\ \ln(\ln q) &= b \ln N_b + b' \end{aligned} \tag{3.22}$$

and N_b is the basis size. For the hydrogen atom, Schmidt and Ruedenburg [98] recommended the following parameters: a = 0.3243, a' = -3.6920, b = -0.4250, b' = 0.9280. Since the external magnetic field only increases the confinement in the horizontal direction, we may expect eqn. (3.21) to be equally useful for generating longitudinal exponents β_j for the AGTO basis.

The choice of α_j is more subtle. Jones, Ortiz, and Ceperley [94] used several tempered sequences of the types

$$\alpha_j = \beta_j, \quad 2\beta_j, \quad 4\beta_j, \quad 8\beta_j, \quad \cdots \tag{3.23}$$

For convenience, we refer to the first sequence ($\alpha_j = \beta_j$) as the primary sequence, and the second, the third, the fourth, … sequences as the secondary sequences in our discussion. The primary JOC sequence in eqn. (3.23) is obviously as same as the spherical GTOs, for which the transverse and longitudinal exponents are the same. However for the second JOC sequence, the transverse exponents α_j's are twice the longitudinal exponents β_j's, and for the third sequence, $\alpha_j = 4\beta_j$, etc. The basis set is the sum of all those sequences. The total number of basis functions is N_b multiplied by the number of different sequences. Reference 94 used 2-5 sequences in the expansion of HF orbitals. Obviously, when several sequences are included, which is necessary for large B fields, very large basis sets can result.

Kravchenko and Liberman [97] chose

$$\alpha_j = \beta_j + B\Delta_{KL}, \beta_j + 1.2B\Delta_{KL}, \beta_j + 0.8B\Delta_{KL}, \beta_j + 1.4B\Delta_{KL}, \beta_j + 0.6B\Delta_{KL} \qquad (3.24)$$

where Δ_{KL} is a value between 0 and 0.3 which minimizes the basis set truncation error compared to more accurate results. Here we still refer to the sequences in eqn. (3.24) as primary and secondary sequences. In each KL sequence, the differences between the transverse and longitudinal exponents are the same for all the basis functions. An improvement of KL basis sets over JOC basis sets is that the former have shorter secondary sequences, which helps to keep basis size within reason. Namely, the second and the third KL sequences have lengths of one-half of KL primary sequence, e.g., N_b /2 is used in eqns. (3.21) and (3.22) to generate them, and the fourth and fifth KL sequences have lengths of N_b /4.

Becken *et al.* [11] used a seemingly different algorithm to optimize both α_j and β_j in the same spirit of minimizing the one-particle HF energy, H atom or He^+ in a B field, but they did not give enough details for one to repeat their optimization procedure.

Optimized AGTO Basis Sets

In this section, I give some numerical illustrations of the basis set issues. These examples illustrate the importance, difficulties, and what can be expected from a reasonably well-optimized basis.

Our goal is set to reduce basis set error in the total energy of a light atom to below one milihartree. This criterion is based on two considerations. One is the observation by Orestes, Marcasso, and Capelle that the magnitude of current effects in CDFT is of the same order as the accuracy reached by modern DFT functionals [37]. They compared atomic ionization energies from experiment with DFT-based calculations. A typical

difference is 0.4eV, or 15 *m*H. To study the current effect in CDFT, we need to reduce the basis set errors to considerably below this value. Another factor considered is the well-known standard of chemical accuracy, usually taken to be 1 kcal/mol, or 1.6 *m*H. It turns out that this goal is much harder to reach for multi-electron atoms in a large B field than for the field-free case. Two systems I choose for comparison are the hydrogen and carbon atoms. There are extensive tabulations for the magnetized hydrogen atom [78], and even more accurate data from the algebraic method [80] against which to compare. However, the hydrogen atom does not include electron-electron interaction, which is exactly the subject of our interest. For the carbon atom, our comparison mainly will be made with numerical Hartree-Fock data [90]. Without external field, the correlation energy of the C atom is about 0.15 Hartree [99], two orders of magnitude larger than our goal. This difference also makes the choice of one *m*H basis set error plausible.

Examine the zero-field case first. It is well known that the non-relativistic energy of the hydrogen atom is exactly -0.5 Hartree. For the carbon atom, the numerical HF data taken from reference 90 are treated as the exact reference. Calculated HF energies in various basis sets are listed in Table 3-1, together with basis set errors in parentheses. We first tested the widely used 6-31G basis sets. Those basis sets are obtained from the GAMESS code [100]. In primitive Gaussians, they include up through 4*s* for the hydrogen, and 10*s*4*p* for the carbon atom. As expected, the accuracies in total energy that they deliver increase only slightly after de-contraction. A sequence of exponents derived from eqn. (3.21) with length $N_b = 8$ has a comparable size with the 6-31G basis for the carbon atom. It gives rather bad results, but recall that a significant deficiency of GTOs is that they cannot describe the nuclear cusp condition. By adding five tighter *s* orbitals

extrapolated from eqn. (3.21) with j = 9,10,…,13, the basis set error is reduced by 99%. To further reduce the remaining 1.6 mH error, higher angular momentum orbitals are required. Addition of four d orbitals and removal of the tightest, unnecessary p orbital gives a 13s7p4d basis set, with only 0.8 mH truncation error left. A larger basis set, 20s11p6d, similarly constructed from the N_b = 16 sequence by adding 4 tighter s orbitals has error only of 0.05 mH.

Table 3-1 Basis set effect on the HF energies of the H and C atoms with $B = 0$ (energies in Hartree)

Basis Set [a]	Hydrogen atom	Carbon atom
6-31G	-0.498233 (0.001767)	-37.67784 (0.01312)
De-contracted 6-31G	-0.498655 (0.001345)	-37.67957 (0.01139)
Sequence N_b = 8	-0.499974 (0.000026)	-37.51166 (0.17930)
N_b = 8, plus 5 tighter s	-0.499989 (0.000011)	-37.68938 (0.00158)
13s7p4d	-0.499989 (0.000011)	-37.69018 (0.00078)
Sequence N_b = 16	-0.49999992(0.00000008)	-37.68949 (0.00147)
20s11p6d	-0.49999996(0.00000004)	-37.69091 (0.00005)
∞	-0.5	-37.69096 [b]

(a) see text for definitions;
(b) from reference 90;
(c) numbers in parentheses are basis set errors.

The situation changes greatly when a substantial external B field is added. Let us first take the example of the H atom ground state in a field B = 10 au. Its energy is known accurately to be -1.747 797 163 714 Hartree [80]. The sequence of N_b = 16 included in Table 3-1 works remarkably well for the field-free energy, but gives 24% error in the B = 10 au field. See Table 3-2. Adding a sequence of d orbitals that has same length and same exponents as that for the s orbitals, which doubles the basis size, reduces the error by 80%. Further supplementation by g and i orbitals in the same way decreases the error by another order of magnitude. But this is still far from satisfactory. To reduce the basis set error below 1 μH, higher angular momentum basis with l up to 20 must be included. Obviously, this is a very inefficient approach. The basis sets used by Jones, Ortiz, and

Ceperley [94] (see eqn. 3.23) converge the total energy more rapidly than these spherical bases. The primary sequence in the JOC basis sets is the same as the spherical basis, but subsequent secondary sequences double the transverse exponents α_j's successively. With four sequences the error is less than 1% of the error in a spherical basis set having the same size. Another significant gain can be obtained if we move to the KL basis sets [97] (see eqn. 3.24). Here we choose $\Delta_{KL} = 0.18$, which is obtained by searching with a step of 0.01 to minimize the basis set truncation error. Including only the primary KL sequence gains about the accuracy of the three-sequence JOC basis set. Recall that the subsequent KL secondary sequences have shorter lengths than the primary one (refer to the discussion after eqn. 3.24). Specifically, the second and the third sequences have length of $N_b/2 = 8$, and the fourth and the fifth sequences have length of $N_b/4 = 4$. Thus, the basis size will be 16 + 8 + 8 + 4 + 4 = 40 if we include five KL sequences, with accuracy of 1 μH.

Table 3-2 Basis set errors for the ground state energy of the hydrogen atom in B = 10 au. (energies in Hartree)

Basis size	Spherical	JOC [a]	KL [b]	Optimized	Eqn. (3.26)
16	0.419 8	0.419 787 28	0.003 738 20	0.000 000 60	0.001 044 51
32	0.081 5	0.027 124 87	0.000 005 39	0.000 000 36	0.000 000 50
48	0.021 7	0.001 008 57			
64	0.008 1	0.000 075 02			
40			0.000 001 12	0.000 000 30	0.000 000 28

(a) Jones-Ortiz-Ceperley basis sets, see ref [94] and eqn. (3.23);
(b) Kravchenko-Liberman basis sets, see ref [97] and eqn. (3.24). Δ_{KL} is chosen to be 0.18.

However, this does not mean there is no opportunity left for basis set optimization. Starting from the primary sequence in the KL basis set, we then searched in the parameter space $\{\alpha_j\}$ to minimize the total energy of the H atom. First, the energy gradient in

parameter space is calculated, then a walk is made in the steepest descent direction. These two steps are repeated until

$$\frac{\partial E}{\partial \alpha_j} = 0 \tag{3.25}$$

The error left in this optimized basis set is only 0.6 μH, six orders of magnitude smaller than the error of a spherical basis set of the same size! The resulting exponents are listed in Table 3-3, together with the coefficients used in the wavefunction expansion. Addition of the same secondary KL sequences can further reduce the remaining error by one half. This improvement is not as spectacular as that for the KL basis set because those exponents have already been optimized. It is worth mentioning that, while it is easy to optimize the basis set for the H atom fully, it is very hard to do so for multi-electron atoms. We usually only get partially optimized results, but by including secondary sequences, the basis error can be greatly reduced, as demonstrated here.

Table 3-3 Optimized basis set and expansion coefficients for the wavefunction of the hydrogen atom in B = 10 au.

j	Coefficients	α_j	β_j	$\alpha_j - \beta_j$
1	0.000493	1.8886	0.0573	1.8313
2	0.011007	2.8640	0.1247	2.7393
3	0.184818	2.4462	0.2717	2.1745
4	0.372811	2.5541	0.5917	1.9624
5	0.277663	2.6442	1.2890	1.3552
6	0.132857	3.7690	2.8077	0.9613
7	0.050662	6.7855	6.1159	0.6696
8	0.019285	13.9048	13.3221	0.5827
9	0.007139	29.3287	29.0190	0.3097
10	0.002772	64.4702	63.2111	1.2591
11	0.000955	139.3854	137.6904	1.6950
12	0.000418	301.7122	299.9260	1.7862
13	0.000114	655.1166	653.3180	1.7986
14	0.000082	1424.8988	1423.0988	1.8000
15	-0.000001	3101.6845	3099.8845	1.8000
16	0.000021	6754.1687	6752.3659	1.8028

From Table 3-3, we see that the wavefunction is mainly expanded in basis j = 3, 4, 5, 6, and $\alpha_j - \beta_j$ is not a constant as the KL sequences suggest. The smaller the exponent, the larger the difference between the transverse and the longitudinal exponents. This is quite understandable. A smaller exponent means that the electron density extends far from the nucleus, and the magnetic field will overpower the nuclear attraction, thus the distortion from the field-free spherical shape will be relatively larger. In the limit of $\beta_j \to 0$, which can be equivalently thought of as the large B limit, or zero nuclear charge, the electron wavefunction is a Landau orbital with an exponential parameter $\alpha_j = a_B = \frac{B}{4}$. The opposite limit, $\beta_j \to \infty$, corresponds to $B = 0$, for which $\alpha_j = \beta_j$. A natural measure of the orbital exponents is a_B. Now we can make an explicit construction (discussed below) which incorporates all these behaviors, namely

$$\alpha_j = \beta_j + \frac{B}{20}\left\{4\left[1+\frac{4}{b(\gamma)}\frac{\beta_j}{B}\right]^{-2} + \left[1+\frac{4}{b(\gamma)}\frac{\beta_j}{B}\right]^{-1/2}\right\} \tag{3.26}$$

where $b(\gamma) = -0.16\left[\tan^{-1}(\gamma)\right]^2 + 0.77\tan^{-1}(\gamma) + 0.74$ (3.27)

$$\beta_j = pq^j \qquad j = 1, 2, \cdots N_b. \tag{3.28}$$

and $\gamma = B/Z^2$ is the reduced field strength for an effective nuclear charge Z. The parameters p and q are defined in eqn. (3.22). For the innermost electrons, Z is close to the bare nuclear charge; for the outmost electrons in a neutral atom, it is close to unity. Nevertheless, accurate Z values do not need to be provided. Nominal values turn out to be good enough for the input to eqn. (3.26). Secondary sequences are defined similarly as in

KL basis set, using a factor of 1.2, 0.8, 1.4, and 0.6 for the second, third, fourth, and fifth sequences, respectively.

Next I show how eqn. (3.26) was obtained. Start from the basis set of one sequence $N_b = 16$. Full basis set optimizations were done for H, He^{+}, Li^{++}, Be^{+++}, C^{5+} and O^{7+} in reduced fields $\gamma = 0.1$, 0.5, 1, 2, 5, 10, 20, 50, 100, 200, 500, 800, 1000, 2000, and 4000. Results for $\gamma = 0.1$, 1, 10, and 100 are plotted in Fig. 3-1. The first observation is that data points for different nuclear charges with the same γ are on the same curve. One can show that this must be the case. Suppose the wavefunction for the hydrogen atom in an external B field is $\psi_H(\vec{r}, B)$,

$$\left[-\frac{\nabla^2}{2}-\frac{1}{r}+\frac{B^2}{8}\left(x^2+y^2\right)\right]\psi_H(\vec{r}, B)=E_H\psi_H(\vec{r}, B) \tag{3.29}$$

Scaling $\vec{r} \to Z\vec{r}$ leads to

$$\left[-\frac{\nabla^2}{2Z^2}-\frac{1}{Zr}+\frac{Z^2B^2}{8}\left(x^2+y^2\right)\right]\psi_H(Z\vec{r}, B)=E_H\psi_H(Z\vec{r}, B)$$

$$\left[-\frac{\nabla^2}{2}-\frac{Z}{r}+\frac{\left(Z^2B\right)^2}{8}\left(x^2+y^2\right)\right]\psi_H(Z\vec{r}, B)=\left(Z^2E_H\right)\psi_H(Z\vec{r}, B)$$

The Hamiltonian on the left side is the same as that of a hydrogen-like atom with nuclear charge Z in an external field $B' = Z^2B$. The scaled hydrogen-atom wavefunction is precisely the eigenfunction of this Hamiltonian with energy of Z^2E_H. Now we expand $\psi_H(\vec{r}, B)$ in the optimized basis set,

$$\psi_H(\vec{r}, B)=\sum_j a_j N_j \rho^{n_{\rho_j}} z^{n_{z_j}} e^{-\alpha_j\rho^2-\beta_j z^2} e^{im\varphi} \tag{3.30}$$

and the scaled wavefunction is

$$\psi_Z\left(\vec{r},Z^2B\right)=\psi_H\left(Z\vec{r},B\right)=\sum_j a_j N_j Z^{n_{\rho_j}+n_{z_j}}\rho^{n_{\rho_j}}z^{n_{z_j}}e^{-\alpha'_j\rho^2-\beta'_j z^2}e^{im\varphi} \tag{3.31}$$

where $\alpha'_j=Z^2\alpha_j,\quad \beta'_j=Z^2\beta_j$. Obviously, $\dfrac{\alpha'_j-\beta'_j}{B'}=\dfrac{\alpha_j-\beta_j}{B}$ and $\dfrac{\beta'_j}{B'}=\dfrac{\beta_j}{B}$.

Another observation is that the curvatures for different γ values are slightly different. To describe the rapid decrease in the small β_j/B region and the slowly decaying long tail, we used a fixed combination of inverse square and inverse square root terms, which proved to be superior to a single reciprocal function. In Fig. 3-2, the functional forms are compared with data points from optimized basis sets for γ = 1.

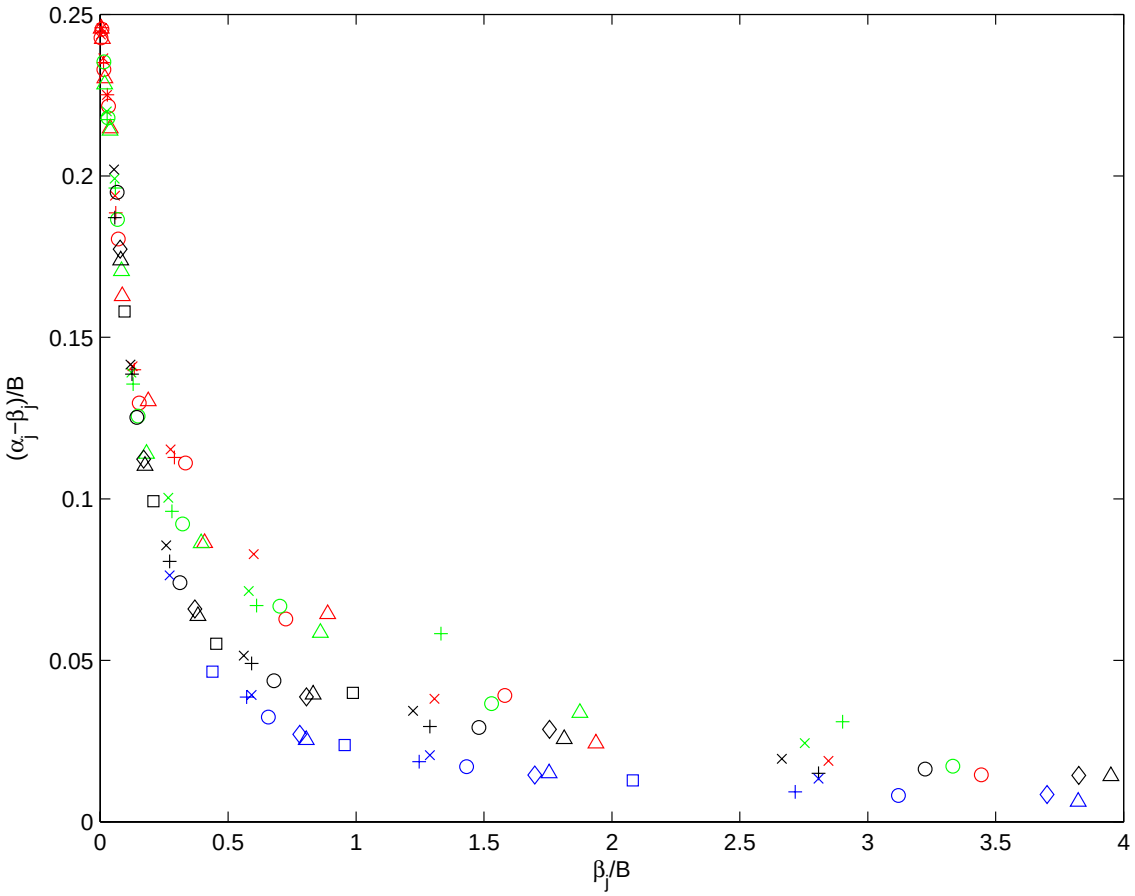

FIG. 3-1 Exponents of optimized basis sets for the H(+), He^{+}(x), Li^{++}(o), Be^{+++}(Δ), C^{5+}(◊) and O^{7+}(□) in reduced magnetic fields γ = 0.1 (blue), 1 (black), 10 (green), and 100 (red).

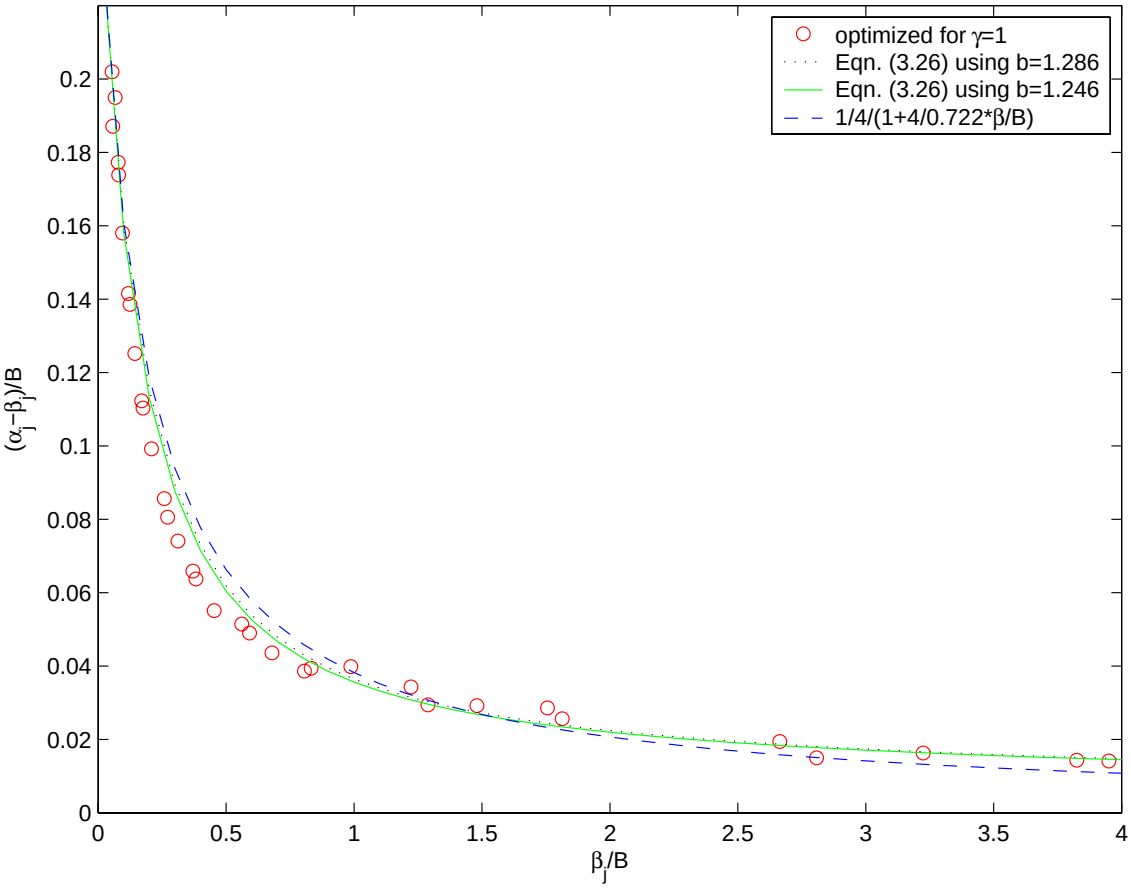

FIG. 3-2 Fitting the parameter $b(\gamma=1)$ using the function (3.26). Fitted result is 1.286, compare to the calculated value 1.246 from eqn. (3.27). Two curves are shown by dotted black line and solid green line. They are almost indistinguishable in the graph. A reciprocal fitting result $\frac{B}{4}\left(1+\frac{4}{0.722}\frac{\beta_j}{B}\right)^{-1}$ is also shown by a dashed blue line.

A calculation using the basis set derived from eqn. (3.26) also is included in Table 3-2. The new primary sequence outperforms the KL primary sequence by a factor of four, but by including only the second and the third sequences, the basis set is almost saturated, compared to other, more slowly converging basis sets. Another advantage of the present basis set is the explicit expressions eqns. (3.26) and (3.27), whereas searching for the best parameter Δ_{KL} in the KL basis sets is quite time consuming.

Table 3-4 Test of basis sets including 1, 2, and 3 sequences on the energies of the hydrogen atom in B fields (energies in Hartree, negative signs are omitted)

State	B (au.)	1 sequence	2 sequences	3 sequences	Reference 80	Reference 78[a]	Reference 76
$1s$	0.1	0.5475263	0.5475263	0.547526461	0.547526480401	0.5475265	
	1	0.83109	0.8311680	0.83116886	0.831168896733	0.831169	0.83116892
	10	1.74675	1.747781	1.74779694	1.747797163714	1.747797	1.74779718
	100	3.78933	3.789790	3.78980395	3.789804236305	3.78905/90250	3.7898043
	1000	7.66224	7.662419	7.66242306	7.662423247755	7.66205/65	7.6624234
	4000	11.20372	11.204139	11.20414499	11.204145206603		
	10000	14.14037	14.140959	14.14096829			14.14097
$2p_0$	1	0.25991	0.2600055	0.26000652	0.260006615944	0.2600066	0.260007
	10	0.38263	0.382641	0.38264977	0.382649848306	0.38264875/5180	0.382650
	1000	0.49248	0.4924948	0.49249495	0.4924950	0.492495	
$2p_{-1}$	1	0.45658	0.456596	0.45659703	0.456597058424	0.45659705	
	10	1.12521	1.125415	1.12542217	1.125422341840	1.1254225	
	100	2.63472	2.634756	2.63476052	2.634760665299	2.634740/95	
	1000	5.63792	5.638413	5.63842079	5.63842108	5.638405/35	
$3d_{-1}$	10	0.33890	0.3389555	0.33895610	0.3389561898	0.33895610/45	
	1000	0.48696	0.4869775	0.48697789	0.4869777	0.48697795	
$3d_{-2}$	10	0.90813	0.908212	0.90821466	0.9082147755	0.9082115/235	
	1000	4.80432	4.805094	4.80511012	4.80511067	4.8051095/125	
$4f_{-2}$	100	0.42767	0.427756	0.42775840		0.4277585	
$4f_{-3}$	10	0.78773	0.787768	0.78776910		0.7877685/705	
	1000	4.30738	4.308344	4.30836962		4.3083700/05	
$5g_{-4}$	1	0.26570	0.266184	0.26618782		0.26618770/875	
	100	1.75448	1.754848	1.75485593		1.754856	
	1000	3.96338	3.964471	3.96450833		3.9645095	

(a) Numbers before/after slashes are the upper/lower bounds to the energy.

The basis set constructed from eqn. (3.26) not only works well for 1*s* electrons, but also for higher excited states. Table 3-4 includes some test results on the hydrogen atom in a wide range of *B* fields. The primary sequence was derived from eqns. (3.26) through (3.28) using $N_b = 16$. Extrapolations to $j > N_b$ or $j \leq 0$ were made for extremely tight or diffuse orbitals whenever necessary. The averaged basis set error for the primary sequence is 0.3 *m*H, which is reduced to 7 μH if the second sequence is added. With three sequences, the accuracy of our basis sets reaches 1 μH level. Notice that energies quoted from reference 76 are slightly lower than the more accurate algebraic results [80]. This implies that Ivanov and Schmelcher's data are not necessarily upper bounds to the energy. We need to keep this in mind when we compare our results with theirs.

Table 3-5 Energies for high angular momentum states of the hydrogen atom in *B* fields (*B* in au; energy in Hartree)

State	$B = 1$	$B = 10$	$B = 100$	$B = 1000$
$5g_{-4}$	-0.2661880	-0.7080264	-1.7548563	-3.9645100
$6h_{-5}$	-0.2421928	-0.6499941	-1.6252244	-3.7061998
$7i_{-6}$	-0.2239757	-0.6051943	-1.5238725	-3.5018527
$8j_{-7}$	-0.2095131	-0.5691841	-1.4415788	-3.3343126
$9k_{-8}$	-0.1976562	-0.5393750	-1.3728860	-3.1933035
$10l_{-9}$	-0.1876974	-0.5141408	-1.3143222	-3.0722218

The accuracy of the previous basis sets can be improved further by increasing N_b and including the fourth and the fifth sequences. Using larger basis sets having five sequences with the primary sequence derived from $N_b = 28$, we obtained energies of -5.638 421 065, -4.805 110 65, -4.308 370 6, and -3.964 510 0 for the H atom $2p_{-1}$, $3d_{-2}$, $4f_{-3}$, and $5g_{-4}$ states in $B = 1000$, respectively. Their accuracy is at the same level as the best available data in the literature (see Table 3-4). There are no specific difficulties for the higher angular momentum states in our expansion. The energy values for the excited

states with quantum numbers $l = -m = 4, 5, \ldots, 9$ of the hydrogen atom in B fields are listed in Table 3-5. Those values will be used in the next step, construction of Table 3-6.

Actually we do not need to use the entire sequences generated from eqns. (3.26) through (3.28). In the expansion of nonzero angular momentum orbitals, very tight basis functions (j close to N_b) are not necessary, but extrapolation to negative j may be required in order to include very diffuse basis functions. Table 3-6 lists the subsets which have accuracy of 1 μH. The one to five segments in each basis set means the ranges of j values selected from the primary and the subsequent secondary sequences. Numbers underlined identify the negative j values. N_b values used for the five sequences are 16, 8, 8, 4, and 4. Also recall a factor of 1.2, 0.8, 1.4, and 0.6 is used for the second, third, fourth, and fifth sequences, respectively. Numbers in parentheses are the sizes of the basis sets.

Table 3-6 Basis sets for the hydrogen atom in B fields with accuracy of 1 μH (B in au)

State	$B = 0$	$B = 1$	$B = 10$	$B = 100$	$B = 1000$
$1s$	1-14(14)	2-14,1-3,1-2(18)	1-16,2-6,2-6(26)	4-20,2-8,2-6(29)	4-21,4-10,5-10(31)
$2p_0$	1-7(9)	0-8,0-3,3(14)	0-10,1-5(16)	1-12,2-5(16)	1-14,3-5(17)
$2p_{-1}$	1-7(9)	1-9,0-3,3(14)	1-11,5,2-6(17)	3-14,4-8,3-6(21)	4-16,4-10,5-10(26)
$3d_{-1}$	3-4(8)	1-6,0-3,0-3(16)	0-8,1-5,2-3(16)	0-10,1-6,2(18)	1-12,2-6,3(18)
$3d_{-2}$	2-4(7)	0-7,1-3,0-3(15)	1-8,3-5,2-6(16)	3-12,3-7,3-7(20)	4-15,4-10,4-7(23)
$4f_{-2}$	5-2(8)	1-5,0-3,0-3(15)	0-7,1-4,1-5(17)	0-10,1-6,2-3(19)	1-12,2-6,3(18)
$4f_{-3}$	4-2(7)	0-4,0-3,0-4(14)	1-7,2-5,2-6(16)	3-11,1-7,1-7(23)	3-14,2-8,4-7,3,3(25)
$5g_{-3}$	4-0(5)	1-5,1-2,0-1(13)	0-7,1-4,1(13)	0-9,1-5,2-3(17)	1-11,2-6,3-4(18)
$5g_{-4}$	4-0,2-1(7)	0-4,0-3,0-4(14)	1-6,2-5,1-3(13)	2-11,1-7,3-6(21)	3-13,3-8,4-7,3,3(23)
$6h_{-5}$	5-2,4-1(8)	0-4,0-3,0-3(13)	1-6,2-5,1-3(13)	2-10,3-7,2-5(18)	3-13,3-8,4-7,3,3(23)
$7i_{-6}$	6-2,5-3(8)	1-2,0-2,0-3(11)	1-5,2-5,1-3(12)	2-10,1-5,3-6(18)	3-13,3-8,4-7,3,3(23)
$8j_{-7}$		1-2,0-2,0-3(11)	1-5,2-5,1-3(12)	2-10,2-6,3,2,2(17)	3-13,3-8,4-7,3,3(23)
$9k_{-8}$			1-5,2-5,1-2(11)	2-9,2-6,3,2,2(16)	3-12,3-8,4-6,3,3(21)
$10l_{-9}$			1-5,2-5,1-2(11)	2-9,2-6,3,2,2(16)	3-12,3-8,4-6,3,3(21)

While the previous optimization scheme is quite impressive for the hydrogen atom in a B field, we want to know whether it also works equivalently well for multi-electron atoms. Thus we do another case study, the carbon atom in the same field $B = 10$ au. Its

ground state configuration is $1s^2 2p_{-1} 3d_{-2} 4f_{-3} 5g_{-4}$, and HF energy is -44.3872 Hartree from calculations on a numerical grid [90]. The performance of various basis sets is summarized in Table 3-7.

Table 3-7 Basis set effect on the HF energies of the carbon atom in B = 10 au.

Basis set	Basis size	HF energy (Hartree)	Error(Hartree)
Spherical(*spdfghi*)	112	-43.6157	0.7715
2sequences, JOC	160	-44.1572	0.2300
3sequences, JOC	240	-44.3529	0.0343
1sequence, KL	80	-44.1629	0.2243
2sequences, KL	120	-44.3824	0.0048
3sequences, KL	160	-44.3863	0.0009
5sequences, KL	200	-44.3867	0.0005
1sequence, present	50	-44.3859	0.0013
2sequences, present	72	-44.38704	0.0002
3sequences, present	91	-44.38714	<0.0001

The spherical basis set includes 16s16p16d16f16g16h16i orbitals. Again it gives a large basis set error. For the KL basis sets, I used the same parameter as before, Δ_{KL} = 0.18. Its accuracy can also be improved greatly by systematic augmentation of secondary sequences. However, the basis size will be increased considerably. Based on the previous detailed study on the basis set for the hydrogen atom, here we prescribe a procedure to construct the basis set for a multi-electron atom in a B field, with the C atom as the example.

We first assign the effective nuclear charge Z_{eff} for each electron roughly. The approach is by approximate isoelectronic sequences. Since the 1s electrons feel the whole strength of the nuclear attraction, we use 6 for them. For the 2p electron, the nucleus is screened by the two 1s electrons, so we use 4, and so forth. Next basis functions are generated according to eqns. (3.26) through (3.28) using N_b = 16, 8, 8, 4, 4 for the primary, the second, …, the fifth sequences. To use Table 3-6 as guidance in selecting

subsets of basis functions from the previously generated sequences, first recall the scaling argument after eqn. (3.29). The 1*s* wavefunction with an effective nuclear charge $Z_{eff,1s}$ = 6 in a field B = 10 can be scaled from the hydrogen atom 1*s* wavefunction in a field $B' = B / Z_{eff,1s}^2 = 0.28$. The value of B' falls in the range of 0 to 1. By inspection of Table 3-6, we find a sufficient choice of basis set includes the first through the fourteenth elements in the primary, 1-3 elements in the second, and 1-2 in the third sequences. But do not forget the scaling factor. Since the C atom 1*s* wavefunction is tighter than the H atom 1*s* wavefunction approximately by $Z_{eff,1s} = 6$ times, the basis function exponents used in the expansion of the C atom 1*s* orbital should be larger than those used for the H atom by $Z_{eff,1s}^2 = 36$ times (recall eqns. 3.30 and 3.31). Remember the exponents β_j's consist of a geometrical series (eqn. 3.28). The increase of the exponents amounts to a shift of $\log_q Z_{eff,1s}^2 = \dfrac{2\ln 6}{\ln 2.18} = 4.6$ elements in the primary sequence, and a shift of $\dfrac{2\ln 6}{\ln 2.84} = 3.4$ elements in the second and the third sequences. Hence, we should pick the 5-19, 4-7, and 4-6 elements in the primary, the second, and the third sequences, respectively. Basis function selections for other electron orbitals are similar. The final basis set is 22*s*19*p*16*d*21*f*13*g,* which is summarized in Table 3-8. Among the total of 91 gaussians in this basis set, 50 are from the primary, 22 from the second, and 19 from the third sequences. From Table 3-7, we can see the accuracy of this basis set is remarkably higher than that of the others. By using only the primary sequence, the error left is close to 1 *m*H. Supplementation with the second sequence reduces the error to 0.2 *m*H. We estimate the error of the 3-sequence present basis to be less than 0.1 *m*H.

Table 3-8 Construction of the AGTO basis set for the carbon atom in B = 10 au.

Orbital	Z_{eff}	$B' = B / Z_{eff}^2$	H atom basis	shifts	C atom basis
1s	6	0.28	1-14, 1-3, 1-2	4.6, 3.4, 3.4	5-19, 4-7, 4-6
2p_{-1}	4	0.63	1-9, 0-3, 3	3.6, 2.6, 2.6	2-13, 2-6, 5-6
3d_{-2}	3	1.1	0-7, 1-3, 0-3	2.8, 2.1, 2.1	2-10, 3-5, 2-5
4f_{-3}	2	2.5	0-7, 0-5, 0-6	1.8, 1.3, 1.3	2-9, 1-6, 1-7
5g_{-4}	1	10	1-6, 2-5, 1-3	0, 0, 0	1-6, 2-5, 1-3

One may wonder why this procedure works so well, or even why it works at all. The main reason is that each electron orbital can be approximated by a hydrogen-like problem fairly closely. For example, the overlap between the 1s HF orbital for the carbon atom in B = 10 and the 1s orbital for C^{5+} in the same field is 0.998. See Table 3-9. Actually by adjusting the nuclear charge to 5.494 and 5.572, the overlaps for 1s spin down and spin up orbitals with their corresponding hydrogen-like counterparts reach the maxima of 0.9998 and 0.9999, respectively. Other orbitals are similar.

Table 3-9 Overlaps between HF orbitals for the carbon atom in B = 10 au and hydrogen-like systems in the same field

Orbital	Z_{eff}	overlap	Z'_{eff}	overlap
1s, ↓	6	0.99773	5.494	0.99984
1s, ↑	6	0.99838	5.572	0.99989
2p_{-1}	4	0.99967	3.944	0.99968
3d_{-2}	3	0.99974	3.145	0.99983
4f_{-3}	2	0.99731	2.644	0.99986
5g_{-4}	1	0.98224	2.108	0.99981

Now that we have a systematic way to construct reasonably accurate basis sets for atoms in a B field. In the next section, I will use those basis sets for the DFT and CDFT studies.

CHAPTER 4
ATOMS IN UNIFORM FIELDS – NUMERICAL RESULTS

Comparison with Data in Literature

I did extensive unrestricted Hartree-Fock (UHF) and conventional DFT calculations on the atoms He, Li, Be, B, C, and their positive ions Li^+, Be^+, B^+ in a large range of B fields with basis sets constructed according to the procedure outlined in the previous chapter. Total energies are compiled in appendix B. Ground states are indicated in orange. Data available from the literature are also included for comparison.

The UHF calculations were primarily for purposes of validation. The agreement of our calculations with those from other groups is excellent. For the helium atom, our HF energies are generally slightly lower than those by Jones, Ortiz, and Ceperley [91, 94]. Their earlier calculations used an STO expansion [91] which is labeled as JOC-HF1 in Table B-1. Later they utilized JOC basis sets within AGTO [94] (also refer eqn. 3.23), which we call JOC-HF2. Presumably the small distinction between their data and ours results from better optimized basis sets I generated, as already illustrated in the previous chapter. This observation is supported by the generally closer agreement of their anisotropic basis set results with ours (in contrast to their spherical basis results). One notable exception to the overall agreement is the $1s4f_{-3}$ state in $B = 800$ au. Our result is -23.42398 Hartree versus theirs -23.4342. Another is $1s3d_{-2}$ at $B = 560$ au: -21.59002 versus their -21.5954 Hartree. The reason for these discrepancies is unclear. It may be some peculiarity of the basis for a particular field strength. For other atoms and ions, the data for comparison are mainly from the series of studies by Ivanov and Schmelcher [86,

88-90]. Our HF energies generally match or are slightly higher than theirs, and the overall agreement is quite satisfactory. Differences are usually less than 0.1 *m*H, far surpassing our goal of 1 *m*H accuracy for the basis set. The remaining differences arise, presumably from our basis set truncation error and their numerical mesh errors. As for any basis-set based calculations, we can only use a finite number of basis functions, which will cause basis set truncation error. Since this error in our calculation is always positive (by the variational principle), one can use our data as an upper bound for the HF energies. However, the numerical error in Ivanov and Schmelcher's 2D HF mesh method seems to tend to be negative. Recall the comparison made in Table 3-4 for the hydrogen atom. Their energies are always lower than the more accurate algebraic result [80]. Another indication is the zero field atomic energies. For example, the HF energy for the beryllium atom is known accurately to be -14.57302316 Hartree [101], which agrees well with our result of -14.57302, but Ivanov and Schmelcher gave a lower value of -14.57336 [88]. They commented that this configuration has large correlation energy and the contribution from the $1s^2 2p^2$ configuration should be considered, but did not specify whether their result was from single determinant or multi-determinant calculation. Since multi-configuration HF (MCHF) is not our main interest here, our data are solely from single configuration HF calculations. They also noted that the precision of their mesh approach decreases for the $1s^2 2s^2$ configuration in a strong field. This can also contribute to the discrepancy. From previous observations, one may speculate that the true HF energies lie between our data and theirs. Furthermore, the accuracy of our data is ready to be improved by invoking a larger basis set, but this is not necessary for the purpose of the present study.

There are fewer DFT calculations for atoms in *B* fields than HF studies. As far as I know, appendix B is the first extensive compilation of magnetized atomic energies based on modern DFT functionals. I chose PW92 [69] for LDA and PBE [70] for GGA calculations. For the field-free case, the present results agree well with published data [102]. Since reference 102 only gave spin non-polarized DFT energies for spherically distributed densities (which is no problem for the helium and beryllium atoms), one needs to use fractional occupation numbers in other atoms for comparison. For example, in the carbon atom, two *p* electrons are placed in six spin orbitals, $p_{-1}^{\uparrow,\downarrow}$, $p_{0}^{\uparrow,\downarrow}$, and $p_{+1}^{\uparrow,\downarrow}$ with equal occupation number of 1/3 for each of them. Actually there are more accurate data for the VWN functional [67]. My results differ from those from reference 67 by no more than 5 μH if I choose the VWN functional, either for spin-polarized or spin non-polarized energies, neutral atoms or their positive ions.

Comparison of non-vanishing *B* field DFT calculations is handicapped by the different magnetic field grids on which different authors present their results, and by the different functionals implemented. The functional due to Jones [103], which is at the level of the local density approximation, was used by Neuhauser, Koonin, and Langanke [104], and by Braun [84]. The simple Dirac exchange-only functional was used by Relovsky and Ruder [83], and by Braun [84]. When I choose the Dirac exchange functional, good agreement is found with Braun's data. However, no application of density-gradient-dependent fiunctionals on atoms in a strong magnetic field is found in the literature so far as I can tell.

For the CDFT study, the present work apparently is the first fully self-consistent calculation on atoms in large *B* fields based on the VRG functional. The most closely

related study is the perturbative implementation of the VRG functional by Orestes, Marcasso, and Capelle [37] on the atomic ionization energies in vanishing *B* field.

For comparison, CI results are available for helium, lithium, and beryllium atoms, and their positive ions in external fields [7, 8, 11-13, 77, 105]. Those data will be treated as the most reliable ones in my comparison.

Magnetic Field Induced Ground State Transitions

The most drastic change of the ground state atoms caused by an external magnetic field is a series of configuration transitions from the field-free ground state to the high-field limit ground state. It is well known that for the field-free case, two competing factors — the spherical nucleus attractive potential and the electron-electron interactions — lead to the shell structure of atoms. This structure is perturbed slightly if the external field is relatively small, but when the field is strong enough that the Lorentz forces exerted on the electrons are comparable to nuclear attraction and electron repulsions, the original shell structure is crushed, and the electrons make a new arrangement. Thus, a series of configuration transitions happens as the *B* field becomes arbitrarily large. In the large-field limit, the ground state is a fully spin-polarized state in which the electrons take the minimum value of spin Zeeman energy. Ivanov and Schmelcher further analyzed the spatial distribution of electrons and described the high-field limit ground state "... with no nodal surfaces crossing the *z* axis (the field axis), and with nonpositive magnetic quantum numbers decreasing from $m = 0$ to $m = -N + 1$, where N is the number of electrons" [76]. In Hartree-Fock language, the high field configuration is $1s2p_{-1}3d_{-2}4f_{-3}\cdots$. In this regime, the magnetic field is the dominant factor, and coulombic forces can be treated as small perturbations. A cylindrical separation of the *z* part from *x* and *y* parts is usually

made for the electron state. Its motion in the *xy* plane is described by a Landau orbital, and the question is reduced to a quasi-1D problem. This technique is often referred to as the adiabatic approximation, valid only in the limit of very large field. Many early investigations on matter in a *B* field concentrated on this regime [103, 104, 106].

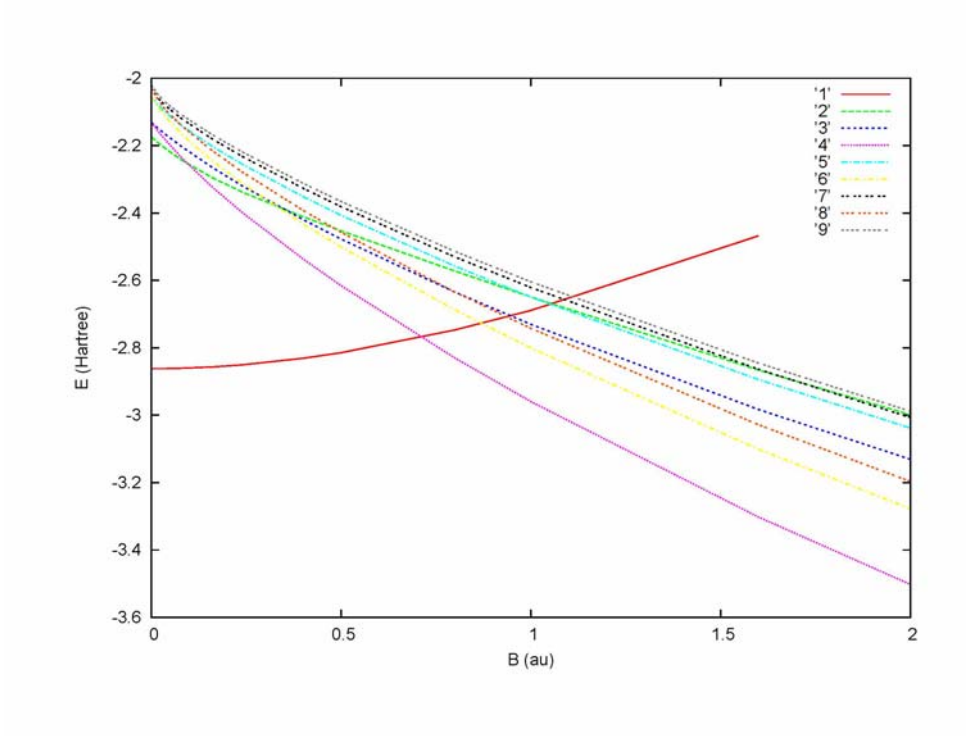

FIG. 4-1 UHF total energies for different electronic states of the helium atom in *B* fields. Curves 1 to 9 represent configurations $1s^2$, 1s2s, $1s2p_0$, $1s2p_{-1}$, $1s3d_{-1}$, $1s3d_{-2}$, $1s4f_{-2}$, $1s4pf_{-3}$, and $1s5g_{-3}$, respectively.

The most difficult part is the region of intermediate *B* field, for which both cylindrical and spherical expansions are inefficient, and where the ground state configurations can only be determined by explicit, accurate calculations. Figure 4-1 displays the HF energies of various configurations for the helium atom in *B* fields as listed in Table B-1, which includes one singlet state and eight triplet states. Curves 1 to 9 represent configurations of $1s^2$, 1s2s, $1s2p_0$, $1s2p_{-1}$, $1s3d_{-1}$, $1s3d_{-2}$, $1s4f_{-2}$, $1s4pf_{-3}$, and $1s5g_{-3}$, respectively. Each configuration belongs to a spin subspace according to its total

spin z component. For convenience, we use the inexact terminology of "local ground state" and "global ground state". For a specific field strength, the configuration which has the lowest energy within a spin subspace is called the local ground state for this spin-multiplet. Among them, the one taking the minimum regardless of its spin is called the global ground state. Thus in Fig. 4-1, the singlet state remains as the global ground state until B reaches 0.71 au., then a configuration transition to $1s2p_{-1}$ occurs. This triplet state is the global ground state for B fields larger than 0.71 au. Atoms with more electrons can have more complicated series of configuration transitions. For example, the carbon atom undergoes six transitions with seven electronic configurations involved being the ground states in different regions of B field strengths [90]. This scenario is basically the same if one uses DFT or CI energies instead of HF energies, except the crossing points for different configurations usually change.

Atomic Density Profile as a Function of B

Within each configuration, the electron density is squeezed toward the z axis with increasing B field. This follows from energy minimization: the electron density shrinks toward the z axis to alleviate the corresponding diamagnetic energy increment (expectation of $B^2(x^2+y^2)/8$). Figure 4-2 shows the density profiles for the $1s^2$ and $1s2p_{-1}$ states of the helium atom at field strengths B = 0, 0.5, 1, and 10 au. The transverse shrinkage is quite evident. However, this shrinkage increases the electron repulsion energy. A configuration transition therefore will happen at some field strength (for He, B = 0.71 au.), accompanied by a change of quantum numbers, and eventually a spin flip. Note Figs. 4-2 (a), (b), and (g). The energy increase in the diamagnetic term caused by

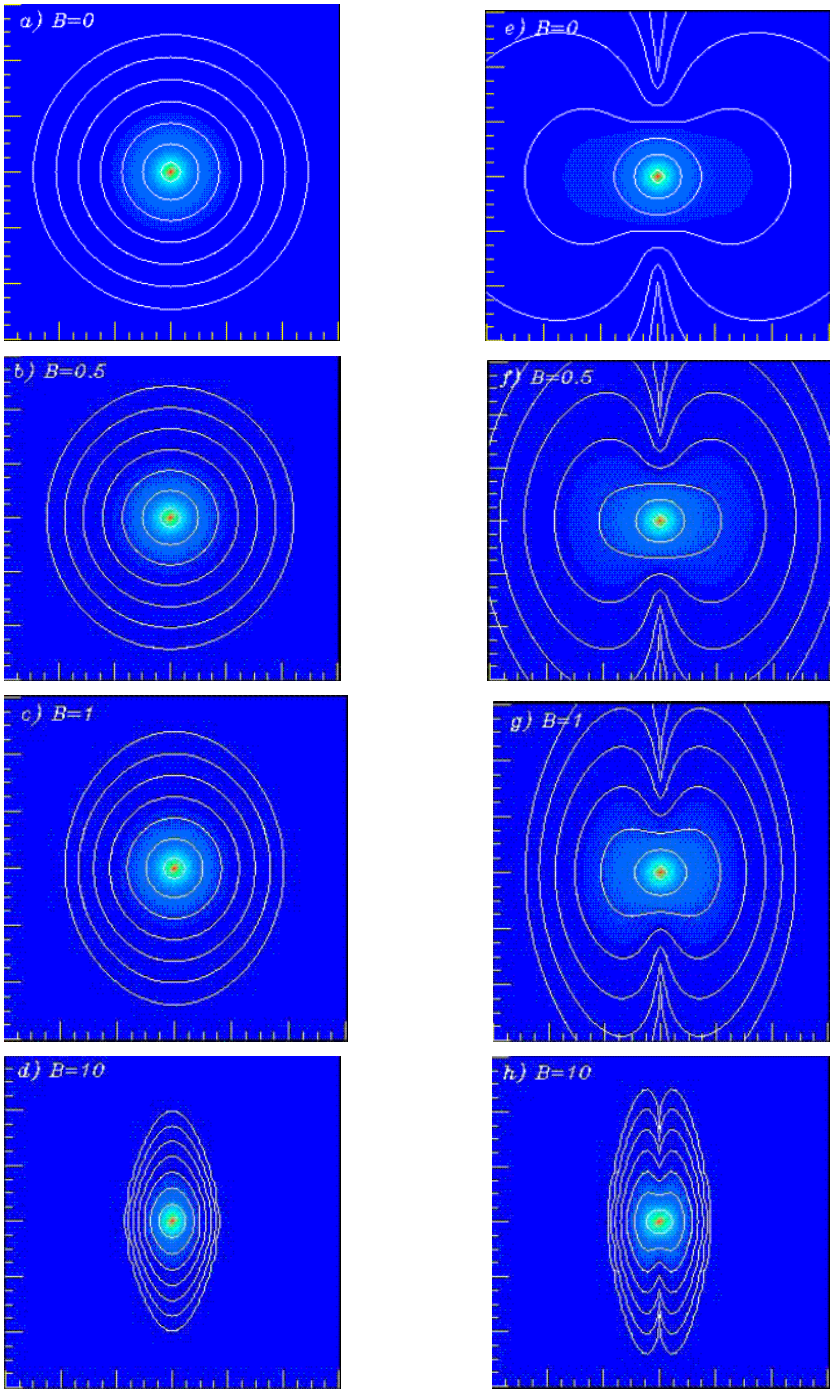

FIG. 4-2 Cross-sectional view of the HF total electron densities of the helium atom $1s^2$ (panels *a*-*d*) and $1s2p_{-1}$ (panels *e*-*h*) states as a function of magnetic field strength. Each large tick mark is 2 bohr radii. The *B* field orientation is in the plane of the paper from bottom to top. The density at the outermost contour lines is $10^{-6}\,a_0^{-3}$, with a factor of 10 increase for each neighboring curves. Panels (*a*), (*b*), (*g*), and (*h*) are global ground states. See text for details.

the electron density expansion in the new spin-configuration for the global ground state is more than compensated by the accompany energy lowering of the Zeeman and electron-electron repulsion terms. In fact, the same net lowering can occur (and sometimes does occur) without change of spin symmetry.

Total Atomic Energies and Their Exchange and Correlation Components

Atomic total energies of He, Li, Be, B, C, and their positive ions Li^+, Be^+, B^+ in a large range of B fields within the HF, DFT-LDA, and DFT-GGA approximations are compiled in Appendix B. The exchange-correlation energy E_{xc}, and its exchange and correlation components E_x, E_c corresponding to the total energies in appendix B, are given in appendix C. As is conventional, the HF correlation energy is defined as the difference between the CI total atomic energy and HF total energy tabulated in appendix B. DFT exchange and correlation energies are defined at the self-consistent electron densities within the corresponding XC energy functionals (LDA or PBE). Keep in mind that exchange and correlation energies are not defined identically in the wavefunction and DFT approaches; recall the discussion in Chap.1, particularly eqn. (1.11).

Because energies of different states in different field strengths vary considerably, we compare their differences from the corresponding CI total energies. Figure 4-3 shows those differences for the HF and DFT total atomic energies of helium atom $1s^2$, $1s2p_0$, and $1s2p_{-1}$ states as functions of B field strength. Since the HF calculation includes exchange exactly, the difference for the HF energy is the negative of the conventional correlation energy E_c^{HF} (the superscript "HF" is for clarify). First we observe that the conventional correlation energies for the states $1s2p_0$ and $1s2p_{-1}$ are extremely small.

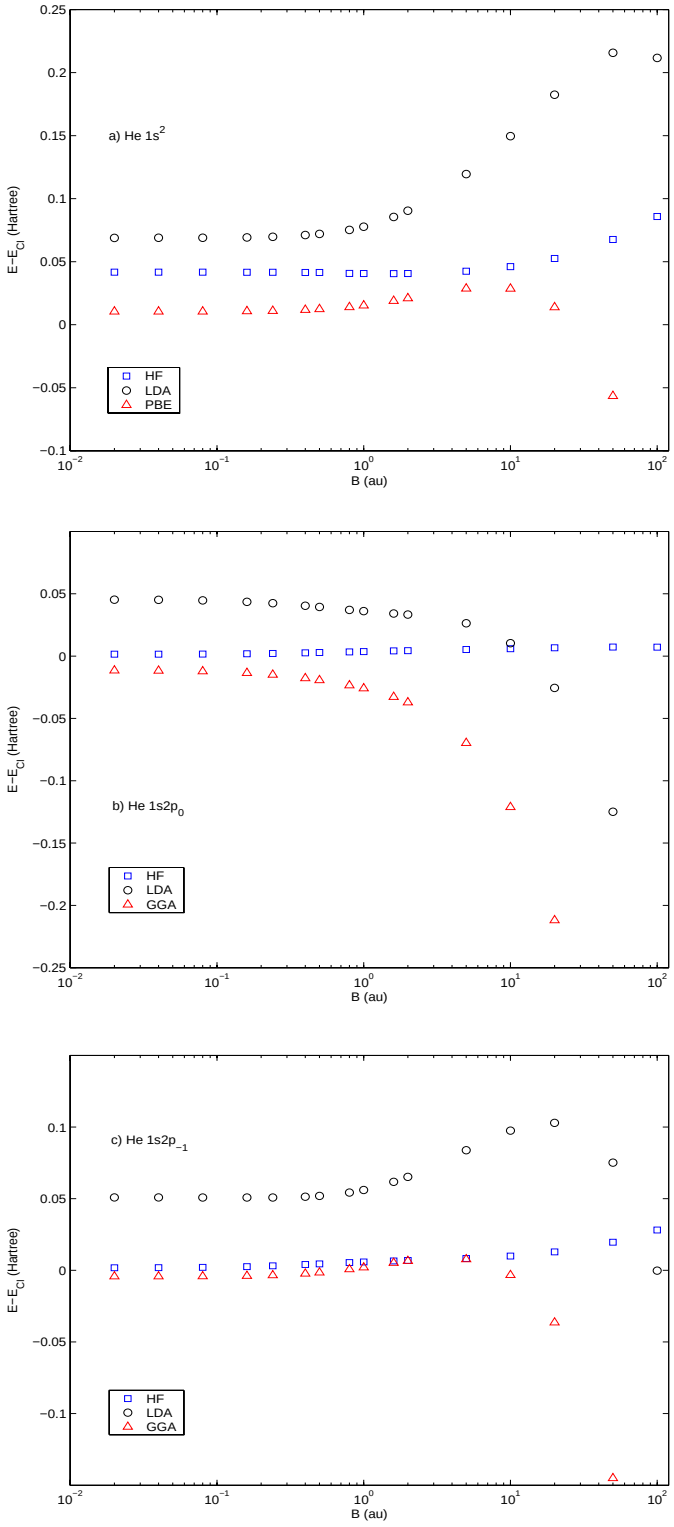

FIG. 4-3 Differences of the HF and DFT total atomic energies of the helium atom $1s^2$, $1s2p_0$, and $1s2p_{-1}$ states with respect to the corresponding CI energies as functions of B field strength. Blue squares □: HF; Black circles o: DFT-LDA; Red triangles Δ: DFT-GGA.

This is because the 1s and 2p electrons in the atom are well separated, unlike the two 1s electrons in the $1s^2$ configuration. The increase of the absolute value of E_c^{HF} in the large B field regime for the two states $1s^2$ and $1s2p_{-1}$ seems to be the result of the compression of electron densities illustrated in Fig. 4-2. The PBE generalized gradient functional gives extremely good results for both the singlet state $1s^2$, and triplet sates $1s2p_0$ and $1s2p_{-1}$ when the B field magnitude is less than 1 au. Both LDA and GGA approximations fail in the large field regime, $B > 10$ au. Notice the similar performance of DFT functionals for the two triplet states $1s2p_0$ and $1s2p_{-1}$. The former one does not carry paramagnetic current density, thus there is no CDFT current correction for this configuration, whereas the later one is a current-carrying state. This observation implies that the success or failure of these particular LDA and PBE functionals is not because they omit current terms.

The success of DFT calculations mainly depends on accurate approximations for the system exchange and correlation energies. As given in detail in Chap. 1, DFT exchange and correlation energies differ subtly from conventional exchange and correlation energies. The DFT quantities refer to the auxiliary KS determinant (and include a kinetic energy contribution) whereas the conventional quantities are defined with respect to the HF determinant. Nevertheless, conventional exchange-correlation energies often are used as the quantity to approximate in DFT exchange-correlation functionals, mostly for pragmatic reasons. The difficulty is that exact DFT quantities and KS orbitals are only available for a few, very small systems. One of those is discussed in the next chapter. For most systems, the exact KS orbitals are unknown. However, there

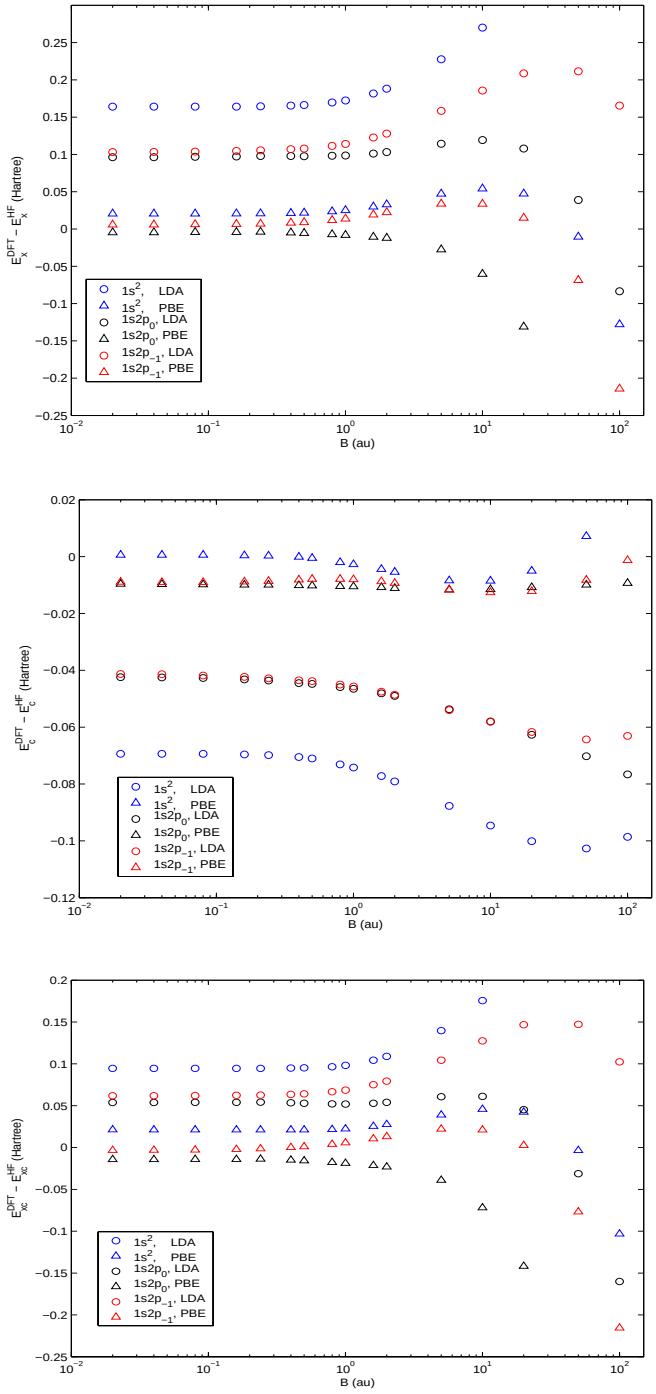

FIG. 4-4 Differences of DFT exchange (top panel), correlation (middle panel), and exchange-correlation (bottom panel) energies with HF ones, for the helium atom in *B* fields.

are abundant HF and correlated calculations for many finite systems, providing good reference densities and energies. To gain a better understanding of the behavior of DFT exchange and correlation approximations, we make a separate comparison of DFT exchange-correlation energies with the HF ones in Fig. 4-4. Note that "DFT exchange" here means the E_x term in a particular functional and not exact DFT exchange calculated from KS orbitals.

We can see from Fig. 4-4 that the LDA approximation shows its typical underestimation of exchange and overestimation of correlation energies. The PBE functional gives good approximations to the exchange and correlation energies separately when the *B* field is less than 1 au., but it seriously overestimates the exchange when $B>10$ au., while the correlation energy does not depend on the field strength very much. Since exchange dominates the XC energies, the error in the exchange term overwhelms the correlation term in large *B* fields. Of course both the LDA and PBE functionals are based on analysis of the field-free electron gas, in which the exchange-correlation hole is centered at the position of the electron, and only the spherically averaged hole density enters. This picture breaks down for an atom in a large *B* field. Because of the strong confinement from the *B* field, there is strong angular correlation among electrons. The XC hole is not centered at the electron, and is not isotropic. Moreover, the external *B* field will effectively elongate XC hole as well as the electron density. If one wishes to improve XC functionals for applications in the large *B* field regime, those factors need to be considered. Another observation from Fig. 4-4 is that PBE overestimates the correlation energies for the two triplet states, in which the HF correlation is very small. This presumably is due to the imperfect cancellation of self-interactions in the functional.

The lithium positive ion is a two-electron system isoelectronic with neutral He. It has approximately the same correlation energy as that of the helium atom in the field-free case. For non-vanishing field, recall the scaling argument for the wavefunction of hydrogen-like atoms in a *B* field. The deformation of the atomic density induced by the *B* field is measured by its reduced strength $\gamma = B / Z^2$, rather than by its absolute value *B*, where *Z* is the nuclear charge (refer to eqns. 3.30 and 3.31 and discussion). Of course, the atomic configuration is another important factor. For the same electronic configuration, the helium atom in $B = 5$ au. and the lithium positive ion in $B = 10$ au. have about the same γ values. Indeed they have about the same HF and PBE correlation energies. On the other hand, an attempt at a similar comparison between the lithium atom and the beryllium ion is obscured by two factors. One is the large correlation energy between the two 1*s* electrons for the doublet states. The effect of the external *B* field on its correlation energy is hardly discernable in the studied range. For the quadruplet state, notice the tabulated conventional correlation energy for the beryllium ion is much smaller in magnitude than that of the lithium atom, giving rise to the suspicion of systematic errors existing in those data. Also notice that the conventional correlation energy of the lithium atom $1s2p_{-1}3d_{-2}$ state in vanishing *B* field is even larger than that of its ground state $1s^2 2s$. Since the electrons are well-separated in the $1s2p_{-1}3d_{-2}$ state, its correlation energy is expected to be smaller than that of a more compact state. Even for vanishing *B* field, large discrepancies on the correlated energies are found in the literature. For example, Al-Hujaj and Schmelcher gave -14.6405 Hartree for the ground state of the beryllium atom from a full CI calculation [8], versus -14.66287 Hartree from a frozen-core approximation by Guan *et al.* [7]. The difference is more than 20 *m*H. This shows it is

difficult to systematically extract atomic correlation energies from the literature, especially for non-vanishing field data.

The DFT functionals investigated here fail spectacularly in a large *B* field, mainly from their exchange part. However, the PBE correlation still gives a large portion of the correlation energy even though its performance degrades somewhat with increasing *B* field. On the other hand, the HF approximation is more robust than DFT-based calculations and includes exchange exactly, but it totally neglects correlation. From those analyses, it seems a better estimation to the total atomic energies in a large *B* field may be achieved by combining HF exact exchange and PBE correlation energy rather than using solely the HF or DFT approximations.

Ionization Energies and Highest Occupied Orbitals for Magnetized Atoms

Because of the magnetic-field-induced configuration transitions for both magnetized atoms and their positive ions, atomic ionization energies are not monotonic increasing or decreasing smooth functions of the applied *B* field. This is already obvious from Koopmans' theorem and the UHF total energies in Fig. 4-1. Here we use the total energy difference between the neutral atom and its positive ion, ΔE_{SCF}, for estimation of the ionization energy. For each field strength, the ground state configurations for the atom and its positive ion must be determined first. Table 4-1 and Fig. 4-5 show the change of ionization energies of the atoms He, Li, and Be with increasing *B* field. Results from different methods are close. For the beryllium atom, a frozen-core calculation [7] gave a larger ionization energy, by 26 *m*H, in the near-zero-field region than the one derived from Al-Hujaj and Schmelcher's data [8]. This difference is mainly caused by the lower ground state atomic energy obtained in the former reference, which has already been mentioned near the end of the previous section.

Table 4-1 Atomic ionization energies in magnetic fields (energy in Hartree)

Atom	Configurations	B(au)	HF	CI	LDA	PBE
He[a]	$1s^2 \rightarrow 1s$	0	0.8617	0.9034	0.8344	0.8929
		0.02	0.8516	0.8933	0.8244	0.8828
		0.04	0.8415	0.8831	0.8142	0.8727
		0.08	0.8208	0.8625	0.7935	0.8520
		0.16	0.7782	0.8199	0.7506	0.8092
		0.24	0.7340	0.7756	0.7059	0.7647
		0.4	0.6409	0.6824	0.6113	0.6706
		0.5	0.5798	0.6212	0.5492	0.6089
	$1s2p_{-1} \rightarrow 1s$	0.8	0.4687	0.4741	0.4199	0.4734
		1	0.5187	0.5245	0.4685	0.5225
		1.6	0.6438	0.6504	0.5887	0.6452
		2	0.7132	0.7201	0.6549	0.7136
		5	1.0734	1.0816	0.9978	1.0739
		10	1.4394	1.4493	1.3519	1.4527
		20	1.9061	1.9190	1.8161	1.9554
		50	2.7182	2.7378	2.6627	2.8829
		100	3.5161	3.5442	3.5445	3.8593
Li	$1s^22s \rightarrow 1s^2$	0	0.1963	0.2006	0.2011	0.2054
		0.01	0.2012	0.2056	0.2059	0.2102
		0.02	0.2068	0.2136	0.2135	0.2178
		0.05	0.2177	0.2254	0.2226	0.2269
		0.1	0.2329	0.2403	0.2380	0.2425
	$1s^22p_{-1} \rightarrow 1s^2$	0.2	0.2587	0.2614	0.2691	0.2729
		0.5	0.3699	0.3750	0.3844	0.3870
		1	0.5025	0.5111	0.5216	0.5226
		2	0.6995	0.7113	0.7226	0.7229
	$1s2p_{-1}3d_{-2} \rightarrow 1s2p_{-1}$	3	0.7525		0.7572	0.7635
		5	0.9475	0.9555	0.9558	0.9644
		10	1.2877	1.2982	1.3074	1.3219
Be	$1s^22s^2 \rightarrow 1s^22s$	0	0.2956	0.3158	0.3318	0.3306
		0.001	0.2951	0.3159	0.3313	0.3302
		0.01	0.2905	0.3112	0.3267	0.3255
		0.02	0.2852	0.3313	0.3214	0.3203
		0.05	0.2683	0.2911	0.3047	0.3035
	$1s^22s2p_{-1} \rightarrow 1s^22s$	0.1	0.3234	0.3242	0.3304	0.3312
		0.2	0.3941	0.3941	0.4010	0.4019
		0.3	0.4531	0.4597	0.4603	0.4612
	$1s^22s2p_{-1} \rightarrow 1s^22p_{-1}$	0.4	0.4687	0.4758	0.4677	0.4717
		0.5	0.4710	0.4749	0.4713	0.4758
		0.6	0.4696	0.4767	0.4718	0.4766
		0.8	0.4593	0.4650	0.4663	0.4718
	$1s^22p_{-1}3d_{-2} \rightarrow 1s^22p_{-1}$	1	0.4559	0.4455	0.4575	0.4636
		2	0.6231	0.6217	0.6257	0.6336
	$1s2p_{-1}3d_{-2}4f_{-3} \rightarrow 1s2p_{-1}3d_{-2}$	5	0.8787	0.8772	0.8895	0.9019
		10	1.1973	1.1959	1.2223	1.2401

(a) Exact energies are used for the one-electron system He^+.

Table 4-2 Eigenvalues for the highest occupied orbitals of magnetized atoms (energy in Hartree)

Atom	Configuration	B (au)	HOMO	HF	LDA	PBE
He	$1s^2$	0	$1s$	-0.91795	-0.5702	-0.5792
		0.02		-0.90789	-0.5601	-0.5692
		0.04		-0.89771	-0.5499	-0.5589
		0.08		-0.87699	-0.5289	-0.5379
		0.16		-0.83412	-0.4848	-0.4940
		0.24		-0.78942	-0.4383	-0.4476
		0.4		-0.69501	-0.3387	-0.3485
		0.5		-0.63298	-0.2728	-0.2829
	$1s2p_{-1}$	0.8	$2p_{-1}$	-0.47120	-0.3184	-0.3184
		1		-0.52183	-0.3529	-0.3532
		1.6		-0.64824	-0.4389	-0.4408
		2		-0.71820	-0.4867	-0.4900
		5		-1.07974	-0.7379	-0.7502
		10		-1.44629	-0.9994	-1.0230
		20		-1.91388	-1.3424	-1.3824
		50		-2.72841	-1.9648	-2.0381
		100		-3.52994	-2.6077	-2.7192
Li	$1s^22s$	0	$2s$	-0.19636	-0.1162	-0.1185
		0.01		-0.20122	-0.1211	-0.1234
		0.02		-0.20668	-0.1282	-0.1306
		0.05		-0.21778	-0.1364	-0.1389
		0.1		-0.23293	-0.1487	-0.1516
	$1s^22p_{-1}$	0.2	$2p_{-1}$	-0.25885	-0.1728	-0.1751
		0.5		-0.37038	-0.2529	-0.2549
		1		-0.50398	-0.3472	-0.3489
		2		-0.70293	-0.4873	-0.4903
	$1s2p_{-1}3d_{-2}$	5	$3d_{-2}$	-0.95259	-0.6626	-0.6763
		10		-1.29348	-0.9139	-0.9355
Be	$1s^22s^2$	0	$2s$	-0.30927	-0.2058	-0.2061
		0.01		-0.30417	-0.2007	-0.2010
		0.02		-0.29888	-0.1953	-0.1957
		0.05		-0.28186	-0.1779	-0.1783
	$1s^22s2p_{-1}$	0.1	$2p_{-1}$	-0.33120	-0.1959	-0.1961
		0.2		-0.40159	-0.2560	-0.2566
		0.3		-0.46016	-0.3046	-0.3054
		0.4	$2s$	-0.47732	-0.3108	-0.3163
		0.5		-0.47908	-0.3099	-0.3161
		0.6		-0.47722	-0.3064	-0.3134
		0.8		-0.46613	-0.2953	-0.3037
	$1s^22p_{-1}3d_{-2}$	1	$3d_{-2}$	-0.46092	-0.3105	-0.3180
		2		-0.62799	-0.4283	-0.4391
	$1s2p_{-1}3d_{-2}4f_{-3}$	5	$4f_{-3}$	-0.88345	-0.6259	-0.6421
		10		-1.20284	-0.8671	-0.8908

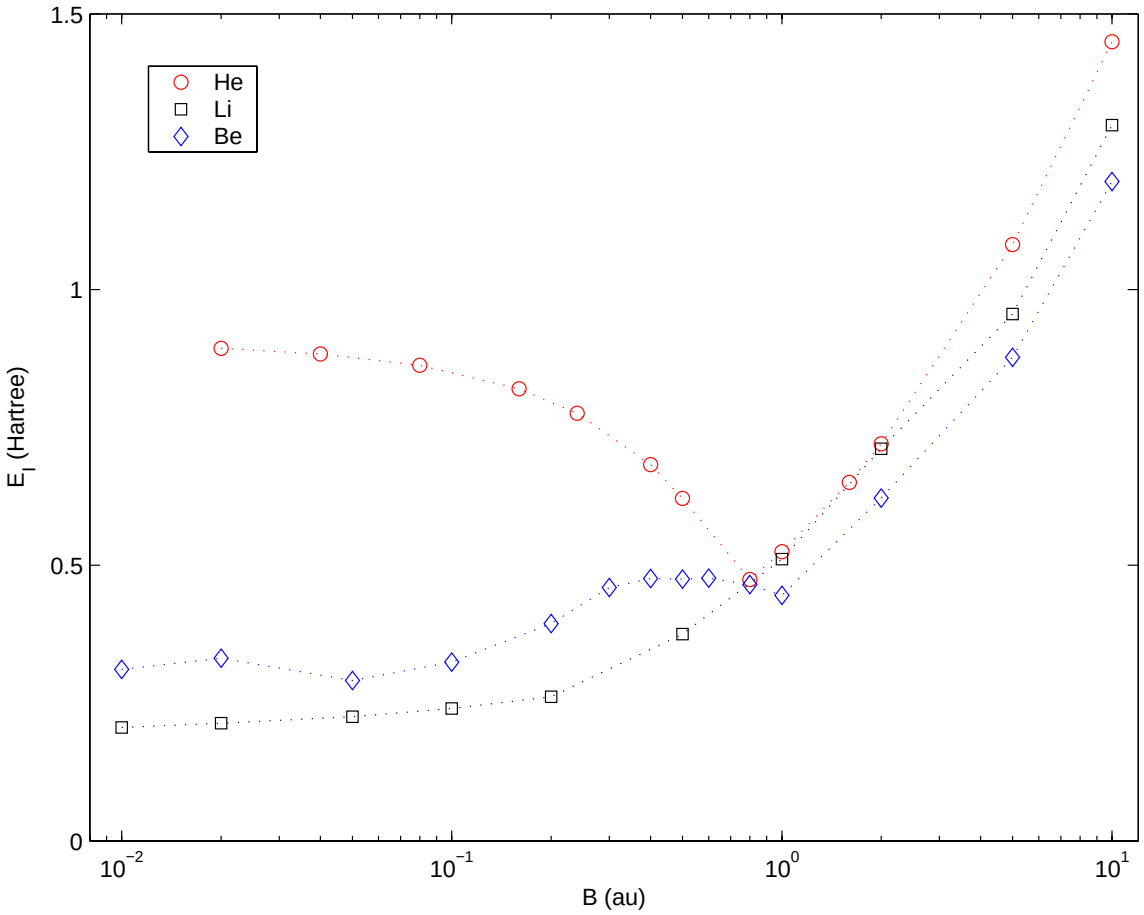

FIG. 4-5 Atomic ground state ionization energies with increasing *B* field. Data plotted are from CI calculations shown in Table 4-1. Dotted lines are the guides to the eye.

Even though the ionization energies in both the low and intermediate field regions are rather complicated as the result of atomic configuration changes, their behaviors are similar for the strong field limit configurations. This is an indication that the original atomic shell structure has been effectively obliterated by the field.

Eigenvalues of the highest occupied orbitals are reported in Table 4-2. In all the cases, the HF orbital energies give the closest approximation to the atomic ionization energies, with an average deviation of only 7.6 *m*H. KS eigenvalues, as usual, significantly underestimate the ionization energy. This is because both LDA and PBE

functionals give approximate potentials too shallow compared with the exact DFT XC potential. Self-interaction correction (SIC) could significantly improve these values, but we will not pursue it further here, because our focus is on E_{xc} functionals that are not explicitly orbitally dependent.

Current Density Correction and Other Issues

Advancement in CDFT, especially in applications, is hindered by the lack of reliable, tractable functionals. In comparison with the vast literature of ordinary DFT approximate XC functionals, the total number of papers about CDFT approximate functional is substantially less than 50. The earliest proposed functional, also the most widely investigated one as of today, is the VRG functional [14-16]. Even for it there are no conclusive results for $B \neq 0$ in the literature. Here we examine this functional in detail for atoms in a B field, and show the problems inherent in it. The analysis indicates that the VRG functional is not cast in a suitable form, at least for magnetized atoms. The choice of vorticity $\vec{\nu} = \nabla \times \frac{\vec{j}_p}{n}$ as the basic variable to ensure gauge-invariance, which is the central result of references 14-16, needs to be critically re-examined.

The challenge to implementing CDFT is, somewhat paradoxically, that the current effect is presumably small. We do not expect that the current correction within CDFT will drastically change the DFT densities. Therefore the first question we encountered is which DFT functional should be used as a reference for the CDFT calculations. If the variation in outcomes that results from different choices of DFT functionals is much larger than the CDFT corrections, which seems to be the case in many situations, the predictability of the calculation is jeopardized. Of course, there is no easy answer to this question. Indeed, DFT functionals themselves are still undergoing improvement.

Here we made the conventional DFT choice of using the LDA as the starting point. Even though not the most accurate one, the LDA is among the best understood DFT functionals. It is also easy to implement. Using self-consistent KS orbitals obtained from LDA calculation for the helium atom $1s2p_{-1}$ state in a field $B = 1$ au., I plotted various quantities that are important in CDFT along the z and ρ directions in Fig. 4-6.

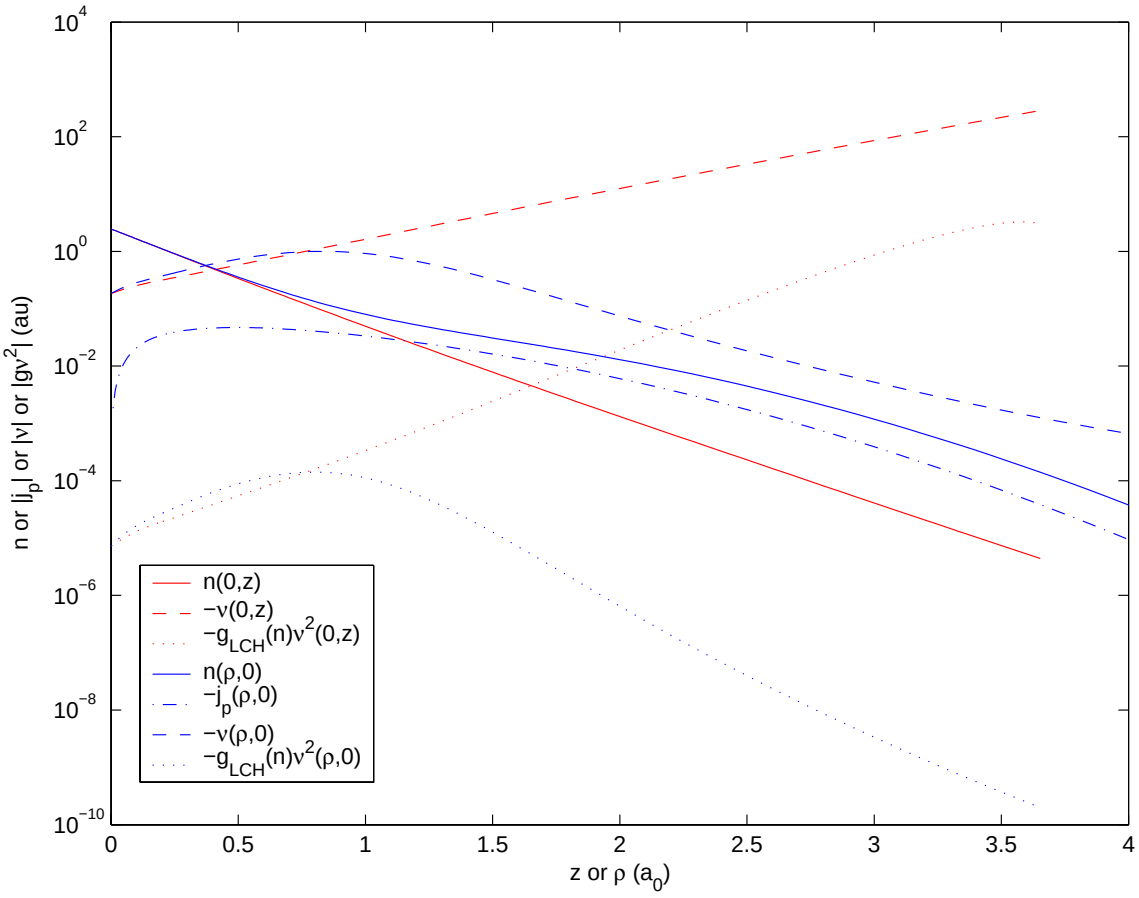

FIG. 4-6 Various quantities (electron density n, paramagnetic current density j_p, vorticity $\boldsymbol{v}$, and the current correction to the exchange-correlation energy density, $g\boldsymbol{v}^2$, in the VRG functional) for the helium atom $1s2p_{-1}$ state in $B = 1$ au. All quantities are evaluated from the LDA KS orbitals and plotted along the z and ρ axes (cylindrical coordinates).

Exponential decay of electron density was already seen in Fig. 4-2. Because the current density along the z axis is zero, it does not appear in Fig. 4-6. However, $\vec{v}$ is not zero on that axis. On the contrary, it diverges at the two poles of the atom. This

divergence causes large values of $g(n)\nu^2$, the energy density correction within the VRG functional (recall eqns. 1.39 and 2.9). If the pre-factor $g(n)$ does not decay fast enough to cancel this divergence, a convergence problem in the SCF solution of the CDFT KS equation will happen. Also notice that the electron density decays very rapidly along the z axis. At $z = 3a_0$, the density is already smaller than $10^{-4}a_0^{-3}$. Remember the function $g(n)$ was fitted to data points with $r_s \le 10a_0$, thus in the low-density region it is not well-defined. Different fits to the same set of original data points vary considerably (refer to eqns. 1.41 through 1.46). Furthermore, even the accuracy of the original data set to be fitted is questionable at $r_s \sim 10a_0$. Even were these problems to be resolved, the underlying behavior shown in Fig. 4-6 would remain. The largest correction relative to ordinary DFT given by the VRG functional is at the places where the electron density and the current density are both almost zero, which is obviously peculiar if not outright unphysical. This peculiar (and difficult) behavior is rooted in the choice of $\vec{v}$ as the basic variable in the CDFT functional.

To avoid the divergence problem, we introduced a rapidly decaying cutoff function. Details were given in chapter 2 (also recall eqns. 2.15 and 2.16). Using parameters $n_{cutoff} = 10^{-3}a_0^{-3}, \alpha_{cutoff} = 2a_0^{-1}$ for the cutoff function, Table 4-3 lists some of the calculated results within the VRG approximation for the fully spin-polarized states of the helium, lithium, and beryllium atoms at several selected field strengths. An estimation of the current effect is to evaluate the VRG functional using the LDA Kohn-Sham orbitals. Results for that estimation are listed in the third column of Table 4-3. This scheme can be thought as a non-self-consistent post-DFT calculation. Fully self-consistent CDFT

calculations were also accomplished when the *B* field is not too large, and they verified the LDA-based estimates. When the *B* field is larger than roughly 5 au., SCF convergence problems return because of the pathological behavior of VRG functional.

Table 4-3 CDFT corrections to LDA results within VRG approximation (parameters $n_{cutoff} = 10^{-3} a_0^{-3}, \alpha_{cutoff} = 2a_0^{-1}$ are used for the cutoff function, ΔE in Hartree)

Atom and State	*B* (au)	Non-SCF ΔE^{VRG}	SCF ΔE^{VRG}	$\Delta\varepsilon^{HOMO}$
He $1s2p_{-1}$	0	-0.0022	-0.0021	0.0001
	0.24	-0.0031	-0.0031	-0.0013
	0.5	-0.0045	-0.0047	-0.0029
	1	-0.0077	-0.0081	-0.0071
	5	-0.036		
	10	-0.074		
	100	-0.81		
Li $1s2p_{-1}3d_{-2}$	0	-0.0070	-0.0071	0.0002
	2	-0.027	-0.029	-0.0077
	5	-0.065		
	10	-0.129		
Be $1s2p_{-1}3d_{-2}4f_{-3}$	1	-0.025	-0.026	-0.0017
	5	-0.085		
	10	-0.166		

Putting these concerns aside, consider Table 4-3. By design, the current correction given by the VRG functional is negative. It strongly depends on the particular atomic configuration. Within each configuration, the VRG contribution increases with increasing *B* field. Besides total atomic energies, the eigenvalues of the highest occupied KS orbitals are also slightly lowered by including the current term, but it helps little in bringing the HOMO energies closer to the ionization energies. This error, of course, is the well-known self-interaction problem.

Because of the use of a cutoff function, these CDFT calculations can at best be thought of as semi-quantitative. This is because the current corrections strongly depend

on the chosen cutoff function. Use of different cutoff parameters gives quite different results (see Table 4-4), an outcome which is really undesirable. Of course, all of this is because the VRG functional does not provide a suitable form for either the low density or the high-density regions, nor do we know its correct asymptotic expression.

Table 4-4 Effect of cutoff function on CDFT corrections for the helium atom $1s2p_{-1}$ state in magnetic field $B = 1$ au. (energy in Hartree)

$n_{cutoff}\left(a_0^{-3}\right)$	$\alpha_{cutoff}\left(a_0^{-1}\right)$	Non-SCF ΔE^{VRG}
0.005	2.0	-0.004
0.001	2.0	-0.008
0.001	1.0	-0.010
0.0001	2.0	-0.025
0.00001	2.0	-0.064

It is unsurprising that the VRG functional fails when applied to atomic systems in a strong magnetic field. It was developed from the study of the moderately dense to dense HEG in a weak magnetic field, for which Landau orbitals were used as approximations. This physical situation is quite different from a finite system. First, electron and paramagnetic current densities vary considerably within an atom, and the low density regions ($r_s > 10a_0$) are non-negligible. Secondly, there is not a direct relationship between $\vec{j}_p\left(\vec{r}\right)$ and the external B field as there is for the HEG. The question whether the electron gas remains homogeneous after imposing a substantial B field is even unclear. If the field induces some form of crystallization, the basic picture based on which the VRG functional proposed is completely lost. The analysis and numerical studies in this chapter suggest the picture of Landau orbitals used for the HEG may not be applicable at all for the atomic-like systems. Unlike the LDA, also based on the HEG, it seems that the VRG functional is too simple to encompass the essential physics of the atomic systems.

A more fundamental question is whether $\vec{v}(\vec{r})$ is a suitable basic variable in gauge-invariant CDFT as Vignale and Rasolt required [14-16]. While it is appealing from a purely theoretical perspective, our numerical results on atomic systems in *B* fields suggest it is an inappropriate choice, or at least an awkward one, from the application perspective. Largely due to the choice of $\vec{v}(\vec{r})$ as the basic variable in the VRG functional, it gives unphysical results in our tests. Recently, Becke proposed a current-dependent functional to resolve the discrepancy of atomic DFT energies of different multiplicity of open-shell atoms [107]. Since this functional is based on the analysis of atomic systems, it may be more suitable for application to magnetized atoms than the VRG functional. There are significant technical barriers to its use. Nonetheless, we hope to investigate this functional in the future.

Before attempting (sometimes in effect, guessing) better forms for the CDFT functional, we need to know some exact CDFT results to serve as touchstones for any possible proposed functional, This is the major task of the next chapter.

Finally, one additional comment remains to be made about the results presented in this chapter. Relativistic effects and the effects due to finite nuclear mass are not considered. Those effects can be important for matter in super-strong fields ($B > 10^4$ au), in which regime the adiabatic approximation will be applicable. But for the field strengths involved in this chapter, both effects should be negligible.

CHAPTER 5
HOOKE'S ATOM AS AN INSTRUCTIVE MODEL

In DFT, the need for accurate approximations to the electronic exchange-correlation energy E_{xc} has motivated many studies of a model system often called Hooke's atom (HA) in the DFT literature [108-121]. The basic HA is two electrons interacting by the Coulomb potential but confined by a harmonic potential rather than the nuclear-electron attraction. This system is significant for DFT because, for certain values of the confining constant, exact analytical solutions for various states of the HA are known [108, 111]. For other confining strengths, it can be solved numerically also with correlation effects fully included [113]. Since the DFT universal functional is *independent* of the external potential and the HA differs from atomic He (and isoelectronic ions) *only* by that potential, exact solutions of the HA allow construction of the exact E_{xc} functional and comparative tests of approximate functionals for such two-electron systems. Given that much less is known about the approximate functionals in CDFT than ordinary DFT, it would be of considerable value to the advancement of CDFT to have corresponding exact solutions for the HA in an external magnetic field.

Hooke's Atom in Vanishing *B* Field

There is a long history of investigating this problem. The system Hamiltonian reads

$$\hat{H}_{tot} = -\frac{1}{2}\left[\nabla_1^2 + \nabla_2^2\right] + \frac{\omega^2}{2}(r_1^2 + r_2^2) + \frac{1}{r_{12}} \tag{5.1}$$

where $\vec{r}_i \ (i = 1, 2)$ are the spatial coordinates of the electrons, and ω the confinement frequency. Hartree atomic units are used throughout. By introducing center of mass (CM) and relative coordinates,

$$\begin{aligned} \vec{R} &= \frac{1}{2}(\vec{r}_2 + \vec{r}_1) \\ \vec{r} &= \vec{r}_2 - \vec{r}_1 \equiv \vec{r}_{12} \end{aligned} \tag{5.2}$$

(when I deal with the relative motion part, $\vec{r}$ always means $\vec{r}_{12}$), the Hamiltonian eqn. (5.1) becomes

$$\hat{H}_{tot} = \hat{H}_{CM} + \hat{H}_r \tag{5.3}$$

where $\hat{H}_{CM} = -\frac{1}{4}\nabla^2_{\vec{R}} + \omega^2 R^2$ (5.4)

$$\hat{H}_r = -\nabla^2_{\vec{r}} + \frac{1}{4}\omega^2 r^2 + \frac{1}{r} \tag{5.5}$$

The solution to the three-dimensional oscillator problem (5.4) can be found in any undergraduate QM textbook. It is the relative motion Schrödinger problem, defined by eqn. (5.5), that has been treated variously by different authors. Laufer and Krieger used the numerical solution to the relative motion problem to construct the exact DFT quantities, and found that, although most approximate functionals generate rather accurate total energies for this model system, the corresponding approximate XC potentials are significantly in error [113]. In 1989, Kais, Herschbach, and Levine found one analytical solution to the HA relative motion problem by dimensional scaling [108]. Samanta and Ghosh obtained solutions by adding an extra linear term to the Hamiltonian [110]. Later, Taut obtained a sequence of exact solutions for certain specific confinement frequencies [111], and used them in studies of DFT functionals [114-116].

A basic observation about the HA follows from the Pauli principle, which requires the total wavefunction to be antisymmetric. Because the CM part is always symmetric under particle exchange $\vec{r}_1 \leftrightarrow \vec{r}_2$, if the relative motion part is symmetric (e.g. *s* or *d*–like orbitals), the spin part must be anti-symmetric, thus a spin singlet state; otherwise a spin triplet state. Thus we can concern ourselves with the spatial relative motion problem alone.

Since the Hamiltonian (5.5) is spherically symmetric, the relative motion wave-function can be written as the product of a spherical harmonic and a radial part. The radial part is in turn decomposed into a gaussian decaying part (ground state wavefunction of a harmonic oscillator) and a polynomial part. In some special conditions, the polynomial has only a finite number of terms, and thus the wavefunction is expressed explicitly in a closed form. Here I proceed slightly differently from the approach in reference 111. Insertion of the relative motion wavefunction

$$\psi_r\left(\vec{r}\right) = Y_{lm}\left(\theta,\varphi\right) r^l e^{-\omega r^2/4} \sum_{k=0}^{\infty} a_k r^k \tag{5.6}$$

in $\hat{H}_r \psi_r\left(\vec{r}\right) = E_r \psi_r\left(\vec{r}\right)$ and a little algebra give the recursion relation

$$-\left(k+2\right)\left(k+2l+3\right)a_{k+2} + a_{k+1} + \left[\left(k+l+\frac{3}{2}\right)\omega - E_r\right]a_k = 0 \tag{5.7}$$

Suppose the polynomial part in eqn. (5.6) terminates at the *n*th term, e.g. $a_n \neq 0$ and $a_{k>n} = 0$. The recursion relation (5.7) for $k = n$ immediately gives

$$E_{r,n,l} = \left(l+n+\frac{3}{2}\right)\omega \tag{5.8}$$

Repeatedly invoking eqn. (5.7) for $k = n\text{-}1, n\text{-}2, \ldots, 0, -1$, we get an expression for a_{-1} which by definition must be zero, in terms of ω. Frequencies which make this expression be zero are the ones that correspond to analytical solutions with eigenvalues given by eqn. (5.8).

Table 5-1 Confinement frequencies ω for HA that have analytical solutions to eqn. (5.5) (see eqn. 5.8 for their eigenvalues)

n	$l = 0$	$l = 1$	$l = 2$	$l = 3$
1	0.50000000000000	0.25000000000000	0.16666666666667	0.12500000000000
2	0.10000000000000	0.05555555555556	0.03846153846154	0.02941176470588
3	0.03653726559926	0.02211227585113	0.01583274147996	0.01232668925503
	0.38012940106740	0.20936920563036	0.14620429555708	0.11267331074497
4	0.01734620322217	0.01122668987403	0.00827862455572	0.00655187269690
	0.08096840351940	0.04778618566245	0.03423838224700	0.02675808522737
5	0.00957842801556	0.00653448467629	0.00494304416061	0.00397054409092
	0.03085793692937	0.01942406484507	0.01426990657388	0.01130595881607
	0.31326733875878	0.18237478381198	0.13126853074700	0.10313090450042
6	0.00584170375528	0.00415579376716	0.00321380796521	0.00261635006133
	0.01507863770249	0.01002629075547	0.00753956664388	0.00605214259197
	0.06897467166559	0.04231138533718	0.03104720074689	0.02465640755471
7	0.00382334430066	0.00281378975218	0.00221804190308	0.00182765149628
	0.00849974006449	0.00591291799966	0.00454144170886	0.00369051896040
	0.02696238772621	0.01743843557070	0.01305357779085	0.01048109720372
	0.26957696177107	0.16282427466688	0.11975836716865	0.09546288545482
8	0.00263809218012	0.00199650951781	0.00160027228709	0.00133306668779
	0.00526419387919	0.00380045768734	0.00297472273003	0.00244506933776
	0.01342801519820	0.00910586669888	0.00694983975395	0.00564110607268
	0.06058986425144	0.03819659970201	0.02852875778009	0.02293923879074
9	0.00189655882218	0.00146924333165	0.00119499503998	0.00100531643239
	0.00348659634110	0.00259554123244	0.00206608391617	0.00171616534853
	0.00767969351968	0.00542189229787	0.00421416844040	0.00345660786555
	0.02409197815100	0.01589809508448	0.01207319134740	0.00979689471802
	0.23835310967398	0.14785508696009	0.11054467575052	0.08912851417778
10	0.00140897933719	0.00111335083551	0.00091728359398	0.00077860389150
	0.00242861494144	0.00185491303393	0.00149877344939	0.00125702179525
	0.00481042669358	0.00351289521069	0.00277638397339	0.00230004951343
	0.01216213038015	0.00837269574743	0.00646564069324	0.00529550074157
	0.05433349965263	0.03496458370680	0.02647749580751	0.02150263695791

An example may be helpful. Consider $l = 0$, and $n = 3$. According to the previously prescribed procedure, we get $E_r = \frac{9}{2}\omega$, $a_2 = \frac{a_3}{\omega}$, $a_1 = \frac{a_2 - 12a_3}{2\omega} = \frac{(1-12\omega)a_3}{2\omega^2}$,

$$a_0 = \frac{a_1 - 6a_2}{3\omega} = \frac{(1-24\omega)a_3}{6\omega^3}, \qquad a_{-1} = \frac{a_0 - 2a_1}{4\omega} = \frac{(1-30\omega+72\omega^2)a_3}{24\omega^4}.$$

To ensure that the last expression vanishes requires that the confinement frequency be $\omega = \frac{5 \pm \sqrt{17}}{24}$, or $\omega = 0.3801294, 0.0365373$. The solution corresponding to the smaller frequency turns out to be a ground state, while the other one is an excited state.

Confinement frequencies corresponding to analytical solutions for $l = 0, 1, 2, 3$ and $n \leq 10$ are compiled in Table 5-1. This tabulation includes more angular momentum quantum numbers and more significant figures than that presented by Taut [111]. For $n \geq 3$, there are several solutions. The smallest frequency corresponds to a ground state, the others are for excited states.

Hooke's Atom in *B* Field, Analytical Solution

When the HA is placed in an external magnetic field, its lateral confinement can exceed its vertical confinement. It is well known that the magnetic field can greatly complicate the motion of a columbic system. Even for the one-electron system (H atom), substantial effort is required to get highly accurate results in a *B* field [79-82]. Only recently have calculations on the He atom in a high field been pushed beyond the HF approximation [11-13]. As far as I know, no exact solutions are reported in the literature for the 3D Hooke's atom in an external magnetic field. Taut only gave analytical solutions for a 2D HA in a perpendicular *B* field [117]. Here I present the exact analytical solutions to the magnetized HA [122]. When the nuclear attraction in the He

atom is replaced by a harmonic potential, our exact analytical results can serve as a stringent check on the accuracy of the correlated calculations just mentioned.

With an external magnetic field chosen along the *z* axis, the system Hamiltonian becomes

$$\hat{H}_{tot} = \frac{1}{2}\left[(\frac{\nabla_1}{i} + \vec{A}(\vec{r}_1))^2 + (\frac{\nabla_2}{i} + \vec{A}(\vec{r}_2))^2 \right] + \frac{\omega^2}{2}(r_1^2 + r_2^2) + \frac{1}{r_{12}} + \hat{H}_{spin} \tag{5.9}$$

where $\hat{H}_{spin} = -\left(s_{1z} + s_{2z}\right) B$ is the spin part of the Hamiltonian, $s_{iz}\ (i = 1,2)$ are the *z* components of the spin, and $\vec{A}(\vec{r})$ is the external vector potential. A similar separation of the CM and the relative motion parts is done as in the case of the $B = 0$ HA:

$$\hat{H}_{tot} = \hat{H}_{CM} + \hat{H}_r + \hat{H}_{spin} \tag{5.10}$$

$$\hat{H}_{CM} = \frac{1}{4}(\frac{\nabla_{\vec{R}}}{i} + 2\vec{A}(\vec{R}))^2 + \omega^2 R^2 = \frac{1}{4}(-\nabla_{\vec{R}}^2 + 4\omega^2 R^2 + B^2 R^2 \sin^2\Theta + 2MB) \tag{5.11}$$

$$\hat{H}_r = (\frac{\nabla_{\vec{r}}}{i} + \frac{1}{2}\vec{A}(\vec{r}))^2 + \frac{1}{4}\omega^2 r^2 + \frac{1}{r} = -\nabla_{\vec{r}}^2 + \frac{1}{4}\omega^2 r^2 + \frac{1}{16}B^2 r^2 \sin^2\theta + \frac{1}{2}mB + \frac{1}{r}$$

$$= -\nabla_{\vec{r}}^2 + \omega_\rho^2 \rho^2 + \omega_z^2 z^2 + \frac{m}{2}B + \frac{1}{r} \tag{5.12}$$

Here $\omega_\rho = \sqrt{\frac{\omega^2}{4} + \frac{B^2}{16}}, \quad \omega_z = \frac{\omega}{2};$ (5.13)

$\rho = \sqrt{x^2 + y^2}$, m and M are magnetic quantum numbers for the relative and CM motion parts. In these expressions, the Coulomb gauge has been chosen.

$$\vec{A}(\vec{r}) = \frac{1}{2}\vec{B} \times \vec{r} \tag{5.14}$$

The solution for the CM part is (un-normalized)

$$\psi_{CM}(\vec{R}) = \exp(-\omega Z^2 - \frac{\Omega_L \mathrm{P}^2}{2}) \cdot \mathrm{P}^{|M|} \cdot H_{N_Z}(\sqrt{2\omega}Z) \cdot {}_1F_1(-N_\mathrm{P}, |M| + 1, \Omega_L \mathrm{P}^2) \cdot \exp(iM\Phi) \tag{5.15}$$

with eigenvalue of

$$E_{CM} = (N_Z + \frac{1}{2})\omega + \frac{M}{2}B + \left(N_{\mathrm{P}} + \frac{|M|+1}{2} \right)\Omega_L \tag{5.16}$$

where $\mathrm{P} = R\sin\Theta, \Omega_L = \sqrt{4\omega^2 + B^2}$, H_{N_Z} is N_Z th order Hermite polynomial. ${}_1F_1$ is the confluent hypergeometric function (or Kummer function) [123]. $N_Z, N_{\mathrm{P}} = 0, 1, 2, \ldots$ are the quantum numbers.

The relative motion eignvalue problem from eqn. (5.12) generally cannot be solved analytically in either spherical or cylindrical coordinates. The difficulty of solving the Schrödinger equation that corresponds to eqn. (5.12) lies in the different symmetries of the confining potential (cylindrical) and electron-electron interaction term (spherical). Since the effective potential in eqn. (5.12) $V(\vec{r}) = \omega_\rho^2\rho^2 + \omega_z^2 z^2 + \frac{1}{r}$ is expressed as a combination of cylindrical coordinate variables (ρ, z) and the spherical coordinate variable *r*, it proves convenient also to express the relative-motion wavefunction in those combined, redundant variables $\psi_r(\vec{r}) = \psi_r(\rho, z, r(\rho, z), \varphi)$. In part motivated by the expected asymptotic behavior, we choose the form

$$\psi_r(\vec{r}) = e^{-\frac{\omega_z}{2}z^2 - \frac{\omega_\rho}{2}\rho^2} \rho^{|m|} z^{\pi_z} u(r, z) e^{im\varphi} \tag{5.17}$$

where $\pi_z = 0$ for even *z* parity, 1 for odd *z* parity. Then $\left(\hat{H}_r - E_r\right)\psi_r(\vec{r}) = 0$ yields

$$\left\{ -\frac{\partial^2}{\partial r^2} - \frac{\partial^2}{\partial z^2} - \frac{2z}{r}\frac{\partial^2}{\partial z \partial r} - \frac{2}{r}\left[1 + \pi_z + |m| + (\omega_\rho - \omega_z)z^2 - \omega_\rho r^2\right]\frac{\partial}{\partial r} + 2\left(\omega_z z - \frac{\pi_z}{z}\right)\frac{\partial}{\partial z} + \frac{1}{r} - \tilde{E} \right\} u(r, z) = 0 \tag{5.18}$$

where $\tilde{E} = E_r - \frac{m}{2}B - (2\pi_z + 1)\omega_z - 2(|m| + 1)\omega_\rho$. (5.19)

To avoid messy notation, no quantum numbers are appended to $\tilde{E}$. This differential equation is not easy to solve either. To proceed, we make a direct, double power-series expansion

$$u(r,z) = \sum_{n_r,n_z=0}^{\infty} A_{n_r,n_z} r^{n_r} z^{n_z} \tag{5.20}$$

to transform eqn. (5.18) into a recurrence relation,

$$-2(n_r+2)(\omega_\rho-\omega_z)A_{n_r+2,n_z-2} - (n_r+2)\left[n_r+3+2(|m|+\pi_z+n_z)\right]A_{n_r+2,n_z} + A_{n_r+1,n_z}$$

$$+\left[2(n_r\omega_\rho+n_z\omega_z)-\tilde{E}\right]A_{n_r,n_z} - (n_z+\pi_z+1)(n_z+\pi_z+2)A_{n_r,n_z+2} = 0 \tag{5.21}$$

where $A_{i,j} = 0$ for $i < 0$, or $j < 0$, or $j = 2k+1$. We seek values of $\tilde{E}$, ω_ρ, ω_z for which the right side of eqn. (5.20) terminates at finite order. Assume the highest power of *z* that appears is N_z, $\left(A_{i,j>N_z} = 0\right)$, where N_z is an even number. For $N_z > 2$, generally there is no solution to the set of equations that follow from eqn. (5.21). However, a judicious choice,

$$\omega_\rho = 2\omega_z,\ \tilde{E} = 2N_z\omega_z \tag{5.22}$$

allows us to set $A_{i,j} = 0$ for $2i + j > N_z$, since there are $\frac{N_z}{2}+1$ recurrence relations of eqn. (5.21) with $2n_r + n_z = N_z$ that then are satisfied automatically. This is the special case, $\omega_\rho = 2\omega_z = \omega$, which corresponds to imposition of an external field *B* upon a HA with magnitude

$$B = 2\sqrt{3}\omega \tag{5.23}$$

Now we find values of ω_z that correspond to analytical solutions. Repeated application of eqn. (5.21) for each combination of $-1 \le n_r \le \frac{N_z}{2}-2$,

$N_z - 2(n_r + 1) \geq n_z \geq 2$, allows us to express all the coefficients $\left\{ A_{0<i\leq\frac{N_z}{2},0\leq j\leq N_z-2i} \right\}$ in terms of $\left\{A_{0,0<j\leq N_z}\right\}$. Invoking eqn. (5.21) for $n_z = 0$, $-1 \leq n_r \leq \frac{N_z}{2} - 1$, gives $\frac{N_z}{2} + 1$ homogenous linear equations involving $\left\{A_{0,0\leq j\leq N_z}\right\}$. To have non-trivial solutions, the determinant of this set of equations must be zero, a requirement which reduces to finding the roots of a polynomial equation in ω_z. Energy eigenvalues can be easily found by substituting eqns. (5.22), (5.23) and (5.13) into (5.19),

$$E_r = \left[\left(N_z + \pi_z + 2|m| \right) + \frac{5}{2} + \sqrt{3}m \right] \omega \tag{5.24}$$

Here I give an explicit example for $m = \pi_z = 0$, $N_z = 6$. Its relative motion energy is $E_r = \left(6 + \frac{5}{2} \right) \omega = 17\omega_z$, First we set all the coefficients $A_{i,j} = 0$ for $2i + j > 6$. The four equations derived from eqn. (5.21) are already satisfied for (n_r, n_z) = (3,0), (2,2), (1,4), and (0,6). Repeatedly invoking the recursion relation (5.21) for $n_r = -1$, $n_z = 6, 4, 2$, we find $A_{1,4}$, $A_{1,2}$, and $A_{1,0,}$ expressed in terms of $A_{0,2}$, $A_{0,4}$, and $A_{0,6.}$

$$A_{1,4} = \frac{A_{0,6}}{2\omega_z},$$

$$A_{1,2} = \frac{A_{0,4} - 10A_{1,4}}{2\omega_z} = \frac{\omega_z A_{0,4} - 5A_{0,6}}{2\omega_z^2},$$

$$A_{1,0} = \frac{-6A_{1,2} + A_{0,2}}{2\omega_z} = \frac{\omega_z^2 A_{0,2} - 3\omega_z A_{0,4} + 15A_{0,6}}{2\omega_z^3};$$

Use eqn. (5.21) again twice for $n_r = 0$, $n_z = 4, 2$,

$$A_{2,2} = -\frac{4\omega_z A_{0,4} - A_{1,4} + 30A_{0,6}}{4\omega_z} = \frac{1-60\omega_z}{8\omega_z^2} A_{0,6} - A_{0,4},$$

$$A_{2,0} = -\frac{14A_{2,2} - A_{1,2} + 8\omega_z A_{0,2} + 12A_{0,4}}{4\omega_z} = \frac{2\omega_z\left(4\omega_z + 1\right)A_{0,4} + (420\omega_z - 17)A_{0,6}}{16\omega_z^3} - 2A_{0,2};$$

Employ eqn. (5.21) one more time for $n_r = 1, n_z = 2$ to obtain

$$A_{3,0} = -\frac{4\omega_z A_{1,2} - A_{2,2} + 12A_{1,4}}{6\omega_z} = -\frac{A_{0,4}}{2\omega_z} + \frac{1-28\omega_z}{48\omega_z^2} A_{0,6}.$$

Now, all the coefficients are expressed in terms of $A_{0,2}$, $A_{0,4}$, and $A_{0,6.}$ The next step is to apply eqn. (5.21) for $n_z = 0, n_r = -1, 0, 1, 2$. We have a set of four homogeneous equations,

$$A_{0,0} - 2A_{1,0} = 0,$$

$$A_{1,0} - 12\omega_z A_{0,0} - 6A_{2,0} - 2A_{0,2} = 0,$$

$$-8\omega_z A_{1,0} - 12A_{3,0} + A_{2,0} - 2A_{1,2} = 0,$$

$$-4\omega_z A_{2,0} + A_{3,0} - 2A_{2,2} = 0.$$

Substitute the expressions for $A_{1,0}, A_{2,0}, A_{3,0}, A_{1,2}, A_{2,2}$ and rearrange,

$$\frac{1}{\omega_z^3}\left[\omega_z^3 A_{0,0} - \omega_z^2 A_{0,2} + 3\omega_z A_{0,4} - 15A_{0,6}\right] = 0,$$

$$\frac{1}{8\omega_z^3}\left[-96\omega_z^4 A_{0,0} + 4\omega_z^2\left(1 + 20\omega_z\right)A_{0,2} - 6\omega_z\left(3 + 4\omega_z\right)A_{0,4} + \left(111 - 1260\omega_z\right)A_{0,6}\right] = 0,$$

$$\frac{1}{16\omega_z^3}\left[-96\omega_z^3 A_{0,2} + 2\omega_z\left(1 + 140\omega_z\right)A_{0,4} - 3\left(7 + 116\omega_z\right)A_{0,6}\right] = 0,$$

$$\frac{1}{48\omega_z^3}\left[384\omega_z^4 A_{0,2} - 48\omega_z^2 A_{0,4} + \left(1 + 164\omega_z - 4320\omega_z^2\right)A_{0,6}\right] = 0.$$

To have non-trivial solutions for $A_{0,0}$, $A_{0,2}$, $A_{0,4}$, and $A_{0,6}$, the determinant for their coefficients must be zero. This requirement is equivalent to the polynomial equation

$$8\omega_z^6\left(20611584\omega_z^4-1946560\omega_z^3+50256\omega_z^2-420\omega_z+1\right)=0$$

There is a standard procedure for solving the fourth power polynomial equation [123]. Here I give the nonzero solutions to the above equation

$$\omega_z=\frac{1}{8}\left\{x_{1,2,3}\pm\left[\frac{35812423+\dfrac{57433337575}{34506x_{1,2,3}}}{1234762704}-x_{1,2,3}^2\right]^{1/2}\right\}+\frac{4345}{184032},$$

where $x_i=\left\{\dfrac{2\sqrt{34759}}{40257}\cos\left[\dfrac{1}{3}\cos^{-1}\left(\dfrac{5633902\sqrt{34759}}{1208188081}\right)+(i-1)\dfrac{2\pi}{3}\right]+\dfrac{35812423}{3704288112}\right\}^{1/2}$.

Numerical evaluation gives

$\omega_z=$ 0.058442857785651984438171351463682719599670165 1, (third excitation)

0.023049151903381566126688606498588074755937494 8, (second excitation)

0.004045735148095486158383252973769735050229535 4, (ground state)

0.008902352537240638115915196297484075010786000 6. (first excitation)

The smallest frequency corresponds to a ground state, others correspond to excited states. Remember those states are not for the same confinement strength, hence not the same physical system.

Table 5-2 lists all the frequencies that correspond to closed-form analytical solutions for m = 0, 1, 2 and $N_z=2,4,6,8,10$, including both positive and negative z parities.

For each frequency found in the previous step, the corresponding eigenvector $\left\{A_{0,0\le j\le N_z}\right\}$ determines the vector of all the coefficients $\left\{A_{0<i\le\frac{N_z}{2},0\le j\le N_z-2i}\right\}$. Table 5-3 gives explicitly some of the solutions to eqn. (5.12).

Table 5-2 Confinement frequencies ω_z which have analytical solutions to eqn. (5.12) ($\omega_z = \omega/2, B = 2\sqrt{3}\omega$, see eqn. 5.24 for their eigenvalues)

π_z	N_z	state	$m = 0$	$m = 1$	$m = 2$
0	2	g	0.08333333333333(1)	0.05000000000000	0.03571428571429
	4	g	0.01337996093554(5)	0.01000000000000	0.00778702514725
		e	0.03958614075938	0.02500000000000(4)	0.01938688789623
	6	g	0.00404573514810	0.00343014626071	0.00291641684372
		e	0.00890235253724	0.00606707008623	0.00468524599259
		e	0.02304915190338	0.01711506721549	0.01417651105557
		e	0.05844285778565	0.03965895252427	0.03017655861841
	8	g	0.00169910717517	0.00151575652301	0.00135563312154
		e	0.00326661504755	0.00253598704899	0.00203265499562
		e	0.00563875253622	0.00412145134063	0.00339412325617
		e	0.01040942255739	0.00824400136608	0.00670121318725
		e	0.01653602158660	0.01329159554766	0.01137236016318
		e	0.03180329263192	0.02138083910939	0.01706956908545
	10	g	0.00086575722262	0.00079244596296	0.00072696957550
		e	0.00147907803884	0.00126081972751	0.00107688670338
		e	0.00241664809384	0.00181507622152	0.00147682860631
		e	0.00334850037594	0.00292405665076	0.00255098333227
		e	0.00397594182269	0.00318249275883	0.00273000792956
		e	0.00736429574821	0.00526294300755	0.00417905341741
		e	0.01303363861242	0.01091689148853	0.00954248742578
		e	0.01973176390413	0.01510846119750	0.01275915629739
		e	0.04608252623918	0.03333142555505	0.02636159496028
1	2	g	0.03571428571429	0.02777777777778(2)	0.02272727272727(3)
	4	g	0.00707894326171	0.00591390023109	0.00504676075803
		e	0.02581579358039	0.01964372058675	0.01616733845868
	6	g	0.00254580870206	0.00223524705023	0.00197793631977
		e	0.00563638108171	0.00451759211533	0.00379720216639
		e	0.01883419465413	0.01489720978500	0.01259718274291
		e	0.02725999959457	0.02265588831769	0.01934687713121
	8	g	0.00119038526800	0.00107801657618	0.00097964051831
		e	0.00217041875920	0.00183191437804	0.00158115925765
		e	0.00436490208339	0.00352808023992	0.00300865314483
		e	0.00573812529618	0.00498357626059	0.00437993535596
		e	0.01453566471300	0.01198041559842	0.01037221561899
		e	0.02126492440705	0.01697086960871	0.01435335804110
	10	g	0.00064917903905	0.00059949900156	0.00055475656842
		e	0.00105825552161	0.00093052390433	0.00082578168452
		e	0.00178623911003	0.00148750195578	0.00128288767589
		e	0.00215173389288	0.00193434188304	0.00174595176146
		e	0.00344914023386	0.00286801805941	0.00249502584282
		e	0.00477115358052	0.00395655886157	0.00340206703840
		e	0.01179464597863	0.01002739489760	0.00884019961249
		e	0.01632356905207	0.01328778382152	0.01143529433090
		e	0.02247241353174	0.01936642452391	0.01698248977049

(a) g = ground state; e = excited state;
(b) Numbers in parentheses are the listing number in Table 5-3.

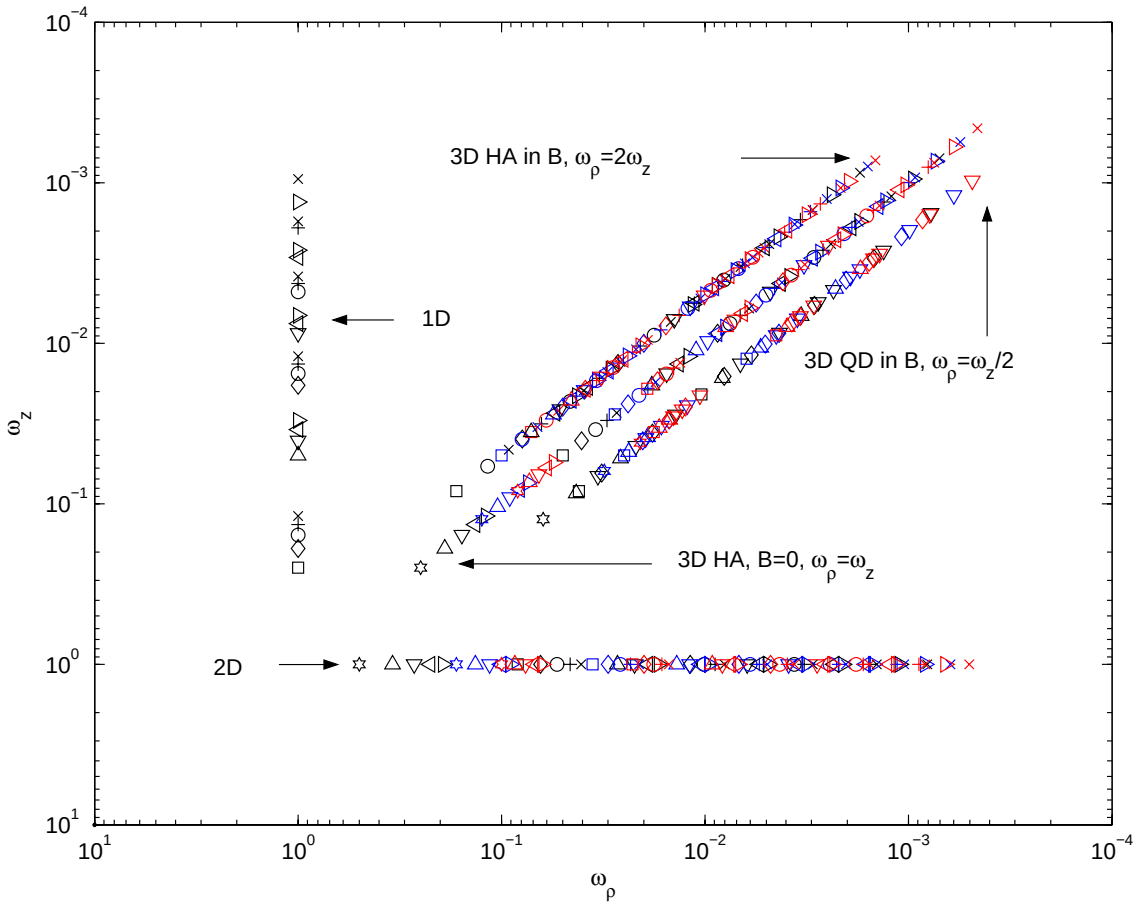

FIG. 5-1 Confinement strengths subject to analytical solution to eqn. (5.12). For 1D, $\omega_\rho = \infty$ has been shifted to $\omega_\rho = 1$. For 2D, $\omega_z = \infty$ has been shifted to $\omega_z = 1$. Hexagon, square, up-triangle, diamond, down-triangle, circle, left-triangle, plus, right-triangle, and x-mark stand for the highest order of z in 1D, ρ in 2D, r in the 3D spherical HA, $t = (r \pm z)/2$ in QD, in the polynomial part of the relative motion wavefunctions being 1,2,…,10, respectively. For HA in a B field, they stand for $N_z + \pi_z$. Black, blue, and red symbols are for $m = 0$, 1, 2, respectively. For spherical HA, only $\pi_z = 0$ is included. Notice its odd parity $(\pi_z = 1, m)$ and even parity states $(\pi_z = 0, m+1)$ are degenerate.

For another case of $\omega_\rho = \omega_z / 2$, which can be thought as a two-electron quantum dot (QD) in a suitable magnetic field, one can also find analytical solutions to eqn. (5.12) for some specific confinement frequencies. Together with two limiting cases of 1D and 2D, they are summarized in reference 122. Figure 5-1 shows those frequencies subject to analytical solutions to the electron relative motion part.

Table 5-3 Some solutions to eqn. (5.12) for confinement potential $\omega = 2\omega_z, B = 2\sqrt{3}\omega$

#	ω	Relative Motion Wavefunction
1	$1/6$	$e^{-\left(z^2+2\rho^2\right)/24}\left(1+r/2+z^2/12\right)$
2	$1/18$	$e^{-\left(z^2+2\rho^2\right)/72}\rho z\left(1+r/6+z^2/108\right)e^{i\varphi}$
3	$1/22$	$e^{-\left(z^2+2\rho^2\right)/88}\rho^2 z\left(1+r/8+z^2/176\right)e^{2i\varphi}$
4	$1/20$	$e^{-\left(z^2+2\rho^2\right)/80}\rho\left(1+r/4-z^2/40+\rho^2/80-rz^2/160-z^4/3200\right)e^{i\varphi}$
5	$\frac{25-3\sqrt{17}}{472}$	$e^{-\omega\left(z^2+2\rho^2\right)/4}\left(1+\frac{r}{2}+\frac{1-22\omega}{48}rz^2+\frac{1+2\omega}{24}r^2+\frac{1-18\omega}{8}z^2+\frac{11-314\omega}{11328}z^4\right)$

Hooke's Atom in *B* Field, Numerical Solution

For arbitrary ω and *B* values, eqn. (5.12) does not have an analytical solution. To have a clear picture for the dependence of the HA system behavior upon increasing ω or *B* field, more data points are essential.

Expansion of the wavefunction in terms of spherical harmonics is satisfactory when the *B* field is not too large. For large *B* values, Landau orbitals are used for expansion. Consider the low-field expansion first.

Spherical expansion:

$$\psi_r^m(\vec{r}) = \sum_l \frac{1}{r} f_{lm}(r) Y_{lm}(\theta,\varphi) \tag{5.25}$$

Insertion of the foregoing expansion together with the Hamiltonian (5.12) in the relative motion Schrödinger equation gives a set of coupled differential equations,

$$-E_r f_{lm}(r) - \frac{d^2}{dr^2} f_{lm}(r) + \sum_{l'} V_{eff}^{ll'm}(r) f_{l'm}(r) = 0$$

$$(l = 0, 2, 4, \ldots \text{ or } l = 1, 3, 5, \ldots) \tag{5.26}$$

where the effective potential is

$$V_{eff}^{ll'm}(r)=\left\langle Y_{lm}(\theta,\varphi)\left|\frac{l(l+1)}{r^2}+\frac{1}{r}+\frac{m}{2}B+\frac{\omega^2}{4}r^2+\frac{B^2}{16}r^2\sin^2\theta\right|Y_{l'm}(\theta,\varphi)\right\rangle$$
$$=\delta_{ll'}\left(\frac{l(l+1)}{r^2}+\frac{1}{r}+\frac{m}{2}B+\frac{\omega^2}{4}r^2+\frac{B^2}{24}r^2\right)-\frac{B^2}{24}r^2\sqrt{\frac{2l+1}{2l'+1}}(l0,20\,|\,l'0)(lm,20\,|\,l'm) \tag{5.27}$$

and $(lm,l''m''\,|\,l'm')$ is a Clebsch-Gordon coefficient. This procedure is very similar to Ruder *et al*.'s method for treating the hydrogen atom in strong magnetic fields[78]. The numerical solver for eqn. (5.26) was obtained from reference 124, with appropriate modifications made to adapt it to this problem.

Next turn to the strong field case, which requires a cylindrical expansion. The expansion used is:

Cylindrical expansion:

$$\psi_r^m(\vec{r})=\sum_n g_{nm}(z)\phi_{nm}^{Lan}(\rho,\varphi) \tag{5.28}$$

$$-E_r g_{nm}(z)-\frac{d^2}{dz^2}g_{nm}(z)+\sum_{n'}V_{eff}^{nn'm}(z)g_{n'm}(z)=0 \qquad (n = 0, 1, 2, \ldots) \tag{5.29}$$

where the effective potential

$$V_{eff}^{nn'm}(z)=\left\langle\phi_{nm}^{Lan}(\rho,\varphi)\left|\frac{1}{r}\right|\phi_{n'm}^{Lan}(\rho,\varphi)\right\rangle+\delta_{nn'}\left[\frac{\omega^2}{4}z^2+\frac{m}{2}B+2\omega_L\left(2n+|m|+1\right)\right] \tag{5.30}$$

and $\omega_L=\dfrac{\Omega_L}{4}=\dfrac{\sqrt{4\omega^2+B^2}}{4}$.

Calculating the effective potential $V_{eff}^{nn'm}(z)$ is not trivial. I followed Pröschel *et al.*'s scheme [125]. Details are included in appendix D.

By use of a similar argument as in reference 90, we can screen out the configurations pertaining to the HA global ground states in *B* field, which are (m = 0, $\pi_z=0$), (m = -1, $\pi_z=0$), and (m = -3, $\pi_z=0$). Energies for the relative motion and spin

parts are compiled in Table E-1 and E.2 for two angular frequencies, ω = 0.5, 0.1, respectively. States are labeled by their conserved quantities as $\nu^{\,2S+1}m^{(-)^{\pi_z}}$, where (2*S*+1) is the spin multiplicity, and ν is the degree of excitation within a given subspace. Their field-free notations are also included (e.g. 1*s*, 2*p*, …). The larger confinement frequency corresponds to the first analytical solution found by Kais, Herschbach, and Levine [108], and is also the most widely studied one. The smaller frequency has two analytical solutions, one for the 1*s* state in $B = 0$ and another for the $2p_{-1}$ state in $B = \sqrt{3}/5$. A sixteen spherical function expansion gives the relative motion energy of the latter state to be 0.4767949192445 Hartree, pleasingly accurate compared to the analytical result

$$E_r = \left[\left(N_z + \pi_z + 2|m|\right) + \frac{5}{2} + \sqrt{3}m\right]\omega = \left[\left(2+0+2\right) + \frac{5}{2} - \sqrt{3}\right] * 0.1 = 0.47679491924311$$

For Tables E.1 and E.2, numbers in parentheses denote the number of radial functions used in expansion (5.25); numbers in brackets are the number of Landau orbitals used in eqn. (5.28). It is easy to see that, in the low field regime ($B < 1$ au.), the spherical expansion outperforms the cylindrical expansion. However, its quality degrades as the *B* field increases. As Jones *et al.* have found and as is physically obvious, the high field regime is very demanding for a spherical basis [93]. Note in Table E-2, for $B = 10$ au., the spherical expansion corresponds to $l_{\max} = 48{,}49$. Clearly, it cannot go much further on practical grounds.

The analytical solution for the singlet state of $\omega = \frac{1}{10}$ in vanishing *B* field is

$$\psi_r(\vec{r}) = \frac{1}{\sqrt{10\pi\left(240 + 61\sqrt{5\pi}\right)}}\left(1 + \frac{r}{2} + \frac{r^2}{20}\right)e^{-\frac{r^2}{40}} \qquad (5.31)$$

with eigenvalue $E_r = \frac{7}{20}$, ($\omega = \frac{1}{10}$, $m = 0$, $B = 0$, singlet)

Its density distribution is

$$n(r)=\frac{\sqrt{2}}{10\pi\left(240+61\sqrt{5\pi}\right)}\left\{\sqrt{\frac{2}{5\pi}}\left(r^2+45\right)e^{-\frac{r^2}{5}}+\left[\frac{r^4+190r^2+2875}{100}+\left(\frac{r^3}{5}+10r+\frac{35}{r}\right)erf\left(\frac{r}{\sqrt{10}}\right)\right]e^{-\frac{r^2}{10}}\right\} \quad (5.32)$$

For very small B field, the diamagnetic term in eqn. (5.12) can be treated as a perturbation. Thus the first order correction

$$E_r^{(1)}(B\to 0)=\frac{B^2}{16}\int\left|\psi_r(\vec{r})\right|^2 r^2\sin^2\theta d\vec{r}=\frac{B^2}{16}\cdot\frac{8\pi}{3}\int_0^\infty\psi_r^2(r)r^4dr=2.228B^2$$

Compared with the second column in Table E-2, this diamagnetic correction term is quite accurate up to $B = 0.1$ au.

In super-strong fields ($B >> 1$), one expects the adiabatic approximation to be applicable. The electron-electron interaction term is treated as a perturbation. By omitting the $\frac{1}{r}$ term in eqn. (5.12), the resulting Hamiltonian looks very similar to eqn.(5.11), and an analytical unperturbed solution exists

$$\lim_{B\to\infty}\psi_r^{(0)}=e^{-\frac{\omega}{4}z^2-\frac{\omega_L}{2}\rho^2}\cdot\rho^{|m|}\cdot H_{n_z}\left(\sqrt{\frac{\omega}{2}}z\right)\cdot{}_1F_1\left(-n_\rho,|m|+1,\omega_L\rho^2\right)\cdot e^{im\varphi} \quad (5.33)$$

$$\lim_{B\to\infty}E_r^{(0)}(B)=\left(n_z+\frac{1}{2}\right)\omega+\left(n_\rho+\frac{|m|+1}{2}\right)4\omega_L+\frac{m}{2}B \quad (5.34)$$

For the three configurations included in Table E-2, $n_z = n_\rho = 0$, the preceding two equations are reduce to

$$\lim_{B\to\infty}\psi_r^{(0)}=e^{-\frac{\omega}{4}z^2-\frac{\omega_L}{2}\rho^2}\cdot\rho^{|m|}\cdot e^{im\varphi} \quad (5.33')$$

$$\lim_{B\to\infty} E_r^{(0)}(B) = \frac{\omega}{2} + 2\left(|m|+1\right)\omega_L + \frac{m}{2}B$$

$$= \frac{\omega}{2} + \frac{1}{2}\sqrt{4\omega^2 + B^2} + \frac{m}{2}\left(B + \frac{|m|}{m}\sqrt{4\omega^2 + B^2} \right) \qquad (5.34')$$

$$= \frac{B}{2} + \frac{\omega}{2} + (1-m)\frac{\omega^2}{B}$$

As can be seen in Table E-2, the first term $\frac{B}{2}$ in eqn. (5.34') dominates all other energy components in the high field limit. The first two terms comprise the zero point energy of the magnetized oscillator.

One might attempt a perturbative calculation for the interacting term $\frac{1}{r}$ using the wavefunction (5.33'). The result is really disappointing. Choose the singlet state (m = 0, $\omega = \frac{1}{10}$, B = 1000), and evaluate the expectation value of $\frac{1}{r}$. We get 1.25 Hartree, which is far off from the desired value of ~0.3. The immediate response is to go to the second order, but soon we will see that the result does not get any better. From eqn. (5.34) we can see that the most important states involved are $n_z = 2, 4, 6, \cdots$

$$E_r^{(2)} = \frac{\left| \left\langle n_z = 0 \left| \frac{1}{r} \right| n_z = 2 \right\rangle \right|^2}{-2\omega} + \frac{\left| \left\langle n_z = 0 \left| \frac{1}{r} \right| n_z = 4 \right\rangle \right|^2}{-4\omega} + \cdots$$

$$= -2.487 - 0.782 - \cdots$$

A standard perturbative calculation does not perform very well. This is because the most significant contribution of the term $\frac{1}{r}$ is from the small r region, exactly the place where the B field can least affect the wavefunction. If we "graft" the correlation part in

eqn. (5.31) to eqn. (5.33'), and use this guessed wavefunction $\left(1+\frac{r}{2}+\frac{r^2}{20}\right)e^{-\frac{\omega}{4}z^2-\frac{\omega_L}{2}\rho^2}$ to evaluate the expectation value of $\frac{1}{r}$ term, we get 0.365 Hartree, which is not too bad. This is one demonstration that the *B* field does not affect the short-distance electron interaction too much.

Phase Diagram for Hooke's Atom in *B* Field

As with what we have seen in the previous chapter for real atoms, application of an external magnetic field also causes a series of configuration changes for HA. For the helium atom, there is only one transition from $1s^2$ state to $1s2p_{-1}$ state, but there are more configurations involved for the HA. To see a complete picture of the evolution of this model system with increasing *B* field, the spin energy should also be considered (recall

Table 5-4 Field strengths for configuration changes for the ground states of Hooke's atom

ω	B_{c1}* (au)	B_{c2}** (au)
0.001896558822	0.0002047	0.00177
0.0038233443	0.000522	0.00445
0.01	0.00187	0.01625
0.02	0.00466	0.04172
0.05	0.01523	0.14596
0.1	0.03642	0.3785
0.2	0.0849	0.987
0.5	0.2493	3.54
1	0.547	9.36
2	1.172	24.91
4	2.47	67.05
10	6.48	247.1
20	13.29	
40	27.06	
100	68.74	

* For the transition from singlet state (m = 0) to triplet state (m = -1);
** For the transition within triplet state, from m = -1 configuration to the maximum density droplet (MDD) state, which has m = -3.

eqn. 5.10). However, the CM motion part can be neglected, since it is the same for all the states that could possibly be the ground state.

For vanishing B field, the ground state of a HA is a singlet state (one electron spin up, the other spin down). With increasing B field, sooner or later the spin down electron will be flipped, and a triplet state becomes the ground state. Further increase of the field will cause configuration transitions within triplet states, and the m value becomes more and more negative. Table 5-4 lists the critical field strengths for the first two transitions. The ground state phase diagram in the $\omega - B$ plane is shown in Fig. 5-2.

For the confinement frequency $\omega = 0.1$ considered in the previous section, the first transition occurs at $B \approx 0.036$, accompanied by a spin flip (singlet to triplet). The m = -1 configuration remains as the ground state until B is increased to 0.38 au., then the m = -3 state takes over. This establishes that the m = -1 configuration is the global ground state at $B = \frac{\sqrt{3}}{5} = 0.34641$ au.

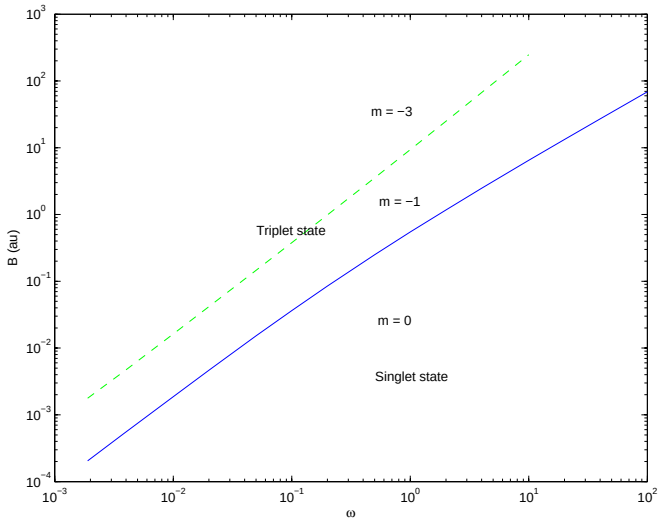

FIG. 5-2 Phase diagram for the Hooke's atom in B fields

Electron Density and Paramagnetic Current Density

With the wavefunction of the Hooke's Atom, we can easily get its electron density distribution by integrating out one variable.

$$n(\vec{r}) = 2\int \left|\psi_{CM}\left(\vec{r}+\frac{\vec{r}'}{2}\right)\psi_r(\vec{r}')\right|^2 d\vec{r}' \tag{5.35}$$

This 3D integral can be reduced to a 2D integral. First we express the CM motion part as the product of a Landau orbital and a function about *Z*,

$$\psi_{CM}\left(\vec{R}\right) = g_{NM}(Z)\phi_{NM}^{Lan}(P,\phi) \tag{5.36}$$

Next notice that $\left|\psi_r(\vec{r}')\right|^2$ does not depend on φ'. Thus

$$n(\vec{r}) = n(\rho, z)$$

$$= 4\int_0^\infty \left[\int_0^\pi \left|\phi_{NM}^{Lan}\left(\left(\rho^2+\rho'^2/4+\rho\rho'\cos\varphi'\right)^{1/2},\phi\right)\right|^2 d\varphi'\right]\left[\int_{-\infty}^{\infty} g_{NM}^2\left(z+\frac{z'}{2}\right)\left|\psi_r(\rho',z',\varphi')\right|^2 dz'\right]\rho' d\rho' \tag{5.37}$$

where ϕ is the azimuthal angle of $\vec{r}+\frac{\vec{r}'}{2}$ but it is a dummy variable, thus not need to be evaluated. Another dummy variable is φ' in $\left|\psi_r(\vec{r}')\right|^2$. They facilitate the separation of integrals $\int d\varphi'$ and $\int dz'$. Otherwise, the separation in eqn. (5.37) is not possible.

Recall from Chap. 1 that the paramagnetic current density $\vec{j}_p(\vec{r})$ is the expectation value of the $\vec{J}_p^{op}(\vec{r})$ operator

$$\vec{j}_p(\vec{r}) = \iint \psi_{CM}^*\left(\vec{R}\right)\psi_r^*(\vec{r}_{12})\vec{J}_p^{op}(\vec{r})\psi_{CM}\left(\vec{R}\right)\psi_r(\vec{r}_{12})\,d\vec{R}\,d\vec{r}_{12} \tag{5.38}$$

where $\vec{J}_p^{op}(\vec{r}) = \frac{1}{2i}\left[\hat{\Psi}^+(\vec{r})\nabla\hat{\Psi}(\vec{r}) - \hat{\Psi}(\vec{r})\nabla\hat{\Psi}^+(\vec{r})\right]$ (5.39)

Here the relative coordinate is explicitly labeled as $\vec{r}_{12} = \vec{r}_2 - \vec{r}_1$ to avoid confusion, and $\hat{\Psi}^+(\vec{r})$ and $\hat{\Psi}(\vec{r})$ are second quantized field creation and annihilation operators. After substitution we reach the following expression

$$\vec{j}_p(\vec{r}) = \hat{\varphi}_{\vec{r}} j_p(\rho, z)$$

$$= \hat{\varphi}_{\vec{r}} m \int_0^{\infty} \left[4 \int_0^{\pi} \left| \phi_{NM}^{Lan} \left(\left(\rho^2 + \rho'^2/4 + \rho\rho' \cos\varphi' \right)^{1/2}, \phi \right) \right|^2 \cos\varphi' d\varphi' \right] \left[\int_{-\infty}^{\infty} g_{NM}^2 \left(z + \frac{z'}{2} \right) \left| \psi_r(\rho', z', \varphi') \right|^2 dz' \right] d\rho' \tag{5.40}$$

The integrals in eqns (5.37) and (5.40) are evaluated numerically, using a 20-point Gauss-Legendre integral for $\int d\varphi'$, and a 40-point Gauss-Laguerre quadrature integral for $\int dz'$ and $\int d\rho'$ [126].

Next I use the ground state of HA with confinement frequency $\omega = \frac{1}{10}$ in $B = \frac{\sqrt{3}}{5}$ for example, which has an analytical wavefunction. Its CM part can be easily obtained from eqn. (5.15) and eqn. (5.16),

$$\psi_{CM}(\vec{R}) = \frac{\sqrt{2}}{(5\pi)^{3/4}} e^{-\frac{Z^2}{10} - \frac{P^2}{5}}, \text{ with eigenvalue } E_{CM} = \frac{1}{4}. \tag{5.41}$$

Its relative motion part is

$$\psi_r(\vec{r}) = A \left(1 + \frac{r}{4} + \frac{z^2}{40} \right) \rho \cdot e^{-\frac{z^2 + 2\rho^2}{40}} e^{-i\varphi} \tag{5.42}$$

where the normalization factor is

$$A = \left\{ \frac{25\pi}{4} \left[114\sqrt{5\pi} + 300 + 55\sqrt{2}\, \mathrm{Re}\left(\tanh^{-1}\left(\frac{3}{\sqrt{8}} \right) \right) \right] \right\}^{-1/2} = 0.007569227363.$$

with eigenvalue of $E_r = \dfrac{13-2\sqrt{3}}{20}$.

For Hooke's atom, the total electron number $N = 2$. The pair density for this example is

$$\bar{n}_2(r) = \frac{1}{4\pi N}\int \left|\psi_r(\vec{r})\right|^2 d\Omega_{\vec{r}}$$

$$= -\frac{A^2}{32}\left\{2\left(4r^2+10r+35\right)e^{-r^2/20} + i\sqrt{5\pi}\left(r^3+6r^2+21r+20+\frac{70}{r}\right)erf\left(\frac{ir}{\sqrt{20}}\right)e^{-r^2/10}\right\} \quad (5.43)$$

where $erf(x)$ is the error function. One can integrate this expression to make a check,

$4\pi\int_0^\infty \bar{n}_2(r)\,r^2 dr = \dfrac{1}{2}$, just as expected, since $4\pi\dfrac{1}{4\pi N}\int\left|\psi_r(\vec{r})\right|^2 d\vec{r} = \dfrac{1}{N} = \dfrac{1}{2}$.

Its electron density is

$$n(\vec{r}) = 2\int\left|\psi_{CM}\left(\vec{r}+\frac{\vec{r}'}{2}\right)\psi_r(\vec{r}')\right|^2 d\vec{r}'$$

$$= \frac{4A^2}{(5\pi)^{3/2}}\int_0^\infty\left\{\left[\int_{-\infty}^{+\infty} e^{-\frac{\left(z+\frac{z'}{2}\right)^2}{5}}\left(1+\frac{\sqrt{z'^2+\rho'^2}}{4}+\frac{z'^2}{40}\right)^2 e^{-\frac{z'^2}{20}}dz'\right]\rho'^2 e^{-\frac{\rho'^2}{10}}\left[\int_0^{2\pi} e^{-\frac{2}{5}\left(\rho^2+\frac{\rho'^2}{4}+\rho\rho'\cos\varphi'\right)}d\varphi'\right]\right\}\rho' d\rho' \quad (5.44)$$

and paramagnetic current density

$$\vec{j}_p(\vec{r}) = -\hat{\varphi}_r\cdot\frac{4A^2}{(5\pi)^{3/2}}\int_0^\infty\left\{\left[\int_{-\infty}^{+\infty} e^{-\frac{\left(z+\frac{z'}{2}\right)^2}{5}}\left(1+\frac{\sqrt{z'^2+\rho'^2}}{4}+\frac{z'^2}{40}\right)^2 e^{-\frac{z'^2}{20}}dz'\right]\rho'^2 e^{-\frac{\rho'^2}{10}}\left[\int_0^{2\pi} e^{-\frac{2}{5}\left(\rho^2+\frac{\rho'^2}{4}+\rho\rho'\cos\varphi'\right)}\cos\varphi' d\varphi'\right]\right\}d\rho' \quad (5.45)$$

Their distributions are shown in Fig. 5-3. The difficulty involved in using

$\vec{v} = \nabla\times\left(\vec{j}_p/n\right)$ as a CDFT parameter is evident from studying that figure.

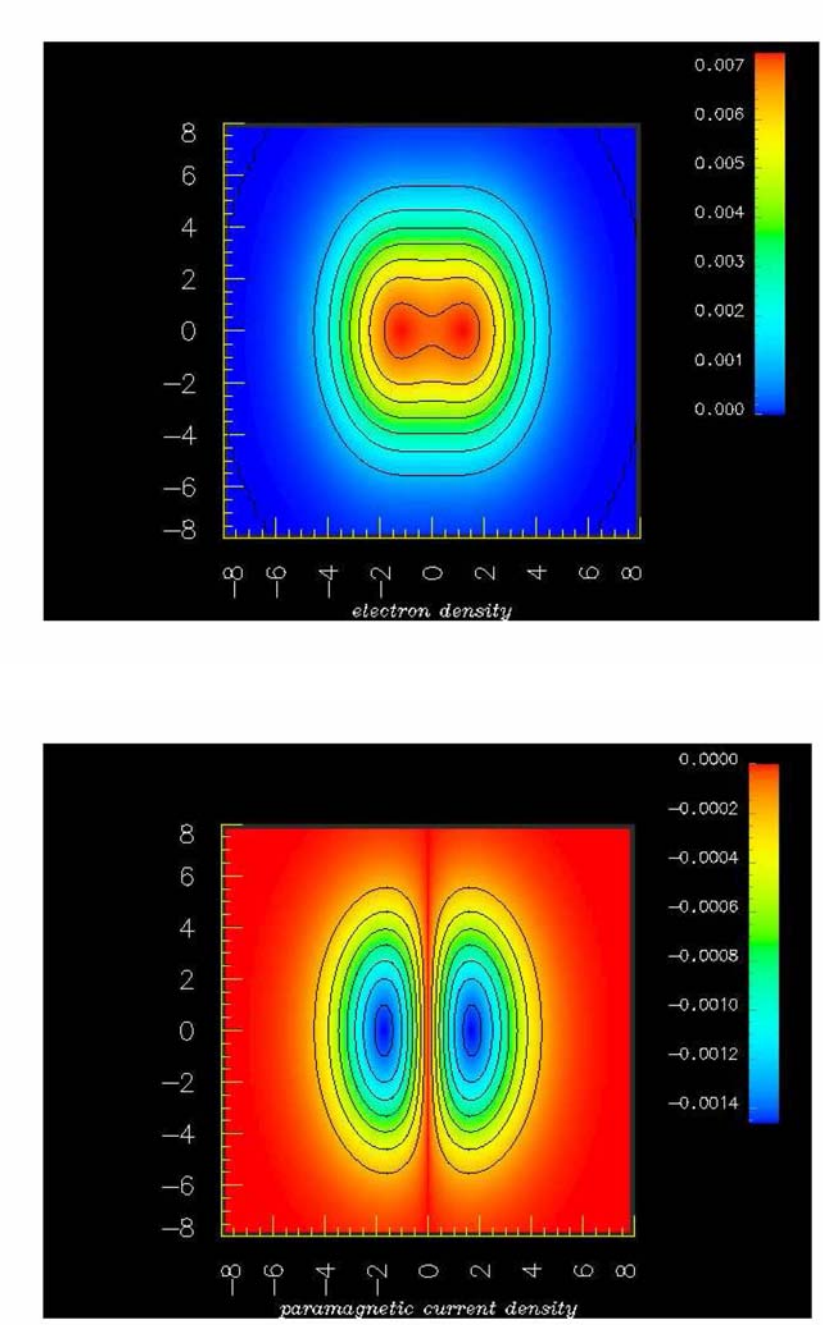

FIG. 5-3 Cross-sectional view of the electron density $n(\rho, z)$ (upper) and paramagnetic current density $j_p(\rho, z)$ (bottom) for the ground state HA with ω = 1/10 in $B = \sqrt{3}/5$. The B field orientation is in the plane of the paper from bottom to top.

Their large *r* limits are (large *r* means that both *z* and ρ become arbitrarily large):

$$\lim_{\substack{\rho\to\infty \\ z\to\infty}} n(\vec{r}) = \frac{\sqrt{2}}{400} A^2 z^4 \left(\rho^2 + 5\right) e^{-\frac{z^2}{10} - \frac{\rho^2}{5}} \tag{5.46}$$

$$\lim_{\substack{\rho\to\infty \\ z\to\infty}} \vec{j}_p(\vec{r}) = -\hat{\varphi}_r \cdot \frac{\sqrt{2}}{400} A^2 z^4 \rho\, e^{-\frac{z^2}{10} - \frac{\rho^2}{5}} \tag{5.47}$$

Now we are ready to construct exact KS orbitals for this state of the HA.

Construction of Kohn-Sham Orbitals from Densities

The Hooke's atom singlet ground state can be inverted easily to obtain KS orbitals [113], since the spatial parts are the same for two KS particles. Each of them contributes one half of the total density, thus the KS orbital is just the square root of one half of the total density. (for KS orbitals, $\vec{r}$ always means $\vec{r}_1$ or $\vec{r}_2$)

Singlet state (*m* = 0):

$$\phi_1^{KS}(\vec{r}) = \phi_2^{KS}(\vec{r}) = \sqrt{\frac{n(\vec{r})}{2}} \tag{5.48}$$

However, we need to use a current-carrying ground state to study the paramagnetic current effect within the framework of CDFT. Those are triplet states. According to CDFT, the KS system must generate the exact electron density and paramagnetic current density. A choice of triplet KS orbitals that fulfills this requirement for this two-electron system is as follows:

Triplet state (*m* = -1):

$$\phi_1^{KS}(\vec{r}) = \left|\phi_1^{KS}(\vec{r})\right| = \sqrt{n(\vec{r}) - \left|\phi_2^{KS}(\vec{r})\right|^2}$$

$$\phi_2^{KS}(\vec{r}) = e^{-i\varphi}\left|\phi_2^{KS}(\vec{r})\right| = e^{-i\varphi}\sqrt{-\rho j_p(\rho, z)} \tag{5.49}$$

I did this construction independently before becoming aware of a similar procedure having been used in reference 127. Their model is a 2D quantum dot, whereas my model is the 3D magnetized HA. An issue not addressed in reference 127 is that the orbitals so constructed should be properly normalized, otherwise the construction is invalid (or at least, incomplete). Numerical checking proves that the constructed KS orbitals in eqn. (5.49) indeed are normalized. For the special analytical solution to the ground state of $\left(\omega=\frac{1}{10}, B=\frac{\sqrt{3}}{5}\right)$, one can demonstrate this rigorously as follows.

With the expression (5.45) for $\vec{j}_p(\vec{r})$, let us rearrange the integrals,

$$\int\left|\phi_2^{KS}(\vec{r})\right|^2 d\vec{r}=-\int \rho j_p(\rho,z)\,d\vec{r}=2\frac{2A^2}{(5\pi)^{3/2}}2\pi\int_0^{\infty} I_1 I_2 \rho'^2 e^{-\frac{\rho'^2}{10}}d\rho'$$

where $I_1=\int_{-\infty}^{+\infty}\int_{-\infty}^{+\infty} e^{-\frac{(z+z'/2)^2}{5}}\left(1+\frac{\sqrt{\rho'^2+z'^2}}{4}+\frac{z'^2}{40}\right)^2 e^{-\frac{z'^2}{20}}dzdz'$

$$I_2=\int_0^{2\pi}\int_0^{\infty} e^{-\frac{2}{5}\left(\rho^2+\rho'^2/4+\rho\rho'\cos\varphi'\right)}\rho^2 d\rho\cos\varphi' d\varphi'$$

To evaluate I_2, consider the following two identities,

$$I_3=\int_0^{2\pi}\left[erf\left(\frac{\rho'\cos\varphi}{\sqrt{10}}\right)-1\right]e^{\rho'^2\cos^2\varphi/10}\cos\varphi d\varphi=\frac{2\sqrt{10\pi}}{\rho'}\left(e^{\rho'^2/10}-1\right)$$

$$I_4=\int_0^{2\pi}\left(15+\rho'^2\cos^2\varphi\right)\left[erf\left(\frac{\rho'\cos\varphi}{\sqrt{10}}\right)-1\right]e^{\frac{\rho'^2\cos^2\varphi}{5}}\cos\varphi d\varphi=4\sqrt{10\pi}\left[\frac{5}{\rho'}\left(e^{\frac{\rho'^2}{10}}-1\right)+\frac{\rho'}{2}\left(e^{\frac{\rho'^2}{10}}-\frac{1}{2}\right)\right]$$

Thus,

$$I_2=-e^{-\frac{\rho'^2}{10}}\int_0^{2\pi}\left\{\frac{5}{8}\rho'\cos\varphi'+\frac{\sqrt{10\pi}}{16}\left(5+\rho'^2\cos^2\varphi'\right)\left[erf\left(\frac{\rho'\cos\varphi'}{\sqrt{10}}\right)-1\right]e^{\frac{\rho'^2\cos^2\varphi'}{10}}\right\}\cos\varphi' d\varphi'$$

$$= -e^{-\frac{\rho'^2}{10}}\left\{\frac{5\pi}{8}\rho' + \frac{\sqrt{10\pi}}{16}\left(I_4 - 10I_3\right)\right\}$$

$$= \frac{5\pi}{4}\rho'$$

The integral $\int dz$ is easy, $\int_{-\infty}^{+\infty} e^{-\frac{(z+z'/2)^2}{5}} dz = \sqrt{5\pi}$. Finally,

$$\int \left|\phi_2^{KS}(\vec{r})\right|^2 d\vec{r} = 2\pi A^2 \int_0^{\infty} \rho' d\rho' \int_{-\infty}^{+\infty} dz' e^{-\frac{z'^2}{20} - \frac{\rho'^2}{10}} \left(1 + \frac{r'}{4} + \frac{z'^2}{40}\right)^2 \rho'^2$$

$$= \int \left|\psi_r(\vec{r}')\right|^2 d\vec{r}' = 1.$$

By construction, $\phi_1^{KS}(\vec{r})$ is also properly normalized provided $\phi_2^{KS}(\vec{r})$ is normalized.

The large *r* limits for the two KS orbitals in the previous example are,

$$\lim_{\substack{\rho\to\infty \\ z\to\infty}} \phi_1^{KS}(\vec{r}) = \frac{2^{1/4}\sqrt{5}}{20} Az^2 e^{-\frac{z^2}{20} - \frac{\rho^2}{10}} \tag{5.50}$$

$$\lim_{\substack{\rho\to\infty \\ z\to\infty}} \phi_2^{KS}(\vec{r}) = \frac{2^{1/4}}{20} Az^2 \rho e^{-\frac{z^2}{20} - \frac{\rho^2}{10}} e^{-i\varphi} \tag{5.51}$$

Exact DFT/CDFT Energy Components and Exchange-correlation Potentials

Each of the energy components can be calculated straightforwardly according to their definitions. Recall discussion in Chapter 1, the kinetic energy for the KS system, T_s, is the expectation value of the kinetic energy operator with respect to the KS orbitals. The difference between T_{tot} and T_s, namely T_c, is the kinetic energy contribution to the DFT correlation energy. The exact exchange energy is calculated from the single-determinant (i.e. HF) exchange formula but with the KS orbitals. *J* is the classical electrostatic energy, and E_c the DFT correlation energy.

$$T_s = t_1 + t_2 = \left\langle \phi_1^{KS} \left| \frac{-\nabla^2}{2} \right| \phi_1^{KS} \right\rangle + \left\langle \phi_2^{KS} \left| \frac{-\nabla^2}{2} \right| \phi_2^{KS} \right\rangle \tag{5.52}$$

$$T_c = T_{tot} - T_s = \left\langle \psi_r \left| -\nabla^2 \right| \psi_r \right\rangle + \frac{\omega + \sqrt{4\omega^2 + B^2}}{4} - T_s \tag{5.53}$$

$$E_x^{exact} = -\frac{1}{2} \sum_{i,j=1}^{2} \iint \frac{\phi_i^{KS}(\vec{r}_1)^* \phi_j^{KS}(\vec{r}_2)^* \phi_j^{KS}(\vec{r}_1) \phi_i^{KS}(\vec{r}_2)}{r_{12}} d\vec{r}_1 d\vec{r}_2 \tag{5.54}$$

$$J = \frac{1}{2} \iint \frac{n(\vec{r}) n(\vec{r}')}{|\vec{r} - \vec{r}'|} d\vec{r} d\vec{r}' \tag{5.55}$$

If we define $V_c^{exact} = E_{ee} - J - E_x^{exact} = \int \frac{|\psi_r(\vec{r})|^2}{r} d\vec{r} - J - E_x^{exact}$ (5.56)

then $E_c^{exact} = V_c^{exact} + T_c$ (5.57)

$$E_{xc}^{exact} = E_x^{exact} + E_c^{exact} \tag{5.58}$$

Notice that for a spin singlet state (m = 0), the exchange energy cancels the electron self-interaction exactly, and $E_x^{exact} = -\frac{J}{2}$. Various energy components for the HA without B field and in a B field for the two confinement frequencies ω = 1/2, 1/10 are listed in Tables E.3 through E.7. Other energy components can be obtained from eqns. (5.52) through (5.58).

As already noted, only results for the HA in a vanishing B field are found in the literature. The most widely studied example is ω = 1/2 [109, 112, 118, 119]. Another frequency ω = 0.0019, which also has an analytical solution (refer to Table 5-1 for the more accurate value corresponding to l = 0, n = 9), was used as a strong-correlation example [114, 115, 120]. Several other frequencies which do not have analytical solutions were investigated from numerical solutions [113]. Cioslowski and Pernal even

did Padé approximants for various quantities in a large range of frequencies [121]. The calculated data in appendix E agree with those given in the literature quite well.

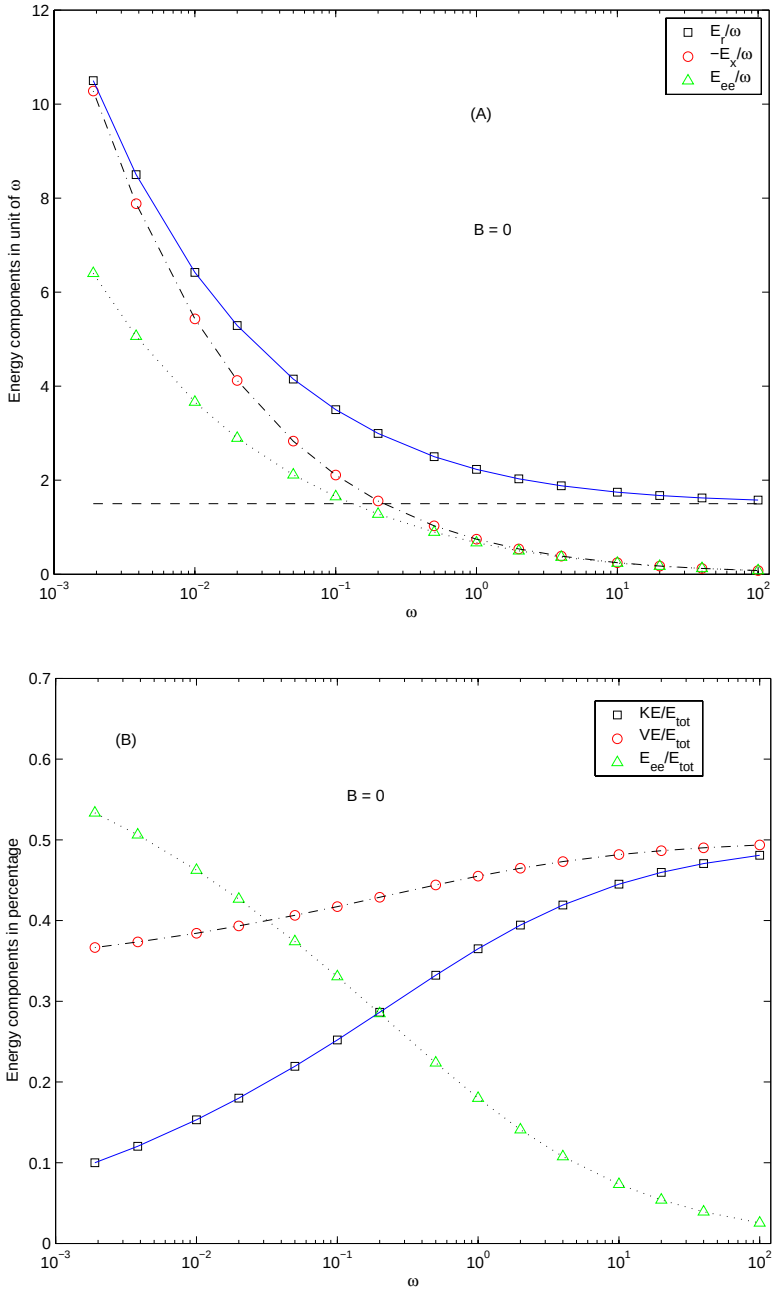

FIG. 5-4 Energy components of HA with $B = 0$. Curves are guides to the eye. In the upper panel, the relative motion total energy E_r (□), negative of the exchange energy $-E_x$ (o), and two-electron interaction energy E_{ee} (Δ) are in units of ω. In panel B, the total kinetic KE (□), potential VE (o), and two-electron E_{ee} (Δ) energies are shown as percentages of the total energy.

Figure 5-4 shows the change in energy contributions with respect to confinement frequency ω without a magnetic field. In the first panel, the energy is divided by ω. The horizontal dashed line is three halves, which is the energy of a 3D harmonic oscillator, and also the relative motion energy for a non-interacting HA. The blue curve is the relative motion total energy. Clearly it goes to the non-interacting limit as ω goes to infinity. The dash dotted curve is the negative of the exchange energy. The dotted curve shows the total electron-electron interaction energy. The difference between them is the static part of the correlation energy, whose percentage contribution to the total energy is significant for very small ω, but negligible in the large-ω limit. Because of this, the small-ω region is also referred to as the strong-correlation regime, while the large-ω region is the weak-correlation regime. This trend is also obvious in panel (B), which displays the percentages of kinetic, external potential, and electron-electron interaction energies in the total energy. Again, both kinetic and potential energies tend to their non-interacting limit, 50%, when ω goes to infinity.

There are only a few papers on the numerical construction of CDFT exchange-correlation vector potential from a supplied density and paramagnetic current density. Besides the work in reference 127 on a 2D QD, Lee and Handy constructed exchange-only vector potentials for 3D systems from HF reference densities by introducing Lagrange multipliers [128]. Again they got involved in the insufficient basis set problem.

In the previous section we have already constructed exact KS orbitals, hence we can invert the CDFT Kohn-Sham eqns. (2.6) and (2.7) to obtain the exact XC potentials for the HA. Since the spin singlet state ($m = 0$) does not carry a current density, there is no CDFT correction to this state. Consider the inversion of the spin triplet state with

m = -1. Notice that $\phi_1^{KS}(\vec{r})$ is an s-like orbital and $\vec{A}_{xc}(\vec{r}) = \hat{\varphi} A_{xc}(\rho, z)$, thus the s-like orbital does not "feel" the vector XC potential, that is $\frac{1}{i}\vec{A}_{xc} \cdot \nabla \phi_1^{KS}(\vec{r}) = 0$. The KS equations for the two KS orbitals therefore are

$$\left[-\frac{\nabla^2}{2} + \left(\tilde{\upsilon}_{ext}(\vec{r}) + \upsilon_H(\vec{r}) + \upsilon_{xc}^{cdft}(\vec{r}) \right) - \frac{B}{2} \right] \phi_1^{KS}(\vec{r}) = \varepsilon_1 \phi_1^{KS}(\vec{r})$$

$$\left[-\frac{\nabla^2}{2} + \left(\tilde{\upsilon}_{ext}(\vec{r}) + \upsilon_H(\vec{r}) + \upsilon_{xc}^{cdft}(\vec{r}) \right) - B + \frac{1}{i}\vec{A}_{xc}(\vec{r}) \cdot \nabla \right] \phi_2^{KS}(\vec{r}) = \varepsilon_2 \phi_2^{KS}(\vec{r})$$

where $\tilde{\upsilon}_{ext}(\vec{r}) = \frac{\omega^2}{2} r^2 + \frac{B^2}{8} r^2 \sin^2\theta$. Hence,

$$\upsilon_{xc}^{cdft}(\vec{r}) = \varepsilon_1 + \frac{1}{2}\frac{\nabla^2 \phi_1^{KS}(\vec{r})}{\phi_1^{KS}(\vec{r})} - \left(\tilde{\upsilon}_{ext}(\vec{r}) + \upsilon_H(\vec{r}) \right) + \frac{B}{2} \tag{5.59}$$

$$-\frac{\vec{A}_{xc}(\vec{r})}{\rho} = \hat{\varphi}_r \left[\left(\varepsilon_2 + \frac{B}{2} - \varepsilon_1 \right) + \frac{1}{2}\left(\frac{\nabla^2 \phi_2^{KS}(\vec{r})}{\phi_2^{KS}(\vec{r})} - \frac{\nabla^2 \phi_1^{KS}(\vec{r})}{\phi_1^{KS}(\vec{r})} \right) \right] \tag{5.60}$$

As Laufer and Krieger pointed out, KS eigenvalues can be found by exploring the large-r limiting behaviors of the KS orbitals [113]. We again use the example of the triplet ground state m = -1, ω = 1/10 in a field $B = \sqrt{3}/5$. Use eqns. (5.50) and (5.51) for their large-r expressions,

$$\varepsilon_1 = \lim_{\substack{\rho\to\infty \\ z\to\infty}} \frac{\left(-\frac{1}{2}\nabla^2 + \tilde{\upsilon}_{ext}(\vec{r}) - \frac{B}{2} \right) \phi_1^{KS}(\vec{r})}{\phi_1^{KS}(\vec{r})} = \frac{9 - 2\sqrt{3}}{20}$$

$$\varepsilon_2 = \lim_{\substack{\rho\to\infty \\ z\to\infty}} \frac{\left(-\frac{1}{2}\nabla^2 + \tilde{\upsilon}_{ext}(\vec{r}) \right) \phi_2^{KS}(\vec{r})}{\phi_2^{KS}(\vec{r})} - B = \frac{13 - 4\sqrt{3}}{20}.$$

It is interesting to observe that ε_2 is just as same as the relative motion energy (excluding the spin part), like Laufer and Krieger's conclusion for the field-free case [113]. Besides, ε_1 equals the relative motion energy (excluding Zeeman energies) for the non-interacting HA with same parameters $\left(\omega = \frac{1}{10}, B = \frac{\sqrt{3}}{5}\right)$, e.g. by omitting $\frac{1}{r}$ repulsion term.

Comparison of Exact and Approximate Functionals

There are two ways to compare the exact KS results obtained in the previous sections with various approximate functionals. The first is to evaluate the approximate functionals using exact densities. The other is to use self-consistent orbitals. Here we choose the former method. Exact and approximate exchange and correlation energies are compiled in Tables E-8 through E-12. Exchange-correlation energies evaluated at the SCF densities are found to be close to those using exact densities.

The chosen functionals include the widely used LDA approximation [69], as well as the gradient-dependent PBE [70], and BLYP [72-75]. A recently proposed current-corrected functional, jPBE [32], is also included.

As already emphasized there are far fewer CDFT functionals than DFT functionals. For practical purposes, the only one available is the VRG local approximation already discussed [14-16]. As shown in previous chapters, this function is rather ill-behaved and requires introduction of a cutoff function. Disappointingly, the current correction term is rather sensitive to the decay rate of that cutoff function. Nevertheless, this is the only functional realistically available, so I tested it.

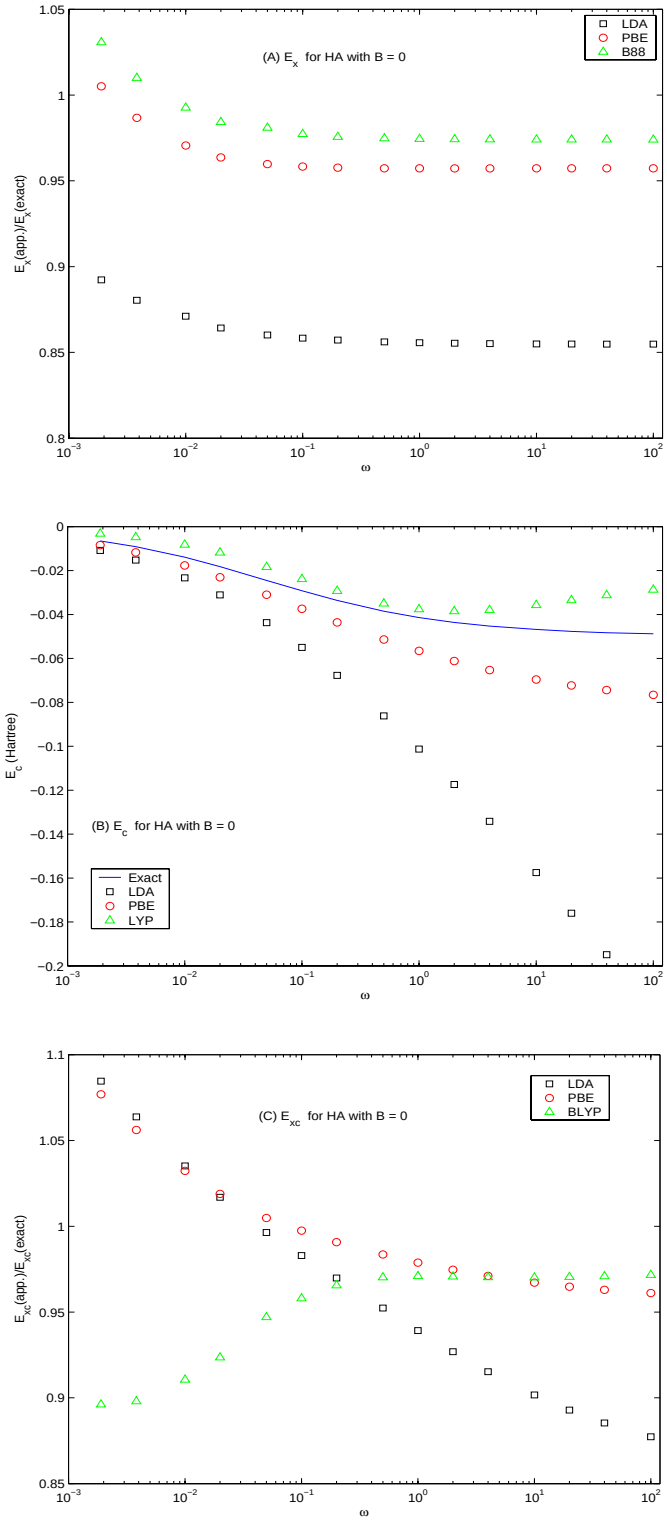

FIG. 5-5 Comparison of exact and approximate XC functionals for the HA with different confinement frequency ω in vanishing B field ($B = 0$). All energy values are evaluated at the exact densities. Exchange and XC are expressed as ratios to the exact ones. Correlation uses absolute values.

Look at the field-free case first. Since it is a singlet state, there is no CDFT current correction. Exact and approximate exchange, correlation, and XC energies are compared in Fig. 5-5. The exchange and XC panels use the ratio of approximate energies to the exact ones. It is well known that LDA underestimates exchange. In this example LDA misses about 15% of the exchange energy, while GGA omits less than 5%. However, in the strong-correlation regime, the GGA can slightly overestimate E_x.

In the correlation panel, an absolute energy scale was used. The blue curve presents the exact correlation energy. We can see that PBE slightly overestimates and LYP underestimates correlation energy, but both are more accurate than LDA. For the sum of exchange and correlation, both PBE and BLYP give quite accurate results in the weak-correlation regime, but there is little improvement over LDA in the strong-correlation regime.

Now turn to the non-vanishing B field cases. Figures 5-6 and 5-7 show the effect of the B field on E_{xc} for HA with ω = 1/2, 1/10, respectively. The left hand panels are for singlet states; right hand ones for triplet states. From top to bottom, the panels are exchange, correlation, and XC energies. We see that as the B field increases, GGAs tend to overestimate exchange. For correlation energy, both LDA and GGA give results almost independent of B field, hence are incapable of including the field effect. Apparently because of error cancellation, GGAs can still predict an accurate E_{xc} for the singlet state, but overestimate E_{xc} significantly for the triplet state at large B field.

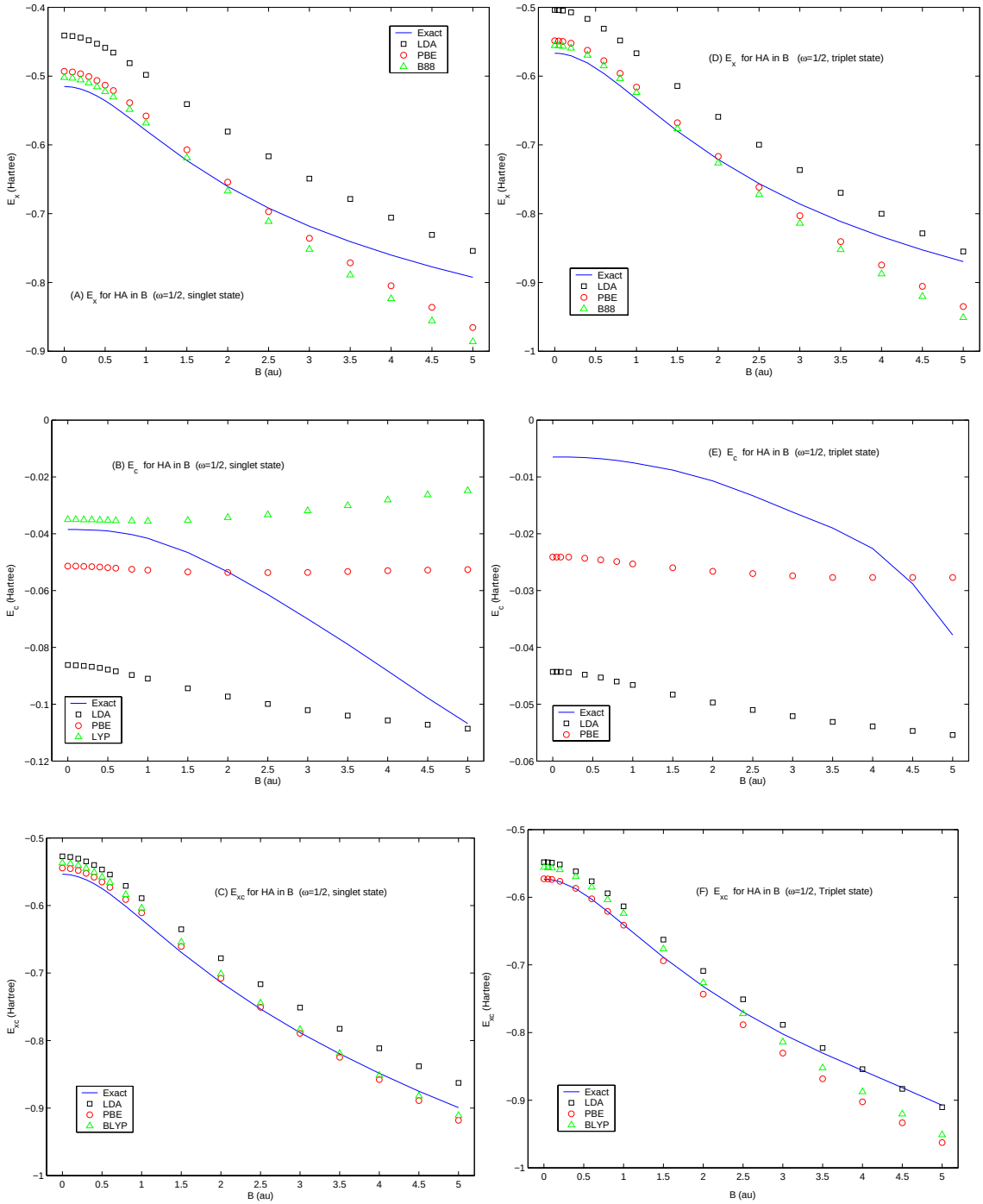

FIG. 5-6 Comparison of exact (curve) and approximate (symbols) exchange (upper panels), correlation (middle panels), and XC (bottom panels) energies of the HA with $\omega = 1/2$ in B fields. Left panels are for singlet state, right panels for triplet state. Blue lines are exact values. Black squares (□) are for LDA, red circles (o) for PBE, and green triangles (Δ) for BLYP.

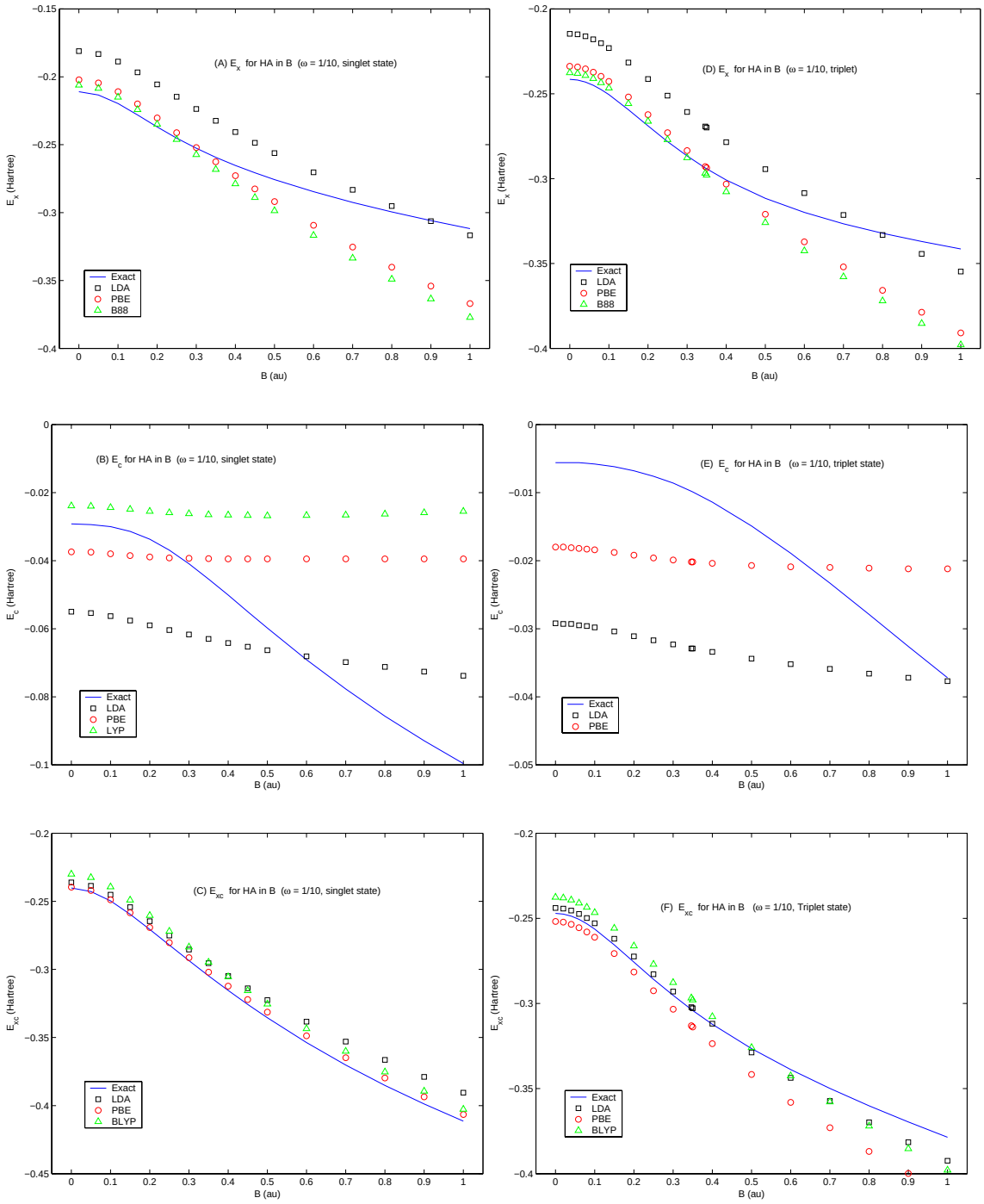

FIG. 5-7 Same as Fig. 5-6, except for $\omega = 1/10$.

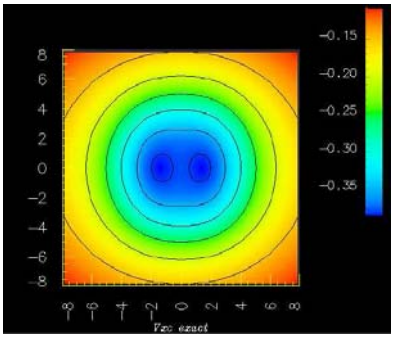

$(a)\ \upsilon_{xc}^{cdft,exact}\left(\rho,z\right)$

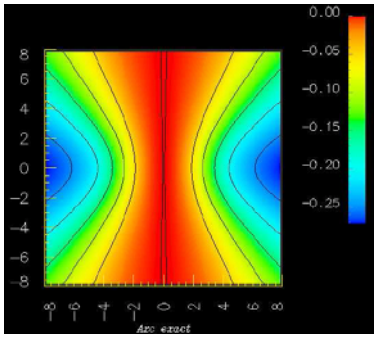

$(e)\ \vec{A}_{xc}\left(\vec{r}\right)=\hat{\varphi}A_{xc}^{cdft,exact}\left(\rho,z\right)$

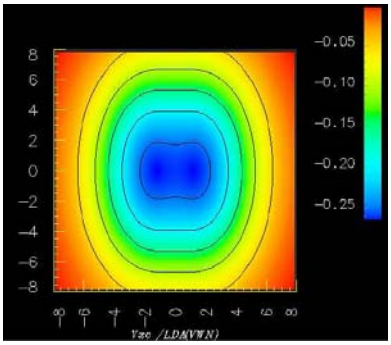

$(b)\ \upsilon_{xc}^{LDA}\left(\rho,z\right)$

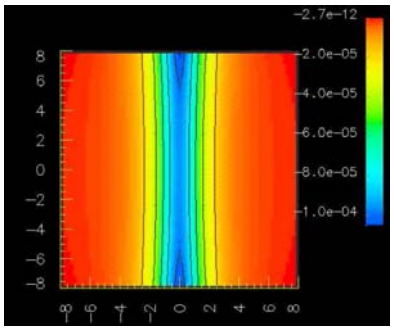

$(f)\ \hat{z}\cdot\vec{v}\left(\vec{r}\right)=\hat{z}\cdot\nabla\times\left(\vec{j}_p/n\right)$

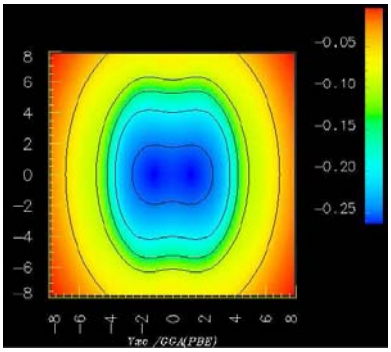

$(c)\ \upsilon_{xc}^{PBE}\left(\rho,z\right)$

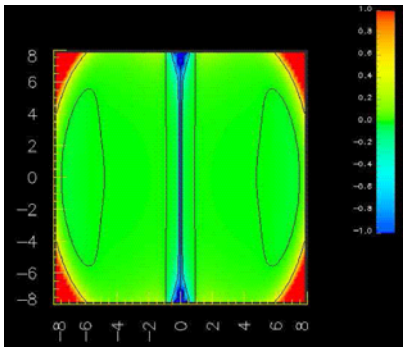

$(g)\ A_{xc}^{VRG}\left(\rho,z\right)$

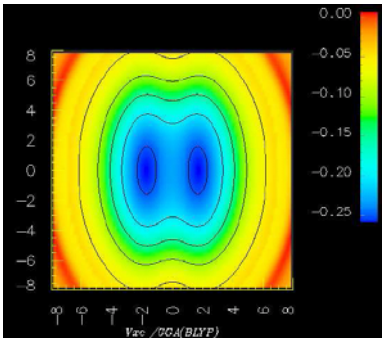

$(d)\ \upsilon_{xc}^{BLYP}\left(\rho,z\right)$

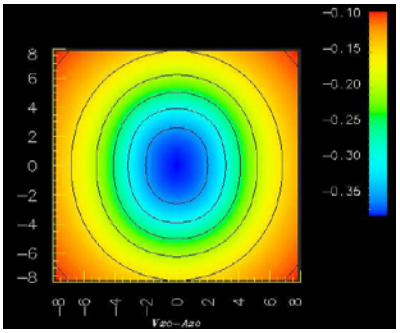

$(h)\ \upsilon_{xc}^{cdft,exact}-A_{xc}^{exact}/\rho$

FIG. 5-8 Cross-sectional views of the exact and approximate XC potentials for the ground state HA with ω = 1/10 in $B=\sqrt{3}/5$. The B field orientation is in the plane of the paper from bottom to top. Each large tick mark is 2 bohr radii.

Exact and approximate DFT and CDFT XC potentials for the ground state HA with ω = 1/10 in $B = \sqrt{3}/5$ are shown in Fig. 5-8. All the quantities are evaluated with exact densities. All the approximate potentials (panels b – d) are too shallow compared with the exact CDFT scalar XC potential, and none of them shares the shape of the exact one. This is similar to the observation for the vanishing B field case [120].

Matters are worse for the vector XC potential. The VRG approximation for the vector potential is very wrong. As with what we have found for real atoms, this functional gives essentially nothing but two singular points (actually singular cuts if my plot were larger) at two poles. The origin of this pathological behavior becomes clear if one looks at the distribution of $\vec{v} = \nabla \times \frac{\vec{j}_p}{n}$, which has only significant values at two poles of either a HA or a real atom. Once again we see that even though $\vec{v}$ is a gauge-invariant combination, an attractive feature from a purely theoretical perspective, it seems an awkward choice (at best) as the basic variable in CDFT for practical calculation. One measure for the paramagnetic current contribution is $\int \vec{j}_p(\vec{r}) \cdot \vec{A}_{xc}(\vec{r}) d\vec{r}$. Using exact values for the previous example, I get 0.0282 Hartree, which is clearly non-negligible. However, from the VRG functional, $\Delta E_{xc}^{VRG}\left[n^{exact}(\vec{r}), \vec{v}^{exact}(\vec{r})\right] = -0.0024$ Hartree.

Previously I mentioned that none of the approximate functionals generates a high quality XC scalar potential. This remark needs some modification in the case that both the scalar and vector potentials are considered simultaneously. Recall that the ground state is a triplet. For the two KS orbitals, the p-like orbital "feels" both the XC scalar and the vector potentials. Their total effect is shown in the last panel of Fig. 5-8. LDA gives

closest approximation to the total XC potentials in the outer part, where the *p*-like orbital has significant distribution, even though the LDA potential is still too shallow. For the *s*-like orbital $\phi_1^{KS}(\vec{r})$, which "feels" only the scalar XC potential, the small-*r* region is more important. Again LDA did a good job at this region.

Table 5-5 SCF results for HF and approximate DFT functionals (energy in Hartree)

system	energy	HF	LDA/VWN	GGA/PBE	GGA/jPBE	GGA/BLYP
	T_s	0.63303	0.62746	0.63280		0.63226
$\omega = 1/2$	J	1.02983	1.02258	1.02696	as	1.02896
$B = 0$	E_{xc}	-0.51492	-0.52377	-0.54317	left	-0.53642
	E_{tot}	2.03844	2.02623	2.00904		2.01653
	T_s	0.30470	0.30763	0.31110	0.31190	0.31017
$\omega = 1/10$	J	0.49797	0.48241	0.48427	0.48560	0.48285
$B = \sqrt{3}/5$	E_{xc}	-0.29804	-0.29775	-0.31035	-0.31288	-0.29442
	E_{tot}	0.38969	0.38072	0.36966	0.36775	0.38478

To check the non-SCF effects, Table 5-5 gives energy contributions from the SCF calculation using HF and several approximate DFT functionals on two special cases which have analytical solutions. For HF, E_{xc} means exchange energy only. Those SCF results are consistent with previous direct evaluation of the approximate functionals. This suggests our previous observations will remain the same were self-consistent orbitals to be used.

CHAPTER 6
SUMMARY AND CONCLUSION

In this dissertation, atom-like systems in strong magnetic fields are investigated by different theoretical methods, with special emphasis on DFT and CDFT descriptions.

An atom in strong magnetic fields is an interesting and challenging problem itself. Most current theoretical studies are still at the level of HF calculations. Besides the inherent complexity of the system, one barrier of the application of well-developed first principle methods on this system is the lack of well-adapted, high quality basis sets. The anisotropic Gaussian basis is suitable for the description of this system, but an efficient, systematic way for basis set optimization is desired, since the optimizing step needs to be done for each atomic configuration and for each field strength. The procedure presented in Chapter 3, specifically, eqns. (3.26) and (3.27), give an explicit construction. I have shown that basis sets constructed thus work extremely well when compared to fully numerical calculations. They may facilitate more accurate numerical studies on atoms in strong fields.

Comparison HF and DFT calculations are done systematically for helium through carbon atoms in a wide range of magnetic fields. Extensive tabulations are given in appendices on the DFT calculations based on modern functionals, LDA and PBE. A CDFT functional, VRG, is also tested. Those investigations contribute to our understanding on the performance and limitations of modern DFT and CDFT functionals, and are suggestive for improving and extending those functionals to describe atomic systems in a strong field.

An exactly soluble model system in DFT and CDFT, Hooke's atom, is studied in detail. For some specific confinement strengths and *B* fields, we developed exact analytical solutions that provide benchmarks against which other methods can be compared.

Exact KS orbitals are constructed for the HA from its electron density and paramagnetic current density. Exact DFT and CDFT energy components, especially exchange and correlation energies, together with approximate ones from modern functionals, are compiled extensively. Exact and approximate XC scalar and vector potentials are also compared. Those comparisons provide useful guidance for the advancement of DFT and CDFT functionals.

We are aware that this study is only at the inception stage of CDFT development. Little is known about the current-correction part. The quantity $\vec{v}(\vec{r})$ does not seem to be a wholly suitable variable in CDFT. Nevertheless, some formal properties about $E_{xc}^{cdft}[n,\vec{j}_p]$ are known for years, mostly from scaling arguments. With our exact KS orbitals, detailed examination of the effect of *B* field on the exchange-correlation hole is also possible. The combination of these two approaches will be helpful to the progress on better CDFT exchange-correlation functionals, or, perhaps, an equivalent gauge-invariant formulation of current contribution to DFT that is better adapted to computational implementation.

APPENDIX A
HAMILTONIAN MATRIX ELEMENTS IN SPHERICAL GAUSSIAN BASIS

In an ordinary GTO basis, the overlap, kinetic, and nuclear attraction integrals are easily obtained in closed form:

$$I\left(l,m,\alpha;l',m',\beta\right)=\left\langle G_{lm}^{\alpha}\mid G_{l'm'}^{\beta}\right\rangle=N_{lm}^{\alpha}N_{l'm'}^{\beta}\delta_{ll'}\delta_{mm'}\frac{\Gamma\left(l+\frac{3}{2}\right)}{2\left(\alpha+\beta\right)^{l+\frac{3}{2}}} \tag{A.1}$$

$$-\frac{1}{2}\left\langle G_{lm}^{\alpha}\mid\nabla^{2}\mid G_{l'm'}^{\beta}\right\rangle=-2\alpha\beta N_{lm}^{\alpha}N_{l'm'}^{\beta}\delta_{ll'}\delta_{mm'}\frac{\Gamma\left(l+\frac{5}{2}\right)}{\left(\alpha+\beta\right)^{l+\frac{5}{2}}} \tag{A.2}$$

$$-Z_{N}\left\langle G_{lm}^{\alpha}\mid\frac{1}{r}\mid G_{l'm'}^{\beta}\right\rangle=-Z_{N}N_{lm}^{\alpha}N_{l'm'}^{\beta}\delta_{ll'}\delta_{mm'}\frac{l!}{\left(\alpha+\beta\right)^{l+\frac{3}{2}}} \tag{A.3}$$

It is also possible to work out the coulomb integral directly in the spherical Gaussian basis, but that would be hard and tedious. To make use of the general formula of the electron repulsion integrals in Hermite Gaussians, we first transform a spherical Gaussian or the product of two spherical Gaussians to a linear combination of Hermite Gaussians.

A Hermite Gaussian centered at the point A is defined as

$$f\left(\vec{n},\alpha,\vec{A};\vec{r}\right)=\partial_{\vec{A}}^{\vec{n}}e^{-\alpha\left|\vec{r}-\vec{A}\right|^{2}} \tag{A.4}$$

where the operator $\partial_{\vec{A}}^{\vec{n}}$ is for the abbreviation of

$$\partial_{\vec{A}}^{\vec{n}}=\frac{\partial^{n_x}}{\partial A_x^{n_x}}\frac{\partial^{n_y}}{\partial A_y^{n_y}}\frac{\partial^{n_z}}{\partial A_z^{n_z}} \tag{A.5}$$

and $\vec{n} = (n_x, n_y, n_z)$.

For example,

$$G^{\alpha}_{1\bar{1}}(\vec{r})\, G^{\beta}_{11}(\vec{r}) = \frac{32}{3}\sqrt{\frac{2}{\pi}}(\alpha\beta)^{\frac{5}{4}} r^2 e^{-(\alpha+\beta)r^2} \left|Y_{11}(\theta,\varphi)\right|^2$$

$$= 2\left(\frac{2}{\pi}\right)^{\frac{3}{2}} (\alpha\beta)^{\frac{5}{4}} \left\{ \frac{f(\vec{0}, \alpha+\beta, \vec{0}; \vec{r})}{\alpha+\beta} + \frac{f(200, \alpha+\beta, \vec{0}; \vec{r}) + f(020, \alpha+\beta, \vec{0}; \vec{r})}{4(\alpha+\beta)^2} \right\}$$

Thus, we only need to evaluate the coulomb integral of two Hermite Gaussians,

$$\left[f(\vec{n}, \alpha, \vec{A}; \vec{r}) \middle| f(\vec{n}', \beta, \vec{C}; \vec{r}') \right] = \int d\vec{r} d\vec{r}' \frac{f(\vec{n}, \alpha, \vec{A}; \vec{r}) f(\vec{n}', \beta, \vec{C}; \vec{r}')}{|\vec{r} - \vec{r}'|} \tag{A.6}$$

Specifically for $\vec{A} = \vec{C} = \vec{0}$,

$$\left[f(\vec{n}, \alpha, \vec{0}; \vec{r}) \middle| f(\vec{n}', \beta, \vec{0}; \vec{r}') \right] = \partial^{\vec{n}}_{\vec{A}} \partial^{\vec{n}'}_{\vec{C}} \left[f(\vec{0}, \alpha, \vec{A}; \vec{r}) \middle| f(\vec{0}, \beta, \vec{C}; \vec{r}') \right] \Big|_{\vec{A}=\vec{C}=0}$$

$$= \frac{2\pi^{\frac{5}{2}}}{\alpha\beta\sqrt{\alpha+\beta}} (-)^{n'} \int_0^1 du \left[\partial^{\vec{n}+\vec{n}'}_{\vec{A}} e^{-\frac{\alpha\beta}{\alpha+\beta}|\vec{A}-\vec{C}|^2 u^2} \right] \Bigg|_{\vec{A}=\vec{C}=0}$$

$$= \frac{2\pi^{\frac{5}{2}}}{\alpha\beta\sqrt{\alpha+\beta}} \frac{\left(-\frac{\alpha\beta}{\alpha+\beta}\right)^{\frac{n+n'}{2}}}{n+n'+1} \prod_{i=x,y,z} \frac{(n_i + n_i')!}{\left(\frac{n_i + n_i'}{2}\right)!} \quad , \quad \text{for } n_i + n_i' = \textit{even integers};$$

$$0, \qquad \text{otherwise.} \tag{A.7}$$

where $n = n_x + n_y + n_z$, and $n' = n'_x + n'_y + n'_z$.

The diamagnetic term integral,

$$\left\langle G^{\alpha}_{lm} \middle| x^2 + y^2 \middle| G^{\beta}_{l'm'} \right\rangle = N^{\alpha}_{lm} N^{\beta}_{l'm'} \left\langle Y_{lm} \middle| \sin^2\theta \middle| Y_{l'm'} \right\rangle \int_0^{\infty} r^{l+l'+4} e^{-(\alpha+\beta)r^2} dr$$

$$= \frac{1}{3} N_{lm}^{\alpha} N_{l'm'}^{\beta} \delta_{mm'} \left[\delta_{ll'} - \sqrt{\frac{2l+1}{2l'+1}} (l0,20|l'0)(lm,20|l'm) \right] \frac{\Gamma\left(l+\frac{5}{2}\right)}{(\alpha+\beta)^{5/2}} \tag{A.8}$$

where $(lm, l''m''|l'm')$ is a Clebsch-Gordon coefficient.

Both vector and scalar XC potential terms were integrated numerically on a mesh, 600 radial points and 180 points in the polar angle.

$$-i\left\langle G_{lm}^{\alpha} \left| \vec{A}_{xc}(\vec{r}) \cdot \nabla \right| G_{l'm'}^{\beta} \right\rangle = m\delta_{mm'} N_{lm}^{\alpha} N_{l'm'}^{\beta} \int_0^{\infty} r^{l+l'+1} e^{-(\alpha+\beta)r^2} \cdot 2\pi \left[\int_0^{\pi} Y_{lm}^{*} Y_{l'm'} A_{xc}(r,\theta) d\theta \right] dr \tag{A.9}$$

$$\left\langle G_{lm}^{\alpha} \left| \upsilon_{xc}^{dft/cdft}(\vec{r}) \right| G_{l'm'}^{\beta} \right\rangle = \delta_{mm'} N_{lm}^{\alpha} N_{l'm'}^{\beta} \int_0^{\infty} r^{l+l'+2} e^{-(\alpha+\beta)r^2} \cdot 2\pi \left[\int_0^{\pi} Y_{lm}^{*} Y_{l'm'} \upsilon_{xc}^{dft/cdft}(r,\theta) \sin\theta d\theta \right] dr \tag{A.10}$$

APPENDIX B
ATOMIC ENERGIES FOR ATOMS HE, LI, BE, B, C AND THEIR POSITIVE IONS LI^+, BE^+, B^+ IN MAGNETIC FIELDS

Table B-1 Atomic energies of the Helium atom in *B* fields. Energies in Hartree, *B* in au. JOC-HF1 is from reference 91 with spherical STO expansion; JOC-HF2 from reference 94 in which JOC basis sets (see eqn. 3.23) within AGTO were used; Correlated data are from CI calculations in references 11 through 13, except those labeled by "d", which are from fixed-phase quantum Monte Carlo calculations in reference 93. All other columns are from present study. Ground states are indicated in orange clolor. See notes following the table.

State	*B*	Present HF	JOC-HF1[a]	JOC-HF2[b]	Correlated[c]	LDA	PBE
$1s^2$	0	-2.86168	-2.8617		-2.903351	-2.8344	-2.8929
	0.02	-2.86160			-2.903270	-2.8344	-2.8928
	0.04	-2.86136			-2.903036	-2.8341	-2.8926
	0.08	-2.86042	-2.8604		-2.902083	-2.8331	-2.8916
	0.16	-2.85665			-2.898290	-2.8290	-2.8876
	0.24	-2.85043	-2.8504		-2.892035	-2.8223	-2.8811
	0.4	-2.83101	-2.8310		-2.872501	-2.8014	-2.8607
	0.5	-2.81445			-2.855859	-2.7838	-2.8435
	0.8	-2.74684	-2.7468		-2.787556	-2.7124	-2.7736
	1	-2.68888			-2.729508	-2.6518	-2.7142
	1.6	-2.46739			-2.507952	-2.4224	-2.4890
	2	-2.28914			-2.329780	-2.2393	-2.3088
	4	-1.17629	-1.1762		-1.21901[d]	-1.1068	-1.1908
	5	-0.53244			-0.574877	-0.4554	-0.5462
	8	1.59127	0.168		1.54628[d]	1.6860	1.5764
	10	3.11063			3.064582	3.2142	3.0932
	20	11.31961			11.267051	11.4496	11.2809
	40	29.01211				29.1592	28.9175
	50	38.14391			38.076320	38.2920	38.0198
	80	66.09209				66.2303	65.8794
	100	85.00418			84.918313	85.1300	84.7336
	160	142.45118				142.5276	142.0151
	200	181.10639				181.1452	180.5661
	240	219.94017				219.9398	219.2999
	400	376.32909				376.1681	375.3224
	500	474.58300				474.3228	473.3680
	560	533.65483				533.3361	532.3207
	800	770.54396				769.9995	768.7679
	1000	968.44540				967.7225	966.3336
	2000	1961.1249				1959.610	1957.599

Table B-1 (*continued*)

State	*B*	Present HF	JOC-HF1[a]	JOC-HF2[b]	Correlated[c]	LDA	PBE
1s2s	0	-2.17425	-2.1742		-2.175220	-2.1203	-2.1768
	0.02	-2.19348			-2.194461	-2.1395	-2.1961
	0.04	-2.21124			-2.212236	-2.1573	-2.2139
	0.08	-2.24291	-2.2429	-2.2425	-2.243958	-2.1891	-2.2459
	0.16	-2.29512			-2.296318	-2.2421	-2.2994
	0.24	-2.33824			-2.339560	-2.2866	-2.3446
	0.4	-2.41124	-2.4112	-2.4111	-2.412723	-2.3640	-2.4239
	0.5	-2.45283			-2.454347	-2.4090	-2.4705
	0.8	-2.57211	-2.5712	-2.5720	-2.573615	-2.5382	-2.6038
	1	-2.64918			-2.650655	-2.6204	-2.6882
	1.6	-2.86616	-2.8632	-2.8659	-2.867620	-2.8477	-2.9219
	2	-2.99824			-2.999708	-2.9846	-3.0629
	4	-3.54362	-3.5114	-3.5435	-3.54353[d]	-3.5466	-3.6437
	5	-3.76667			-3.768199	-3.7761	-3.8817
	8	-4.32036	-4.2891	-4.3202	-4.31429[d]	-4.3463	-4.4744
	10	-4.62594			-4.627450	-4.6616	-4.8030
	20	-5.77102			-5.772448	-5.8480	-6.0441
	40	-7.25443		-7.2543		-7.3984	-7.6751
	50	-7.81400			-7.815256	-7.9874	-8.2972
	80	-9.13864		-9.1385		-9.3909	-9.7848
	100	-9.84199			-9.843074	-10.1416	-10.5831
	160	-11.49473		-11.4945		-11.9202	-12.4820
	200	-12.36634				-12.8667	-13.4967
	240	-13.12269		-13.1223		-13.6929	-14.3847
	400	-15.46711		-15.4668		-16.2827	-17.1819
	500	-16.60183				-17.5522	-18.5600
	560	-17.20526		-17.2046		-18.2315	-19.2992
	800	-19.22890		-19.2286		-20.5313	-21.8113
	1000	-20.59486				-22.1027	-23.5360
	2000	-25.36396				-27.7150	-29.7493
$1s2p_0$	0	-2.13133	-2.1314		-2.132910	-2.0873	-2.1439
	0.02	-2.15087			-2.152378	-2.1071	-2.1639
	0.04	-2.16929			-2.170822	-2.1257	-2.1825
	0.08	-2.20350	-2.2035	-2.2031	-2.205130	-2.1604	-2.2173
	0.16	-2.26467			-2.266575	-2.2230	-2.2801
	0.24	-2.31988			-2.322032	-2.2796	-2.3370
	0.4	-2.41975	-2.4196	-2.4197	-2.422361	-2.3820	-2.4401
	0.5	-2.47732			-2.480172	-2.4408	-2.4995
	0.8	-2.63483	-2.6347	-2.6347	-2.638222	-2.6011	-2.6617
	1	-2.73016			-2.733813	-2.6977	-2.7597
	1.6	-2.98302	-2.9828	-2.9827	-2.987185	-2.9530	-3.0199
	2	-3.13076			-3.135142	-3.1018	-3.1723
	4	-3.71910	-3.7141	-3.7186	-3.72389[d]	-3.6952	-3.7830
	5	-3.95398			-3.959235	-3.9329	-4.0289
	8	-4.52888	-4.4861	-4.5282	-4.53277[d]	-4.5175	-4.6357
	10	-4.84263			-4.848590	-4.8383	-4.9697
	20	-6.00482			-6.011488	-6.0370	-6.2234
	40	-7.49328		-7.4932		-7.5940	-7.8623

Table B-1 (*continued*)

State	*B*	Present HF	JOC-HF1[a]	JOC-HF2[b]	Correlated[c]	LDA	PBE
$1s2p_0$	50	-8.05222			-8.059466	-8.1843	-8.4864
	80	-9.37260		-9.3724		-9.5901	-9.9776
	100	-10.07281			-10.079973	-10.3416	-10.7777
	160	-11.71716		-11.7170		-12.1223	-12.6810
	200	-12.58420				-13.0700	-13.6981
	240	-13.33662		-13.3364		-13.8973	-14.5883
	400	-15.66948		-15.6691		-16.4911	-17.3924
	500	-16.79906				-17.7627	-18.7744
	560	-17.39990		-17.3996		-18.4433	-19.5159
	800	-19.41540		-19.4150		-20.7480	-22.0364
	1000	-20.77640				-22.3233	-23.7673
	2000	-25.53090				-27.9510	-30.0030
$1s2p_{-1}$	0	-2.13133	-2.1314		-2.133149	-2.0821	-2.1370
	0.02	-2.16035			-2.162112	-2.1113	-2.1664
	0.04	-2.18730			-2.189128	-2.1383	-2.1934
	0.08	-2.23646	-2.2365	-2.2353	-2.238504	-2.1877	-2.2427
	0.16	-2.32260			-2.325189	-2.2744	-2.3291
	0.24	-2.39927			-2.402393	-2.3516	-2.4059
	0.4	-2.53674	-2.5336	-2.5366	-2.540763	-2.4894	-2.5431
	0.5	-2.61555			-2.620021	-2.5681	-2.6216
	0.8	-2.83021	-2.8299	-2.8301	-2.835619	-2.7814	-2.8349
	1	-2.95969			-2.965504	-2.9095	-2.9635
	1.6	-3.30222	-3.3017	-3.3016	-3.308774	-3.2471	-3.3036
	2	-3.50205			-3.508911	-3.4437	-3.5024
	4	-4.29844	-4.2950	-4.2980	-4.30587[d]	-4.2273	-4.2977
	5	-4.61725			-4.625491	-4.5417	-4.6178
	8	-5.40041	-5.3793	-5.4000	-5.40452[d]	-5.3162	-5.4077
	10	-5.82951			-5.839475	-5.7420	-5.8428
	20	-7.42770			-7.440556	-7.3377	-7.4770
	40	-9.48827		-9.4882		-9.4184	-9.6149
	50	-10.26449			-10.28410	-10.2090	-10.4292
	80	-12.10132		-12.1011		-12.0950	-12.3754
	100	-13.07665			-13.10478	-13.1050	-13.4198
	160	-15.36930		-15.3690		-15.5026	-15.9049
	200	-16.57907				-16.7810	-17.2331
	240	-17.62932		-17.6289		-17.8983	-18.3956
	400	-20.88777		-20.8876		-21.4084	-22.0585
	500	-22.46665				-23.1332	-23.8638
	560	-23.30677		-23.3066		-24.0572	-24.8326
	800	-26.12655		-26.1264		-27.1911	-28.1255
	1000	-28.03209				-29.3371	-30.3870
	2000	-34.69865				-37.0248	-38.5309
$1s3d_{-1}$	0	-2.05557	-2.0556		-2.055629	-2.0035	-2.0592
	0.02	-2.08225			-2.082319	-2.0305	-2.0865
	0.04	-2.10413			-2.104234	-2.0530	-2.1094
	0.08	-2.14084	-2.1408	-2.1403	-2.141017	-2.0910	-2.1481
	0.16	-2.20200			-2.202291	-2.1542	-2.2127
	0.24	-2.25559			-2.256006	-2.2094	-2.2690

Table B-1 (*continued*)

State	*B*	Present HF	JOC-HF1[a]	JOC-HF2[b]	Correlated[c]	LDA	PBE
$1s3d_{-1}$	0.4	-2.35154	-2.3508	-2.3512	-2.352208	-2.3083	-2.3695
	0.5	-2.40669			-2.407521	-2.3651	-2.4270
	0.8	-2.55775	-2.5525	-2.5528	-2.559005	-2.5202	-2.5843
	1	-2.64947			-2.650973	-2.6141	-2.6796
	1.6	-2.89411	-2.8741	-2.8938	-2.896192	-2.8636	-2.9335
	2	-3.03792			-3.040304	-3.0099	-3.0827
	4	-3.61580	-3.6053	-3.6156	-3.61588[d]	-3.5963	-3.6839
	5	-3.84820			-3.851883	-3.8321	-3.9267
	8	-4.41969	-4.3470	-4.4193	-4.40580[d]	-4.4126	-4.5267
	10	-4.73271			-4.737490	-4.7313	-4.8570
	20	-5.89611			-5.902110	-5.9217	-6.0960
	40	-7.39013		-7.3900		-7.4646	-7.7118
	50	-7.95152			-7.959094	-8.0487	-8.3258
	80	-9.27773		-9.2773		-9.4375	-9.7908
	100	-9.98090			-9.989376	-10.1791	-10.5757
	160	-11.63164		-11.6315		-11.9342	-12.4402
	200	-12.50169				-12.8673	-13.4351
	240	-13.25654		-13.2562		-13.6812	-14.3053
	400	-15.59593		-15.5955		-16.2305	-17.0422
	500	-16.72819				-17.4790	-18.3884
	560	-17.33035		-17.3302		-18.1468	-19.1112
	800	-19.34981		-19.3495		-20.4068	-21.5638
	1000	-20.71314				-21.9503	-23.2428
	2000	-25.47417				-27.4561	-29.3136
$1s3d_{-2}$	0	-2.05517	-2.0556		-2.055635	-2.0024	-2.0571
	0.02	-2.09057			-2.090760	-2.0382	-2.0933
	0.04	-2.11905			-2.119167	-2.0670	-2.1225
	0.08	-2.16632	-2.1663	-2.1659	-2.166519	-2.1148	-2.1712
	0.16	-2.24437			-2.244776	-2.1938	-2.2513
	0.24	-2.31214			-2.312786	-2.2624	-2.3206
	0.4	-2.43230	-2.4310	-2.4320	-2.433466	-2.3845	-2.4433
	0.5	-2.50087			-2.502362	-2.4542	-2.5132
	0.8	-2.68753	-2.6824	-2.6871	-2.689916	-2.6441	-2.7031
	1	-2.80039			-2.803296	-2.7589	-2.8178
	1.6	-3.10079	-3.0801	-3.1005	-3.104935	-3.0636	-3.1234
	2	-3.27738			-3.282141	-3.2423	-3.3031
	4	-3.98909	-3.9611	-3.9890	-3.99144[d]	-3.9603	-4.0288
	5	-4.27663			-4.284050	-4.2500	-4.3227
	8	-4.98705	-4.8724	-4.9866	-4.97560[d]	-4.9660	-5.0509
	10	-5.37808			-5.387931	-5.3607	-5.4531
	20	-6.84153			-6.854811	-6.8428	-6.9669
	40	-8.73864		-8.7385		-8.7792	-8.9512
	50	-9.45533			-9.476057	-9.5157	-9.7076
	80	-11.15470		-11.1540		-11.2732	-11.5158
	100	-12.05871			-12.088566	-12.2148	-12.4864
	160	-14.18753		-14.1875		-14.4506	-14.7958
	200	-15.31278				-15.6429	-16.0302
	240	-16.29062		-16.2905		-16.6851	-17.1106

Table B-1 (*continued*)

State	*B*	Present HF	JOC-HF1[a]	JOC-HF2[b]	Correlated[c]	LDA	PBE
$1s3d_{-2}$	400	-19.32952		-19.3286		-19.9597	-20.5142
	500	-20.80454				-21.5688	-22.1915
	560	-21.59002		-21.5954		-22.4310	-23.0915
	800	-24.22930		-24.2283		-25.3550	-26.1503
	1000	-26.01525				-27.3575	-28.2510
	2000	-32.27676				-34.5328	-35.8136
$1s4f_{-2}$	0	-2.03125	-2.0313		-2.031254	-1.9776	-2.0321
	0.02	-2.06215			-2.062177	-2.0103	-2.0651
	0.04	-2.08431			-2.084414	-2.0336	-2.0891
	0.08	-2.12033	-2.1197	-2.1201	-2.120532	-2.0712	-2.1279
	0.16	-2.18008			-2.180271	-2.1331	-2.1914
	0.24	-2.23257			-2.232769	-2.1870	-2.2466
	0.4	-2.32686	-2.3118	-2.3268	-2.327166	-2.2836	-2.3454
	0.5	-2.38120			-2.381601	-2.3392	-2.4021
	0.8	-2.53039	-2.5253	-2.5299	-2.531094	-2.4914	-2.5571
	1	-2.62115			-2.622067	-2.5837	-2.6512
	1.6	-2.86378	-2.8503	-2.8637	-2.865215	-2.8297	-2.9022
	2	-3.00670			-3.008432	-2.9743	-3.0500
	4	-3.58255	-3.5648	-3.5823	-3.58366[d]	-3.5557	-3.6465
	5	-3.81470			-3.817900	-3.7900	-3.8877
	8	-4.38646	-4.3398	-4.3861	-4.38303[d]	-4.3677	-4.4844
	10	-4.70001			-4.704423	-4.6852	-4.8133
	20	-5.86663			-5.872256	-5.8714	-6.0469
	40	-7.36567		-7.3654		-7.4089	-7.6554
	50	-7.92889			-7.935933	-7.9907	-8.2664
	80	-9.25902		-9.2549		-9.3736	-9.7237
	100	-9.96402			-9.971845	-10.1117	-10.5041
	160	-11.61837		-11.6182		-11.8577	-12.3571
	200	-12.48998				-12.7855	-13.3455
	240	-13.24601		-13.2459		-13.5947	-14.2094
	400	-15.58829		-15.5879		-16.1278	-16.9261
	500	-16.72161				-17.3679	-18.2634
	560	-17.32426		-17.3240		-18.0311	-18.9786
	800	-19.34508		-19.3448		-20.2748	-21.4099
	1000	-20.70912				-21.8066	-23.0781
	2000	-25.47179				-27.2681	-29.0676
$1s4f_{-3}$	0	-2.03125	-2.0313		-2.031255	-1.9764	-2.0303
	0.02	-2.06949			-2.069509	-2.0172	-2.0715
	0.04	-2.09691			-2.096967	-2.0460	-2.1010
	0.08	-2.14149	-2.1412	-2.1406	-2.141582	-2.0914	-2.1475
	0.16	-2.21484			-2.214999	-2.1656	-2.2233
	0.24	-2.27873			-2.278994	-2.2301	-2.2889
	0.4	-2.39242	-2.3916	-2.3923	-2.392988	-2.3447	-2.4052
	0.5	-2.45746			-2.458243	-2.4104	-2.4716
	0.8	-2.63477	-2.6344	-2.6344	-2.636282	-2.5893	-2.6520
	1	-2.74210			-2.744109	-2.6976	-2.7611
	1.6	-3.02805	-3.0270	-3.0275	-3.031517	-2.9859	-3.0513
	2	-3.19635			-3.200682	-3.1554	-3.2222

Table B-1 (*continued*)

State	*B*	Present HF	JOC-HF1[a]	JOC-HF2[b]	Correlated[c]	LDA	PBE
$1s4f_{-3}$	4	-3.87602	-3.8689	-3.8759	-3.88056[d]	-3.8388	-3.9132
	5	-4.15121			-4.160555	-4.1153	-4.1936
	8	-4.83222	-4.7802	-4.8318	-4.83102[d]	-4.7997	-4.8893
	10	-5.20761			-5.222402	-5.1774	-5.2741
	20	-6.61486			-6.636961	-6.5973	-6.7242
	40	-8.44270		-8.4426		-8.4541	-8.6273
	50	-9.13392			-9.169700	-9.1605	-9.3529
	80	-10.77406		-10.7734		-10.8463	-11.0881
	100	-11.64710			-11.697425	-11.7494	-12.0196
	160	-13.70423		-13.7044		-13.8936	-14.2360
	200	-14.79217				-15.0370	-15.4207
	240	-15.73789		-15.7378		-16.0363	-16.4576
	400	-18.67851		-18.6784		-19.1756	-19.7238
	500	-20.10658				-20.7178	-21.3334
	560	-20.86724		-20.8674		-21.5441	-22.1968
	800	-23.42398		-23.4342		-24.3457	-25.1316
	1000	-25.15479				-26.2639	-27.1469
	2000	-31.22698				-33.1339	-34.3978
$1s5g_{-3}$	0	-2.01997				-1.9605	-2.0146
	0.02	-2.05277				-1.9995	-2.0540
	0.04	-2.07425				-2.0239	-2.0791
	0.08	-2.10912		-2.1089	-2.10950[d]	-2.0607	-2.1171
	0.16	-2.16749				-2.1215	-2.1796
	0.24	-2.21905			-2.21919[d]	-2.1745	-2.2340
	0.4	-2.31208		-2.3120	-2.31133[d]	-2.2698	-2.3316
	0.5	-2.36585				-2.3247	-2.3877
	0.8	-2.51380		-2.5133	-2.51328[d]	-2.4751	-2.5415
	1	-2.60397				-2.5665	-2.6349
	1.6	-2.84546		-2.8451	-2.84601[d]	-2.8105	-2.8843
	2	-2.98790				-2.9541	-3.0313
	4	-3.56275		-3.5607	-3.74971[d]	-3.5322	-3.6251
	5	-3.79480				-3.7656	-3.8656
	8	-4.36680		-4.3664	-4.36666[d]	-4.3413	-4.4605
	10	-4.68070				-4.6579	-4.7885
	20	-5.84934				-5.8413	-6.0193
	40	-7.35154		-7.3514		-7.3756	-7.6240
	50	-7.91592				-7.9560	-8.2336
	80	-9.24860		-9.2476		-9.3356	-9.6868
	100	-9.95479				-10.0717	-10.4649
	160	-11.61154		-11.6106		-11.8125	-12.3118
	200	-12.48420				-12.7374	-13.2968
	240	-13.24104		-13.2408		-13.5439	-14.1576
	400	-15.58525		-15.5847		-16.0679	-16.8640
	500	-16.71928				-17.3031	-18.1935
	560	-17.32225		-17.3216		-17.9637	-18.9068
	800	-19.34395		-19.3436		-20.1980	-21.3262
	1000	-20.70844				-21.7231	-22.9845
	2000	-25.47211				-27.1590	-28.9289

Notes for Table B-1:

(a) Spherical STO basis expansion. Data from M. D. Jones, G. Ortiz, and D. M. Ceperley, Phys. Rev. A **54**, 219 (1996);

(b) Anisotropic GTO basis, from M.D. Jones, G. Ortiz, and D.M. Ceperley, Phys. Rev. A **59**, 2875 (1999);

(c) Anisotropic GTO basis CI calculations except data labled by (d). For magnetic quantum number M = 0, M = -1, and M = -2,-3, data are from W. Becken, P. Schmelcher, and F.K. Diakonos, J. Phys. B **32**, 1557 (1999) W. Becken and P. Schmelcher, J. Phys. B **33**, 545 (2000), and Phys. Rev. A **63**, 053412 (2001), respectively;

(d) Fixed-Phase Quantum Monte Carlo calculations, from M.D. Jones, G. Ortiz, and D.M. Ceperley, Int. J. Quant. Chem. **64**, 523 (1997).

Table B-2 Atomic energies of the Lithium singly positive ion, Li^+, in *B* fields. Energies in Hartree, *B* in au. Numerical HF is from reference 86; CI from reference 77. All others from present study. Ground states are indicated in orange.

State	*B*	Present HF	Numerical HF	CI	LDA	PBE
$1s^2$	0	-7.23641	-7.23642	-7.277191	-7.1422	-7.2567
	0.01	-7.23643	-7.23641	-7.277327	-7.1422	-7.2568
	0.02	-7.23645	-7.23639	-7.277376	-7.1423	-7.2569
	0.05	-7.23623	-7.23623	-7.277336	-7.1420	-7.2566
	0.1	-7.23567	-7.23567	-7.276897	-7.1414	-7.2560
	0.2	-7.23345	-7.23345	-7.274673	-7.1391	-7.2537
	0.5	-7.21798	-7.21798	-7.259522	-7.1228	-7.2377
	1	-7.16401	-7.16401	-7.205547	-7.0663	-7.1822
	2	-6.96299	-6.96300	-7.004453	-6.8577	-6.9769
	3	-6.66237	-6.66237		-6.5482	-6.6718
	4	-6.28590			-6.1630	-6.2913
	5	-5.85050	-5.85051	-5.891947	-5.7192	-5.8525
	5.4	-5.66264		-5.704147	-5.5281	-5.6635
	7	-4.84724	-4.84725		-4.7005	-4.8441
	10	-3.11091	-3.11092	-3.153453	-2.9446	-3.1029
	20	3.74896	3.74896		3.9618	3.7599
	50	27.96465	27.96465		28.2462	27.9452
	100	72.09338	72.09337		72.4153	71.9934
	200	164.66868	164.66867		164.9937	164.3926
	500	452.00319	452.0032		452.1999	451.2283
	1000	939.87972	939.87976		939.7871	938.3857
	2000	1925.2140			1924.543	1922.523
$1s2p_{-1}$	0	-5.02468	-5.02469	-5.026321	-4.9386	-5.0301
	0.01	-5.03961	-5.03963	-5.041247	-4.9535	-5.0450
	0.02	-5.05440	-5.05442	-5.056040	-4.9683	-5.0598
	0.05	-5.09795	-5.09797	-5.099595	-5.0119	-5.1033
	0.1	-5.16787	-5.16789	-5.169539	-5.0818	-5.1732
	0.2	-5.29872	-5.29873	-5.300455	-5.2125	-5.3038
	0.5	-5.64005	-5.64006	-5.643726	-5.5534	-5.6444
	1	-6.11462	-6.11462	-6.119216	-6.0264	-6.1171

Table B-2 (*continued*)

State	*B*	Present HF	Numerical HF	CI	LDA	PBE
$1s2p_{-1}$	2	-6.89407	-6.89408	-6.899768	-6.8001	-6.8922
	3	-7.54672	-7.54672		-7.4458	-7.5409
	4	-8.11772			-8.0101	-8.1089
	5	-8.62942	-8.62943	-8.636273	-8.5155	-8.6183
	5.4	-8.82072		-8.827671	-8.7044	-8.8089
	7	-9.52491	-9.52492		-9.4000	-9.5112
	10	-10.65131	-10.65131	-10.659060	-10.5135	-10.6369
	20	-13.42974	-13.42974		-13.2670	-13.4258
	50	-18.52547	-18.52548		-18.3463	-18.5834
	100	-23.69994	-23.69994		-23.5452	-23.8753
	200	-30.26077	-30.26077		-30.1973	-30.6627
	500	-41.50392	-41.50393		-41.7541	-42.4946
	1000	-52.32301	-52.3230		-53.0628	-54.1191
	2000	-65.47655			-67.0601	-68.5692

Table B-3 Atomic energies of the Lithium atom in *B* fields. Energies in Hartree, *B* in au. Numerical HF is from reference 86; CI from reference 77, except those labeled by (c), which are from reference 105. All others from present study. Ground states are indicated in orange.

State	*B*	Present HF	Numerical HF[a]	CI	LDA	PBE
$1s^2 2s$	0	-7.43274	-7.43275	-7.477766[b]	-7.3433	-7.4621
	0.001	-7.43325	-7.43326	-7.478032[b]	-7.3438	-7.4627
	0.002	-7.43364	-7.43375		-7.3442	-7.4631
	0.009	-7.43712	-7.43713	-7.4821719[c]	-7.3477	-7.4666
	0.01	-7.43759	-7.43760	-7.482888[b]	-7.3481	-7.4670
	0.018	-7.44125	-7.44125	-7.4863018[c]	-7.3518	-7.4707
	0.02	-7.44328	-7.44214	-7.490983[b]	-7.3558	-7.4747
	0.05	-7.45397	-7.45398	-7.502724[b]	-7.3646	-7.4835
	0.054	-7.45536	-7.45537	-7.5004678[c]	-7.3660	-7.4849
	0.1	-7.46856	-7.46857	-7.517154[b]	-7.3794	-7.4985
	0.126	-7.47407	-7.47408	-7.5193718[c]	-7.3851	-7.5043
	0.17633	-7.48162	-7.48162		-7.3931	-7.5126
	0.18	-7.48203	-7.48204	-7.5275049[c]	-7.3935	-7.5131
	0.2	-7.48400	-7.48400	-7.533495[b]	-7.3957	-7.5154
	0.5	-7.47740	-7.47741	-7.528055[b]	-7.3948	-7.5170
	0.54	-7.47350	-7.47351	-7.5197262[c]	-7.3919	-7.5146
	0.900	-7.42504	-7.42504	-7.4710527[c]	-7.3530	-7.4808
	1	-7.40878	-7.40879	-7.458550[b]	-7.3392	-7.4683
	1.260	-7.36225	-7.36226		-7.2982	-7.4305
	5	-6.08810	-6.08811	-6.136918[b]	-6.0481	-6.2195
	10	-3.35784	-3.35777	-3.406556[b]	-3.3276	-3.5438
$1s^2 2p_{-1}$	0	-7.36494	-7.36509	-7.407126[b]	-7.2788	-7.3970
	0.009	-7.37380	-7.37387	-7.4185656[c]	-7.2878	-7.4063
	0.01	-7.37475	-7.37481	-7.416994[b]	-7.2888	-7.4072
	0.018	-7.38213	-7.38218	-7.4268977[c]	-7.2962	-7.4146
	0.02	-7.38391	-7.38397		-7.2980	-7.4164

Table B-3 (*continued*)

State	*B*	Present HF	Numerical HF[a]	CI	LDA	PBE
$1s^2 2p_{-1}$	0.05	-7.40841	-7.40844	-7.451086[b]	-7.3226	-7.4411
	0.054	-7.41138	-7.41141	-7.4562839[c]	-7.3256	-7.4441
	0.1	-7.44173	-7.44176	-7.484773[b]	-7.3565	-7.4750
	0.126	-7.45648	-7.45650	-7.5018829[c]	-7.3715	-7.4901
	0.17633	-7.48160	-7.48162		-7.3973	-7.5158
	0.18	-7.48328	-7.48330	-7.5291175[c]	-7.3990	-7.5175
	0.2	-7.49218	-7.49220	-7.536032[b]	-7.4082	-7.5266
	0.5	-7.58787	-7.58790	-7.634547[b]	-7.5072	-7.6247
	0.54	-7.59707	-7.59709	-7.645730[c]	-7.5167	-7.6341
	0.9	-7.65627	-7.65628	-7.707054[c]	-7.5775	-7.6944
	1	-7.66652	-7.66653	-7.716679[b]	-7.5879	-7.7048
	1.26	-7.68285	-7.68288	-7.735013[c]	-7.6040	-7.7211
	1.8	-7.67655	-7.67657	-7.729627[c]	-7.5955	-7.7143
	2	-7.66245	-7.66246	-7.715709[b]	-7.5803	-7.6998
	2.153	-7.64784	-7.64785		-7.5647	-7.6849
	2.16	-7.64710	-7.64711		-7.5639	-7.6842
	2.5	-7.60350	-7.60351		-7.5179	-7.6399
	3	-7.51515	-7.51516		-7.4258	-7.5506
	3.6	-7.37637	-7.37638	-7.425857[c]	-7.2824	-7.4108
	4	-7.26672			-7.1697	-7.3006
	5	-6.94229	-6.94230	-7.002346[b]	-6.8378	-6.9752
	5.4	-6.79515	-6.79517	-6.8361629[c]	-6.6879	-6.8279
	10	-4.61775	-4.61777	-4.684076[b]	-4.4845	-4.6542
$1s2p_{-1}3d_{-2}$	0	-5.08355	-5.08379	-5.142319[b]	-5.0057	-5.0975
	0.1	-5.32136	-5.32140	-5.341030[b]	-5.2440	-5.3357
	0.5	-5.97050	-5.97052	-5.982253[b]	-5.8880	-5.9820
	1	-6.57079	-6.57081	-6.582361[b]	-6.4853	-6.5805
	1.8	-7.34721	-7.34723		-7.2576	-7.3545
	2	-7.52002	-7.52003	-7.530125[b]	-7.4293	-7.5268
	2.153	-7.64784	-7.64785		-7.5563	-7.6543
	2.16	-7.65360	-7.65361		-7.5620	-7.6600
	2.5	-7.92531	-7.92532		-7.8318	-7.9311
	3	-8.29920	-8.29920		-8.2030	-8.3044
	4	-8.97475			-8.8735	-8.9797
	5	-9.57693	-9.57694	-9.591769[b]	-9.4713	-9.5827
	5.4	-9.80146	-9.80147		-9.6943	-9.8079
	10	-11.93900	-11.93902	-11.957294[b]	-11.8209	-11.9588
	20	-15.16261	-15.16260		-15.0438	-15.2274
	50	-21.05051	-21.0505		-20.9843	-21.2681
	100	-27.01926	-27.0192		-27.0769	-27.4789
	200	-34.58498	-34.5850		-34.8991	-35.4725
	500	-47.55828	-47.5583		-48.5639	-49.4845
	1000	-60.05888	-60.0589		-62.0240	-63.3419
	2000	-75.28238			-78.7973	-80.6829

(a) From M. V. Ivanov and P. Schmelcher, Phys. Rev. A **57**, 3793 (1998);
(b) From O.-A. Al-Hujaj and P. Schmelcher, Phys. Rev. A **70**, 033411 (2004);
(c) From X. Guan and B. Li, PRA **63**, 043413 (2001).

Table B-4 Atomic energies of the Beryllium singly positive ion, Be^+, in B fields. Energies in Hartree, B in au. Numerical HF is from reference 88; CI from reference 8, except those labeled by (c), which are from frozen core approximation in reference 7. All others from present study. Ground states are indicated in orange.

State	B	Present HF	Numerical HF[a]	CI	LDA	PBE
$1s^2 2s$	0	-14.27746	-14.27747	-14.3247[b]	-14.1147	-14.2993
	0.001	-14.27796	-14.27797	-14.3251[b]	-14.1152	-14.2998
	0.002	-14.27846	-14.27846	-14.32226[c]	-14.1157	-14.3003
	0.004	-14.27953		-14.32326[c]	-14.1169	-14.3015
	0.01	-14.28241	-14.28241	-14.3296[b]	-14.1196	-14.3043
	0.02	-14.28724	-14.28725	-14.33105[c]	-14.1245	-14.3091
	0.05	-14.30110	-14.30111	-14.3482[b]	-14.1383	-14.3230
	0.1	-14.32206	-14.32207	-14.3694[b]	-14.1593	-14.3440
	0.2	-14.35648	-14.35648	-14.4038[b]	-14.1938	-14.3787
	0.3	-14.38211		-14.42588[c]	-14.2197	-14.4048
	0.4	-14.40046	-14.40046	-14.44420[c]	-14.2383	-14.4237
	0.5	-14.41281	-14.41282	-14.4606[b]	-14.2511	-14.4368
	0.6	-14.42021		-14.46390[c]	-14.2590	-14.4452
	0.7	-14.42350		-14.46700[c]	-14.2629	-14.4495
	0.8	-14.42334		-14.46697[c]	-14.2634	-14.4506
	1	-14.41477	-14.41478	-14.4630[b]	-14.2567	-14.4451
	2	-14.28223	-14.28225	-14.3300[b]	-14.1376	-14.3353
	5	-13.55017	-13.55019	-13.5971[b]	-13.4306	-13.6537
	10	-11.57651	-11.57652	-11.6231[b]	-11.4662	-11.7269
$1s^2 2p_{-1}$	0	-14.13090	-14.13093	-14.1741[b]	-13.9771	-14.1593
	0.01	-14.14085	-14.14087	-14.1841[b]	-13.9871	-14.1696
	0.05	-14.17913	-14.17916	-14.2216[b]	-14.0254	-14.2079
	0.1	-14.22387	-14.22390	-14.2672[b]	-14.0702	-14.2526
	0.2	-14.30404	-14.30406	-14.3476[b]	-14.1506	-14.3329
	0.3	-14.37399		-14.41738[c]	-14.2208	-14.4030
	0.4	-14.43597	-14.43599	-14.47926[c]	-14.2830	-14.4652
	0.5	-14.49161	-14.49163	-14.5358[b]	-14.3390	-14.5211
	0.6	-14.54207		-14.58512[c]	-14.3897	-14.5717
	0.7	-14.58819		-14.63109[c]	-14.4361	-14.6179
	0.8	-14.63057		-14.67332[c]	-14.4787	-14.6604
	1	-14.70590	-14.70591	-14.7520[b]	-14.5543	-14.7358
	2	-14.95180	-14.95181	-15.0000[b]	-14.7988	-14.9807
	5	-14.96818	-14.96820	-15.0184[b]	-14.7975	-14.9890
	10	-13.75772	-13.75733	-13.8087[b]	-13.5532	-13.7690
	20	-9.21789	-9.217910		-8.9640	-9.2287
	50	10.42839	10.42836		10.7504	10.3674
$1s2p_{-1}3d_{-2}$	0	-9.41049	-9.41056	-9.4156[b]	-9.2941	-9.4253
	0.1	-9.68350	-9.68356	-9.6888[b]	-9.5670	-9.6984
	0.2	-9.91871	-9.91878	-9.9243[b]	-9.8010	-9.9327
	0.5	-10.51254	-10.51259	-10.5188[b]	-10.3904	-10.5235
	1	-11.31310	-11.31312	-11.3203[b]	-11.1854	-11.3205
	2	-12.59205	-12.59206	-12.6002[b]	-12.4567	-12.5942
	5	-15.42816	-15.42817	-15.4367[b]	-15.2744	-15.4206

Table B-4 (*continued*)

State	*B*	Present HF	Numerical HF[a]	CI	LDA	PBE
$1s2p_{-1}3d_{-2}$	10	-18.82017	-18.820184	-18.8283[b]	-18.6433	-18.8096
	20	-23.61200	-23.612005		-23.4113	-23.6181
	50	-32.61958	-32.61959		-32.4163	-32.7191
	100	-41.93409	-41.93414		-41.7890	-42.2079
	200	-53.90637	-53.90638		-53.9257	-54.5138
	500	-74.73620	-74.73619		-75.2754	-76.2067
	1000	-95.07510	-95.07513		-96.4008	-97.7251
	2000	-120.11944	-120.11947		-122.7839	-124.6704

(a) From M. V. Ivanov and P. Schmelcher, Eur. Phys. J. D **14**, 279 (2001);
(b) From O.-A. Al-Hujaj and P. Schmelcher, Phys. Rev. A **70**, 023411 (2004);
(c) FromX. Guan, B. Li, and K. T. Taylor, J. Phys. B **36**, 2465 (2003).

Table B-5 Atomic energies of the Beryllium atom in *B* fields. Energies in Hartree, *B* in au. Numerical HF is from reference 88; CI from reference 8, except those labeled by (c), which are from frozen core approximation in reference 7. All others from present study. Ground states are indicated in orange.

State	*B*	Present HF	Numerical HF[a]	CI	LDA	PBE
$1s^22s^2$	0	-14.57302	-14.57336	-14.6405[b]	-14.4465	-14.6299
	0.001	-14.57304	-14.57336	-14.6410[b]	-14.4465	-14.6300
	0.01	-14.57288	-14.57322	-14.6408[b]	-14.4463	-14.6298
	0.02	-14.57244	-14.57279	-14.66238[c]	-14.4459	-14.6294
	0.03	-14.57173			-14.4452	-14.6287
	0.04	-14.57072			-14.4442	-14.6277
	0.05	-14.56944	-14.56986	-14.6393[b]	-14.4430	-14.6265
	0.07	-14.56605	-14.56657		-14.4396	-14.6232
	0.1	-14.55897		-14.6298[b]	-14.4327	-14.6163
	0.5	-14.30723	-14.32860	-14.3882[b]	-14.1861	-14.3721
	1	-13.79426	-13.89120	-13.9220[b]	-13.6858	-13.8762
$1s^22s2p_{-1}$	0.01	-14.52688	-14.52690	-14.5744[b]	-14.3714	-14.5568
	0.02	-14.54136	-14.54138	-14.59170[c]	-14.3859	-14.5713
	0.03	-14.55551			-14.4000	-14.5854
	0.04	-14.56931			-14.4138	-14.5992
	0.05	-14.58279	-14.58281	-14.6142[b]	-14.4272	-14.6126
	0.07	-14.60878	-14.60879		-14.4531	-14.6386
	0.1	-14.64546		-14.6936[b]	-14.4897	-14.6752
	0.15	-14.70106	-14.70108	-14.75127[c]	-14.5452	-14.7308
	0.2	-14.75063		-14.7979[b]	-14.5948	-14.7806
	0.3	-14.83519	-14.83520	-14.88560[c]	-14.6800	-14.8660
	0.3185	-14.84904	-14.84905		-14.6940	-14.8801
	0.4	-14.90463		-14.95507[c]	-14.7507	-14.9369
	0.5	-14.96262	-14.96264	-15.0107[b]	-14.8103	-14.9969
	0.6	-15.01170		-15.06181[c]	-14.8615	-15.0483
	0.8	-15.08987		-15.13834[c]	-14.9450	-15.1322
	1	-15.14895	-15.14899	-15.1982[b]	-15.0103	-15.1981
	2	-15.30813	-15.30815	-15.3551[b]	-15.2027	-15.3960

Table B-5 (*continued*)

State	*B*	Present HF	Numerical HF[a]	CI	LDA	PBE
$1s^2 2s 2p_{-1}$	5	-15.25182	-15.25183	-15.3002[b]	-15.1799	-15.4007
$1s^2 2p_{-1} 3d_{-2}$	0.1	-14.37791		-14.4082[b]	-14.2326	-14.4153
	0.2	-14.51754		-14.5492[b]	-14.3705	-14.5540
	0.3	-14.63365	-14.63369		-14.4854	-14.6698
	0.4	-14.73393			-14.5849	-14.7700
	0.5	-14.82270	-14.82272	-14.8530[b]	-14.6732	-14.8590
	0.6	-14.90260			-14.7529	-14.9391
	0.8	-15.04230			-14.8924	-15.0794
	1	-15.16176	-15.16178	-15.1975[b]	-15.0118	-15.1994
	2	-15.57494	-15.57496	-15.6217[b]	-15.4245	-15.6143
	3	-15.79983			-15.6469	-15.8400
	4	-15.90158			-15.7448	-15.9423
	4.501	-15.91624	-15.91626		-15.7573	-15.9573
	5	-15.91025	-15.91027	-15.9493[b]	-15.7491	-15.9517
	10	-15.04641	-15.04644	-15.0875[b]	-14.8638	-15.0963
	20	-10.97097	-10.97100		-10.7632	-11.0544
	50	7.83402	7.83395		8.0441	7.6128
$1s 2p_{-1} 3d_{-2} 4f_{-3}$	1	-11.72872	-11.72880	-11.7358[b]	-11.6049	-11.7440
	2	-13.16959	-13.16961	-13.1762[b]	-13.0384	-13.1831
	3	-14.35015			-14.2142	-14.3635
	4	-15.38048			-15.2407	-15.3945
	4.501	-15.85572			-15.7143	-15.8704
	5	-16.30689	-16.30690	-16.3139[b]	-16.1639	-16.3225
	10	-20.01751	-20.01753	-20.0242[b]	-19.8656	-20.0497
	20	-25.23248	-25.23250		-25.0850	-25.3181
	30	-29.11101			-28.9821	-29.2579
	40	-32.28414	-32.28415		-32.1803	-32.4941
	50	-35.00766	-35.00768		-34.9326	-35.2806
	100	-45.10513	-45.10519		-45.1927	-45.6795
	200	-58.08260	-58.08264		-58.5053	-59.1944
	500	-80.67355	-80.67357		-82.0025	-83.1010
	1000	-102.75472	-102.7548		-105.3481	-106.9144
	2000	-129.97904	-129.9790		-134.6277	-136.8618

(a) From M. V. Ivanov and P. Schmelcher, Eur. Phys. J. D **14**, 279 (2001);
(b) From O.-A. Al-Hujaj and P. Schmelcher, Phys. Rev. A **70**, 023411 (2004);
(c) FromX. Guan, B. Li, and K. T. Taylor, J. Phys. B **36**, 2465 (2003).

Table B-6 Atomic energies of the Boron singly positive ion, B^+, in *B* fields. Energies in Hartree, *B* in au. Numerical HF is from reference 89; All others from present study. Ground states are indicated in orange.

State	*B*	Present HF	Numerical HF	LDA	PBE
$1s^2 2s^2$	0	-24.23757	-24.23758	-24.0373	-24.2934
	0.01	-24.23751	-24.23752	-24.0372	-24.2934
	0.05	-24.23592	-24.23593	-24.0357	-24.2918

Table B-6 (*continued*)

State	*B*	Present HF	Numerical HF	LDA	PBE
$1s^2 2s^2$	0.07	-24.23434	-24.23435	-24.0341	-24.2903
	0.07811	-24.23355	-24.23356	-24.0333	-24.2895
	0.1	-24.23099	-24.23100	-24.0308	-24.2870
	0.2	-24.21160	-24.21161	-24.0115	-24.2679
	0.3	-24.18034	-24.18047	-23.9805	-24.2372
	0.4	-24.13837	-24.13926	-23.9389	-24.1959
	0.5	-24.08691	-24.08953	-23.8879	-24.1454
	1	-23.72226	-23.75518	-23.5270	-23.7872
$1s^2 2s 2p_{-1}$	0	-24.12015	-24.12078	-23.8855	-24.1418
	0.01	-24.13570	-24.13573	-23.9005	-24.1569
	0.05	-24.19396	-24.19399	-23.9588	-24.2152
	0.07	-24.22223	-24.22226	-23.9870	-24.2435
	0.07811	-24.23353	-24.23356	-23.9983	-24.2548
	0.1	-24.26357	-24.26360	-24.0283	-24.2848
	0.2	-24.39242	-24.39245	-24.1571	-24.4136
	0.3	-24.50850	-24.50852	-24.2732	-24.5298
	0.4	-24.61321	-24.61324	-24.3780	-24.6348
	0.5	-24.70796	-24.70798	-24.4730	-24.7300
	0.6	-24.79399	-24.79401	-24.5595	-24.8166
	0.8	-24.94405	-24.94408	-24.7109	-24.9685
	1	-25.07023	-25.07026	-24.8391	-25.0970
	1.5	-25.31062	-25.31064	-25.0867	-25.3456
	1.6761	-25.37642	-25.37644	-25.1556	-25.4149
	1.8143	-25.42280	-25.42283	-25.2046	-25.4643
	2	-25.47886	-25.47889	-25.2643	-25.5246
	2.5	-25.60152		-25.3976	-25.6596
	3	-25.69387	-25.69390	-25.5005	-25.7648
	4	-25.81860	-25.81863	-25.6430	-25.9132
	5	-25.88462	-25.88465	-25.7212	-25.9981
	10	-25.54205	-25.54207	-25.3982	-25.7121
$1s^2 2p_{-1} 3d_{-2}$	0	-23.39306	-23.39320	-23.1756	-23.4268
	0.1	-23.61603	-23.6162	-23.3984	-23.6499
	0.5	-24.24283	-24.2429	-24.0200	-24.2733
	1	-24.78666	-24.78674	-24.5594	-24.8153
	1.5	-25.20281	-25.20288	-24.9730	-25.2304
	1.8143	-25.42277	-25.42282	-25.1917	-25.4499
	2	-25.54102	-25.54108	-25.3092	-25.5679
	2.5	-25.82390		-25.5902	-25.8500
	3	-26.06393	-26.06397	-25.8282	-26.0892
	4	-26.44417	-26.44420	-26.2042	-26.4680
	5	-26.71996	-26.71999	-26.4753	-26.7423
	7	-27.03668	-27.03671	-26.7819	-27.0567
	8	-27.10172	-27.10174	-26.8418	-27.1209
	10	-27.08414	-27.08417	-26.8140	-27.1024
	20	-25.06408	-25.06410	-24.7520	-25.0900
	50	-10.65832	-10.65835	-10.2914	-10.7602
$1s 2p_{-1} 3d_{-2} 4f_{-3}$	0	-15.23729	-15.237424	-15.0882	-15.2612
	1	-18.07234	-18.07243	-17.9049	-18.0849

Table B-6 (*continued*)

State	*B*	Present HF	Numerical HF	LDA	PBE
$1s2p_{-1}3d_{-2}4f_{-3}$	5	-24.01516	-24.01520	-23.8148	-24.0139
	7	-26.16678	-26.16682	-25.9571	-26.1641
	8	-27.14062	-27.14064	-26.9270	-27.1381
	10	-28.93502	-28.93504	-28.7145	-28.9341
	20	-36.02017	-36.02020	-35.7813	-36.0431
	30	-41.38293	-41.38296	-41.1416	-41.4429
	40	-45.81146	-45.81149	-45.5765	-45.9137
	50	-49.63541	-49.63544	-49.4122	-49.7823
	100	-63.94724	-63.947265	-63.8180	-64.3235
	200	-82.55704	-82.55711	-82.6656	-83.3703
	500	-115.33673		-116.1676	-117.2772
	1000	-147.71740		-149.6245	-151.1968
	2000	-187.99218		-191.7212	-193.9542

Table B-7 Atomic energies of the Boron atom in *B* fields. Energies in Hartree, *B* in au. Numerical HF is from reference 89; Ground states are indicated in orange.

State	*B*	Present HF	Numerical HF	LDA	PBE
$1s^2 2s^2 2p_{-1}$	0.01	-24.54011	-24.54018	-24.3632	-24.6174
	0.05	-24.57671	-24.57679	-24.3997	-24.6540
	0.07	-24.59334	-24.59340	-24.4163	-24.6706
	0.07811	-24.59977		-24.4227	-24.6770
	0.1	-24.61625	-24.61631	-24.4391	-24.6934
	0.2	-24.67629	-24.67634	-24.4989	-24.7534
	0.3	-24.71433	-24.71439	-24.5370	-24.7919
	0.4	-24.73414	-24.73424	-24.5573	-24.8126
	0.5	-24.73877	-24.73975	-24.5627	-24.8185
	1	-24.60461	-24.63172	-24.4367	-24.6953
$1s^2 2s 2p_0 2p_{-1}$	0.01	-24.47095	-24.47112	-24.2536	-24.5083
	0.05	-24.54806	-24.54823	-24.3305	-24.5853
	0.07	-24.58519	-24.58536	-24.3675	-24.6223
	0.07811	-24.59998	-24.60015	-24.3822	-24.6370
	0.1	-24.63915	-24.63932	-24.4212	-24.6760
	0.2	-24.80494	-24.80511	-24.5856	-24.8406
	0.3	-24.95164	-24.95180	-24.7307	-24.9862
	0.4	-25.08238	-25.08255	-24.8599	-25.1159
	0.5	-25.19978	-25.19996	-24.9759	-25.2325
	0.6	-25.30594	-25.30612	-25.0808	-25.3380
	0.8	-25.49085	-25.49103	-25.2635	-25.5220
	1	-25.64692	-25.64711	-25.4179	-25.6777
	1.5	-25.94975	-25.94997	-25.7182	-25.9814
	1.6761	-26.03495	-26.03522	-25.8030	-26.0674
	1.8143	-26.09592		-25.8639	-26.1293
	2	-26.17107	-26.17110	-25.9392	-26.2059
	5	-26.79526	-26.79531	-26.5919	-26.8851
$1s^2 2s 2p_{-1} 3d_{-2}$	1	-25.56896	-25.56899	-25.3483	-25.6074
	1.5	-25.93109	-25.93113	-25.7194	-25.9812

Table B-7 (*continued*)

State	*B*	Present HF	Numerical HF	LDA	PBE
$1s^2 2s 2p_{-1} 3d_{-2}$	1.6761	-26.03517	-26.03522	-25.8276	-26.0903
	1.8143	-26.11044	-26.11049	-25.9064	-26.1697
	2	-26.20410	-26.20413	-26.0050	-26.2692
	2.23984	-26.31433	-26.31437	-26.1219	-26.3873
	2.4779	-26.41397	-26.41401	-26.2282	-26.4947
	2.5	-26.42279	-26.42283	-26.2376	-26.5043
	5	-27.12857	-27.12860	-26.9889	-27.2731
$1s^2 2p_0 2p_{-1} 3d_{-2}$	1	-25.36887	-25.36901	-25.2182	-25.4660
	1.5	-25.80947	-25.80961	-25.6638	-25.9134
	1.8143	-26.04216		-25.8986	-26.1492
	2	-26.16559	-26.16572	-26.0246	-26.2759
	2.23984	-26.31425	-26.31437	-26.1753	-26.4274
	2.4779	-26.45005	-26.45018	-26.3130	-26.5660
	2.5	-26.46211	-26.46224	-26.3252	-26.5784
	3	-26.71284	-26.71297	-26.5795	-26.8347
	4	-27.10845	-27.10860	-26.9807	-27.2408
	5	-27.39426	-27.39442	-27.2706	-27.5363
	10	-27.77130	-27.77139	-27.6590	-27.9591
$1s^2 2p_{-1} 3d_{-2} 4f_{-3}$	1	-25.20248	-25.20257	-24.9789	-25.2387
	2	-26.11853	-26.11859	-25.8903	-26.1567
	2.4779	-26.45012	-26.45018	-26.2208	-26.4896
	2.5	-26.46426	-26.46431	-26.2348	-26.5038
	3	-26.76014	-26.76019	-26.5297	-26.8011
	4	-27.23762	-27.23765	-27.0051	-27.2814
	5	-27.59735	-27.59737	-27.3627	-27.6439
	7	-28.05666	-28.05669	-27.8174	-28.1092
	7.957	-28.17992	-28.17996	-27.9384	-28.2355
	8	-28.18421	-28.18424	-27.9426	-28.2400
	10	-28.27942	-28.27946	-28.0333	-28.3422
	50	-13.06551	-13.06555	-12.8236	-13.3414
$1s 2p_{-1} 3d_{-2} 4f_{-3} 5g_{-4}$	1	-18.45800	-18.45809	-18.2958	-18.4798
	5	-24.83952	-24.83956	-24.6556	-24.8668
	7	-27.12782	-27.12785	-26.9412	-27.1632
	7.957	-28.11827		-27.9309	-28.1581
	8	-28.16147	-28.16150	-27.9741	-28.2015
	10	-30.06359	-30.06363	-29.8759	-30.1138
	20	-37.55464	-37.55469	-37.3796	-37.6684
	30	-43.21386	-43.213901	-43.0648	-43.3998
	40	-47.88388	-47.883924	-47.7676	-48.1443
	50	-51.91495	-51.91499	-51.8351	-52.2500
	100	-66.99696	-66.99699	-67.1195	-67.6908
	200	-86.60730	-86.60738	-87.1424	-87.9436
	500	-121.16486	-121.16488	-122.8141	-124.0823
	1000	-155.32948	-155.3296	-158.5373	-160.3385
	2000	-197.86533	-197.8655	-203.6173	-206.1782

Table B-8 Atomic energies of the Carbon atom in *B* fields. Energies in Hartree, *B* in au. Numerical HF is from reference 90; Ground states are indicated in orange.

State	*B*	Present HF	Numerical HF	LDA	PBE
$1s^2 2s^2 2p_0 2p_{-1}$	0	-37.69090	-37.69096	-37.4680	-37.7944
	0.01	-37.70580	-37.7059	-37.4829	-37.8093
	0.05	-37.76304	-37.7633	-37.5400	-37.8664
	0.1	-37.82994	-37.8302	-37.6066	-37.9330
	0.2	-37.94835	-37.9486	-37.7241	-38.0506
	0.3	-38.04780	-38.0479	-37.8224	-38.1492
	0.4	-38.13006	-38.1302	-37.9035	-38.2306
	0.5	-38.19664	-38.1973	-37.9689	-38.2964
$1s^2 2s 2p_0 2p_{-1} 2p_{+1}$	0.1	-37.78785	-37.7882	-37.5080	-37.8355
	0.2	-37.95500	-37.9552	-37.6737	-38.0013
	0.3	-38.10236	-38.1026	-37.8191	-38.1471
	0.4	-38.23206	-38.2323	-37.9468	-38.2753
	0.5	-38.34613	-38.3464	-38.0591	-38.3881
	0.6	-38.44601	-38.4467	-38.1573	-38.4869
	0.8	-38.61100	-38.6116	-38.3196	-38.6506
	1	-38.73696	-38.7373	-38.4438	-38.7761
$1s^2 2s 2p_0 2p_{-1} 3d_{-2}$	0.4	-38.16215	-38.1624	-37.8764	-38.2027
	0.5	-38.35375	-38.3541	-38.0673	-38.3935
	0.6	-38.53370	-38.5339	-38.2462	-38.5727
	0.8	-38.86300	-38.8632	-38.5731	-38.9006
	1	-39.15752	-39.1577	-38.8652	-39.1941
	2	-40.27685	-40.2769	-39.9767	-40.3135
	3	-41.04743	-41.0477	-40.7464	-41.0903
	4	-41.63173	-41.6319	-41.3355	-41.6861
	5	-42.10143	-42.1016	-41.8142	-42.1717
	10	-43.47679	-43.4769	-43.2522	-43.6525
$1s^2 2p_0 2p_{-1} 3d_{-2} 4f_{-3}$	1	-38.40409	-38.4043	-38.1922	-38.5107
	2	-39.76198	-39.7621	-39.5550	-39.8769
	3	-40.77794	-40.7780	-40.5769	-40.9029
	4	-41.58847	-41.5886	-41.3931	-41.7233
	5	-42.25476	-42.2549	-42.0645	-42.3992
	7	-43.27693	-43.2771	-43.0950	-43.4400
	8	-43.66834	-43.6685	-43.4900	-43.8406
	10	-44.26570	-44.2659	-44.0938	-44.4562
	11	-44.48601		-44.3170	-44.6856
	12	-44.66133	-44.6615	-44.4952	-44.8702
$1s^2 2p_{-1} 3d_{-2} 4f_{-3} 5g_{-4}$	1	-37.81283	-37.8130	-37.5149	-37.8497
	5	-42.06075	-42.0608	-41.7472	-42.1113
	7	-43.21948	-43.2195	-42.9043	-43.2802
	8	-43.67332	-43.6734	-43.3576	-43.7393
	10	-44.38714	-44.3872	-44.0704	-44.4637
	11	-44.66223		-44.3451	-44.7443
	12	-44.89040	-44.8905	-44.5730	-44.9780
	15	-45.33461	-45.3348	-45.0168	-45.4394
	20	-45.44642	-45.4465	-45.1298	-45.5816
$1s 2p_0 2p_{-1} 3d_{-2} 4f_{-3} 5g_{-4}$	1	-28.01924	-28.0195	-27.9066	-28.1223

Table B-8 (*continued*)

State	B	Present HF	Numerical HF	LDA	PBE
$1s2p_0 2p_{-1} 3d_{-2} 4f_{-3} 5g_{-4}$	5	-35.96005	-35.9601	-35.8547	-36.0840
	10	-42.52763	-42.5277	-42.4404	-42.6918
	11	-43.64185		-43.5586	-43.8148
	12	-44.70921	-44.7094	-44.6300	-44.8911
	15	-47.67672	-47.6770	-47.6103	-47.8869
	20	-52.02805	-52.0282	-51.9852	-52.2884
	30	-59.27456	-59.2747	-59.2851	-59.6420
	50	-70.51859	-70.5187	-70.6485	-71.1076
$1s2p_{-1} 3d_{-2} 4f_{-3} 5g_{-4} 6h_{-4}$	1	-26.78405	-26.7843	-26.5823	-26.8134
	5	-35.18143	-35.1815	-34.9563	-35.2215
	10	-42.07983	-42.0799	-41.8560	-42.1517
	15	-47.50012	-45.5002	-47.2857	-47.6090
	20	-52.08898	-52.0890	-51.8882	-52.2377
	30	-59.74324	-59.7433	-59.5777	-59.9760
	40	-66.10717	-66.1073	-65.9830	-66.4261
	50	-71.62837	-71.6285	-71.5491	-72.0335
	100	-92.45517	-92.4552	-92.6194	-93.2756
	200	-119.81264	-119.8127	-120.4671	-121.3785
	500	-168.52468	-168.5248	-170.4975	-171.9285
	1000	-217.14114	-217.1413	-220.9602	-222.9850
	2000	-278.16083	-278.1612	-285.0006	-287.8708

APPENDIX C
EXCHANGE AND CORRELATION ENERGIES OF ATOMS HE, LI, BE, AND POSITIVE IONS LI^+, BE^+ IN MAGNETIC FIELDS

All energies in Hartree; B in au; Negative signs are omitted. E_c^{HF} values are derived from the energy difference between the correlated calculations and HF energies listed in Appendix B. Notice the correlated data may be from different sources. Refer to Appendix B for the cited references.

Table C-1 Exchange and correlation energies of the Helium atom in magnetic fields

B	E_x^{HF}	E_c^{HF}	E_{xc}^{HF}	E_x^{LDA}	E_c^{LDA}	E_{xc}^{LDA}	E_x^{PBE}	E_c^{PBE}	E_{xc}^{PBE}
$1s^2$									
0	1.0258	0.0417	1.0674	0.8618	0.1111	0.9729	1.0051	0.0411	1.0462
0.02	1.0258	0.0417	1.0675	0.8618	0.1111	0.9729	1.0052	0.0411	1.0462
0.04	1.0259	0.0417	1.0676	0.8619	0.1111	0.9730	1.0053	0.0411	1.0464
0.08	1.0264	0.0417	1.0681	0.8624	0.1111	0.9735	1.0058	0.0411	1.0469
0.16	1.0284	0.0416	1.0701	0.8642	0.1112	0.9755	1.0077	0.0412	1.0489
0.24	1.0316	0.0416	1.0732	0.8671	0.1114	0.9786	1.0108	0.0413	1.0520
0.4	1.0410	0.0415	1.0825	0.8756	0.1120	0.9876	1.0197	0.0416	1.0613
0.5	1.0485	0.0414	1.0899	0.8823	0.1124	0.9947	1.0268	0.0419	1.0687
0.8	1.0759	0.0407	1.1166	0.9063	0.1138	1.0201	1.0523	0.0427	1.0950
1	1.0964	0.0406	1.1371	0.9241	0.1148	1.0389	1.0713	0.0433	1.1147
1.6	1.1616	0.0406	1.2021	0.9799	0.1178	1.0977	1.1316	0.0450	1.1766
2	1.2048	0.0406	1.2454	1.0167	0.1197	1.1364	1.1718	0.0460	1.2178
5	1.4830	0.0424	1.5254	1.2555	0.1301	1.3856	1.4357	0.0508	1.4864
10	1.8186	0.0460	1.8647	1.5485	0.1406	1.6891	1.7644	0.0545	1.8189
20	2.2820	0.0526	2.3346	1.9629	0.1527	2.1155	2.2346	0.0576	2.2922
50	3.1300	0.0676	3.1975	2.7514	0.1703	2.9217	3.1404	0.0604	3.2009
100	3.9856	0.0859	4.0715	3.5876	0.1845	3.7721	4.1134	0.0614	4.1747
1s2s									
0	0.7435	0.0010	0.7445	0.6322	0.0431	0.6753	0.7310	0.0123	0.7433
0.02	0.7441	0.0010	0.7450	0.6327	0.0432	0.6758	0.7315	0.0123	0.7438
0.04	0.7455	0.0010	0.7465	0.6340	0.0433	0.6773	0.7329	0.0124	0.7453
0.08	0.7502	0.0010	0.7513	0.6384	0.0436	0.6820	0.7375	0.0125	0.7500
0.16	0.7616	0.0012	0.7628	0.6492	0.0442	0.6935	0.7489	0.0129	0.7618
0.24	0.7722	0.0013	0.7735	0.6596	0.0448	0.7044	0.7603	0.0129	0.7733
0.4	0.7884	0.0015	0.7898	0.6772	0.0458	0.7231	0.7806	0.0128	0.7934
0.5	0.7958	0.0015	0.7973	0.6868	0.0464	0.7332	0.7922	0.0128	0.8050
0.8	0.8136	0.0015	0.8151	0.7127	0.0477	0.7604	0.8232	0.0131	0.8363
1	0.8251	0.0015	0.8266	0.7288	0.0485	0.7773	0.8422	0.0132	0.8554
1.6	0.8625	0.0015	0.8639	0.7747	0.0503	0.8249	0.8953	0.0135	0.9088
2	0.8881	0.0015	0.8896	0.8037	0.0513	0.8549	0.9288	0.0136	0.9424
5	1.0589	0.0015	1.0604	0.9871	0.0563	1.0434	1.1419	0.0141	1.1560

Table C-1 (*continued*)

B	E_x^{HF}	E_c^{HF}	E_{xc}^{HF}	E_x^{LDA}	E_c^{LDA}	E_{xc}^{LDA}	E_x^{PBE}	E_c^{PBE}	E_{xc}^{PBE}
1s2s									
10	1.2666	0.0015	1.2681	1.2098	0.0612	1.2709	1.4040	0.0144	1.4185
20	1.5510	0.0014	1.5524	1.5239	0.0667	1.5906	1.7782	0.0147	1.7929
50	2.0645	0.0013	2.0657	2.1222	0.0749	2.1971	2.5010	0.0148	2.5158
100	2.5769	0.0011	2.5780	2.7557	0.0816	2.8372	3.2752	0.0147	3.2898
$1s2p_0$									
0	0.7332	0.0016	0.7348	0.6356	0.0438	0.6794	0.7358	0.0111	0.7469
0.02	0.7333	0.0015	0.7348	0.6370	0.0439	0.6809	0.7379	0.0111	0.7490
0.04	0.7349	0.0015	0.7364	0.6385	0.0440	0.6825	0.7394	0.0112	0.7506
0.08	0.7400	0.0016	0.7416	0.6432	0.0443	0.6876	0.7442	0.0114	0.7556
0.16	0.7524	0.0019	0.7543	0.6551	0.0451	0.7003	0.7565	0.0118	0.7683
0.24	0.7644	0.0022	0.7666	0.6665	0.0458	0.7124	0.7682	0.0121	0.7803
0.4	0.7869	0.0026	0.7895	0.6890	0.0471	0.7361	0.7917	0.0127	0.8044
0.5	0.7999	0.0029	0.8028	0.7022	0.0477	0.7499	0.8054	0.0131	0.8185
0.8	0.8364	0.0034	0.8398	0.7383	0.0493	0.7876	0.8436	0.0138	0.8574
1	0.8592	0.0037	0.8628	0.7606	0.0502	0.8108	0.8673	0.0142	0.8815
1.6	0.9226	0.0042	0.9267	0.8215	0.0523	0.8738	0.9331	0.0150	0.9481
2	0.9614	0.0044	0.9658	0.8583	0.0534	0.9118	0.9734	0.0155	0.9889
5	1.1898	0.0053	1.1951	1.0755	0.0590	1.1344	1.2172	0.0169	1.2340
10	1.4425	0.0060	1.4484	1.3233	0.0640	1.3872	1.5028	0.0175	1.5203
20	1.7681	0.0067	1.7748	1.6602	0.0694	1.7296	1.8990	0.0175	1.9165
50	2.3227	0.0072	2.3299	2.2838	0.0774	2.3611	2.6469	0.0171	2.6640
100	2.8526	0.0072	2.8597	2.9360	0.0838	3.0198	3.4425	0.0165	3.4591
$1s2p_{-1}$									
0	0.7276	0.0018	0.7295	0.6239	0.0430	0.6669	0.7210	0.0107	0.7317
0.02	0.7281	0.0018	0.7298	0.6249	0.0431	0.6680	0.7223	0.0107	0.7331
0.04	0.7307	0.0018	0.7325	0.6273	0.0432	0.6706	0.7248	0.0108	0.7356
0.08	0.7385	0.0020	0.7405	0.6347	0.0438	0.6785	0.7323	0.0110	0.7433
0.16	0.7562	0.0026	0.7588	0.6515	0.0449	0.6964	0.7495	0.0114	0.7609
0.24	0.7732	0.0031	0.7763	0.6677	0.0459	0.7136	0.7661	0.0117	0.7777
0.4	0.8046	0.0040	0.8086	0.6976	0.0475	0.7451	0.7963	0.0121	0.8085
0.5	0.8229	0.0045	0.8274	0.7150	0.0483	0.7633	0.8139	0.0124	0.8263
0.8	0.8744	0.0054	0.8798	0.7629	0.0504	0.8132	0.8625	0.0133	0.8758
1	0.9066	0.0058	0.9124	0.7924	0.0515	0.8438	0.8928	0.0138	0.9066
1.6	0.9955	0.0066	1.0021	0.8729	0.0541	0.9270	0.9762	0.0153	0.9915
2	1.0495	0.0069	1.0563	0.9215	0.0555	0.9769	1.0271	0.0162	1.0432
5	1.3654	0.0082	1.3736	1.2070	0.0622	1.2692	1.3316	0.0199	1.3514
10	1.7213	0.0100	1.7313	1.5357	0.0681	1.6039	1.6876	0.0226	1.7102
20	2.1979	0.0129	2.2107	1.9892	0.0746	2.0639	2.1829	0.0251	2.2080
50	3.0525	0.0196	3.0721	2.8410	0.0839	2.9249	3.1211	0.0278	3.1489
100	3.9053	0.0281	3.9334	3.7398	0.0912	3.8310	4.1194	0.0294	4.1489
$1s3d_{-1}$									
0	0.6690	0.0001	0.6691	0.5672	0.0379	0.6051	0.6627	0.0097	0.6724
0.02	0.6718	0.0001	0.6718	0.5695	0.0382	0.6077	0.6651	0.0098	0.6749
0.04	0.6765	0.0001	0.6766	0.5739	0.0387	0.6126	0.6700	0.0100	0.6800
0.08	0.6854	0.0002	0.6856	0.5826	0.0397	0.6223	0.6798	0.0104	0.6902
0.16	0.6993	0.0003	0.6996	0.5968	0.0411	0.6379	0.6965	0.0109	0.7073
0.24	0.7104	0.0004	0.7108	0.6082	0.0420	0.6503	0.7095	0.0112	0.7207

Table C-1 (*continued*)

B	E_x^{HF}	E_c^{HF}	E_{xc}^{HF}	E_x^{LDA}	E_c^{LDA}	E_{xc}^{LDA}	E_x^{PBE}	E_c^{PBE}	E_{xc}^{PBE}
$1s3d_{-1}$									
0.4	0.7287	0.0007	0.7293	0.6276	0.0435	0.6711	0.7314	0.0117	0.7431
0.5	0.7387	0.0008	0.7396	0.6384	0.0442	0.6826	0.7435	0.0120	0.7554
0.8	0.7663	0.0013	0.7675	0.6681	0.0459	0.7139	0.7761	0.0126	0.7886
1	0.7835	0.0015	0.7850	0.6866	0.0468	0.7334	0.7963	0.0129	0.8092
1.6	0.8325	0.0021	0.8345	0.7384	0.0489	0.7873	0.8528	0.0135	0.8664
2	0.8632	0.0024	0.8656	0.7705	0.0501	0.8205	0.8880	0.0139	0.9019
5	1.0543	0.0037	1.0580	0.9655	0.0557	1.0212	1.1061	0.0154	1.1215
10	1.2780	0.0048	1.2828	1.1939	0.0608	1.2547	1.3679	0.0164	1.3843
20	1.5783	0.0060	1.5843	1.5077	0.0664	1.5741	1.7343	0.0171	1.7515
50	2.1099	0.0076	2.1175	2.0906	0.0744	2.1649	2.4281	0.0176	2.4457
100	2.6322	0.0085	2.6407	2.6997	0.0808	2.7804	3.1655	0.0176	3.1831
$1s3d_{-2}$									
0	0.6722	0.0005	0.6726	0.5676	0.0380	0.6056	0.6607	0.0103	0.6710
0.02	0.6744	0.0002	0.6746	0.5713	0.0384	0.6097	0.6657	0.0103	0.6761
0.04	0.6799	0.0001	0.6800	0.5766	0.0390	0.6156	0.6716	0.0106	0.6822
0.08	0.6910	0.0002	0.6912	0.5869	0.0401	0.6270	0.6834	0.0110	0.6943
0.16	0.7086	0.0004	0.7090	0.6035	0.0417	0.6451	0.7020	0.0116	0.7136
0.24	0.7227	0.0006	0.7234	0.6170	0.0428	0.6598	0.7170	0.0120	0.7291
0.4	0.7463	0.0012	0.7475	0.6404	0.0444	0.6848	0.7421	0.0127	0.7548
0.5	0.7594	0.0015	0.7609	0.6537	0.0452	0.6989	0.7560	0.0131	0.7690
0.8	0.7951	0.0024	0.7975	0.6907	0.0472	0.7379	0.7940	0.0137	0.8077
1	0.8174	0.0029	0.8204	0.7141	0.0483	0.7624	0.8177	0.0140	0.8318
1.6	0.8806	0.0041	0.8847	0.7797	0.0508	0.8305	0.8847	0.0148	0.8994
2	0.9201	0.0048	0.9248	0.8203	0.0522	0.8725	0.9266	0.0152	0.9417
5	1.1654	0.0074	1.1729	1.0671	0.0589	1.1260	1.1869	0.0175	1.2044
10	1.4563	0.0099	1.4661	1.3577	0.0648	1.4225	1.4995	0.0196	1.5191
20	1.8551	0.0133	1.8684	1.7614	0.0713	1.8327	1.9383	0.0216	1.9598
50	2.5828	0.0207	2.6035	2.5221	0.0806	2.6026	2.7722	0.0237	2.7959
100	3.3180	0.0299	3.3478	3.3260	0.0879	3.4139	3.6606	0.0248	3.6854
$1s4f_{-2}$									
0	0.6506	0.0000	0.6506	0.5533	0.0360	0.5892	0.6452	0.0090	0.6542
0.02	0.6561	0.0000	0.6561	0.5562	0.0365	0.5927	0.6489	0.0091	0.6580
0.04	0.6622	0.0001	0.6623	0.5617	0.0372	0.5989	0.6554	0.0093	0.6647
0.08	0.6715	0.0002	0.6718	0.5712	0.0384	0.6096	0.6669	0.0097	0.6765
0.16	0.6848	0.0002	0.6850	0.5848	0.0399	0.6246	0.6831	0.0101	0.6932
0.24	0.6949	0.0002	0.6951	0.5952	0.0409	0.6360	0.6956	0.0104	0.7060
0.4	0.7115	0.0003	0.7118	0.6125	0.0423	0.6548	0.7162	0.0108	0.7271
0.5	0.7206	0.0004	0.7210	0.6221	0.0430	0.6650	0.7275	0.0110	0.7385
0.8	0.7458	0.0007	0.7465	0.6485	0.0446	0.6930	0.7578	0.0116	0.7694
1	0.7618	0.0009	0.7627	0.6651	0.0454	0.7105	0.7766	0.0119	0.7885
1.6	0.8072	0.0014	0.8086	0.7120	0.0475	0.7595	0.8293	0.0125	0.8419
2	0.8360	0.0017	0.8377	0.7413	0.0487	0.7900	0.8623	0.0129	0.8752
5	1.0180	0.0032	1.0212	0.9240	0.0542	0.9782	1.0691	0.0143	1.0833
10	1.2352	0.0044	1.2396	1.1419	0.0593	1.2011	1.3201	0.0152	1.3353
20	1.5305	0.0056	1.5361	1.4441	0.0649	1.5090	1.6741	0.0159	1.6900
50	2.0590	0.0070	2.0661	2.0088	0.0728	2.0816	2.3463	0.0165	2.3627
100	2.5815	0.0078	2.5894	2.6002	0.0793	2.6795	3.0648	0.0165	3.0813

Table C-1 (*continued*)

B	E_x^{HF}	E_c^{HF}	E_{xc}^{HF}	E_x^{LDA}	E_c^{LDA}	E_{xc}^{LDA}	E_x^{PBE}	E_c^{PBE}	E_{xc}^{PBE}
$1s4f_{-3}$									
0	0.6518	0.0000	0.6518	0.5561	0.0363	0.5925	0.6472	0.0096	0.6568
0.02	0.6588	0.0000	0.6588	0.5594	0.0369	0.5963	0.6517	0.0097	0.6614
0.04	0.6663	0.0001	0.6664	0.5658	0.0378	0.6036	0.6595	0.0099	0.6694
0.08	0.6776	0.0001	0.6777	0.5766	0.0390	0.6157	0.6720	0.0104	0.6823
0.16	0.6941	0.0002	0.6942	0.5921	0.0406	0.6327	0.6903	0.0108	0.7012
0.24	0.7070	0.0003	0.7073	0.6043	0.0417	0.6460	0.7045	0.0112	0.7157
0.4	0.7283	0.0006	0.7289	0.6246	0.0433	0.6679	0.7277	0.0118	0.7395
0.5	0.7401	0.0008	0.7408	0.6360	0.0440	0.6800	0.7403	0.0121	0.7524
0.8	0.7721	0.0015	0.7736	0.6675	0.0459	0.7133	0.7741	0.0130	0.7872
1	0.7920	0.0020	0.7941	0.6874	0.0468	0.7342	0.7952	0.0135	0.8088
1.6	0.8484	0.0035	0.8519	0.7439	0.0493	0.7931	0.8541	0.0148	0.8689
2	0.8838	0.0043	0.8881	0.7794	0.0506	0.8299	0.8914	0.0153	0.9066
5	1.1059	0.0093	1.1152	1.0000	0.0570	1.0570	1.1251	0.0173	1.1424
10	1.3732	0.0148	1.3880	1.2648	0.0628	1.3275	1.4106	0.0187	1.4293
20	1.7436	0.0221	1.7657	1.6356	0.0692	1.7048	1.8150	0.0201	1.8351
50	2.4251	0.0358	2.4608	2.3378	0.0783	2.4161	2.5880	0.0215	2.6096
100	3.1176	0.0503	3.1679	3.0815	0.0856	3.1670	3.4142	0.0222	3.4365

Table C-2 Exchange and correlation energies of the Li^+ ion in magnetic fields

B	E_x^{HF}	E_c^{HF}	E_{xc}^{HF}	E_x^{LDA}	E_c^{LDA}	E_{xc}^{LDA}	E_x^{PBE}	E_c^{PBE}	E_{xc}^{PBE}
$1s^2$									
0	1.6517	0.0408	1.6925	1.3962	0.1336	1.5299	1.6170	0.0441	1.6611
0.01	1.6517	0.0409	1.6925	1.3962	0.1336	1.5299	1.6169	0.0441	1.6611
0.02	1.6516	0.0409	1.6925	1.3962	0.1336	1.5298	1.6169	0.0441	1.6611
0.05	1.6517	0.0411	1.6929	1.3963	0.1336	1.5299	1.6170	0.0441	1.6612
0.1	1.6519	0.0412	1.6931	1.3964	0.1336	1.5301	1.6172	0.0442	1.6613
0.2	1.6526	0.0412	1.6938	1.3971	0.1337	1.5307	1.6178	0.0442	1.6620
0.5	1.6574	0.0415	1.6990	1.4013	0.1339	1.5352	1.6224	0.0443	1.6666
1	1.6734	0.0415	1.7149	1.4153	0.1344	1.5498	1.6373	0.0446	1.6819
2	1.7250	0.0415	1.7664	1.4600	0.1362	1.5962	1.6851	0.0456	1.7307
5	1.9233	0.0414	1.9647	1.6297	0.1422	1.7719	1.8698	0.0487	1.9185
5.4	1.9498	0.0415	1.9913	1.6523	0.1429	1.7953	1.8947	0.0491	1.9437
10	2.2288	0.0425	2.2713	1.8923	0.1501	2.0425	2.1601	0.0522	2.2122
$1s2p_{-1}$									
0	1.1486	0.0016	1.1502	0.9956	0.0535	1.0491	1.1393	0.0114	1.1507
0.01	1.1486	0.0016	1.1503	0.9956	0.0535	1.0491	1.1393	0.0114	1.1507
0.02	1.1487	0.0016	1.1504	0.9957	0.0535	1.0492	1.1394	0.0114	1.1508
0.05	1.1495	0.0016	1.1511	0.9964	0.0536	1.0500	1.1402	0.0114	1.1515
0.1	1.1520	0.0017	1.1537	0.9988	0.0537	1.0525	1.1426	0.0114	1.1540
0.2	1.1605	0.0017	1.1623	1.0074	0.0541	1.0615	1.1517	0.0116	1.1633
0.5	1.1963	0.0037	1.1999	1.0412	0.0555	1.0967	1.1861	0.0121	1.1982
1	1.2579	0.0046	1.2625	1.0991	0.0576	1.1567	1.2450	0.0128	1.2578
2	1.3710	0.0057	1.3766	1.2034	0.0606	1.2640	1.3517	0.0142	1.3659
5	1.6540	0.0069	1.6608	1.4595	0.0662	1.5257	1.6195	0.0173	1.6368

Table C-2 (*continued*)

B	E_x^{HF}	E_c^{HF}	E_{xc}^{HF}	E_x^{LDA}	E_c^{LDA}	E_{xc}^{LDA}	E_x^{PBE}	E_c^{PBE}	E_{xc}^{PBE}
$1s2p_{-1}$									
5.4	1.6869	0.0070	1.6939	1.4893	0.0667	1.5560	1.6510	0.0176	1.6686
10	2.0118	0.0077	2.0195	1.7843	0.0715	1.8558	1.9661	0.0201	1.9863

Table C-3 Exchange and correlation energies of the Lithium atom in magnetic fields

B	E_x^{HF}	E_c^{HF}	E_{xc}^{HF}	E_x^{LDA}	E_c^{LDA}	E_{xc}^{LDA}	E_x^{PBE}	E_c^{PBE}	E_{xc}^{PBE}
$1s^22s$									
0	1.7813	0.0450	1.8263	1.5144	0.1502	1.6645	1.7514	0.0510	1.8024
0.001	1.7812	0.0448	1.8260	1.5144	0.1502	1.6645	1.7514	0.0510	1.8024
0.009	1.7813	0.0451	1.8264	1.5145	0.1502	1.6646	1.7515	0.0510	1.8025
0.01	1.7814	0.0453	1.8266	1.5144	0.1502	1.6646	1.7514	0.0510	1.8024
0.018	1.7816	0.0451	1.8266	1.5147	0.1502	1.6649	1.7517	0.0510	1.8027
0.02	1.7801	0.0477	1.8278	1.5145	0.1502	1.6647	1.7516	0.0510	1.8026
0.05	1.7836	0.0488	1.8324	1.5165	0.1504	1.6669	1.7536	0.0511	1.8047
0.054	1.7840	0.0451	1.8291	1.5169	0.1504	1.6673	1.7539	0.0511	1.8051
0.1	1.7891	0.0486	1.8377	1.5216	0.1508	1.6724	1.7589	0.0514	1.8103
0.126	1.7924	0.0453	1.8377	1.5248	0.1511	1.6758	1.7622	0.0515	1.8137
0.18	1.7995	0.0455	1.8450	1.5313	0.1516	1.6829	1.7692	0.0518	1.8210
0.2	1.8021	0.0495	1.8516	1.5338	0.1518	1.6856	1.7719	0.0519	1.8238
0.5	1.8339	0.0507	1.8846	1.5661	0.1541	1.7202	1.8079	0.0524	1.8603
0.54	1.8372	0.0462	1.8834	1.5698	0.1543	1.7241	1.8123	0.0524	1.8647
0.9	1.8616	0.0460	1.9076	1.6009	0.1558	1.7567	1.8493	0.0527	1.9020
1	1.8678	0.0498	1.9175	1.6091	0.1561	1.7653	1.8592	0.0528	1.9120
5	2.1753	0.0488	2.2241	1.9330	0.1675	2.1005	2.2295	0.0563	2.2858
10	2.5201	0.0487	2.5689	2.2720	0.1777	2.4497	2.6187	0.0593	2.6780
$1s^2p_{-1}$									
0	1.7502	0.0422	1.7923	1.4905	0.1485	1.6390	1.7261	0.0495	1.7755
0.009	1.7497	0.0448	1.7945	1.4908	0.1485	1.6393	1.7268	0.0495	1.7762
0.01	1.7497	0.0422	1.7920	1.4908	0.1485	1.6393	1.7268	0.0495	1.7763
0.018	1.7503	0.0448	1.7950	1.4913	0.1486	1.6399	1.7273	0.0495	1.7768
0.05	1.7547	0.0427	1.7974	1.4954	0.1490	1.6444	1.7315	0.0497	1.7812
0.054	1.7554	0.0449	1.8003	1.4961	0.1490	1.6451	1.7322	0.0497	1.7819
0.1	1.7648	0.0430	1.8078	1.5049	0.1499	1.6548	1.7414	0.0501	1.7914
0.126	1.7703	0.0454	1.8157	1.5101	0.1505	1.6605	1.7469	0.0503	1.7971
0.18	1.7814	0.0458	1.8272	1.5207	0.1515	1.6722	1.7579	0.0506	1.8086
0.2	1.7854	0.0439	1.8292	1.5245	0.1519	1.6764	1.7619	0.0508	1.8127
0.5	1.8385	0.0467	1.8852	1.5758	0.1566	1.7324	1.8147	0.0527	1.8674
0.54	1.8450	0.0487	1.8937	1.5821	0.1571	1.7392	1.8211	0.0529	1.8740
0.9	1.9010	0.0508	1.9518	1.6354	0.1615	1.7969	1.8754	0.0552	1.9306
1	1.9161	0.0502	1.9663	1.6496	0.1626	1.8121	1.8899	0.0559	1.9457
1.26	1.9549	0.0522	2.0071	1.6857	0.1652	1.8508	1.9267	0.0575	1.9842
1.8	2.0339	0.0531	2.0869	1.7580	0.1698	1.9279	2.0014	0.0606	2.0620
2	2.0626	0.0533	2.1159	1.7841	0.1714	1.9555	2.0285	0.0617	2.0902
3.6	2.2806	0.0495	2.3301	1.9796	0.1814	2.1610	2.2343	0.0685	2.3028
5	2.4529	0.0601	2.5130	2.1335	0.1879	2.3214	2.3985	0.0728	2.4713

Table C-3 (*continued*)

B	E_x^{HF}	E_c^{HF}	E_{xc}^{HF}	E_x^{LDA}	E_c^{LDA}	E_{xc}^{LDA}	E_x^{PBE}	E_c^{PBE}	E_{xc}^{PBE}
$1s^2 2p_{-1}$									
5.4	2.4992	0.0410	2.5402	2.1749	0.1895	2.3644	2.4429	0.0738	2.5167
10	2.9587	0.0663	3.0250	2.5879	0.2036	2.7916	2.8900	0.0819	2.9719
$1s2p_{-1}3d_{-2}$									
0	1.2019	0.0588	1.2607	1.0494	0.0634	1.1129	1.1994	0.0158	1.2152
0.1	1.2391	0.0197	1.2588	1.0835	0.0666	1.1501	1.2357	0.0177	1.2535
0.5	1.3816	0.0118	1.3934	1.2104	0.0739	1.2843	1.3677	0.0226	1.3903
1	1.5128	0.0116	1.5243	1.3316	0.0789	1.4105	1.4925	0.0249	1.5174
2	1.7190	0.0101	1.7291	1.5233	0.0851	1.6084	1.6889	0.0275	1.7164
5	2.1788	0.0148	2.1936	1.9497	0.0953	2.0450	2.1320	0.0323	2.1644
10	2.7217	0.0183	2.7400	2.4590	0.1043	2.5633	2.6709	0.0367	2.7076

Table C-4 Exchange and correlation energies of the Be^+ ion in magnetic fields

B	E_x^{HF}	E_c^{HF}	E_{xc}^{HF}	E_x^{LDA}	E_c^{LDA}	E_{xc}^{LDA}	E_x^{PBE}	E_c^{PBE}	E_{xc}^{PBE}
$1s^2 2s$									
0	2.5072	0.0472	2.5545	2.1431	0.1723	2.3154	2.4662	0.0539	2.5201
0.001	2.5072	0.0471	2.5544	2.1431	0.1723	2.3154	2.4662	0.0539	2.5201
0.002	2.5072	0.0438	2.5510	2.1431	0.1723	2.3154	2.4662	0.0539	2.5200
0.004	2.5071	0.0437	2.5508	2.1431	0.1723	2.3153	2.4662	0.0539	2.5200
0.01	2.5072	0.0472	2.5544	2.1431	0.1723	2.3154	2.4662	0.0539	2.5201
0.02	2.5073	0.0438	2.5511	2.1432	0.1723	2.3154	2.4663	0.0539	2.5201
0.05	2.5077	0.0471	2.5548	2.1435	0.1723	2.3159	2.4667	0.0539	2.5205
0.1	2.5091	0.0473	2.5564	2.1449	0.1724	2.3173	2.4681	0.0539	2.5220
0.2	2.5140	0.0473	2.5613	2.1496	0.1727	2.3223	2.4730	0.0541	2.5271
0.3	2.5208	0.0438	2.5646	2.1560	0.1731	2.3291	2.4798	0.0543	2.5341
0.4	2.5285	0.0437	2.5722	2.1634	0.1736	2.3370	2.4876	0.0546	2.5421
0.5	2.5364	0.0478	2.5842	2.1711	0.1740	2.3451	2.4959	0.0548	2.5507
0.6	2.5445	0.0437	2.5881	2.1790	0.1745	2.3534	2.5043	0.0550	2.5593
0.7	2.5523	0.0435	2.5958	2.1867	0.1749	2.3616	2.5127	0.0552	2.5679
0.8	2.5599	0.0436	2.6035	2.1944	0.1753	2.3697	2.5211	0.0553	2.5764
1	2.5742	0.0482	2.6224	2.2092	0.1761	2.3853	2.5375	0.0555	2.5930
2	2.6308	0.0478	2.6786	2.2751	0.1786	2.4537	2.6140	0.0562	2.6701
5	2.7931	0.0469	2.8400	2.4604	0.1832	2.6436	2.8266	0.0578	2.8844
10	3.0887	0.0466	3.1353	2.7576	0.1906	2.9482	3.1641	0.0601	3.2242
$1s^2 2p_{-1}$									
0	2.4804	0.0432	2.5236	2.1278	0.1726	2.3004	2.4489	0.0524	2.5013
0.01	2.4805	0.0433	2.5237	2.1279	0.1726	2.3005	2.4490	0.0524	2.5013
0.05	2.4813	0.0425	2.5238	2.1292	0.1726	2.3018	2.4507	0.0524	2.5032
0.1	2.4838	0.0433	2.5271	2.1315	0.1728	2.3043	2.4531	0.0525	2.5056
0.2	2.4921	0.0436	2.5356	2.1393	0.1734	2.3127	2.4612	0.0528	2.5140
0.3	2.5027	0.0434	2.5461	2.1495	0.1741	2.3236	2.4716	0.0531	2.5247
0.4	2.5144	0.0433	2.5577	2.1605	0.1749	2.3354	2.4829	0.0534	2.5364
0.5	2.5263	0.0442	2.5705	2.1719	0.1757	2.3476	2.4946	0.0538	2.5484
0.6	2.5384	0.0430	2.5814	2.1833	0.1765	2.3598	2.5063	0.0542	2.5605
0.7	2.5503	0.0429	2.5932	2.1947	0.1773	2.3720	2.5179	0.0545	2.5725

Table C-4 (*continued*)

B	E_x^{HF}	E_c^{HF}	E_{xc}^{HF}	E_x^{LDA}	E_c^{LDA}	E_{xc}^{LDA}	E_x^{PBE}	E_c^{PBE}	E_{xc}^{PBE}
$1s^2 2p_{-1}$									
0.8	2.5622	0.0427	2.6049	2.2059	0.1781	2.3840	2.5295	0.0549	2.5844
1	2.5856	0.0461	2.6317	2.2281	0.1795	2.4076	2.5521	0.0557	2.6077
2	2.6978	0.0482	2.7460	2.3329	0.1859	2.5188	2.6593	0.0593	2.7186
5	3.0137	0.0502	3.0639	2.6189	0.1991	2.8179	2.9573	0.0680	3.0253
10	3.4749	0.0510	3.5259	3.0310	0.2128	3.2439	3.3966	0.0769	3.4735
$1s2p_{-1}3d_{-2}$									
0	1.6837	0.0051	1.6888	1.4780	0.0756	1.5536	1.6788	0.0174	1.6962
0.1	1.6984	0.0053	1.7037	1.4920	0.0766	1.5686	1.6942	0.0181	1.7123
0.2	1.7236	0.0056	1.7292	1.5145	0.0779	1.5925	1.7174	0.0191	1.7364
0.5	1.8016	0.0063	1.8078	1.5841	0.0813	1.6654	1.7893	0.0215	1.8109
1	1.9164	0.0072	1.9236	1.6883	0.0853	1.7736	1.8973	0.0238	1.9211
2	2.1048	0.0081	2.1130	1.8623	0.0906	1.9529	2.0762	0.0263	2.1025
5	2.5353	0.0085	2.5439	2.2615	0.0997	2.3612	2.4875	0.0302	2.5177
10	3.0723	0.0081	3.0804	2.7605	0.1081	2.8685	3.0093	0.0343	3.0436

Table C-5 Exchange and correlation energies of the Beryllium atom in magnetic fields

B	E_x^{HF}	E_c^{HF}	E_{xc}^{HF}	E_x^{LDA}	E_c^{LDA}	E_{xc}^{LDA}	E_x^{PBE}	E_c^{PBE}	E_{xc}^{PBE}
$1s^2 2s^2$									
0	2.6669	0.0675	2.7344	2.2903	0.2237	2.5140	2.6336	0.0854	2.7190
0.001	2.6669	0.0680	2.7348	2.2903	0.2237	2.5140	2.6335	0.0854	2.7190
0.01	2.6670	0.0679	2.7349	2.2904	0.2237	2.5141	2.6336	0.0854	2.7191
0.02	2.6672	0.0899	2.7571	2.2906	0.2237	2.5143	2.6338	0.0854	2.7193
0.05	2.6686	0.0699	2.7384	2.2919	0.2239	2.5157	2.6351	0.0856	2.7207
0.1	2.6731	0.0708	2.7440	2.2960	0.2243	2.5204	2.6395	0.0859	2.7254
0.5	2.7390	0.0810	2.8199	2.3583	0.2303	2.5886	2.7054	0.0899	2.7954
1	2.8081	0.1277	2.9358	2.4295	0.2360	2.6655	2.7842	0.0918	2.8761
$1s^2 2s2p_{-1}$									
0.01	2.7211	0.0475	2.7686	2.3394	0.1930	2.5324	2.6752	0.0644	2.7396
0.02	2.7214	0.0503	2.7718	2.3398	0.1930	2.5328	2.6755	0.0644	2.7399
0.05	2.7238	0.0314	2.7552	2.3421	0.1932	2.5353	2.6780	0.0645	2.7425
0.10	2.7312	0.0481	2.7793	2.3494	0.1937	2.5431	2.6854	0.0649	2.7502
0.15	2.7412	0.0502	2.7915	2.3591	0.1943	2.5534	2.6952	0.0653	2.7605
0.2	2.7527	0.0473	2.8000	2.3699	0.1950	2.5649	2.7063	0.0658	2.7721
0.3	2.7769	0.0504	2.8273	2.3929	0.1964	2.5892	2.7297	0.0668	2.7965
0.4	2.8006	0.0504	2.8511	2.4156	0.1978	2.6134	2.7530	0.0677	2.8207
0.5	2.8231	0.0481	2.8712	2.4373	0.1991	2.6364	2.7753	0.0685	2.8438
0.6	2.8439	0.0501	2.8940	2.4577	0.2003	2.6580	2.7962	0.0693	2.8655
0.8	2.8805	0.0485	2.9289	2.4946	0.2026	2.6972	2.8342	0.0706	2.9048
1	2.9109	0.0493	2.9602	2.5269	0.2045	2.7314	2.8675	0.0716	2.9391
2	3.0088	0.0470	3.0558	2.6491	0.2114	2.8605	2.9972	0.0738	3.0710
5	3.3021	0.0484	3.3505	2.9669	0.2252	3.1921	3.3478	0.0787	3.4265
$1s^2 2p_{-1}3d_{-2}$									
0.1	2.5723	0.0303	2.6026	2.2162	0.1855	2.4017	2.5458	0.0587	2.6044
0.2	2.6132	0.0317	2.6449	2.2516	0.1880	2.4397	2.5827	0.0606	2.6433

Table C-5 (*continued*)

B	E_x^{HF}	E_c^{HF}	E_{xc}^{HF}	E_x^{LDA}	E_c^{LDA}	E_{xc}^{LDA}	E_x^{PBE}	E_c^{PBE}	E_{xc}^{PBE}
$1s^2 2p_{-1} 3d_{-2}$									
0.5	2.7135	0.0303	2.7438	2.3414	0.1938	2.5352	2.6771	0.0643	2.7413
1	2.8413	0.0357	2.8771	2.4598	0.2007	2.6605	2.8002	0.0680	2.8682
2	3.0441	0.0468	3.0909	2.6495	0.2107	2.8602	2.9952	0.0738	3.0691
5	3.5314	0.0390	3.5704	3.1011	0.2305	3.3316	3.4635	0.0867	3.5501
10	4.1768	0.0411	4.2179	3.6967	0.2503	3.9470	4.0931	0.0995	4.1926
$1s 2p_{-1} 3d_{-2} 4f_{-3}$									
1	2.1659	0.0071	2.1730	1.9150	0.1064	2.0215	2.1369	0.0371	2.1740
2	2.4496	0.0066	2.4562	2.1769	0.1150	2.2919	2.4085	0.0413	2.4498
5	3.0516	0.0070	3.0586	2.7421	0.1286	2.8707	2.9930	0.0473	3.0403
10	3.7658	0.0067	3.7725	3.4207	0.1406	3.5614	3.7013	0.0527	3.7540

APPENDIX D
EFFECTIVE POTENTIAL INTEGRALS WITH RESPECT TO LANDAU ORBITALS IN EQUATION (5.30)

The explicit expression for the Landau orbitals is

$$\phi_{nm}^{Lan}\left(\rho,\varphi\right)=\frac{1}{a_L\sqrt{\pi}}e^{im\varphi}I_{ns}\left(\frac{\rho^2}{a_L^2}\right)=\left|ns\right\rangle \tag{D.1}$$

where $s=n-m\geq 0$,

$$I_{ns}\left(x\right)=\frac{1}{\sqrt{n!s!}}e^{\frac{x}{2}}x^{\frac{s-n}{2}}\frac{d^s}{dx^s}\left(x^n e^{-x}\right) \tag{D.2}$$

and $a_L=\sqrt{\frac{2}{B}}$ is the Larmor radius.

Consider the expansion $\left\langle \phi_{nm}^{Lan}\left|\frac{1}{r}\right|\phi_{n'm}^{Lan}\right\rangle=\sum_{s''=|m|}^{n+n'-m}b\left(ss',nn';s''\right)\left\langle 0s''\left|\frac{1}{r}\right|0s''\right\rangle$ (D.3)

Comparison of the powers of ρ^2 on both sides immediately yields

$$b\left(ss',nn';s''\right)=\left(-\right)^{s''+|m|}\left(\frac{s!s'!}{n!n'!}\right)^{1/2}\frac{s''!}{\left(s''+|m|\right)!}\sum_{\substack{k=0\\ k+k'=s''-|m|}}^{n}\sum_{k'=0}^{n'}\frac{n!}{k!\left(n-k\right)!}\frac{n'!}{k'!\left(n'-k'\right)!}\frac{\left(s''+|m|\right)!}{\left(k+|m|\right)!\left(s''-k\right)!} \tag{D.4}$$

Here $n\leq s$ and $n'\leq s'$ are assumed without loss of generality.

Three different methods are used for the calculation of the potentials

$$V_s\left(|z|\right)=\left\langle 0s\left|\frac{1}{r}\right|0s\right\rangle=\frac{1}{s!}\int_0^\infty\frac{x^s e^{-x}}{\sqrt{x+z^2}}dx \tag{D.5}$$

in different regions:

For $|z| \le 2$ and $0 \le s \le 8$, closed forms for the integrals are used. See Table D-1, and note that *erf*(*z*) is the usual error function.

Table D-1 Expressions for $V_s(z)$ with $|z| \le 2$ and $0 \le s \le 8$

s	$V_s(z)$
0	$\sqrt{\pi}e^{z^2}\left(1-erf(z)\right)$
1	$z+\frac{\sqrt{\pi}}{2}e^{z^2}\left(1-erf(z)\right)\left(1-2z^2\right)$
2	$\left(\frac{3z}{4}-\frac{z^3}{2}\right)+\frac{\sqrt{\pi}}{8}e^{z^2}\left(1-erf(z)\right)\left(3-4z^2+4z^4\right)$
3	$\left(\frac{5z}{8}-\frac{z^3}{3}+\frac{z^5}{6}\right)+\frac{\sqrt{\pi}}{48}e^{z^2}\left(1-erf(z)\right)\left(15-18z^2+12z^4-8z^6\right)$
4	$\left(\frac{35z}{64}-\frac{25z^3}{96}+\frac{5z^5}{48}-\frac{z^7}{24}\right)+\frac{\sqrt{\pi}}{384}e^{z^2}\left(1-erf(z)\right)\left(105-120z^2+72z^4-32z^6+16z^8\right)$
5	$\left(\frac{63z}{128}-\frac{7z^3}{32}+\frac{19z^5}{240}-\frac{z^7}{40}+\frac{z^9}{120}\right)+\frac{\sqrt{\pi}e^{z^2}}{3840}\left(1-erf(z)\right)\left(945-1050z^2+600z^4-240z^6+80z^8-32z^{10}\right)$
6	$\left(\frac{231z}{512}-\frac{49z^3}{256}+\frac{21z^5}{320}-\frac{3z^7}{160}+\frac{7z^9}{1440}-\frac{z^{11}}{720}\right)$ $+\frac{\sqrt{\pi}e^{z^2}}{46080}\left(1-erf(z)\right)\left(10395-11340z^2+6300z^4-2400z^6+720z^8-192z^{10}+64z^{12}\right)$
7	$\left(\frac{429z}{1024}-\frac{11z^3}{64}+\frac{73z^5}{1280}-\frac{13z^7}{840}+\frac{73z^9}{20160}-\frac{z^{11}}{1260}+\frac{z^{13}}{5040}\right)+\frac{\sqrt{\pi}e^{z^2}}{645120}\left(1-erf(z)\right)$ $*\left(135135-145530z^2+79380z^4-29400z^6+8400z^8-2016z^{10}+448z^{12}-128z^{14}\right)$
8	$\left(\frac{6435z}{16384}-\frac{1287z^3}{8192}+\frac{209z^5}{4096}-\frac{963z^7}{71680}+\frac{107z^9}{35840}-\frac{19z^{11}}{32256}+\frac{z^{13}}{8960}-\frac{z^{15}}{40320}\right)+\frac{\sqrt{\pi}e^{z^2}}{10321920}\left(1-erf(z)\right)$ $*\left(2027025-2162160z^2+1164240z^4-423360z^6+117600z^8-26880z^{10}+5376z^{12}-1024z^{14}+256z^{16}\right)$

For $2 < |z| \le 100$ and $0 \le s \le 8$, and for $|z| \le 100$ and $8 < s$, the expression (D.5) is integrated with the Gauss-Laguerre quadrature formula of order 24 [126].

For $|z| > 100$, we use its large *z* asymptotic expansion

$$V_s(z) = \frac{1}{|z|}\left\{1 - \frac{1}{2}\frac{(s+1)}{z^2} + \frac{3}{8}\frac{(s+1)_2}{z^4} - \frac{5}{16}\frac{(s+1)_3}{z^6} + \frac{35}{128}\frac{(s+1)_4}{z^8} - \frac{63}{256}\frac{(s+1)_5}{z^{10}} + \frac{231}{1024}\frac{(s+1)_6}{z^{12}} - \cdots\right\}$$

where $(s+1)_i = (s+1)(s+2)\cdots(s+i)$. (D.6)

APPENDIX E
ENERGY VALUES FOR HOOKE'S ATOM IN MAGNETIC FIELDS

Table E-1 Relative motion and spin energies for the Hooke's atom in B fields ($\omega = 1/2$, energy in Hartree). Numbers in parentheses denote the number of functions used in the spherical expansion; Numbers in brackets denote the number of functions used in the Landau orbital expansion.

$B(au)$	$1\,^1 0^+\,(1s)$		$1\,^3 0^-\,(2p_0)$		$1\,^3(-1)^+\,(2p_{-1})$	
0	1.250000000	(3)	1.609657060	(3)	1.609657060	(3)
0.0001	1.250000003	(3)	1.609557063	(3)	1.609507066	(3)
0.00015	1.250000008	(3)	1.609507066	(3)	1.609432073	(3)
0.0002	1.250000014	(3)	1.609457071	(3)	1.609357083	(3)
0.0003	1.250000031	(3)	1.609357086	(3)	1.609207112	(3)
0.0005	1.250000086	(3)	1.609157132	(3)	1.608907204	(3)
0.0007	1.250000168	(3)	1.608957201	(3)	1.608607342	(3)
0.001	1.250000342	(3)	1.608657347	(3)	1.608157635	(3)
0.0015	1.250000770	(3)	1.608157707	(3)	1.607408354	(3)
0.002	1.250001368	(3)	1.607658210	(3)	1.606659360	(3)
0.003	1.250003079	(3)	1.606659647	(3)	1.605162235	(3)
0.005	1.250008552	(3)	1.604664247	(3)	1.602171434	(3)
0.007	1.250016762	(3)	1.602671147	(3)	1.599185233	(3)
0.01	1.250034208	(3)	1.599685808	(3)	1.594714556	(3)
0.015	1.250076965	(5)	1.594721740	(5)	1.587286421	(5)
0.02	1.250136820	(5)	1.589772041	(5)	1.579887024	(5)
0.03	1.250307795	(5)	1.579915729	(5)	1.565174407	(5)
0.05	1.250854552	(5)	1.560375249	(5)	1.536093504	(5)
0.07	1.251673646	(5)	1.541063723	(5)	1.507470637	(5)
0.1	1.253410092	(5)	1.512523532	(5)	1.465391042	(5)
0.15	1.257642612	(5)	1.466083307	(5)	1.397514744	(5)
0.2	1.263513190	(5)	1.421024408	(5)	1.332407876	(5)
0.3	1.279947919	(5)	1.334879453	(5)	1.210179577	(5)
0.5	1.329535134	(7)	1.176881544	(7)	0.994625266	(7)
0.7	1.396923698	(7)	1.034429994	(7)	0.81085244	(7)
	1.39703	[24]	1.034433	[12]	0.810855	[20]
1	1.520416489	(9)	0.841222544	(9)	0.5777205	(9)
	1.520519	[24]	0.8412251	[12]	0.577723	[20]
1.5	1.75777857	(9)	0.550811694	(9)	0.2559303	(9)
	1.757872	[24]	0.5508135	[12]	0.255933	[20]
2	2.0112016	(11)	0.279793095	(11)	-0.0246336	(11)
	2.011286	[24]	0.2797945	[12]	-0.024631	[20]
3	2.5296152	(13)	-0.239648205	(13)	-0.539284	(13)
	2.529682	[24]	-0.2396471	[12]	-0.539282	[20]
5	3.5644399	(17)	-1.251756371	(19)	-1.5219222	(19)

Table E-1 (*continued*)

$B(au)$	$1\,^1 0^+ (1s)$		$1\,^3 0^- (2p_0)$		$1\,^3(-1)^+ (2p_{-1})$	
5	3.5644866	[24]	-1.25175534	[12]	-1.521919	[17]
7	4.5886380	(21)	-2.255103373	(21)	-2.497629	(21)
	4.5886734	[24]	-2.25510106	[12]	-2.497623	[14]
10	6.1124882	(25)	-3.756420943	(25)	-3.9672702	(25)
	6.112518	[24]	-3.7564155	[12]	-3.967261	[12]
15	8.6359755	(25)	-6.2564087	(25)	-6.4323365	(25)
	8.636000	[18]	-6.2563985	[12]	-6.432323	[10]
20	11.150104	(25)	-8.755915	(25)	-8.90935	(25)
	11.150138	[15]	-8.7558996	[12]	-8.909340	[9]
30	16.1668	(25)	-13.7548	(25)	-13.8805	(25)
	16.166748	[11]	-13.7549175	[12]	-13.880982	[7]
50	26.187	(25)	-23.747	(25)	-23.837	(25)
	26.18302	[8]	-23.753597	[12]	-23.85238	[5]
70	36.22	(25)	-33.72	(25)	-33.77	(25)
	36.19185	[6]	-33.75201	[12]	-33.83741	[5]
100	51.30	(25)	-48.62	(25)	-48.64	(25)
	51.2025	[5]	-48.7464	[12]	-48.8221	[4]
150	76.49	(25)	-73.38	(25)	-73.37	(25)
	76.224	[4]	-73.726	[12]	-73.7971	[3]
200	101.7	(25)	-98.1	(25)	-98.09	(25)
	101.254	[4]	-98.695	[12]	-98.765	[3]
300	152.2	(25)	-147.5	(25)	-147.56	(25)
	151.332	[3]	-148.618	[12]	-148.683	[3]
500	253.0	(25)	-246.3	(25)	-246.6	(25)
	251.538	[2]	-248.417	[12]	-248.474	[2]
700	353.8	(25)	-345.1	(25)	-345.7	(25)
	351.785	[3]	-348.177	[12]	-348.224	[3]
1000	504.8	(25)	-493.4	(25)	-494.6	(25)
	502.208	[2]	-497.764	[12]	-497.798	[2]

Table E-1 (*continued*)

$B(au)$	$1\,^1(-1)^- (3d_{-1})$	$1\,^1(-2)^+ (3d_{-2})$	$1\,^3(-2)^- (4f_{-2})$	$1\,^3(-3)^+ (4f_{-3})$
0	2.043613898 (3)	2.043613898 (3)	2.503840941 (3)	2.503840941 (3)
0.0001	2.043563903 (3)	2.043513906 (3)	2.503640949 (3)	2.503590952 (3)
0.00015	2.043538910 (3)	2.043463916 (3)	2.503540959 (3)	2.503465965 (3)
0.0002	2.043513920 (3)	2.043413930 (3)	2.503440973 (3)	2.503340984 (3)
0.0003	2.043463947 (3)	2.043313971 (3)	2.503241013 (3)	2.503091037 (3)
0.0005	2.043364034 (3)	2.043114101 (3)	2.502841140 (3)	2.502591206 (3)
0.0007	2.043264164 (3)	2.042914297 (3)	2.502441330 (3)	2.502091459 (3)
0.001	2.043114441 (3)	2.042614712 (3)	2.501841734 (3)	2.501341999 (3)
0.0015	2.042865119 (3)	2.042115730 (3)	2.500842726 (3)	2.500093320 (3)
0.002	2.042616070 (3)	2.041617156 (3)	2.499844113 (3)	2.498845171 (3)
0.003	2.042118784 (3)	2.040621228 (3)	2.497848078 (3)	2.496350457 (3)
0.005	2.041127471 (3)	2.038634258 (3)	2.493860765 (3)	2.491367373 (3)
0.007	2.040140502 (3)	2.036653803 (3)	2.489879796 (3)	2.486392748 (3)
0.01	2.038668190 (3)	2.033695337 (3)	2.483920236 (3)	2.478946667 (3)
0.015	2.036236052 (5)	2.028797129 (5)	2.474019348 (5)	2.466578817 (5)

Table E-1 (*continued*)

$B(au)$	$1\,^1(-1)^-\,(3d_{-1})$		$1\,^1(-2)^+\,(3d_{-2})$		$1\,^3(-2)^-\,(4f_{-2})$		$1\,^3(-3)^+\,(4f_{-3})$	
0.02	2.033831050	(5)	2.023939627	(5)	2.464158094	(5)	2.454263813	(5)
0.03	2.029102424	(5)	2.014346693	(5)	2.444554442	(5)	2.429792279	(5)
0.05	2.019970328	(5)	1.995648582	(5)	2.405822055	(5)	2.381482453	(5)
0.07	2.011270774	(5)	1.977599362	(5)	2.367721481	(5)	2.334015098	(5)
0.1	1.999028635	(5)	1.951736628	(5)	2.311749856	(5)	2.264386593	(5)
0.15	1.980756300	(5)	1.911830624	(5)	2.221578322	(5)	2.152492944	(5)
0.2	1.965100502	(5)	1.875853518	(5)	2.135232658	(5)	2.045703296	(5)
0.3	1.941337955	(5)	1.815247057	(5)	1.973592906	(5)	1.846876266	(5)
0.5	1.921179706	(7)	1.735281511	(7)	1.690498779	(7)	1.502941229	(7)
0.7	1.931222704	(7)	1.701058458	(7)	1.452008304	(7)	1.218792604	(7)
	1.9312234	[12]	1.70105911	[17]	1.45200871	[12]	1.21879300	[13]
1	1.987024019	(9)	1.71190543	(9)	1.15503647	(9)	0.87438094	(9)
	1.9870245	[12]	1.71190608	[16]	1.15503698	[12]	0.87438125	[12]
1.5	2.1451176	(11)	1.83029806	(9)	0.75863481	(11)	0.4338451	(11)
	2.14511795	[12]	1.8302987	[15]	0.75863507	[12]	0.4338454	[11]
2	2.344898761	(11)	2.0134298	(11)	0.42660426	(13)	0.08101563	(11)
	2.34489904	[12]	2.0134306	[14]	0.42660448	[12]	0.0810159	[11]
3	2.795651846	(15)	2.4588635	(15)	-0.15632829	(15)	-0.5139253	(15)
	2.7956525	[12]	2.4588645	[13]	-0.15632796	[12]	-0.5139245	[10]
5	3.76164459	(19)	3.4447447	(19)	-1.21660648	(19)	-1.5623472	(19)
	3.76164552	[12]	3.4447463	[11]	-1.21660545	[12]	-1.5623457	[8]
7	4.75047650	(23)	4.4583592	(23)	-2.23786510	(23)	-2.5626623	(23)
	4.75047867	[12]	4.4583624	[10]	-2.23786247	[12]	-2.5626603	[8]
10	6.24446123	(23)	5.9843736	(23)	-3.7504183	(23)	-4.0452405	(23)
	6.24446471	[12]	5.9843796	[9]	-3.7504143	[12]	-4.0452364	[7]
15	8.7419092	[12]	8.520735	[7]	-6.2570279	[12]	-6.512476	[6]
20	11.24164	[12]	11.04731	[7]	-8.7588054	[12]	-8.98549	[6]
30	16.242351	[12]	16.08239	[6]	-13.759101	[12]	-13.947178	[5]
50	26.24398	[12]	26.11964	[5]	-23.757718	[12]	-23.903968	[4]
70	36.24587	[12]	36.13961	[4]	-33.75560	[12]	-33.880158	[4]
100	51.2518	[12]	51.1588	[4]	-48.7497	[12]	-48.8571	[3]
150	76.272	[12]	76.1872	[3]	-73.729	[12]	-73.8259	[3]
200	101.303	[12]	101.221	[3]	-98.699	[12]	-98.790	[3]
300	151.381	[12]	151.306	[3]	-148.620	[12]	-148.703	[3]
500	251.582	[12]	251.519	[2]	-248.419	[12]	-248.487	[2]
700	351.822	[12]	351.771	[3]	-348.179	[12]	-348.234	[3]
1000	502.236	[12]	502.197	[2]	-497.765	[12]	-497.806	[2]

Table E-2 As in Table E-1, but for $\omega = 1/10$.

$B(au)$	$1\,^1 0^+\,(1s)$		$1\,^3(-1)^+\,(2p_{-1})$		$1\,^3(-3)^+\,(4f_{-3})$	
0	0.35000000	(2)	0.40317279	(2)	0.56141220	(2)
0.0001	0.35000002	(2)	0.40302283	(2)	0.56116226	(2)
0.00015	0.35000005	(2)	0.40294787	(2)	0.56103733	(2)
0.0002	0.35000009	(2)	0.40287293	(2)	0.56091243	(2)
0.0003	0.35000020	(2)	0.40272309	(2)	0.56066271	(2)

Table E-2 (*continued*)

$B(au)$	$1\,^1 0^+\,(1s)$		$1\,^3(-1)^+\,(2p_{-1})$		$1\,^3(-3)^+\,(4f_{-3})$	
0.0005	0.35000056	(2)	0.40242363	(2)	0.56016361	(2)
0.0007	0.35000109	(2)	0.40212443	(2)	0.55966497	(2)
0.001	0.35000223	(2)	0.40167612	(2)	0.55891784	(2)
0.0015	0.35000501	(3)	0.40093028	(3)	0.55767489	(3)
0.002	0.35000891	(3)	0.40018611	(3)	0.55643476	(3)
0.003	0.35002005	(3)	0.39870275	(3)	0.55396296	(3)
0.005	0.35005568	(3)	0.39575601	(3)	0.54905317	(3)
0.007	0.35010912	(3)	0.39283586	(3)	0.54418844	(3)
0.01	0.35022257	(3)	0.38850546	(3)	0.53697577	(3)
0.015	0.35050018	(3)	0.38142058	(3)	0.52517916	(3)
0.02	0.35088769	(4)	0.37450044	(3)	0.51366193	(3)
0.03	0.35198763	(4)	0.36114883	(4)	0.49145730	(4)
0.05	0.35543780	(4)	0.33634307	(4)	0.45028105	(4)
0.07	0.36042632	(5)	0.31391694	(5)	0.41318824	(5)
0.1	0.37036790	(6)	0.28423501	(5)	0.36443746	(6)
	0.37039495	[16]	0.28423695	[16]	0.36443759	[11]
0.15	0.39174385	(7)	0.24317081	(7)	0.29824181	(7)
	0.39177144	[16]	0.24317281	[16]	0.29824194	[11]
0.2	0.41667766	(8)	0.20941540	(8)	0.24581813	(8)
	0.41670496	[16]	0.20941744	[16]	0.24581826	[11]
0.3	0.47039300	(10)	0.15361448	(10)	0.16546431	(10)
	0.47041748	[16]	0.15361649	[16]	0.16546444	[11]
0.34641*	0.49566784	(11)	0.13038476	(11)	0.13465525	(11)
	0.49568856	[16]	0.13038631	[16]	0.13465538	[11]
0.5	0.57826539	(13)	0.05756353	(13)	0.04646911	(13)
	0.57828216	[16]	0.05756521	[16]	0.04646923	[11]
0.7	0.68315870	(16)	-0.03562337	(16)	-0.05498833	(16)
	0.68317018	[16]	-0.03562208	[16]	-0.05498817	[10]
1	0.83731609	(19)	-0.17768011	(20)	-0.19983021	(21)
	0.83732330	[16]	-0.17767924	[16]	-0.19983009	[10]
1.5	1.09080151	(23)	-0.41987130	(24)	-0.43971736	(24)
	1.09080565	[16]	-0.41987081	[16]	-0.43971723	[9]
2	1.34264091	(25)	-0.66554881	(25)	-0.68207522	(24)
	1.34264369	[16]	-0.66554844	[14]	-0.68207516	[9]
3	1.84457872	(25)	-1.16102111	(25)	-1.17273995	(24)
	1.84458030	[16]	-1.16102138	[12]	-1.17274770	[8]
5	2.84626	(25)	-2.15712831	(25)	-2.16347569	(24)
	2.84625158	[15]	-2.15725040	[9]	-2.16442702	[7]
7	3.8473	(25)	-3.15404988	(25)	-3.15378124	(24)
	3.84702797	[13]	-3.15556815	[8]	-3.16073739	[6]
10	5.35	(25)	-4.64435345	(25)	-4.62992050	(24)
	5.34765193	[11]	-4.65425628	[7]	-4.65793294	[6]
15	7.84817795	[10]	-7.15318255	[6]	-7.15571040	[5]
20	10.3484629	[9]	-9.65261533	[6]	-9.65457004	[5]
30	15.3487725	[8]	-14.6520127	[5]	-14.6533896	[4]
50	25.3490515	[6]	-24.6514848	[5]	-24.6523876	[4]
70	35.3491869	[6]	-34.6512350	[4]	-34.6519267	[4]
100	50.3493002	[5]	-49.6510305	[4]	-49.6515572	[3]

Table E-2 (*continued*)

$B(au)$	$1\,^1 0^+\,(1s)$		$1\,^3(-1)^+\,(2p_{-1})$		$1\,^3(-3)^+\,(4f_{-3})$	
150	75.3494006	[5]	-74.6508535	[4]	-74.6512450	[3]
200	100.349458	[4]	-99.6507548	[4]	-99.6510748	[3]
300	150.349524	[4]	-149.650644	[4]	-149.650888	[4]
500	250.349588	[4]	-249.650539	[4]	-249.650716	[4]
700	350.349621	[5]	-349.650486	[5]	-349.650630	[5]
1000	500.349652	[5]	-499.650439	[5]	-499.650557	[5]

*The exact field strength used is $\sqrt{3}/5 = 0.346410161514$.

Table E-3 Contributions to total energy for Hooke's atom in Zero *B* field ($B = 0$, $m = 0$, singlet state, energy in Hartree)

ω	E_r	KE_r	E_{ee}	J	E_c	T_c
0.001896558822	0.019914	0.000852	0.012140	0.038988	-0.006460	0.000893
0.0038233443	0.032498	0.001735	0.019352	0.060288	-0.009114	0.001678
0.01	0.064205	0.004629	0.036635	0.108665	-0.013945	0.003753
0.02	0.105775	0.009437	0.057934	0.164935	-0.018220	0.006314
0.05	0.207490	0.024500	0.105661	0.283102	-0.024481	0.011409
0.1	0.350001	0.051036	0.165299	0.421934	-0.029242	0.016427
0.2	0.598799	0.107379	0.256027	0.623288	-0.033640	0.021977
0.5	1.250000	0.289414	0.447447	1.030251	-0.038510	0.029168
1	2.230121	0.611502	0.671410	1.493432	-0.041385	0.033921
2	4.057877	1.283267	0.994225	2.151368	-0.043611	0.037849
4	7.523219	2.669785	1.455759	3.083973	-0.045286	0.040942
10	17.448685	6.941110	2.377629	4.936774	-0.046848	0.043911
20	33.492816	14.181479	3.419880	7.026041	-0.047663	0.045478
40	64.970125	28.813145	4.895849	9.981397	-0.048252	0.046597
100	157.902068	73.081043	7.826636	15.845961	-0.048781	0.047564

Table E-4 Contributions to the total energy for the Hooke's atom in *B* fields (ω = ½, m=0, singlet state, energy in Hartree)

B (au)	E_r	KE_r	E_{ee}	J	E_c	T_c
0	1.250000	0.289400	0.447461	1.030250	-0.038510	0.029154
0.005	1.250009	0.289402	0.447463	1.030255	-0.038510	0.029154
0.01	1.250034	0.289410	0.447470	1.030269	-0.038510	0.029155
0.02	1.250137	0.289442	0.447497	1.030325	-0.038510	0.029155
0.03	1.250308	0.289494	0.447541	1.030418	-0.038511	0.029156
0.04	1.250547	0.289567	0.447603	1.030547	-0.038512	0.029158
0.05	1.250855	0.289661	0.447683	1.030714	-0.038514	0.029160
0.06	1.251230	0.289775	0.447780	1.030918	-0.038515	0.029163
0.08	1.252185	0.290067	0.448028	1.031435	-0.038520	0.029170
0.1	1.253410	0.290442	0.448345	1.032098	-0.038526	0.029179
0.15	1.257643	0.291740	0.449436	1.034383	-0.038546	0.029210
0.2	1.263513	0.293549	0.450938	1.037534	-0.038576	0.029253

Table E-4 (*continued*)

B (au)	E_r	KE_r	E_{ee}	J	E_c	T_c
0.25	1.270970	0.295860	0.452827	1.041508	-0.038617	0.029309
0.3	1.279948	0.298662	0.455076	1.046251	-0.038671	0.029379
0.35	1.290375	0.301944	0.457652	1.051704	-0.038739	0.029461
0.4	1.302172	0.305691	0.460520	1.057800	-0.038823	0.029557
0.45	1.315255	0.309889	0.463644	1.064472	-0.038924	0.029668
0.5	1.329535	0.314521	0.466988	1.071652	-0.039046	0.029792
0.6	1.361344	0.325020	0.474195	1.087264	-0.039353	0.030084
0.8	1.435650	0.350470	0.489798	1.121801	-0.040259	0.030843
1	1.520416	0.380946	0.505673	1.158171	-0.041581	0.031832
1.5	1.757779	0.473051	0.541104	1.245654	-0.046579	0.035144
2	2.011202	0.579719	0.567825	1.320940	-0.053445	0.039200
2.5	2.269769	0.694704	0.586889	1.383789	-0.061421	0.043585
3	2.529615	0.814589	0.600268	1.436538	-0.069952	0.048049
3.5	2.789340	0.937455	0.609591	1.481470	-0.078930	0.052214
4	3.048455	1.062185	0.616035	1.520370	-0.088319	0.055831
4.5	3.306821	1.188087	0.620421	1.554550	-0.097779	0.059075
5	3.564440	1.314712	0.623321	1.584973	-0.106767	0.062399

Table E-5 Contributions to the total energy for the Hooke's atom in B fields (ω = 1/10, m= 0, singlet state, energy in Hartree)

B (*au*)	E_r	KE_r	E_{ee}	J	E_c	T_c
0	0.350001	0.051035	0.165298	0.421934	-0.029242	0.016427
0.001	0.350003	0.051036	0.165299	0.421936	-0.029242	0.016427
0.005	0.350057	0.051046	0.165320	0.421984	-0.029244	0.016428
0.01	0.350224	0.051081	0.165386	0.422134	-0.029247	0.016433
0.02	0.350889	0.051217	0.165648	0.422730	-0.029264	0.016453
0.03	0.351989	0.051443	0.166078	0.423712	-0.029294	0.016484
0.04	0.353511	0.051764	0.166667	0.425064	-0.029336	0.016529
0.05	0.355439	0.052174	0.167403	0.426764	-0.029395	0.016584
0.06	0.357752	0.052678	0.168271	0.428787	-0.029472	0.016650
0.08	0.363439	0.053971	0.170337	0.433676	-0.029686	0.016815
0.1	0.370368	0.055647	0.172720	0.439473	-0.030002	0.017014
0.15	0.391744	0.061524	0.179133	0.456254	-0.031363	0.017631
0.2	0.416678	0.069685	0.184874	0.473808	-0.033673	0.018356
0.25	0.443245	0.079773	0.189134	0.490349	-0.036916	0.019124
0.3	0.470393	0.091310	0.191852	0.505287	-0.040900	0.019891
0.35	0.497620	0.103826	0.193315	0.518638	-0.045382	0.020622
0.4	0.524712	0.116952	0.193876	0.530627	-0.050134	0.021303
0.45	0.551597	0.130422	0.193840	0.541500	-0.054982	0.021928
0.5	0.578266	0.144061	0.193433	0.551467	-0.059805	0.022496
0.6	0.631021	0.171463	0.192068	0.569294	-0.069104	0.023476
0.7	0.683159	0.198730	0.190471	0.584989	-0.077741	0.024283
0.8	0.734846	0.225742	0.188913	0.599073	-0.085671	0.024953
0.9	0.786204	0.252492	0.187485	0.611875	-0.092936	0.025516
1	0.837317	0.279005	0.186208	0.623623	-0.099608	0.025996

Table E-6 Contributions to the total energy for the Hooke's atom in B fields (ω = 1/2 m= -1, triplet state, energy in Hartree)

B (au)	E_{tot}	E_r	KE_r	E_{ee}	J
0	2.359657	1.609657	0.546492	0.344449	0.923482
0.005	2.352178	1.607171	0.546497	0.344451	0.923486
0.01	2.344740	1.604715	0.546515	0.344457	0.923499
0.05	2.286718	1.586094	0.547070	0.344635	0.923908
0.1	2.217885	1.565391	0.548803	0.345191	0.925181
0.2	2.092310	1.532408	0.555672	0.347376	0.930189
0.3	1.982195	1.510180	0.566921	0.350891	0.938245
0.4	1.886425	1.497909	0.582277	0.355570	0.948964
0.5	1.803642	1.494625	0.601402	0.361214	0.961894
0.6	1.732381	1.499286	0.623930	0.367617	0.976564
0.7	1.671180	1.510852	0.649489	0.374583	0.992528
0.8	1.618662	1.528350	0.677722	0.381937	1.009392
0.9	1.573578	1.550897	0.708301	0.389531	1.026823
1	1.534827	1.577720	0.740928	0.397243	1.044549
1.5	1.407318	1.755930	0.926773	0.434924	1.131722
2	1.343400	1.975366	1.136625	0.468075	1.209795
2.5	1.309802	2.213511	1.359833	0.495899	1.277064
3	1.291855	2.460716	1.591124	0.518997	1.334803
3.5	1.282548	2.712521	1.827601	0.538179	1.384693
4	1.278260	2.966707	2.067649	0.554171	1.428264
4.5	1.276993	3.222107	2.310381	0.567564	1.466746
5	1.277588	3.478078	2.555147	0.578824	1.501046

Table E-6 (*continued*)

B (au)	E_x	E_c	T_c	t_1	*Self-interaction*
0	-0.566825	-0.006452	0.005755	0.334161	0.473258
0.005	-0.566827	-0.006452	0.005755	0.334164	0.473260
0.01	-0.566834	-0.006453	0.005755	0.334172	0.473266
0.05	-0.567061	-0.006454	0.005757	0.334448	0.473474
0.1	-0.567766	-0.006461	0.005764	0.335309	0.474121
0.2	-0.570535	-0.006486	0.005792	0.338722	0.476666
0.3	-0.574985	-0.006529	0.005839	0.344310	0.480759
0.4	-0.580897	-0.006592	0.005905	0.351937	0.486203
0.5	-0.588012	-0.006675	0.005993	0.361436	0.492768
0.6	-0.596065	-0.006781	0.006101	0.372622	0.500212
0.7	-0.604803	-0.006911	0.006231	0.385310	0.508310
0.8	-0.614007	-0.007066	0.006382	0.399323	0.516860
0.9	-0.623490	-0.007248	0.006554	0.414496	0.525692
1	-0.633103	-0.007455	0.006747	0.430681	0.534669
1.5	-0.679926	-0.008828	0.008044	0.522799	0.578743
2	-0.721218	-0.010719	0.009782	0.626700	0.618121
2.5	-0.756291	-0.013343	0.011531	0.737098	0.651969
3	-0.786016	-0.016213	0.013576	0.851443	0.680956
3.5	-0.811429	-0.018955	0.016131	0.968554	0.705960
4	-0.833425	-0.022620	0.018049	1.087906	0.727781
4.5	-0.852694	-0.028757	0.017731	1.209165	0.747048
5	-0.869732	-0.037819	0.014671	1.331989	0.764215

Table E-7 Contributions to the total energy for the Hooke's atom in B fields (ω = 1/10, m = -1, triplet state, energy in Hartree)

B (au)	E_{tot}	E_r	KE_r	E_{ee}	J
0	0.553173	0.403173	0.096200	0.140515	0.391878
0.005	0.545787	0.400756	0.096227	0.140535	0.391925
0.01	0.538630	0.398505	0.096306	0.140596	0.392065
0.02	0.524999	0.394500	0.096623	0.140837	0.392624
0.03	0.512268	0.391149	0.097148	0.141235	0.393547
0.04	0.500417	0.388436	0.097880	0.141784	0.394820
0.05	0.489421	0.386343	0.098814	0.142477	0.396426
0.06	0.479249	0.384846	0.099946	0.143303	0.398344
0.08	0.461230	0.383527	0.102778	0.145314	0.403016
0.1	0.446038	0.384235	0.106326	0.147722	0.408623
0.15	0.418171	0.393171	0.117951	0.154847	0.425321
0.2	0.400837	0.409415	0.132814	0.162525	0.443604
0.25	0.390249	0.430171	0.150170	0.169888	0.461605
0.3	0.383892	0.453614	0.169442	0.176488	0.478385
0.34641*	0.38038476	0.47679492	0.18866537	0.18177953	0.49255431
0.35	0.380183	0.478627	0.190198	0.182154	0.493592
0.4	0.378139	0.504532	0.212112	0.186872	0.507182
0.5	0.376822	0.557564	0.258474	0.193743	0.530008
0.6	0.377270	0.611042	0.307108	0.197884	0.548195
0.7	0.378382	0.664377	0.357120	0.200091	0.563052
0.8	0.379691	0.717380	0.407937	0.201004	0.575571
0.9	0.380997	0.770020	0.459198	0.201083	0.586443
1	0.382222	0.822320	0.510668	0.200644	0.596130
2	0.389439	1.334451	1.023668	0.191409	0.664385
5	0.394749	2.842749	2.536839	0.179678	0.774053
10	0.396743	5.345744	5.046088	0.174667	0.866618

Table E-7 (*continued*)

B (au)	E_x	E_c	T_c	t_1	*Self-interaction*
0	-0.241488	-0.005554	0.004321	0.059488	0.200023
0.005	-0.241513	-0.005555	0.004322	0.059501	0.200047
0.01	-0.241589	-0.005557	0.004324	0.059539	0.200119
0.02	-0.241892	-0.005564	0.004331	0.059692	0.200404
0.03	-0.242391	-0.005576	0.004345	0.059945	0.200874
0.04	-0.243079	-0.005594	0.004363	0.060298	0.201523
0.05	-0.243946	-0.005617	0.004386	0.060748	0.202342
0.06	-0.244980	-0.005646	0.004415	0.061293	0.203319
0.08	-0.247493	-0.005721	0.004488	0.062658	0.205699
0.1	-0.250498	-0.005821	0.004582	0.064366	0.208555
0.15	-0.259365	-0.006201	0.004909	0.069954	0.217050
0.2	-0.268929	-0.006787	0.005363	0.077086	0.226336
0.25	-0.278183	-0.007600	0.005935	0.085400	0.235462
0.3	-0.286649	-0.008643	0.006605	0.094622	0.243950
0.34641*	-0.29366692	-0.00981101	0.00729685	0.10381856	0.25110225
0.35	-0.294176	-0.009909	0.007353	0.104552	0.251625
0.4	-0.300775	-0.011382	0.008154	0.115039	0.258470

Table E-7 (*continued*)

B (au)	E_x	E_c	T_c	t_1	*Self-interaction*
0.5	-0.311571	-0.014863	0.009831	0.137261	0.269929
0.6	-0.319917	-0.018898	0.011496	0.160651	0.279027
0.7	-0.326598	-0.023297	0.013065	0.184798	0.286436
0.8	-0.332173	-0.027896	0.014497	0.209434	0.292668
0.9	-0.337014	-0.032567	0.015779	0.234380	0.298075
1	-0.341352	-0.037224	0.016911	0.259517	0.302890
2	-0.373422	-0.076231	0.023323	0.512690	0.336881
5	-0.428044	-0.145886	0.020445	1.269841	0.391705
10	-0.474958	-0.210271	0.006722	2.604651	0.438010

*The exact field strength used is $\sqrt{3}/5 = 0.346410161514$.

Table E-8 Exact and approximate XC energies for the Hooke's atom in Zero B field (B=0, m = 0, singlet state, energy in Hartree)

ω	E_x^{exact}	E_x^{LDA}	$E_x^{PBE/jPBE}$	E_x^{B88}	E_c^{exact}	E_c^{LDA}	$E_c^{PBE/jPBE}$	E_c^{LYP}
0.00190	-0.0195	-0.0174	-0.0196	-0.0201	-0.0065	-0.0108	-0.0084	-0.0032
0.00382	-0.0301	-0.0265	-0.0297	-0.0304	-0.0091	-0.0152	-0.0117	-0.0048
0.01	-0.0543	-0.0473	-0.0527	-0.0539	-0.0139	-0.0233	-0.0177	-0.0082
0.02	-0.0825	-0.0713	-0.0795	-0.0812	-0.0182	-0.0311	-0.0231	-0.0118
0.05	-0.1416	-0.1218	-0.1359	-0.1389	-0.0245	-0.0437	-0.0310	-0.0184
0.1	-0.2110	-0.1811	-0.2022	-0.2062	-0.0292	-0.0550	-0.0374	-0.0239
0.2	-0.3116	-0.2671	-0.2984	-0.3040	-0.0336	-0.0677	-0.0436	-0.0293
0.5	-0.5151	-0.4410	-0.4931	-0.5021	-0.0385	-0.0862	-0.0514	-0.0350
1	-0.7467	-0.6389	-0.7148	-0.7276	-0.0414	-0.1013	-0.0566	-0.0376
2	-1.0757	-0.9201	-1.0297	-1.0480	-0.0436	-0.1174	-0.0612	-0.0385
4	-1.5420	-1.3186	-1.4761	-1.5021	-0.0453	-0.1342	-0.0653	-0.0380
10	-2.4684	-2.1104	-2.3630	-2.4044	-0.0468	-0.1575	-0.0696	-0.0357
20	-3.5130	-3.0033	-3.3630	-3.4219	-0.0477	-0.1760	-0.0723	-0.0335
40	-4.9907	-4.2663	-4.7777	-4.8611	-0.0483	-0.1949	-0.0744	-0.0312
100	-7.9230	-6.7727	-7.5849	-7.7171	-0.0488	-0.2208	-0.0766	-0.0287

Table E-9 Exact and approximate XC energies for the Hooke's atom in B fields (ω=1/2, m =0, singlet state, energy in Hartree)

B (au)	E_x^{exact}	E_x^{LDA}	E_x^{PBE}	E_x^{B88}	E_c^{exact}	E_c^{LDA}	E_c^{PBE}	E_c^{LYP}
0	-0.5151	-0.4410	-0.4931	-0.5021	-0.0385	-0.0862	-0.0514	-0.0350
0.1	-0.5160	-0.4418	-0.4940	-0.5030	-0.0385	-0.0863	-0.0514	-0.0350
0.2	-0.5188	-0.4441	-0.4966	-0.5056	-0.0386	-0.0865	-0.0515	-0.0351
0.3	-0.5231	-0.4479	-0.5008	-0.5099	-0.0387	-0.0868	-0.0516	-0.0351
0.4	-0.5289	-0.4529	-0.5064	-0.5156	-0.0388	-0.0872	-0.0517	-0.0352
0.5	-0.5358	-0.4589	-0.5133	-0.5226	-0.0390	-0.0878	-0.0519	-0.0353
0.6	-0.5436	-0.4658	-0.5211	-0.5305	-0.0394	-0.0884	-0.0521	-0.0354
0.8	-0.5609	-0.4813	-0.5387	-0.5485	-0.0403	-0.0897	-0.0525	-0.0355
1	-0.5791	-0.4982	-0.5580	-0.5682	-0.0416	-0.0910	-0.0528	-0.0356

Table E-9 (*continued*)

B (au)	E_x^{exact}	E_x^{LDA}	E_x^{PBE}	E_x^{B88}	E_c^{exact}	E_c^{LDA}	E_c^{PBE}	E_c^{LYP}
1.5	-0.6228	-0.5408	-0.6072	-0.6188	-0.0466	-0.0944	-0.0534	-0.0353
2	-0.6605	-0.5807	-0.6541	-0.6670	-0.0534	-0.0973	-0.0536	-0.0343
2.5	-0.6919	-0.6166	-0.6970	-0.7113	-0.0614	-0.0999	-0.0537	-0.0333
3	-0.7183	-0.6491	-0.7358	-0.7518	-0.0700	-0.1021	-0.0536	-0.0319
3.5	-0.7407	-0.6786	-0.7714	-0.7891	-0.0789	-0.1040	-0.0533	-0.0301
4	-0.7602	-0.7057	-0.8048	-0.8236	-0.0883	-0.1057	-0.0530	-0.0281
4.5	-0.7773	-0.7308	-0.8361	-0.8558	-0.0978	-0.1072	-0.0528	-0.0263
5	-0.7925	-0.7541	-0.8655	-0.8861	-0.1068	-0.1086	-0.0526	-0.0248

Table E-10 Exact and approximate XC energies for the Hooke's atom in B fields (ω=1/10, m = 0, singlet state, energy in Hartree)

B (au)	E_x^{exact}	E_x^{LDA}	E_x^{PBE}	E_x^{B88}	E_c^{exact}	E_c^{LDA}	E_c^{PBE}	E_c^{LYP}
0	-0.2110	-0.1811	-0.2022	-0.2061	-0.0292	-0.0550	-0.0374	-0.0239
0.05	-0.2134	-0.1832	-0.2045	-0.2085	-0.0294	-0.0554	-0.0375	-0.0240
0.1	-0.2197	-0.1888	-0.2109	-0.2150	-0.0300	-0.0563	-0.0380	-0.0244
0.15	-0.2281	-0.1967	-0.2199	-0.2242	-0.0314	-0.0576	-0.0385	-0.0249
0.2	-0.2369	-0.2056	-0.2303	-0.2349	-0.0337	-0.0590	-0.0389	-0.0255
0.25	-0.2452	-0.2147	-0.2412	-0.2461	-0.0369	-0.0604	-0.0392	-0.0259
0.3	-0.2526	-0.2237	-0.2521	-0.2573	-0.0409	-0.0617	-0.0393	-0.0262
0.35	-0.2593	-0.2324	-0.2626	-0.2682	-0.0454	-0.0630	-0.0394	-0.0265
0.4	-0.2653	-0.2407	-0.2728	-0.2788	-0.0501	-0.0642	-0.0395	-0.0266
0.45	-0.2707	-0.2486	-0.2826	-0.2889	-0.0550	-0.0653	-0.0395	-0.0267
0.5	-0.2757	-0.2562	-0.2919	-0.2986	-0.0598	-0.0663	-0.0395	-0.0268
0.6	-0.2846	-0.2703	-0.3093	-0.3168	-0.0691	-0.0681	-0.0395	-0.0267
0.7	-0.2925	-0.2832	-0.3254	-0.3335	-0.0777	-0.0698	-0.0395	-0.0266
0.8	-0.2995	-0.2952	-0.3402	-0.3490	-0.0857	-0.0712	-0.0395	-0.0263
0.9	-0.3059	-0.3063	-0.3541	-0.3635	-0.0929	-0.0726	-0.0395	-0.0259
1	-0.3118	-0.3167	-0.3670	-0.3772	-0.0996	-0.0738	-0.0395	-0.0255

Table E-11 Exact and approximate XC energies for the Hooke's atom in B fields (ω=1/2, m=-1, triplet state, energy in Hartree)

B (au)	E_x^{exact}	E_x^{LDA}	E_x^{PBE}	E_x^{jPBE}	E_x^{B88}	E_c^{exact}	E_c^{LDA}	E_c^{PBE}	E_c^{jPBE}
0	-0.5668	-0.5039	-0.5487	-0.5552	-0.5557	-0.0065	-0.0443	-0.0241	-0.0210
0.05	-0.5671	-0.5041	-0.5489	-0.5554	-0.5560	-0.0065	-0.0443	-0.0241	-0.0210
0.1	-0.5678	-0.5048	-0.5496	-0.5561	-0.5567	-0.0065	-0.0443	-0.0241	-0.0210
0.2	-0.5705	-0.5073	-0.5523	-0.5589	-0.5594	-0.0065	-0.0444	-0.0241	-0.0211
0.4	-0.5809	-0.5169	-0.5625	-0.5694	-0.5697	-0.0066	-0.0448	-0.0243	-0.0212
0.6	-0.5961	-0.5311	-0.5777	-0.5850	-0.5850	-0.0068	-0.0453	-0.0246	-0.0213
0.8	-0.6140	-0.5482	-0.5960	-0.6038	-0.6036	-0.0071	-0.0460	-0.0249	-0.0214
1	-0.6331	-0.5668	-0.6160	-0.6244	-0.6239	-0.0075	-0.0466	-0.0253	-0.0215
1.5	-0.6799	-0.6144	-0.6679	-0.6779	-0.6764	-0.0088	-0.0483	-0.0260	-0.0218
2	-0.7212	-0.6592	-0.7167	-0.7284	-0.7263	-0.0107	-0.0497	-0.0266	-0.0218

Table E-11 (*continued*)

B (au)	E_x^{exact}	E_x^{LDA}	E_x^{PBE}	E_x^{jPBE}	E_x^{B88}	E_c^{exact}	E_c^{LDA}	E_c^{PBE}	E_c^{jPBE}
2.5	-0.7563	-0.6998	-0.7615	-0.7747	-0.7721	-0.0133	-0.0510	-0.0270	-0.0218
3	-0.7860	-0.7365	-0.8029	-0.8177	-0.8139	-0.0162	-0.0521	-0.0274	-0.0218
3.5	-0.8114	-0.7697	-0.8406	-0.8568	-0.8522	-0.0190	-0.0531	-0.0277	-0.0217
4	-0.8334	-0.8002	-0.8746	-0.8921	-0.8875	-0.0226	-0.0539	-0.0277	-0.0215
4.5	-0.8527	-0.8286	-0.9056	-0.9246	-0.9204	-0.0288	-0.0547	-0.0277	-0.0212
5	-0.8697	-0.8550	-0.9350	-0.9553	-0.9511	-0.0378	-0.0554	-0.0277	-0.0209
10	-0.9726	-1.0490	-1.1614	-1.1925	-1.1848	-0.0921	-0.0599	-0.0285	-0.0198
20	-1.0701	-1.2993	-1.4679	-1.5144	-1.4903	-0.3119	-0.0655	-0.0267	-0.0163

Table E-12 Exact and approximate XC energies for the Hooke's atom in B fields (ω=1/10, m= -1, triplet state, energy in Hartree)

B (au)	E_x^{exact}	E_x^{LDA}	E_x^{PBE}	E_x^{jPBE}	E_x^{B88}	E_c^{exact}	E_c^{LDA}	E_c^{PBE}	E_c^{jPBE}
0	-0.2415	-0.2147	-0.2338	-0.2366	-0.2376	-0.0056	-0.0292	-0.0180	-0.0162
0.02	-0.2419	-0.2150	-0.2342	-0.2370	-0.2380	-0.0056	-0.0293	-0.0180	-0.0162
0.04	-0.2431	-0.2161	-0.2354	-0.2382	-0.2392	-0.0056	-0.0293	-0.0181	-0.0163
0.06	-0.2450	-0.2179	-0.2373	-0.2401	-0.2410	-0.0056	-0.0295	-0.0182	-0.0163
0.08	-0.2475	-0.2202	-0.2397	-0.2427	-0.2435	-0.0057	-0.0296	-0.0183	-0.0164
0.1	-0.2505	-0.2231	-0.2427	-0.2458	-0.2466	-0.0058	-0.0298	-0.0184	-0.0165
0.15	-0.2594	-0.2316	-0.2519	-0.2552	-0.2558	-0.0062	-0.0304	-0.0188	-0.0167
0.2	-0.2689	-0.2413	-0.2623	-0.2660	-0.2662	-0.0068	-0.0311	-0.0192	-0.0169
0.25	-0.2782	-0.2511	-0.2729	-0.2770	-0.2770	-0.0076	-0.0317	-0.0196	-0.0171
0.3	-0.2866	-0.2607	-0.2835	-0.2879	-0.2877	-0.0086	-0.0323	-0.0199	-0.0172
0.346*	-0.2937	-0.2693	-0.2929	-0.2977	-0.2968	-0.0098	-0.0329	-0.0202	-0.0173
0.35	-0.2942	-0.2699	-0.2936	-0.2984	-0.2979	-0.0099	-0.0329	-0.0202	-0.0173
0.4	-0.3008	-0.2785	-0.3032	-0.3085	-0.3077	-0.0114	-0.0334	-0.0204	-0.0173
0.5	-0.3116	-0.2944	-0.3210	-0.3271	-0.3259	-0.0149	-0.0344	-0.0207	-0.0173
0.6	-0.3199	-0.3085	-0.3372	-0.3440	-0.3425	-0.0189	-0.0352	-0.0209	-0.0172
0.7	-0.3266	-0.3214	-0.3520	-0.3595	-0.3578	-0.0233	-0.0359	-0.0210	-0.0170
0.8	-0.3322	-0.3332	-0.3658	-0.3740	-0.3720	-0.0279	-0.0366	-0.0211	-0.0169
0.9	-0.3370	-0.3443	-0.3787	-0.3876	-0.3853	-0.0326	-0.0372	-0.0212	-0.0167
1	-0.3414	-0.3547	-0.3909	-0.4004	-0.3979	-0.0372	-0.0377	-0.0212	-0.0165

* The exact field strength used is $\sqrt{3}/5 = 0.346410161514$.

LIST OF REFERENCES

1. M. Born and J. R. Oppenheimer, Ann. Physik. **84**, 457 (1927)

2. K. S. Pitzer, Accounts Chem. Res. **12**, 271 (1979)

3. N. Flocke, Wuming Zhu, and S. B. Trickey, J. Phys. Chem. B **109**, 4168 (2005)

4. Wuming Zhu, D. E. Taylor, A. R. Al-Derzi, K. Runge, S. B. Trickey, Ting Zhu, Ju Li, and S. Yip, (submitted to Comp. Mat. Sci.)

5. T. Kinoshita, Phys. Rev. **105**, 1490 (1957)

6. A. Szabo and N. S. Ostlund, *Modern Quantum Chemistry* (McGraw-Hill, New York, 1989)

7. X. Guan, B. Li, and K. T. Taylor, J. Phys. B **36**, 2465 (2003)

8. O.-A. Al-Hujaj and P. Schmelcher, Phys. Rev. A **70**, 023411 (2004)

9. P. Hohenberg and W. Kohn, Phys. Rev. **136**, B846 (1964)

10. W. Kohn and L. J. Sham, Phys. Rev. **140**, A1133 (1965)

11. W. Becken, P. Schmelcher, and F. K. Diakonos, J. Phys. B **32**, 1557 (1999)

12. W. Becken and P. Schmelcher, J. Phys. B **33**, 545 (2000)

13. W. Becken and P. Schmelcher, Phys. Rev. A **63**, 053412 (2001)

14. G. Vignale and M. Rasolt, Phys. Rev. Lett. **59**, 2360 (1987)

15. G. Vignale and M. Rasolt, Phys. Rev. B **37**, 10685 (1988)

16. G. Vignale, M. Rasolt, and D. J. W. Geldart, Adv. Quantum Chem. **21**, 235 (1990)

17. A review article on TF and related theories of atoms and molecules was given by E. H. Lieb, Rev. Mod. Phys. **53**, 603 (1981)

18. E. H. Lieb, *Physics as Natural Philosophy*, ed. by A. Shimory and H. Feshback (MIT Press, Cambridge, MA, 1982)

19. M. Levy, Phys. Rev. A **26**, 1200 (1982)

20. R. M. Dreizler and E. K. U. Gross, *Density Functional Theory* (Springer-Verlag, Berlin, 1990)

21. R. G. Parr and W. Yang, *Density Functional Theory of Atoms and Molecules* (Oxford University Press, Oxford, 1989)

22. *Modern Density Functional Theory, A Tool for Chemistry*, ed. by J. M. Seminario and P. Politzer (Elsevier, New York, 1995)

23. U. von Barth and L. Hedin, J. Phys. C **5**, 1629 (1972)

24. L. M. Sander, H. B. Shore, and L. J. Sham, Phys. Rev. Lett. **31**, 533 (1973)

25. R. K. Kalia and P. Vashishta, Phys. Rev. B **17**, 2655 (1978)

26. N. D. Mermin, Phys. Rev. **137**, A1441 (1965)

27. L. N. Oliveira, W. Kohn, and E. K. U. Gross, Phys. Rev. Lett. **60**, 2430 (1989)

28. A. K. Rajagopal and J. Callaway, Phys. Rev. B **7**, 1912 (1973)

29. E. Runge and E. K. U. Gross, Phys. Rev. Lett. **52**, 997 (1984)

30. S. M. Colwell and N. C. Handy, Chem. Phys. Lett. **217**, 271 (1994)

31. A. M. Lee, S. M. Colwell, and N. C. Handy, Chem. Phys. Lett. **229**, 225 (1994)

32. S. N. Maximoff, M. Ernzerhof, and G. E. Scuseria, J. Chem. Phys. **120**, 2105 (2004)

33. K. Capelle and G. Vignale, Phys. Rev. B **65**, 113106 (2002)

34. W. Kohn, A. Savin, and C. A. Ullrich, Int. J. Quantum Chem. **100**, 20 (2004)

35. S. Erhard and E. K. U. Gross, Phys. Rev. A **53**, R5 (1996)

36. G. Vignale, M. Rasolt and D. J. W. Geldart, Phys. Rev. B **37**, 2502 (1988)

37. E. Orestes, T. Marcasso, and K. Capelle, Phys. Rev. A **68**, 022105 (2003)

38. A. M. Lee, N. C. Handy, and S. M. Colwell, J. Chem. Phys. **103**, 10095 (1995)

39. A. M. Lee, N. C. Handy, and S. M. Colwell, Phys. Rev. A **53**, 1316 (1996)

40. A. G. Ioannou, S. M. Colwell, and R. D. Amos, Chem. Phys. Lett. **278**, 278 (1997)

41. K. Capelle, Phys. Rev. A **60**, R733 (1999)

42. G. Vignale and P. Skudlarski, Phys. Rev. B **46**, 10232 (1992)

43. P. Skudlarski and G. Vignale, Phys. Rev. Lett. **69**, 949 (1992)

44. G. Vignale, P. Skudlarski, and M. Rasolt, Phys. Rev. B **45**, 8494 (1992)

45. P. Skudlarski and G. Vignale, Phys. Rev. B **47**, 16647 (1993)

46. R. W. Danz and M. L. Glasser, Phys. Rev. B **4**, 94 (1971)

47. G. Vignale, Phys. Rev. B **47**, 10105 (1993)

48. S. M. Reimann and M. Manninen, Rev. Mod. Phys. **74**, 1283 (2002), and references therein.

49. S. Viefers, P. S. Deo, S. M. Reimann, M. Manninen, and M. Koskinen Phys. Rev. B **62**, 10668 (2000)

50. B. Tanatar and D. M. Ceperley, Phys. Rev. B **39**, 5005 (1989)

51. D. Levesque, J. J. Weis, and A. H. MacDonald, Phys. Rev. B **30**, 1056 (1984)

52. S. Liu, Phys. Rev. A **54**, 1328 (1996)

53. M. Higuchi and K. Higuchi, Phys. Rev. B **65**, 195122 (2002)

54. K. Higuchi and M. Higuchi, Physica B **312-313**, 534 (2002)

55. A. Holas and N. H. March, Phys. Rev. A **56**, 4595 (1997)

56. K. Capelle and E. K. U. Gross, Phys. Rev. Lett. **78**, 1872 (1997)

57. G. Vignale and W. Kohn, Phys. Rev. Lett. **77**, 2037 (1996)

58. R. Nifosi, S. Conti, and M. P. Tosi, Phys. Rev. B **58**, 12 758 (1998)

59. S. Conti, R. Nifosi, and M. P. Tosi, J. Phys.: Condens. Matter **9**, L475 (1997)

60. M. van Faassen, P. L. de Boeij, R. van Leeuwen, J. A. Berger, and J. G. Snijders, Phys. Rev. Lett. **88**, 186401 (2002)

61. M. van Faassen, P. L. de Boeij, R. van Leeuwen, J. A. Berger, and J. G. Snijders, J. Chem. Phys. **118**, 1044 (2003)

62. P. L. de Boeij, F. Kootstra, J. A. Berger, R. van Leeuwen, and J. G. Snijders, J. Chem. Phys. **115**, 1995 (2001)

63. C. A. Ullrich and G. Vignale, Phys. Rev. B **65**, 245102 (2002)

64. N. T. Maitra, I. Souza, and K. Burke, Phys. Rev. B **68**, 045109 (2003)

65. F. Janak, V. L. Moruzzi, and A. R. Williams, Phys. Rev. B **12**, 1257 (1975)

66. S. H. Vosko, L. Wilk, and M. Nusair, Can. J. Phys. **58**, 1200 (1980)

67. S. Kotochigova, Z. H. Levine, E. L. Shirley, M. D. Stiles, and C. W. Clark, Phys. Rev. A **55**, 191 (1997)

68. J. P. Perdew and A. Zunger, Phys. Rev. B **23**, 5048 (1981)

69. J. P. Perdew and Y. Wang, Phys. Rev. B **45**, 13244 (1992)

70. J. P. Perdew, K. Burke, and M. Ernzerhof, Phys. Rev. Lett. **77**, 3865 (1996)

71. J. P. Perdew, J. A. Chevary, S. H. Vosko, K. A. Jackson, M. R. Pederson, D. J. Singh, and C. Fiolhais, Phys. Rev. B **46**, 6671 (1992)

72. A. D. Becke, Phys. Rev. A **38**, 3098 (1988)

73. C. Lee, W. Yang, and R. G. Parr, Phys. Rev. B **37**, 785 (1988)

74. B. Miehlich, A. Savin, H. Stoll, and H. Preuss, Chem. Phys. Lett. **157**, 200 (1989)

75. B. G. Johnson, P. M. W. Gill, and J. A. Pople, J. Chem. Phys. **98**, 5612 (1993)

76. M. V. Ivanov and P. Schmelcher, Phys. Rev. A **61**, 022505 (2000)

77. O.-A. Al-Hujaj and P. Schmelcher, Phys. Rev. A **70**, 033411 (2004)

78. H. Ruder, G. Wunner, H. Herold, and F. Geyer, *Atoms in Strong Magnetic Fields* (Springer-Verlag, Berlin, 1994)

79. Y. P. Kravchenko, M. A. Liberman, and B. Johansson, Phys. Rev. Lett. **77**, 619 (1996)

80. Y. P. Kravchenko and M. A. Liberman, Phys. Rev. A **54**, 287 (1996)

81. Y. P. Kravchenko and M. A. Liberman, Int. J. Quantum Chem. **62**, 593 (1996)

82. A. Rutkowski and A. Poszwa, Phys. Rev. A **67**, 013412 (2003)

83. B. M. Relovsky and H. Ruder, Phys. Rev. A **53**, 4068 (1996)

84. M. Braun, Phys. Rev. A **65**, 033415 (2002)

85. M. V. Ivanov, J. Phys. B **27**, 4513 (1994)

86. M. V. Ivanov and P. Schmelcher, Phys. Rev. A **57**, 3793 (1998)

87. M. V. Ivanov, Phys. Lett. A **239**, 72 (1998)

88. M. V. Ivanov and P. Schmelcher, Eur. Phys. J. D **14**, 279 (2001)

89. M. V. Ivanov and P. Schmelcher, J. Phys. B **34**, 2031 (2001)

90. M. V. Ivanov and P. Schmelcher, Phys. Rev. A **60**, 3558 (1999)

91. M. D. Jones, G. Ortiz, and D. M. Ceperley, Phys. Rev. A **54**, 219 (1996)

92. M. D. Jones, G. Ortiz, and D. M. Ceperley, Phys. Rev. E **55**, 6202 (1997)

93. M. D. Jones, G. Ortiz, and D. M. Ceperley, Int. J. Quantum Chem. **64**, 523 (1997)

94. M. D. Jones, G. Ortiz, and D. M. Ceperley, Phys. Rev. A **59**, 2875 (1999)

95. S. B. Trickey, J. A. Alford, and J. C. Boettger, Comp. Mat. Sci., Theor. Comp. Chem. 15, **171** (2004) and references therein.

96. K. Runge and J. R. Sabin, Int. J. Quantum Chem. **64**, 561 (1997)

97. Y. P. Kravchenko and M. A. Liberman, Int. J. Quantum Chem. **64**, 513 (1997)

98. M. W. Schmidt and K. Ruedenburg, J. Chem. Phys. **71**, 3951 (1979)

99. F. Sasaki and M. Yoshimine, Phys. Rev. A **9**, 17 (1974)

100. General Atomic and Molecular Electronic Structure System, http://www.msg.ameslab.gov/GAMESS/GAMESS.html, accessed July 1, 2005

101. C. F. Bunge, J. A. Barrientos, A. V. Bunge, and J. A. Cogordan, Phys. Rev. A **46**, 3691 (1992)

102. I.-H. Lee and R. M. Martin, Phys. Rev. B **56**, 7197 (1997)

103. P. B. Jones, Phys. Rev. Lett. **55**, 1338 (1985)

104. D. Neuhauser, S. E. Koonin, and K. Langanke, Phys. Rev. A **36**, 4163 (1987)

105. X. Guan and B. Li, Phys. Rev. A **63**, 043413 (2001)

106. D. Neuhauser, K. Langanke, and S. E. Koonin, Phys. Rev. A **33**, 2084 (1986)

107. A. D. Becke, J. Chem. Phys. **117**, 6935 (2002)

108. S. Kais, D. R. Herschbach, and R. D. Levine, J. Chem. Phys. **91**, 7791 (1989)

109. S. Kais, D. R. Herschbach, N. C. Handy, C. W. Murray, and G. J. Laming, J. Chem. Phys. **99**, 417 (1993)

110. A. Samanta and S. K. Ghosh, Phys. Rev. A **42**, 1178 (1990)

111. M. Taut, Phys. Rev. A **48**, 3561 (1993)

112. D. P. O'Neill and P. M. Gill, Phys. Rev. A **68**, 022505 (2003)

113. P. M. Laufer and J. B. Krieger, Phys. Rev. A **33**, 1480 (1986)

114. C. Fillipi, C. J. Umrigar and M. Taut, J. Chem. Phys. **100**, 1290 (1994)

115. M. Taut, Phys. Rev. A **53**, 3143 (1996)

116. M. Taut, A. Ernst and H. Eschrig, J. Phys. B **31**, 2689 (1998)

117. M. Taut, J. Phys. A **27**, 1045 (1994)

118. Z. Qian and V. Sahni, Phys Rev A **57**, 2527 (1998)

119. E. V. Ludeña, D. Gómez, V. Karasiev, and P. Nieto, Int. J. Quantum Chem. **99**, 297 (2004)

120. K.-C. Lam, F. G. Cruz, and K. Burke, Int. J. Quantum Chem. **69**, 533 (1998)

121. J. Cioslowski and K. Pernal, J. Chem. Phys. **113**, 8434 (2000)

122. W. Zhu and S. B. Trickey, Phys. Rev. A (in press)

123. Z. Wang and D. Guo*, Introduction to Special Function* (Peking Univ. Press, Beijing, China, 2000)

124. A. G. Abrashkevich, D. G. Abrashkevich, M. S. Kaschiev and I. V. Puzynin, Comp. Phys. Comm. **85**, 65 (1995)

125. P. Pröschel, W. Rösner, G. Wunner, H. Ruder and H. Herold, J. Phys. B **15**, 1959 (1982)

126. W. H. Press, S. A. Teukolsky, W. T. Vetterling, and B. P. Flannery, *Numerical Recipes in* C++, (Cambridge Univ. Press, 2002)

127. A. Wensauer and U. Rössler , Phys. Rev. B **69**, 155302 (2004)

128. A. M. Lee and N. C. Handy, Phys. Rev. A **59**, 209 (1999)

BIOGRAPHICAL SKETCH

Wuming Zhu was born on September 11, 1970, in Qixian, Henan province, China. He got a B.S. degree in physics in 1991 from East China Normal University, Shanghai, and a M.S. degree in biophysics in 1994 from the same university under the supervision of Professor Jiasen Chen. He taught for 5 years as an instructor in physics experiments in the Department of Physics, ECNU, before attending the University of Florida in 1999. He started working under the supervision of Professor Samuel B. Trickey in 2000. He married Ms. Xingxing Liu in 2003. He completed his Ph.D. in 2005.